Towards personalized medicine for metastatic urothelial cancer

Maud Rijnders

Towards personalized medicine for metastatic urothelial cancer

Maud Rijnders

Towards personalized medicine for metastatic urothelial cancer

Maud Rijnders

Towards Personalized Medicine for Metastatic Urothelial Cancer

-

De weg naar gepersonaliseerde behandeling van gemetastaseerd urotheelcarcinoom

Proefschrift

ter verkrijging van de graad van doctor aan de
Erasmus Universiteit Rotterdam
op gezag van de
rector magnificus

Prof. dr. A.L. Bredenoord

en volgens besluit van het College voor Promoties.

De openbare verdediging zal plaatsvinden op
woensdag 8 februari 2023 om 10.30 uur

door

Maud Rijnders

geboren te 's-Hertogenbosch

Erasmus University Rotterdam

Printing of this thesis was financially supported by: the department of Medical Oncology of the Erasmus MC Cancer Institute and the Erasmus University Rotterdam.

ISBN: 978-94-6419-717-4
Cover: Ilse Modder | www.ilsemodder.nl
Lay-out: Ilse Modder | www.ilsemodder.nl
Print: Gildeprint Enschede | www.gildeprint.nl

PROMOTIECOMMISSIE

Promotoren:	Prof. dr. R. de Wit Prof. dr. J.E.M.A. Debets
Overige leden:	Prof. dr. P.A.E. Sillevis Smitt Prof. dr. A.C. Dingemans Prof. dr. T.D. de Gruijl
Copromotoren:	Dr. A.A.M. van der Veldt Dr. J.L. Boormans

TABLE OF CONTENTS

CHAPTER 1

General introduction

BLADDER CANCER

Bladder cancer is the 7th most common malignancy diagnosed in males worldwide, whereas the incidence is much lower in women (1). The majority of patients is older than 65 years at time of diagnosis (2). Approximately 90% of bladder cancers are of urothelial origin. Non-urothelial bladder cancers include squamous cell, adeno-, and small cell carcinomas. Tumors can arise along the entire urinary tract, ranging from the urethra and bladder to the ureter and renal pelvis. Risk factors for developing bladder cancer are tobacco smoking, occupational exposure to aromatic benzenes, chronic cystitis, and pelvic radiation for other malignancies, such as prostate and rectal cancer (3-7). Furthermore, patients with Lynch syndrome, a hereditary cancer syndrome caused by a germline mutation in one of the DNA mismatch repair genes, have a lifetime risk of up to 20% of developing upper tract urothelial carcinoma (8). Although bladder cancer is less common in females, women often present with more advanced disease and have worse survival outcomes, possibly as a result of delayed diagnosis or hormone-related factors (9, 10).

DISEASE STAGES OF BLADDER CANCER

The majority of patients with bladder cancer (~70%) have non-muscle invasive disease which is confined to the urothelium or lamina propria (11). Patients with non-muscle invasive bladder cancer (NMIBC) have excellent overall survival outcomes, however many patients experience intravesical recurrences. In about 10-25% of patients with NMIBC, the disease will progress to muscle invasive bladder cancer (MIBC) (12). Approximately 25% of patients present with primary muscle invasive disease. The prognosis of these patients is significantly worse compared to NMIBC; 20-70% of patients with MIBC experience recurrent disease after local curative treatment, and metastatic disease occurs in ~50% of cases (13). A minority of patients (5-15%) with MIBC has metastatic disease at initial disease presentation. Patients with metastatic urothelial cancer (mUC) have a poor prognosis with a 5-year survival rate of less than 15% when treated with conventional regimens (14).

TREATMENT OF BLADDER CANCER

Traditional therapeutic approaches at multiple disease stages

The initial management of NMIBC is aimed at obtaining tumor control and at preservation of a functional bladder. Depending on the risk stratification, patients are treated by transurethral resection of the bladder tumor with or without intravesical

therapy (13). Intravesical therapy can consist of a single postoperative or maintenance instillation with chemotherapy, or multiple installations with *Bacillus Calmette-Guérin* (BCG), which is a live attenuated form of *Mycobacterium bovis*. Following initial therapy, careful surveillance is required for all patients as there is a high risk of recurrence and development of second primary tumors (15-18). For patients who are considered to be BCG-unresponsive, radical cystectomy is recommended as they are at high risk of progression to MIBC and eventual development of metastatic disease (19).

The majority of patients with non-metastatic MIBC is treated with neoadjuvant systemic chemotherapy followed by radical cystectomy. Chemotherapy consists of platinum-based combination regimens of either (standard or dose-dense) MVAC (methotrexate, vinblastine, doxorubicin, and cisplatin) or gemcitabine plus cisplatin (20-23). A subset of patients is not fit for this intense treatment or prefers to preserve their native bladder. For these patients, management by maximal transurethral resection of the bladder tumor followed by concurrent chemoradiotherapy can be considered (24, 25).

Since the late 1980s, palliative systemic chemotherapy has been the backbone of therapy in mUC. Patients with mUC can be treated with combination regimens of MVAC or gemcitabine plus cisplatin. The toxicity profile of gemcitabine plus cisplatin is more favorable and as a result this has become the preferred regimen (14). Notably, more than half of patients with mUC are unfit to receive cisplatin-based chemotherapy due to poor performance status, decreased creatinine clearance, severe hearing loss, peripheral neuropathy, or heart failure (26, 27). Patient who are cisplatin-unfit can be treated with gemcitabine plus carboplatin, which has a milder toxicity profile (28). Until recently, patients with mUC who developed progressive disease after first-line treatment had little treatment options. Single-agent chemotherapy with paclitaxel, docetaxel, or vinflunine have been registered as second-line therapy, however response rates are less than 20% and of short duration (29).

Novel and experimental therapeutic approaches for bladder cancer

Second-line immune checkpoint inhibition for metastatic urothelial cancer

In 2013, T cell therapy for cancer, including immune checkpoint inhibitors (ICI), was designated as scientific breakthrough of the year (30). ICIs disrupt the interaction between co-inhibitory receptors on T cells and their ligands on tumor cells or antigen presenting cells, by which they re-activate T cells to kill tumor cells. ICIs are antibodies that target for instance programmed cell death protein (PD)-1 (pembrolizumab, nivolumab), or its ligand PD-L1 (atezolizumab, durvalumab, avelumab), or cytotoxic T-lymphocyte-associated protein 4 (CTLA4; ipilimumab, tremelimumab). For patients with bladder cancer, the treatment paradigm started to shift in 2014 with the first demonstration of efficacy of an anti-PD-L1 agent in a phase I study of 67 patients with

mUC who experienced progressive disease after chemotherapy (Table 1) (31). In the following years, multiple phase I and II studies were conducted, showing the efficacy of nivolumab, durvalumab, atezolizumab, pembrolizumab and avelumab in the second-line setting (discussed in Chapter 2 of this thesis) (32-38). The median progression-free survival (PFS) and overall survival (OS) in these studies ranged from 1.5 to 2.8 months, and 6.5 to 13 months, respectively (Table 1). Specifically OS with ICIs was better than that of conventional chemotherapy regimens with a median of 7 to 8.5 months (median PFS 2.7 to 4 months) (29). Therefore, in 2016 and 2017 accelerated approvals by the U.S. Food and Drug Administration (FDA) and the European Medicine Agency (EMA) were granted to all five drugs for use as second-line therapy for patients with mUC.

The first head-to head comparison of standard-of-care chemotherapy with an ICI (i.e., pembrolizumab) was performed in the phase III KEYNOTE-045 trial. This study showed superiority of pembrolizumab over chemotherapy with an objective response rate (ORR) of 21% *vs* 11% (p = 0.001), and a median OS of 10.3 *vs* 7.4 months (hazard ratio (HR) 0.73; 95% confidence interval (CI) 0.59-0.91; p = 0.002) respectively (Table 1). In this study, PD-L1 expression was not found to be associated with treatment response to pembrolizumab (39, 40). These outcomes led to the first new approval as second-line treatment for patients with mUC in the Netherlands since 2010 (judged by the "*Nederlandse vereniging voor medische oncologie - commissie ter beoordeling van oncologische middelen (BOM)*")(41). It is noteworthy that a phase III trial comparing atezolizumab to conventional chemotherapy, the IMvigor211 study, failed to show improved outcomes for patients treated with atezolizumab. Patients who had PD-L1 expression on at least 5% of tumor infiltrating immune cells (IC2/3 status) showed similar ORR, and median OS and PFS in both treatment arms (Table 1) (42, 43). These results led to withdrawal of regulatory approval of atezolizumab as second-line therapy in patients with mUC (44). Also, regulatory approval for second-line durvalumab was voluntarily withdrawn by AstraZeneca in 2021 based on the results of the DANUBE trial in the first-line setting (see section below) (45, 46). Approval for pembrolizumab, nivolumab, and avelumab remains (Figure 1), although the latter two ICIs have not been directly compared to conventional chemotherapy. Together, these studies show that efficacy of monotherapy with ICIs in the second-line setting is limited. Finally, combination treatment with nivolumab and ipilimumab was tested in the phase III CheckMate032 trial and showed promising results specifically for the combination of nivolumab (1 mg/kg) plus ipilimumab (3 mg/kg). Although the study design precluded direct comparison with other treatment arms, this regimen resulted in the best ORR of 38%, a median OS of 15.3 months, and a median PFS of 4.9 months (Table 1) (47).

First-line immune checkpoint inhibition for metastatic urothelial cancer

Based on the efficacy of ICIs in patients with chemotherapy-refractory mUC, trials

were also initiated in earlier lines of treatment. The first studies showing efficacy of ICIs in patients who were treatment-naïve and platinum-ineligible were conducted with atezolizumab (48) and pembrolizumab (49), and led to FDA and EMA approvals in this setting in 2017 (Figure 1). In these phase II trials, ORRs of 23% and 24% were observed for atezolizumab and pembrolizumab, respectively (Table 1). In patient with a PD-L1 IC2/3 status (according to the companion diagnostic assay for atezolizumab) who were treated with atezolizumab, ORR was 28%, median OS was 12.3 months (95% CI 6 months to not reached (NR)), and the 12-month OS rate was 52% (48). Subgroup analyses of pembrolizumab treated patients revealed an ORR of 47% for patients with a PD-L1 combined positivity score (CPS) ≥10 (according to the companion diagnostic assay for pembrolizumab), including 20% of patients with a complete response. The median OS was 18.5 months (95% CI, 9.7 months to NR) for these patients, and responses lasted for more than 24 months in 57% of patients (50). An early review of the IMvigor130 and KEYNOTE-361 trials by the data monitoring committee revealed that patients with a low PD-L1 expression status who received ICI monotherapy had decreased survival compared to patients who received chemotherapy (51). As a consequence, the FDA and EMA restricted the first-line use of atezolizumab and pembrolizumab to cisplatin-ineligible patients with high PD-L1 expressing tumors (IC2/3 and CPS ≥10, respectively). Treatment remained non-restricted for patients with mUC who are ineligible for any platinum-based chemotherapy (52, 53).

In follow-up studies, combination therapy of ICIs with chemotherapy were investigated in the first-line setting. In the phase III IMvigor130 study, atezolizumab plus chemotherapy was compared to atezolizumab monotherapy and placebo plus chemotherapy (54). The primary endpoint of PFS was reached for combination treatment *vs* chemotherapy alone (median 8.2 *vs* 6.3 months; HR 0.82; 95% CI 0.70-0.96; p = 0.007; Table 1). However, no OS benefit was observed for the combination *vs* chemotherapy alone in this interim analysis (median 16 *vs* 13 months; HR 0.83; 95% CI, 0.69-1.00; p = 0.027; prespecified p value boundary of 0.007), questioning its clinical value. Formal comparison of chemotherapy *vs* atezolizumab monotherapy has not been performed yet due to the sequential testing design of the study. In a similar manner, efficacy of pembrolizumab plus chemotherapy *vs* pembrolizumab monotherapy *vs* placebo plus chemotherapy was studied in the KEYNOTE-361 study (55). Combination therapy did not improve the median OS (17 *vs* 14.3 months; HR 0.86; 95% CI 0.72-1.02; p = 0.041; prespecified p value boundary of 0.014) and PFS (8.3 *vs* 7.1 months; HR 0.78; 95% CI 0.65-0.93; p = 0.0033; prespecified p value boundary of 0.0019) compared to chemotherapy alone (Table 1). The trial design impeded further testing of pembrolizumab monotherapy *vs* chemotherapy. Finally, durvalumab monotherapy and durvalumab plus tremelimumab *vs* chemotherapy were evaluated in the DANUBE trial (45). Median OS did not improve in patients receiving combination therapy compared to chemotherapy (15 *vs* 12 months; HR 0.85; 95% CI 0.72-1.02; p = 0.075;

Table 1). Also among patients with high levels of PD-L1 expression there was no OS benefit of durvalumab monotherapy compared to chemotherapy (median 14.4 *vs* 12.1 months; HR 0.89; 95% CI 0.71-1.11; p = 0.30). However, the median OS was longer in patients with high PD-L1 expression who were treated with durvalumab plus tremelimumab compared to chemotherapy (17.9 *vs* 12.1 months; HR 0.74; 95% CI 0.59-0.93; p-value not reported). Front-line use of durvalumab is therefore further being investigated in the ongoing NILE trial in combination with tremelimumab and/or chemotherapy (NCT03682068). For now, there is not enough evidence to support the use of ICIs plus chemotherapy in the treatment of chemotherapy-naïve patients with mUC.

Maintenance therapy with immune checkpoint inhibitors for metastatic urothelial cancer

In several tumor types, it has been shown that maintenance therapy with ICI can prolong OS in patients who do not experience progressive disease following ICI (continuation maintenance) or chemotherapy (switch maintenance) (56). The rationale for the switch maintenance approach is that chemotherapy may prime the immune system and deplete immunosuppressive cells resulting in less blockade (besides immune checkpoints) of anti-tumor T cells. Furthermore, this approach may prevent potential cross-resistance and toxicities due to concurrent exposure to two agents. Maintenance therapy is only administered to patients who obtain disease control, which is prognostically favorable compared to rapid disease progression upon chemotherapy. In addition, earlier administration of an ICI increases the likelihood that a patient is able to receive a subsequent therapy, which is currently only possible for 30-50% of patients after first-line chemotherapy (56-59). Maintenance therapy was evaluated for pembrolizumab (60) and avelumab (61) in patients with advanced and mUC. Pembrolizumab or placebo maintenance therapy was administered to patients who achieved at least stable disease upon first-line platinum-based chemotherapy. Analysis revealed a PFS benefit for pembrolizumab *vs* placebo (primary endpoint; median 5.4 *vs* 3.0 months; HR 0.65; p = 0.04) but no OS benefit (secondary endpoint; median 22 *vs* 18.7 months; HR 0.91; 95% CI 0.52-1.59; p = 0.74; Table 1). Better results were reported for avelumab maintenance therapy after initial chemotherapy treatment in the JAVELIN Bladder 100 trial (61). The median OS improved from 14.3 months with best supportive care (BSC) to 21.4 months with avelumab (HR 0.69; 95% CI 0.56-0.86; p = 0.001), and median PFS improved from 2.0 to 3.7 months respectively (HR 0.62; 95% CI 0.52-0.75; p-value not reported; Table **1**). In the subgroup of patients with PD-L1 positive tumors, median OS was not reached *vs* 17 months (HR 0.56; 95% CI 0.40-0.79; p < 0.001), and median PFS was 5.7 *vs* 2.1 months (HR 0.56; 95% CI 0.43-0.73; p-value not reported) in the avelumab and BSC arm, respectively. Based on these results regulatory approval was granted for avelumab maintenance therapy by the FDA, EMA, and Dutch advisory committee BOM (Figure 1; (62-64)).

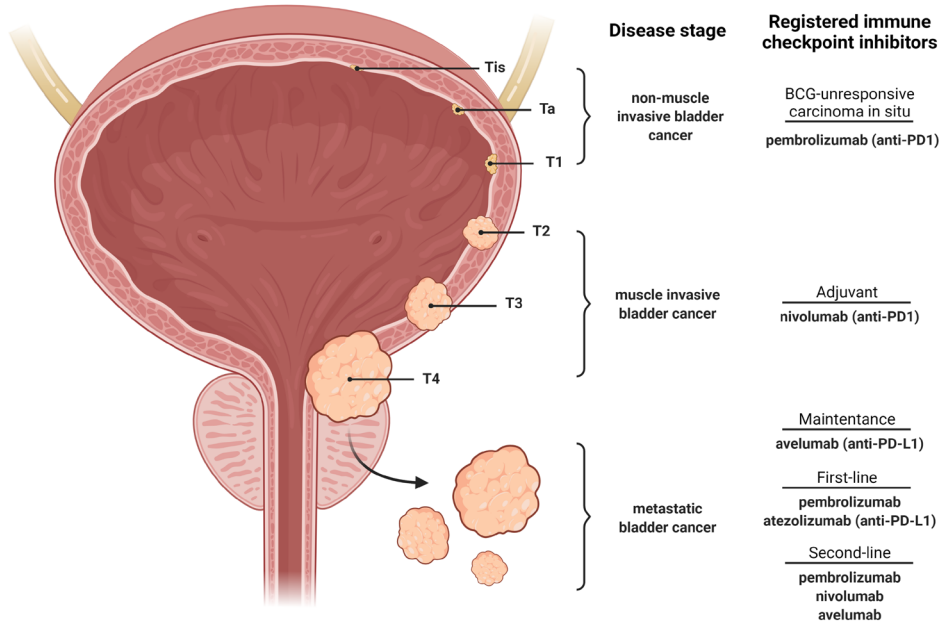

Figure 1. Immune checkpoint inhibitors registered as treatment for patients with different stages of bladder cancer.

Treatment with immune checkpoint inhibitors in patients with primary urothelial cancer

Recently, the first trials reporting efficacy outcomes for ICIs in earlier stages of UC have been published. In NMIBC, pembrolizumab was evaluated in patients with BCG-unresponsive carcinoma in situ of the bladder with or without papillary disease. Radical cystectomy is the recommended treatment for these patients, however this is a major surgical procedure with high morbidity and even mortality rates, and many patients are unable to undergo this procedure because of advanced age, comorbidities, or insufficient performance score. The KEYNOTE-057 trial showed that 39 out of 96 patients (41%) had a complete response after three months of therapy, and this lasted for more than 12 months in 18 of 39 patients (46%). Furthermore, the PFS to muscle-invasive or metastatic disease or death at 12 months was 97% (95% CI 86.0-99.2), and the PFS to worsening of grade or stage or death at 12 months was 83% (95% CI 70.2-90.4). Radical cystectomy could successfully be prevented in these patients. Treatment was generally well tolerated, although 13% of patients did experience grade 3 or 4 treatment-related adverse events. Pembrolizumab was therefore approved as an alternative regimen for BCG-unresponsive carcinoma in situ of the bladder by the FDA (Figure 1) (65, 66).

Neoadjuvant ICIs have been tested for MIBC but have not yet been approved in this setting. In the Pure-01 trial, three cycles of pembrolizumab were administered to patients

with MIBC (stage ≤T3bN0), prior to cystectomy. Twenty-one out of 50 patients (42%) had a pathological complete response (pCR), and in an additional six patients MIBC was downstaged to non-muscle invasive tumors. The pCR rate improved to 54% for patients with PD-L1 positive tumors (CPS ≥10), whereas only two patients with CPS <10 obtained a pCR (67). Efficacy of two cycles of neoadjuvant atezolizumab before cystectomy was studied in the ABACUS trial. A pCR was achieved in 31% (27 out of 88) of all studied patients, whereas this was only 17% in patients with T3 or T4 disease at baseline. In patients who had high PD-L1 expression (≥5% of immune cells) at baseline, the pCR rate was 37% (68).

Combination therapy with two ICIs has also been tested in the neoadjuvant setting. In the NABUCO trial, two cycles of ipilimumab and two cycles of nivolumab were administered preoperatively to 24 patients with MIBC (stage ≤T4aN0-3). Eleven patients (46%) had a pCR, defined as the absence of urothelial cancer cells at radical cystectomy, and in 14 patients (58%) no residual invasive UC was observed. The pCR rate was 40% and 50% in patients with and without lymph node involvement at baseline, and 73% in patients with a PD-L1 CPS ≥10 (69). Additionally, combination therapy with two cycles of durvalumab plus tremelimumab was studied in patients with MIBC (stage ≤T4N0) who were cisplatin-ineligible. A total of 9 out of 24 patients (38%) had a pCR at cystectomy, and downstaging to non-muscle invasive disease was observed in 58% of patients. The pCR rate in patients with T3 or T4 disease was 42%. No association with response was observed for PD-L1 expression on tumor or immune cells (70).

Finally, the efficacy of adjuvant therapy with ICIs following cystectomy is being studied. Adjuvant nivolumab (n = 353 patients) was compared to placebo (n = 356) and showed a significantly improved disease-free survival (DFS) of 21 *vs* 11 months, respectively (71). The 6-month DFS rate was 75% with nivolumab and 60% with placebo (HR 0.70; 98.22% CI 0.55-0.9; p < 0.001), and 75% and 56% (HR 0.55; 98.72% CI 0.35-0.85; p < 0.001) in patients treated with nivolumab or placebo with at least 1% PD-L1 expression in their tumor. The median recurrence-free survival was 23 months in the nivolumab arm *vs* 14 months in the placebo arm. At 6 months 77% of patients treated with nivolumab and 63% of patients treated with placebo were alive and free from recurrence (HR 0.72; 95% CI 0.59-0.89; no p-value reported). This survival benefit was associated with significantly more grade 3 or 4 treatment-related adverse events in the nivolumab *vs* placebo arm (20% and 7.2%). Based on these results nivolumab was approved by the FDA as adjuvant treatment for patients with MIBC (Figure 1) (72). No improvement of DFS was observed for adjuvant therapy with atezolizumab compared to placebo after cystectomy, with a median DFS of 19 *vs* 17 months, respectively (HR 0.89; 95% CI 0.74-1.08; p – 0.24). Also, subgroup analysis of patients with a positive PD-L1 score did not reveal benefit of atezolizumab over placebo (73). Efficacy of adjuvant pembrolizumab is currently being evaluated in the ongoing AMBASSADOR trial (74).

Table 1. Efficacy of immune checkpoint inhibitors in different lines of treatment of patients with advanced and metastatic urothelial cancer.

Trial	Date	Study design	Treatment	Patients (n)	Median OS months (CI)	Hazard ratio OS (CI)	Median PFS months (CI)	Hazard Ratio PFS (CI)	ORR (CI)	CR n (%)	Median DOR in months (CI)
Second-line											
Fradet (40)	2019	Phase III	Pembrolizumab	270	10.1	0.70***	2.1	0.96	21.1%**	25†	NR†
KEYNOTE-045[5]					(8.0-12)[a]	(0.57-0.85)[a]	(2.0-2.2)[a]	(0.79-1.16)[a]	(16-27)[a]	(9.3%)	(1.6-30.0)[b]
			Chemotherapy	272	7.3		3.3		11%	8	4.4
					(6.1-8.1)[a]		(2.4-3.6)[a]		(7.6-15)[a]	(2.9%)	(1.4-29.9)[b]
Bellmunt (39)	2017	Phase III	Pembrolizumab	270	10.3	0.73**	2.1	0.98	21.1%**	19†	NR†
KEYNOTE-045					(8.0-12)[a]	(0.59-0.91)[a]	(2.0-2.2)[a]	(0.81-1.19)[a]	(16-27)[a]	(7%)	(1.6-15.6)[b]
			Chemotherapy	272	7.4		3.3		11.4%	9	4.3
					(6.1-8.3)[a]		(2.3-3.5)[a]		(7.9-16)[a]	(3.3%)	(1.4-15.4)[b]
Powles (42)	2018	Phase III	Atezolizumab	467	11.1[4]	0.87	2.4[4]	1.01	23%[4]	8[4]	15.9[4]†
IMvigor211					(8.6-16)[a]	(0.63-1.21)[a]	(2.1-4.2)[a]	(0.75-1.34)[a]	(16-32)[a]	(7%)	(10.4-NR)[a]
			Chemotherapy	443	10.6[4]		4.2[4]		21.6%[4]	8[4]	8.3[4]
					(8.4-12)[a]		(3.7-5.0)[a]		(15-30)[a]	(7%)	(5.6-13.2)[a]
Sharma (35)	2017	Phase II	Nivolumab	270	8.74		2		19.6%	6	NR
CheckMate275					(6.05-NR)[a]		(1.9-2.6)[a]		(15-25)[a]	(2%)	(7.43-NR)[c]
Rosenberg (34)	2016	Phase II	Atezolizumab	310	7.9		2.1		15%	15	NR
IMvigor210[6]					(6.6-9.3)[a]		(2.1-2.1)[a]		(11-19)[a]	(5%)	(2.0-13.7)[b]
Sharma (47)	2019	Phase I/II	Nivo 3[1]	78	9.9	NA	2.8	NA	25.6%†	8†	30.5†
CheckMate032					(7.3-21)[a]		(1.5-5.3)[a]		(16-37)[a]	(10%)	(8.3-NR)[a]
			Nivo 3 plus ipi 1[2]	104	7.4	NA	2.6	NA	26.9%	8	22.3
					(5.6-11)[a]		(1.4-3.9)[a]		(19-37)[a]	(7.7%)	(12.8-NR)[a]
			Nivo 1 plus ipi 3[3]	92	15.3	NA	4.9	NA	38%	6	22.9
					(10-28)[a]		(2.7-6.6)[a]		(28-49)[a]	(6.5%)	(9.8-NR)[a]
Powles (38)	2017	Phase I/II	Durvalumab	191	18.2		1.5		17.8%	7	NR
					(8.1-NR)[a]		(1.4-1.9)[a]		(13-24)[a]	(3.7%)	(0.9-19.9)[b]
Massard (33)	2016	Phase I/II	Durvalumab	61	NA		NA		31%	NA	NR
									(18-47)[a]		(4.1-49.3)[b]
Sharma (32)	2016	Phase I/II	Nivolumab	78	9.7		2.8		24.4%	5	9.4
CheckMate032					(7.3-16)[c]		(1.5-5.9)[c]		(15-35)[a]	(6%)	(5.7-12.5)[c]
Plimack (36)	2017	Phase Ib	Pembrolizumab	33	13		2		26%	3	10
KEYNOTE-012					(5-20)[b]		(2-4)[b]		(11-46)[a]	(11%)	(4-22+)[b]

Table 1. Continued

Trial	Date	Study design	Treatment	Patients (n)	Median OS months (CI)	Hazard ratio OS (CI)	Median PFS months (CI)	Hazard Ratio PFS (CI)	ORR (CI)	CR n (%)	Median DOR in months (CI)
Patel (37)	2018	Phase I	Avelumab	161	6.5		1.5		17%	9	NR
					(4.8-9.5)[a]		(0-2.3)[a]		(11-24)[a]	(6%)	(42.1-NR)[a]
Powles (31)	2014	Phase I	Anti-PD-L1	67	NA		NA		26%	2	NA
										(3%)	
First-line											
Powles (55)	2021	Phase III	Pembrolizumab	351	17	0.86[7]	8.3	0.78[7]	54.7%†	53†	8.5†
KEYNOTE-361			plus chemotherapy		(15-20)[a]	(0.72-1.02)[a]	(7.5-8.5)[a]	(0.65-0.93)[a]	(49-60)[a]	(15%)	(8.2-11.4)[a]
			Pembrolizumab	307	15.6	0.92[8]	NA	NA	30.3%	34	28.2
					(12-18)[a]	(0.77-1.11)[a]			(25-36)[a]	(11%)	(13.5-NR)[a]
			Placebo plus	352	14.3	NA	7.1	NA	44.9%	43	6.2
			Chemotherapy		(12-17)[a]		(6.4-7.9)[a]		(40-50)[a]	(12%)	(5.8-6.5)[a]
Powles (45)	2020	Phase III	Durvalumab	346	13.2	0.99[9]	2.3	NA	26%†	27†	9.3†
DANUBE			monotherapy		(10-15)[a]	(0.83-1.17)[a]	(1.9-3.5)[a]			(8%)	(5.8-20.5)[a]
			Durvalumab plus	342	15.1	0.85[10]	3.7	NA	36%	27	11.1
			tremelimumab		(13-18)[a]	(0.72-1.02)[a]	(3.4-3.8)[a]			(8%)	(7.9-18.5)[a]
			Chemotherapy	344	12.1	NA	6.7	NA	49%	22	5.7
					(11-140)[a]		(5.7-7.3)[a]			(6%)	(5.6-6.2)[a]
Galsky (54)	2020	Phase III	Atezolizumab plus	451	16	0.83[11]	8.2	0.82**[11]	47%†	56†	8.5†
IMvigor130			chemotherapy		(14-19)[a]	(0.69-1.00)[a]	(6.5-8.3)[a]	(0.70-0.96)[a]	(43-52)[a]	(13%)	(7.2-10.4)[a]
			Atezolizumab	362	15.7	1.02[12]	NA	NA	23%	22	NR
			monotherapy		(13-18)[a]	(0.83-1.24)			(19-28)[a]	(6%)	(15.9-NR)[a]
			Placebo plus	400	13.4	NA	6.3	NA	44%	27	7.6
			chemotherapy		(12-15)[a]		(6.2-7.0)[a]		(39-49)[a]	(7%)	(6.3-8.5)[a]
Vuky (50)	2020	Phase II	Pembrolizumab		11.3		2.2		28.6%	33	30.1
KEYNOTE-052[13]					(9.7-13)[a]		(2.1-3.4)[a]		(24-34)[a]	(8.9%)	(18.1-NR)[a]
Balar (49)	2017	Phase II	Pembrolizumab	370	NA		2.0		24%	17	NR
KEYNOTE-052							(2-3)[a]		(20-29)[a]	(5%)	(9-NR)[a]
Balar (48)	2016	Phase II	Atezolizumab	119	15.9		2.7		23%	11	NR
IMvigor210[14]					(10-NR)[a]		(2.1-4.2)[a]		(16-31)[a]	(9%)	(14.1-NR)[a]

Table 1. Continued

Trial	Date	Study design	Treatment	Patients (n)	Median OS months (CI)	Hazard ratio OS (CI)	Median PFS months (CI)	Hazard Ratio PFS (CI)	ORR (CI)	CR n (%)	Median DOR in months (CI)
Maintenance											
Powles (61)	2020	Phase III	Avelumab	350	21.4	0.69**	3.7	0.62†	9.7%†	21†	NA
JAVELIN					(19-26)[a]	(0.56-0.86)[a]	(3.5-5.5)[a]	(0.52-0,.75)[a]	(6.8-13)[a]	(6%)	
Bladder 100			Best supportive	350	14.3		2.0		1.4%	3	NA
			care		(13-18)[a]		(1.9-2.7)[a]		(0.5-3.3)[a]	(0.9%)	
Galsky (60)	2020	Phase III	Pembrolizumab	55	22	0.91	5.4	0.65*	23%[15]†	5[9]†	NA
					(13-NR)[a]	(0.52-1.59)[a]	(3.1-7.3)[a]			(9%)	
			Placebo	53	18.7		3.0		10%[15]	0[9]	NA
					(11-NR)[a]		(2.7-5.5)[a]			(0%)	

Abbreviations: CI, confidence interval; OS, overall survival; PFS, progression-free survival; ORR, objective response rate; CR, complete response; DOR, duration of response; NR = not reached; NA = not available.
[1]Nivolumab 3 mg/kg, [2]nivolumab 3 mg/kg plus ipilimumab 1 mg/kg, [3]nivolumab 1 mg/kg plus ipilimumab 3 mg/kg. [4]The efficacy analysis was performed in the population of patients with a positive PD-L1 status (PD-L1 expression on at least 5% of tumor infiltrating immune cells). [5]Long term outcomes after a median follow-up of 28 months. [6]Results of cohort 2 of the IMvigor210 trial. [7]Pemrolizumab plus chemotherapy vs chemotherapy alone; differences are not statistically significant per the prespecified p-value boundary of 0.0142 for OS and 0.0019 for PFS. [8]Pembrolizumab alone vs chemotherapy alone. [9] Durvalumab alone vs chemotherapy. [10]Durvalumab plus tremelimumab vs chemotherapy. [11]Atezolizumab plus chemotherapy vs chemotherapy alone. [12]Atezolizumab alone vs chemotherapy alone. [13]Long term outcomes after a minimum follow-up of 2 years. [14]Results of cohort 1 of the IMvigor210 trial. [15]Patients with a complete radiographic response to first-line chemotherapy on study entry were not considered assessable for objective response with pembrolizumab or placebo.
[a] 95% CI, [b] range, [c] inter quartile range.
*Significance levels: * $p < 0.05$, ** $p < 0.01$, *** $p < 0.001$, †not reported*

PREDICTIVE BIOMARKERS USED IN CLINICAL PRACTICE

The studies listed in Table 1 clearly delineate the added value of ICIs in the treatment for patients with UC. Treatment with ICIs is generally well tolerated and some patients develop durable responses. These treatments are however challenged by limited initial response rates , specifically in the first- and second-line setting of mUC. Therefore, multiple studies assessed whether biomarkers can be used to improve selection of patients. Upfront identification of patients who will respond to treatment with ICIs can spare responders from more intensive (combination) treatment regimens and can prevent exposure to a potentially toxic and ineffective therapy in non-responders, thereby also reducing costs of care.

The most studied biomarker for patient selection is PD-L1 expression. Its predictive value in UC is however ambiguous, as portrayed in the studies described earlier. Potential explanations for these conflicting results include the use of different companion diagnostic assays (described in detail in Chapter 3 of this thesis), variable use of primary and metastatic tumor tissues, and varying previous exposure to (chemo)therapy. Currently, selection of patients based on PD-L1 expression is only required for first-line treatment with pembrolizumab and atezolizumab in cisplatin-ineligible patients. Another biomarker that is in use in current clinical practice is the tumor mutational burden (TMB). The FDA has approved high TMB (≥10 mutations/Mbp) as a pan-cancer biomarker for selection of previously treated patients with advanced solid tumors for treatment with pembrolizumab (75, 76). However, the predictive value of TMB for UC specifically, and for other ICIs and different treatment lines remains to be determined.

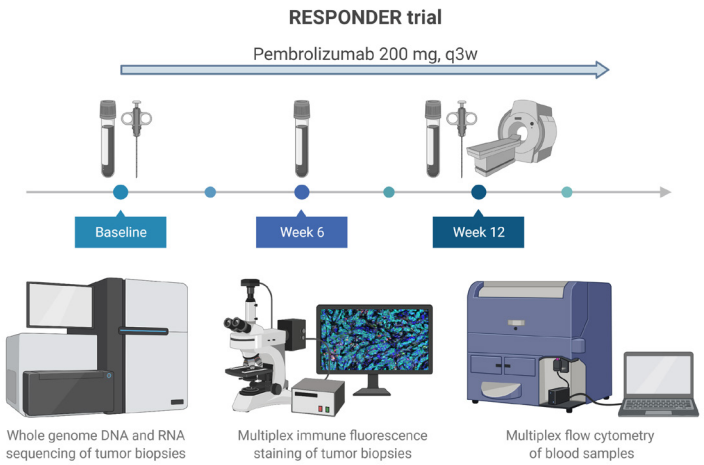

Figure 2. Design of the RESPONDER trial
Schematic overview of the study design, including timeline, sample collection, radiological imaging, and methods used for analysis of samples.

THE RESPONDER TRIAL – A CORE TRIAL TO THIS THESIS

Rationale
Introduction of ICIs has significantly improved treatment of patients with mUC, with durable responses in a selection of patients. However, the results from clinical trials on ICI efficacy in UC described in this chapter also raise questions:

- Why do some patients with UC not benefit from ICIs?
- Why are not all tumor responses durable?
- Why do some ICIs perform better than others, and why does this differ per treatment setting?
- Why does addition of chemotherapy to ICIs not improve patient outcomes?
- Why does PD-L1 expression not predict response to all ICIs at all stages of disease?
- How can we improve stratification of patients for treatment with ICIs?

These questions underscore the need for a biomarker that facilitates effective selection of patients with mUC for ICI therapy. In addition, more research into mechanisms of primary and acquired resistance to ICIs is needed. Together this may result in a more individualized treatment approach for patients with mUC, leading to improved patient outcomes, quality of life, and toxicity and cost-efficiency rates.

Objectives
Our first aim was to identify novel biomarkers associated with therapy response, with a specific focus on response to first- or second-line treatment with pembrolizumab in patients with mUC. Secondly, we aimed to obtain a better understanding of genomic, transcriptomic and immunophenotypic features that are associated with both sensitivity and resistance to pembrolizumab.

Design
A phase II prospective biomarker discovery study was initiated in multiple centers in the Netherlands (Figure 2). In total, 75 patients with mUC were included in this trial. Prior to and during treatment metastatic tumor biopsies and blood samples were collected. Fresh frozen biopsies were used for whole genome DNA and RNA sequencing analysis, and paired formalin-fixed paraffin-embedded biopsies were used for PD-L1 and multiplex immunofluorescence stainings. Blood samples were analyzed by multiparameter flowcytometry to determine numbers of immune cell populations and to study T cell phenotypes in detail. The resulting data were used to study differences between responders and non-responders to treatment, and to investigate dynamic changes in immune profiles during treatment.

THESIS CONTENT

A detailed overview of clinical trials (published before March 2017) on safety and efficacy of ICIs in patients with mUC is provided in **Chapter 2**.

In **Chapter 3** we performed an accurate comparison of four companion diagnostic assays and one research antibody for determination of PD-L1 expression in resection specimens of UC to study their interchangeability.

Chapter 4 describes the results of whole genome and whole transcriptome analysis of freshly obtained metastatic biopsies in a large cohort of patients with mUC. Genomic and transcriptomic subtypes of mUC are described and potential novel targets for (combination) therapy are suggested per transcriptomic subtype and for individual patients.

Immune profiling of sequential blood samples and tumor tissues was performed in **Chapter 5** to investigate whether temporal changes in T cell subsets in blood, and/or their density and location in tumor tissue were associated with efficacy of pembrolizumab in patients with mUC treated in the RESPONDER trial.

In **Chapter 6**, we aimed to identify a novel marker for stratification of patients with mUC by interrogating the entire genome and transcriptome of metastatic tumor biopsies from patients with mUC who were treated with pembrolizumab in the RESPONDER trial. With the intend to identify a blood-based immune marker for response to pembrolizumab, **Chapter 7** describes detailed flow cytometric assessment of 18 immune cell subsets in blood of patients with mUC who were treated with pembrolizumab in the RESPONDER trial.

Finally, **Chapter 8** summarizes the main findings of chapters 3 to 7 and discusses how these findings may affect future individualized ICI therapy for patients with mUC.

REFERENCES

1. Sung, H., et al., *Global Cancer Statistics 2020: GLOBOCAN Estimates of Incidence and Mortality Worldwide for 36 Cancers in 185 Countries.* CA: A Cancer Journal for Clinicians, 2021. **71**(3): p. 209-249.
2. Burger, M., et al., *Epidemiology and risk factors of urothelial bladder cancer.* Eur Urol, 2013. **63**(2): p. 234-41.
3. Freedman, N.D., et al., *Association between smoking and risk of bladder cancer among men and women.* Jama, 2011. **306**(7): p. 737-45.
4. Pashos, C.L., et al., *Bladder cancer: epidemiology, diagnosis, and management.* Cancer Pract, 2002. **10**(6): p. 311-22.
5. Peluchi, C., et al., *Mechanisms of disease: The epidemiology of bladder cancer.* Nat Clin Pract Urol, 2006. **3**(6): p. 327-40.
6. Chrouser, K., et al., *Bladder cancer risk following primary and adjuvant external beam radiation for prostate cancer.* J Urol, 2008. **179**(5 Suppl): p. S7-s11.
7. Kleinerman, R.A., et al., *Second primary cancer after treatment for cervical cancer. An international cancer registries study.* Cancer, 1995. **76**(3): p. 442-52.
8. Harper, H.L., et al., *Upper tract urothelial carcinomas: frequency of association with mismatch repair protein loss and lynch syndrome.* Mod Pathol, 2017. **30**(1): p. 146-156.
9. Liu, S., et al., *The impact of female gender on bladder cancer-specific death risk after radical cystectomy: a meta-analysis of 27,912 patients.* Int Urol Nephrol, 2015. **47**(6): p. 951-8.
10. Scosyrev, E., et al., *Sex and racial differences in bladder cancer presentation and mortality in the US.* Cancer, 2009. **115**(1): p. 68-74.
11. Kirkali, Z., et al., *Bladder cancer: epidemiology, staging and grading, and diagnosis.* Urology, 2005. **66**(6 Suppl 1): p. 4-34.
12. Soukup, V., et al., *Prognostic Performance and Reproducibility of the 1973 and 2004/2016 World Health Organization Grading Classification Systems in Non-muscle-invasive Bladder Cancer: A European Association of Urology Non-muscle Invasive Bladder Cancer Guidelines Panel Systematic Review.* Eur Urol, 2017. **72**(5): p. 801-813.
13. Witjes, J.A., et al., *European Association of Urology Guidelines on Muscle-invasive and Metastatic Bladder Cancer: Summary of the 2020 Guidelines.* Eur Urol, 2021. **79**(1): p. 82-104.
14. von der Maase, H., et al., *Long-term survival results of a randomized trial comparing gemcitabine plus cisplatin, with methotrexate, vinblastine, doxorubicin, plus cisplatin in patients with bladder cancer.* J Clin Oncol, 2005. **23**(21): p. 4602-8.
15. Böhle, A. and P.R. Bock, *Intravesical bacille Calmette-Guérin versus mitomycin C in superficial bladder cancer: formal meta-analysis of comparative studies on tumor progression.* Urology, 2004. **63**(4): p. 682-6; discussion 686-7.
16. Sylvester, R.J., et al., *Bacillus calmette-guerin versus chemotherapy for the intravesical treatment of patients with carcinoma in situ of the bladder: a meta-analysis of the published results of randomized clinical trials.* J Urol, 2005. **174**(1): p. 86-91; discussion 91-2.
17. Hall, M.C., et al., *Guideline for the management of nonmuscle invasive bladder cancer (stages Ta, T1, and Tis): 2007 update.* J Urol, 2007. **178**(6): p. 2314-30.
18. Bosschieter, J., et al., *Value of an Immediate Intravesical Instillation of Mitomycin C in Patients with Non-muscle-invasive Bladder Cancer: A Prospective Multicentre Randomised Study in 2243 patients.* Eur Urol, 2018. **73**(2): p. 226-232.
19. Sylvester, R.J., et al., *European Association of Urology (EAU) Prognostic Factor Risk Groups for Non-muscle-invasive Bladder Cancer (NMIBC) Incorporating the WHO 2004/2016 and WHO 1973 Classification Systems for Grade: An Update from the EAU NMIBC Guidelines Panel.* Eur Urol, 2021. **79**(4): p. 480-488.
20. *Neoadjuvant chemotherapy in invasive bladder cancer: a systematic review and meta-analysis.* Lancet, 2003. **361**(9373): p. 1927-34.
21. Meeks, J.J., et al., *A systematic review of neoadjuvant and adjuvant chemotherapy for muscle-invasive bladder cancer.* Eur Urol, 2012. **62**(3): p. 523-33.
22. Winquist, E., et al., *Neoadjuvant chemotherapy for transitional cell carcinoma of the bladder: a systematic review and meta-analysis.* J Urol, 2004. **171**(2 Pt 1): p. 561-9.
23. *Neoadjuvant chemotherapy in invasive bladder cancer: update of a systematic review and meta-analysis of individual patient data advanced bladder cancer (ABC) meta-analysis collaboration.* Eur Urol, 2005. **48**(2): p. 202-5; discussion 205-6.
24. Giacalone, N.J., et al., *Long-term Outcomes After Bladder-preserving Tri-modality Therapy for Patients with Muscle-invasive Bladder Cancer: An Updated Analysis of the Massachusetts General Hospital Experience.* Eur Urol, 2017. **71**(6): p. 952-960.
25. Efstathiou, J.A., et al., *Long-term outcomes of selective bladder preservation by combined-modality therapy for invasive bladder cancer: the MGH experience.* Eur Urol, 2012. **61**(4): p. 705-11.
26. Galsky, M.D., et al., *Treatment of patients with metastatic urothelial cancer "unfit" for Cisplatin-based chemotherapy.* J Clin Oncol, 2011. **29**(17): p. 2432-8.
27. Galsky, M.D., et al., *A consensus definition of patients with metastatic urothelial carcinoma who are unfit for cisplatin-based chemotherapy.* Lancet Oncol, 2011. **12**(3): p. 211-4.
28. De Santis, M., et al., *Randomized phase II/III trial assessing gemcitabine/carboplatin and methotrexate/carboplatin/vinblastine in patients with advanced urothelial cancer who are unfit for cisplatin-based chemotherapy: EORTC study 30986.* J Clin Oncol, 2012. **30**(2): p. 191-9.
29. Raggi, D., et al., *Second-line single-agent versus doublet chemotherapy as salvage therapy for metastatic urothelial cancer: a systematic review and meta-analysis.* Annals of Oncology, 2016. **27**(1): p. 49-61.

30. Couzin-Frankel, J., *Cancer Immunotherapy.* Science, 2013. **342**(6165): p. 1432-1433.
31. Powles, T., et al., *MPDL3280A (anti-PD-L1) treatment leads to clinical activity in metastatic bladder cancer.* Nature, 2014. **515**(7528): p. 558-562.
32. Sharma, P., et al., *Nivolumab monotherapy in recurrent metastatic urothelial carcinoma (CheckMate 032): a multicentre, open-label, two-stage, multi-arm, phase 1/2 trial.* Lancet Oncol, 2016. **17**(11): p. 1590-1598.
33. Massard, C., et al., *Safety and efficacy of durvalumab (MEDI4736), an anti-programmed cell death ligand-1 immune checkpoint inhibitor, in patients with advanced urothelial bladder cancer.* J Clin Oncol, 2016. **34**(26): p. 3119-3125.
34. Rosenberg, J.E., et al., *Atezolizumab in patients with locally advanced and metastatic urothelial carcinoma who have progressed following treatment with platinum-based chemotherapy: A single-arm, multicentre, phase 2 trial.* Lancet, 2016. **387**(10031): p. 1909-1920.
35. Sharma, P., et al., *Nivolumab in metastatic urothelial carcinoma after platinum therapy (CheckMate 275): a multicentre, single-arm, phase 2 trial.* Lancet Oncol, 2017. **18**(3): p. 312-322.
36. Plimack, E.R., et al., *Safety and activity of pembrolizumab in patients with locally advanced or metastatic urothelial cancer (KEYNOTE-012): a non-randomised, open-label, phase 1b study.* Lancet Oncol, 2017. **18**(2): p. 212-220.
37. Patel, M.R., et al., *Avelumab in metastatic urothelial carcinoma after platinum failure (JAVELIN Solid Tumor): pooled results from two expansion cohorts of an open-label, phase 1 trial.* Lancet Oncol, 2018. **19**(1): p. 51-64.
38. Powles, T., et al., *Efficacy and Safety of Durvalumab in Locally Advanced or Metastatic Urothelial Carcinoma: Updated Results From a Phase 1/2 Open-label Study.* JAMA Oncol, 2017. **3**(9): p. e172411.
39. Bellmunt, J., et al., *Pembrolizumab as Second-Line Therapy for Advanced Urothelial Carcinoma.* 2017.
40. Fradet, Y., et al., *Randomized phase III KEYNOTE-045 trial of pembrolizumab versus paclitaxel, docetaxel, or vinflunine in recurrent advanced urothelial cancer: results of > 2 years of follow-up.* Ann Oncol, 2019.
41. *Pembrolizumab als tweedelijns behandeling bij het urotheelcelcarcinoom.* Medische Oncologie, 2017(8): p. 43-46.
42. Powles, T., et al., *Atezolizumab versus chemotherapy in patients with platinum-treated locally advanced or metastatic urothelial carcinoma (IMvigor211): a multicentre, open-label, phase 3 randomised controlled trial.* Lancet, 2018. **391**(10122): p. 748-757.
43. van der Heijden, M.S., et al., *Atezolizumab Versus Chemotherapy in Patients with Platinum-treated Locally Advanced or Metastatic Urothelial Carcinoma: A Long-term Overall Survival and Safety Update from the Phase 3 IMvigor211 Clinical Trial.* Eur Urol, 2021. **80**(1): p. 7-11.
44. *Roche provides update on Tecentriq US indication in prior-platinum treated metastatic bladder cancer.* 2021 8 March, 2021; Available from: https://www.roche.com/media/releases/med-cor-2021-03-08.htm.
45. Powles, T., et al., *Durvalumab alone and durvalumab plus tremelimumab versus chemotherapy in previously untreated patients with unresectable, locally advanced or metastatic urothelial carcinoma (DANUBE): a randomised, open-label, multicentre, phase 3 trial.* Lancet Oncol, 2020. **21**(12): p. 1574-1588.
46. Kemp, A. *Voluntary withdrawal of Imfinzi indication in advanced bladder cancer in the US.* 2021 22 February, 2021; Available from: https://www.astrazeneca.com/content/astraz/media-centre/press-releases/2021/voluntary-withdrawal-imfinzi-us-bladder-indication.html.
47. Sharma, P., et al., *Nivolumab Alone and With Ipilimumab in Previously Treated Metastatic Urothelial Carcinoma: CheckMate 032 Nivolumab 1 mg/kg Plus Ipilimumab 3 mg/kg Expansion Cohort Results.* J Clin Oncol, 2019. **37**(19): p. 1608-1616.
48. Balar, A.V., et al., *Atezolizumab as first-line treatment in cisplatin-ineligible patients with locally advanced and metastatic urothelial carcinoma: a single-arm, multicentre, phase 2 trial.* Lancet, 2017. **389**(10064): p. 67-76.
49. Balar, A.V., et al., *First-line pembrolizumab in cisplatin-ineligible patients with locally advanced and unresectable or metastatic urothelial cancer (KEYNOTE-052): a multicentre, single-arm, phase 2 study.* Lancet Oncol, 2017. **18**(11): p. 1483-1492.
50. Vuky, J., et al., *Long-Term Outcomes in KEYNOTE-052: Phase II Study Investigating First-Line Pembrolizumab in Cisplatin-Ineligible Patients With Locally Advanced or Metastatic Urothelial Cancer.* J Clin Oncol, 2020. **38**(23): p. 2658-2666.
51. Suzman, D.L., et al., *FDA Approval Summary: Atezolizumab or Pembrolizumab for the Treatment of Patients with Advanced Urothelial Carcinoma Ineligible for Cisplatin-Containing Chemotherapy.* The oncologist, 2019. **24**(4): p. 563-569.
52. *FDA Alerts Health Care Professionals and Oncology Clinical Investigators about an Efficacy Issue Identified in Clinical Trials for Some Patients Taking Keytruda (pembrolizumab) or Tecentriq (atezolizumab) as Monotherapy to Treat Urothelial Cancer with Low Expression of PD-L1.* 2018 20-06-2018; Available from: https://www.fda.gov/Drugs/DrugSafety/ucm608075.htm.
53. *EMA restricts use of Keytruda and Tecentriq in bladder cancer.* 2018 01-06-2018; Available from: http://www.ema.europa.eu/ema/index.jsp?curl=pages/news_and_events/news/2018/05/news_detail_002964.jsp&mid=WC0b01ac058004d5c1.
54. Galsky, M.D., et al., *Atezolizumab with or without chemotherapy in metastatic urothelial cancer (IMvigor130): a multicentre, randomised, placebo-controlled phase 3 trial.* Lancet, 2020. **395**(10236): p. 1547-1557.
55. Powles, T., et al., *Pembrolizumab alone or combined with chemotherapy versus chemotherapy as first-line therapy for advanced urothelial carcinoma (KEYNOTE-361): a randomised, open-label, phase 3 trial.* Lancet Oncol, 2021. **22**(7): p. 931-945.
56. Grivas, P., et al., *Immune Checkpoint Inhibitors as Switch or Continuation Maintenance Therapy in Solid Tumors: Rationale and Current State.* Targeted Oncology, 2019. **14**(5): p. 505-525.
57. Sonpavde, G.P., et al., *Impact of the Number of Cycles of Platinum Based First Line Chemotherapy for Advanced Urothelial Carcinoma.* The Journal of urology, 2018. **200**(6): p. 1207-1214.

58. Galsky, M.D., et al., *Treatment patterns and outcomes in "real world" patients (pts) with metastatic urothelial cancer (UC).* Journal of Clinical Oncology, 2013. **31**(15_suppl): p. 4525-4525.
59. Flannery, K., et al., *Outcomes in patients with metastatic bladder cancer in the USA: a retrospective electronic medical record study.* Future Oncol, 2019. **15**(12): p. 1323-1334.
60. Galsky, M.D., et al., *Randomized Double-Blind Phase II Study of Maintenance Pembrolizumab Versus Placebo After First-Line Chemotherapy in Patients With Metastatic Urothelial Cancer.* J Clin Oncol, 2020. **38**(16): p. 1797-1806.
61. Powles, T., et al., *Avelumab Maintenance Therapy for Advanced or Metastatic Urothelial Carcinoma.* N Engl J Med, 2020. **383**(13): p. 1218-1230.
62. *FDA approves avelumab for urothelial carcinoma maintenance treatment.* 2020 01-07-2020; Available from: https://www.fda.gov/drugs/drug-approvals-and-databases/fda-approves-avelumab-urothelial-carcinoma-maintenance-treatment.
63. *New indication concerns the first-line maintenance treatment of adult patients with locally advanced or metastatic urothelial carcinoma.* 2020 17-12-2020; Available from: https://www.esmo.org/oncology-news/ema-recommends-extension-of-indications-for-avelumab2.
64. *Avelumab als onderhoudsbehandeling bij het urotheelcelcarcinoom van de urinewegen.* Medische Oncologie, 2021(3): p. 37-40.
65. Balar, A.V., et al., *Pembrolizumab monotherapy for the treatment of high-risk non-muscle-invasive bladder cancer unresponsive to BCG (KEYNOTE-057): an open-label, single-arm, multicentre, phase 2 study.* Lancet Oncol, 2021. **22**(7): p. 919-930.
66. *FDA approves pembrolizumab for BCG-unresponsive, high-risk non-muscle invasive bladder cancer.* 2020 01-08-2020; Available from: https://www.fda.gov/drugs/resources-information-approved-drugs/fda-approves-pembrolizumab-bcg-unresponsive-high-risk-non-muscle-invasive-bladder-cancer.
67. Necchi, A., et al., *Pembrolizumab as Neoadjuvant Therapy Before Radical Cystectomy in Patients With Muscle-Invasive Urothelial Bladder Carcinoma (PURE-01): An Open-Label, Single-Arm, Phase II Study.* J Clin Oncol, 2018. **36**(34): p. 3353-3360.
68. Powles, T., et al., *Clinical efficacy and biomarker analysis of neoadjuvant atezolizumab in operable urothelial carcinoma in the ABACUS trial.* Nat Med, 2019. **25**(11): p. 1706-1714.
69. van Dijk, N., et al., *Preoperative ipilimumab plus nivolumab in locoregionally advanced urothelial cancer: the NABUCO trial.* Nat Med, 2020. **26**(12): p. 1839-1844.
70. Gao, J., et al., *Neoadjuvant PD-L1 plus CTLA-4 blockade in patients with cisplatin-ineligible operable high-risk urothelial carcinoma.* Nat Med, 2020. **26**(12): p. 1845-1851.
71. Bajorin, D.F., et al., *Adjuvant Nivolumab versus Placebo in Muscle-Invasive Urothelial Carcinoma.* N Engl J Med, 2021. **384**(22): p. 2102-2114.
72. *FDA approves nivolumab for adjuvant treatment of urothelial carcinoma.* 2021 20-08-2021; Available from: https://www.fda.gov/drugs/resources-information-approved-drugs/fda-approves-nivolumab-adjuvant-treatment-urothelial-carcinoma.
73. Bellmunt, J., et al., *Adjuvant atezolizumab versus observation in muscle-invasive urothelial carcinoma (IMvigor010): a multicentre, open-label, randomised, phase 3 trial.* Lancet Oncol, 2021. **22**(4): p. 525-537.
74. Apolo, A.B., et al., *Alliance A031501: Phase III randomized adjuvant study of MK-3475 (pembrolizumab) in muscle-invasive and locally advanced urothelial carcinoma (MIBC) (AMBASSADOR) versus observation.* Journal of Clinical Oncology, 2019. **37**(7_suppl): p. TPS504-TPS504.
75. Marabelle, A., et al., *Association of tumour mutational burden with outcomes in patients with advanced solid tumours treated with pembrolizumab: prospective biomarker analysis of the multicohort, open-label, phase 2 KEYNOTE-158 study.* Lancet Oncol, 2020. **21**(10): p. 1353-1365.
76. *FDA approves pembrolizumab for adults and children with TMB-H solid tumors.* 2020 17-06-2020; Available from: https://www.fda.gov/drugs/drug-approvals-and-databases/fda-approves-pembrolizumab-adults-and-children-tmb-h-solid-tumors.

CHAPTER 2

Systematic review of immune checkpoint inhibition in urological cancers

Maud Rijnders
Ronald de Wit
Joost L. Boormans
Martijn P.J. Lolkema
Astrid A.M. van der Veldt

Published in European Urology, 2017 Sep;72(3):411-423

ABSTRACT

Context
In patients with advanced and metastatic urological cancers, clinical outcome may be improved by immune checkpoint inhibitors (ICIs).

Objective
To systematically review relevant literature on efficacy and safety of ICIs in patients with advanced and metastatic urothelial cancer (UC), renal cell cancer (RCC), and prostate cancer.

Evidence acquisition
Relevant databases, including Medline, Embase, and the Cochrane Library, were searched up to March 16, 2017. A narrative review of randomized clinical trials (RCTs) was performed.

Evidence synthesis
Six RCTs were included for the systematic review. In platinum-pretreated UC, efficacy of pembrolizumab was superior to chemotherapy, with longer median overall survival (OS; 10.3 vs 7.4 months), a higher objective response rate (ORR; 21.1% vs 11.4%; p = 0.001), and a lower adverse event rate (60.9% vs 90.2%). Three RCTs assessed the safety and efficacy of nivolumab in advanced RCC. The median OS (25.0 vs 19.6 months) and the ORR (25% vs 5%) were higher in patients treated with nivolumab compared with second-line everolimus. In all three studies, the safety profile of nivolumab was favorable. In patients with metastatic castration-resistant prostate cancer, two RCTs were identified, which did not show significant benefits for ipilimumab over placebo. In UC and RCC, there was no conclusive association between programmed cell death receptor ligand 1 (PD-L1) expression in tumor tissue and clinical outcome during pembrolizumab and nivolumab treatment, respectively.

Conclusion
In metastatic UC and RCC, pembrolizumab and nivolumab have superior efficacy and safety to second-line chemotherapy and everolimus, respectively. No beneficial effect of ipilimumab was observed in prostate cancer patients. PD-L1 expression status is currently not suitable as a predictive marker for treatment outcome.

Patient summary
Immune checkpoint inhibitors are able to reactivate the immune system against tumor cells. In second-line setting, pembrolizumab and nivolumab are safe and confer survival benefit in advanced urothelial cell and renal cell cancer, respectively.

INTRODUCTION

Immune checkpoint inhibitors (ICIs) have shown efficacy in the treatment of a variety of solid tumors, including advanced urological cancers (1). Historically, the treatment of urological malignancies included immune modulating agents. In high-risk non–muscle-invasive bladder cancer (NMIBC), adjuvant treatment with intravesical Bacille Calmette Guérin (BCG), a therapy that uses mycobacterial components to activate the immune system, provides a 32% risk reduction in recurrence compared with intravesical chemotherapy (2). In addition, 10–20% of patients with metastatic renal cell cancer (mRCC) experience durable responses upon treatment with high-dose interleukin-2 (3). The first commercially available autologous cell-based vaccination therapy, sipuleucel-T, was found to be effective in metastatic castration-resistant prostate cancer (mCRPC) (4). Although immune modulating therapies have shown efficacy in these specific cases, systemic treatment of advanced and metastatic urological cancers thus far mainly comprises chemotherapy (for urothelial cell cancer (UC) and prostate cancer (PC)), vascular endothelial growth factor (VEGF) pathway inhibitors (for mRCC), and androgen deprivation therapy (for PC).

Over the past 20 years, standard first-line treatment for advanced and metastatic UC has been cisplatin-based chemotherapy (5, 6). However, up to 50% of patients are unfit for cisplatin, mainly due to age-associated impaired renal function, cardiovascular comorbidities, and performance status (7). Furthermore, no effective second-line treatment is available for patients with disease progression after first-line chemotherapy. Single-agent chemotherapy (paclitaxel, docetaxel, or vinflunine) is commonly applied, but only 10% of patients experience a tumor response, and the median overall survival (OS) is around 7 months (8).

In contrast with UC, RCC is highly resistant to chemotherapy and, until the introduction of VEGF pathway inhibitors (eg, sunitinib and sorafenib) in 2005–2006, systemic treatment consisted of interferon-alpha and high-dose interleukin-2 (3). Although VEGF pathway inhibitors, together with mammalian target of rapamycin (mTOR) inhibitors (eg, everolimus), have significantly improved the perspectives of patients with mRCC (9), the median OS for patients with mRCC remains only 12.5 months after first-line targeted therapy (10).

In metastatic PC, androgen deprivation therapy is the backbone of treatment and frequently results in durable responses. Nevertheless, eventually all patients experience progression to mCRPC (11). For the treatment of mCRPC, chemotherapy (docetaxel (12) and cabazitaxel (13)), second-generation antiandrogens such as abiraterone (14) and enzalutamide (15), and radionuclides such as radium-223 (16) have been approved. These agents have improved the survival in patients with mCRPC; however, the median OS

seems to plateau at about 3 years (14, 15).

The current lack of efficacious treatment options for advanced UC, mRCC, and mCRPC underscores the clinical need for new well-tolerated treatment modalities that improve the outcome of patients with urological cancers. ICIs may expand the treatment armamentarium for patients with urological malignancies. Currently available ICIs include monoclonal antibodies that block the function of inhibitory receptors on T cells, resulting in a release of T-cell inhibition. Some tumors manage to escape immune surveillance by expressing the programmed cell death receptor ligand 1 (PD-L1) activating the inhibitory receptors on T cells and thereby preventing clearance by the immune system (17). Interference with this receptor–ligand interaction by ICIs reinvigorates the T-cell–mediated antitumor immune response (18, 19). Thus far, blocking antibodies against programmed cell death 1 (PD-1; eg, nivolumab and pembrolizumab), PD-L1 (eg, atezolizumab), and cytotoxic T-lymphocyte–associated protein 4 (CTLA-4; eg, ipilimumab) have been introduced in the clinic (Figure 1).

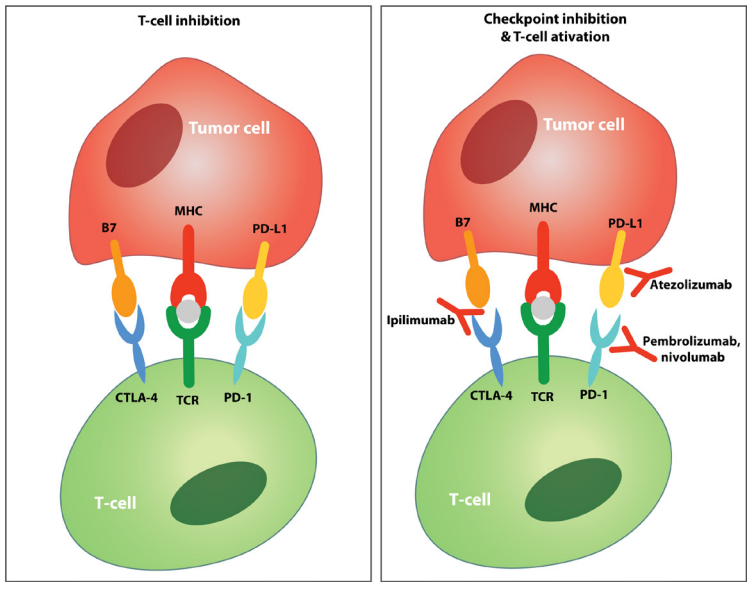

Figure 1. T-cell co-inhibitory receptor expression and checkpoint inhibition.
Tumor cells and antigen presenting cells (APCs) express a specific antigen that is presented to cytotoxic T-cells in a peptide major histocompatibility complex (MHC). T-cells recognize this presented antigen with their T-cell receptor (TCR) and, together with binding of co-stimulatory receptors (eg, CD28) this leads to T-cell activation and subsequently elimination of the (tumor) cell. Interaction of co-inhibitory receptors on T-cells with their ligands on APCs or tumor cells inhibits T-cell activation. Known co-inhibitory receptors are PD-1 (that interacts with its ligand PD-L1) and CTLA-4. Blocking antibodies against these co-inhibitory receptors or their ligands can prevent their interaction and the subsequent inhibition of T-cell activity. CTLA-4 = cytotoxic T lymphocyte–associated protein 4; PD-1 = programmed cell death 1; PD-L1 = programmed cell death receptor ligand 1.

The first hint of antitumor activity of ICIs in urological cancers came from phase I clinical trials, reporting durable responses in metastatic UC and RCC (19, 20). Since then, several pivotal clinical trials evaluating the efficacy of ICIs in urological cancers have been initiated. In this systematic review, we analyzed the efficacy and safety of ICIs in patients with advanced urological cancers, including UC, RCC, and PC.

EVIDENCE ACQUISITION

Search strategy

Up to March 16, 2017, an electronic search of the Medline, Embase, and Cochrane databases, and relevant websites (Web of Science and Google Scholar) was performed by an expert librarian. The search was conducted per Preferred Reporting Items for Systematic Reviews and Meta-Analyses (PRISMA) guidelines (Figure 2) (21). Search terms included the following: "urinary tract cancer, bladder cancer, kidney cancer, prostate cancer, immune checkpoint inhibitors, atezolizumab, avelumab, durvalumab, ipilimumab, nivolumab, pembrolizumab, tremelimumab, anti-PD1, anti-PD-L1, and anti-CTLA-4" (see Supplementary materials for details). The search was completed by manual screening of reference lists from included studies.

Inclusion criteria

The study population consisted of patients (>18 years of age), diagnosed with advanced or metastatic UC, RCC, or PC, who were treated with one of the ICIs targeting PD-1 (nivolumab and pembrolizumab), PD-L1 (atezolizumab, avelumab, and durvalumab), and CTLA-4 (ipilimumab and tremelimumab). The search was limited to studies executed in humans. No restrictions in publication date or language were imposed. During the systematic review process, only prospective, randomized, phase 1, 2, and 3 clinical trials were included, whereas nonrandomized clinical trials (non-RCTs), case reports, editorials, letters, review articles, and conference abstracts were excluded. If multiple analyses of the same clinical study were performed, the most recent or most relevant publication was selected. Primary outcome measures included OS, progression-free survival (PFS), and objective response rate (ORR) according to Response Evaluation Criteria in Solid Tumors (RECIST) (22). Secondary outcomes included adverse events (AEs) and efficacy analyses according to PD-L1 expression status in tumor tissue.

Data extraction

Two independent reviewers (M.R. and A.A.M.V.) assessed relevant articles for study eligibility, and any disagreement on inclusion was resolved by discussion. Using a standardized data extraction form, the following details were extracted: study design, number of patients, patient characteristics, treatment intervention, median duration

of follow-up, survival data, ORR, AEs, and PD-L1 expression status. Data were extracted from all included studies by one reviewer (M.R.) and subsequently checked by a second reviewer (A.A.M.V.) to ensure their accuracy.

Data analysis

Descriptive analyses were used to present the data. Continuous outcomes were described using mean and standard deviation, or alternatively, median and (interquartile) range. For categorical outcomes, frequencies and proportions were used. If reported, hazard ratios (HRs) with confidence intervals (CIs) were mentioned. Owing to the limited number of available studies, no quantitative analysis (ie, meta-analysis) could be performed.

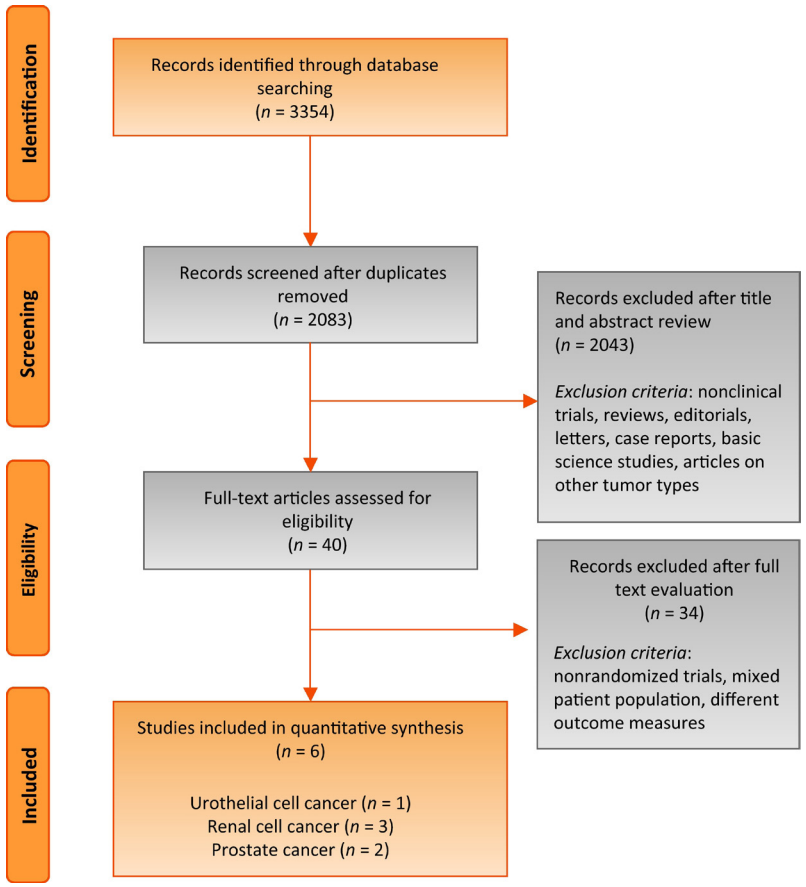

Figure 2. Evidence synthesis flowchart according to PRISMA.
PRISMA = Preferred Reporting Items for Systematic Reviews and Meta-Analyses.

EVIDENCE SYNTHESIS

Study selection

The initial literature search identified 3354 articles. After removing duplicate studies, one reviewer (M.R.) evaluated all titles and abstracts. Finally, 40 publications were identified as potentially relevant and were retrieved for full-text evaluation. According to the inclusion criteria, six randomized phase 1–3 clinical trials were selected for evidence synthesis (one trial on UC, three trials on RCC, and two trials on PC; Table 1). The literature search identified 16 additional non-RCTs addressing the safety and efficacy of ICIs in urological cancer (Supplementary Tables 1 and 2).

Characteristics, efficacy, and PD-L1 status in selected studies

The characteristics, efficacy measures, and PD-L1 status of the included studies are presented in Table 1, Table 2, and Table 3, respectively (see also Supplementary Table 3).

Urothelial cell cancer

For advanced UC, one RCT was identified in which 542 patients with disease progression after first-line platinum-based chemotherapy were randomized to receive pembrolizumab (200 mg intravenously every 3 weeks) or investigator's choice of chemotherapy (docetaxel, paclitaxel, or vinflunine) (23). Patients treated with pembrolizumab had significantly longer median OS than those treated with investigator's choice of chemotherapy (10.3 vs 7.4 months). Although there was no significant between-group difference for PFS (HR for disease progression or death 0.98; 95% CI, 0.81–1.19; p = 0.42), the estimated PFS rate at 12 months was higher for pembrolizumab-treated patients (16.8% vs 6.2%; no HR reported). The ORR was almost two-fold higher for the pembrolizumab group as compared with the chemotherapy group (21.1% vs 11.4%; p = 0.001). Among patients with a tumor response during pembrolizumab treatment, 7% had a complete response and 14.1% had a partial response. In the pembrolizumab group, the median duration of response was not reached, whereas the median response duration was 4.3 months in the chemotherapy group. PD-L1 expression was determined on pretreatment, mainly archival, tumor tissue. A combined positivity score was used, defined as the percentage of PD-L1 expressing tumor and tumor-infiltrating immune cells relative to the total number of tumor cells. Patients in all subgroups experienced benefit from pembrolizumab treatment irrespective of PD-L1 expression. In both pembrolizumab- and chemotherapy-treated patients, shorter OS was observed in those with high PD-L1 expression, defined as a combined positive score of ≥10%.

Renal cell cancer

For advanced RCC and mRCC, three RCTs evaluating the efficacy of nivolumab were identified, including two dose-controlled trials (phases 1b and 2) and one active

comparator-controlled phase 3 trial with everolimus. In these three trials, only clear cell histology was allowed and patients were mainly pretreated with antiangiogenic therapy. In the two dose-controlled trials, patients were randomized to nivolumab at a dose of 0.3, 2, or 10 mg/kg every 3 weeks. These phase 1b and 2 trials were different in patient population, design, and objectives. The phase 1b study demonstrated immune pharmacodynamic effects (eg, changes in circulating chemokines and tumor-associated lymphocytes) irrespective of dose (24), whereas the phase 2 study did not show a significant dose–response effect (25).

In the phase 3 trial, 821 patients with previously treated advanced RCC or mRCC were randomized to everolimus or nivolumab at a dosage of 3 mg/kg every 2 weeks (26). Nivolumab treatment was associated with significantly improved median OS (25.0 vs 19.6 months; HR 0.73; 98.5% CI, 0.57–0.93; p = 0.002). Although the ORR was significantly higher in the nivolumab group than in the everolimus group (25% vs 5%; odds ratio 5.98; 95% CI, 3.68–9.72; p < 0.001), there was no difference in PFS (4.6 vs 4.4 months; HR 0.88; 95% CI, 0.75–1.03; p = 0.11). Overall, eight out of 1080 (<1%) nivolumab-treated patients in the three RCTs (phases 1b, 2, and 3) had a complete response.

In the phase 2 and 3 trials with nivolumab, pretreatment tumor PD-L1 expression was determined as the percentage of PD-L1–positive tumor cells relative to the total number or tumor cells (25, 26). In the phase 2 dosing study, a beneficial effect of higher PD-L1 expression (≥5%) was observed, with a higher ORR and longer OS (25), whereas the phase 3 study showed shorter OS in nivolumab-treated patients with high PD-L1 expression (≥1%; 27.4 vs 21.8 months) (26).

Prostate cancer

For mCRPC, two RCTs were selected in which chemotherapy-naive (n = 602) and docetaxel-pretreated patients (n = 799) were randomized to ipilimumab or placebo (27, 28). In one study, single-dose bone-directed radiotherapy (8 Gy) was given prior to administration of ipilimumab or placebo (28). In both studies, ipilimumab failed to show survival benefit over placebo. However, there was a trend toward improved PFS and a prostate-specific antigen response in ipilimumab-treated patients (27, 28), suggesting some efficacy.

Safety of ICIs in urological cancer

AEs reported in the selected randomized studies are presented in Table 4.

Urothelial cell cancer

Compared with patients with UC treated with chemotherapy, patients treated with pembrolizumab experienced fewer AEs (90.2% vs 60.9% AEs of any grade) (23). In addition,

the incidence of grade 3–4 AEs was more than three times higher in chemotherapy-treated patients. In pembrolizumab-treated patients, grade 3–4 immune-related AEs were observed in 4.5% of the patients, including pneumonitis, colitis, and nephritis. In both treatment groups, four treatment-related AEs resulted in patient death. Treatment-related deaths in the pembrolizumab group resulted from pneumonitis (n = 1), urinary tract obstruction (n = 1), malignant neoplasm progression (n = 1), and unspecified cause (n = 1).

Renal cell cancer

In patients with mRCC treated with nivolumab, fewer treatment-related AEs were reported compared with those in patients in the everolimus group (79% vs 88%) (26). In nivolumab-treated patients, the most common grade 3–4 AEs were fatigue, nausea, and diarrhea. Overall, the incidence of immune-related AEs was limited. In the phase 2 study, there was no association between nivolumab dosage and the number of AEs (25).

Prostate cancer

In the RCT without radiotherapy, the incidence of grade 3–4 AEs in patients with mCRPC treated with ipilimumab was approximately 40%, including 31% grade 3–4 immune-related AEs and nine (2%) treatment-related deaths (27). The most frequently reported AEs included diarrhea (15%), rash (3%), and fatigue (3%). In the RCT with single-dose radiotherapy, grade 3–4 immune-related AEs were reported both in the ipilimumab and in the placebo group (26% vs 11%) (28).

Table 1. Characteristics of randomized clinical trials on immune checkpoint inhibitors in urological cancer.

	Trial	Study design	Population	Patients (n)	Histology subgroups	Line	Previous therapy	Experimental arm	Comparator
Urothelial cell cancer									
Bellmunt 2017 (23)	Keynote-045 (NCT02256436)	Phase 3	Advanced UC	542	Pembrolizumab 68.9% and chemotherapy 73.0% pure transition-cell features	2nd	Platinum-based chemotherapy	200 mg pembrolizumab IV, every 3 weeks	Investigator's choice chemotherapy
Renal cell cancer									
Motzer 2015 (26)	CheckMate 025 (NCT01668784)	Phase 3	Advanced or metastatic RCC	821	100% clear cell RCC	2nd	Anti-angiogenic therapy	3 mg/kg nivolumab IV, every 2 weeks	10 mg everolimus, orally, once daily
Motzer 2015 (25)	NCT01354431	Phase 2	Metastatic RCC	168	100% clear cell RCC	2nd	Anti-angiogenic therapy	0.3, 2 or 10 mg/kg nivolumab IV, every 3 weeks	Other experimental arms
Choueiri 2016 (24)	NCT01358721	Phase 1b	Metastatic RCC	91	100% clear cell RCC	1st,2nd	Systemic therapy, not specified	0.3, 2 or 10 mg/kg nivolumab, every 3 weeks[a]	Other experimental arms
Prostate cancer									
Beer 2017 (27)	NCT01057810	Phase 3	Metastatic CRPC	602	NA	2nd	Anti-androgenic therapy, no chemotherapy for mCRPC	10 mg/kg ipilimumab IV, every 3 weeks for up to 4 doses, followed by maintenance treatment every 12 weeks	Placebo IV, every 3 weeks for up to 4 doses, followed by maintenance treatment every 12 weeks
Kwon 2014 (28)	NCT00861614	Phase 3	Metastatic CRPC	799	Adenocarcinoma	2nd	Anti-androgenic therapy, docetaxel-based chemotherapy for mCRPC	Single-dose bone-directed radiotherapy (8 Gy) followed by 10 mg/kg ipilimumab IV, every 3 weeks for up to 4 doses	Single-dose bone-directed radiotherapy (8 Gy) followed by placebo IV, every 3 weeks for up to 4 doses

UC, urothelial cancer; RCC, renal cell cancer; CRPC, castration resistant prostate cancer; mCRPC, metastatic castration resistant prostate cancer; NA, not available; IV, intravenously; [a] Previously treated population is subdivided in 3 dosage subgroups of 0.3, 2 or 10 mg/kg nivolumab, all treatment-naive patients received 10 mg/kg nivolumab.

Table 2. Efficacy of immune checkpoint inhibitors in randomized clinical trials in urological cancer.

	Treatment	Patients (n)	Median follow up in months (CI)[c,d]	Median OS months (CI)[a,b]	Median PFS months (CI)[a,b]	ORR (CI)[a,b]	CR	PR	SD	PD	NE	Median duration of response in months (CI)[b,c]	Other
Urothelial cell cancer													
Bellmunt 2017 (23)	Pembrolizumab 200 mg	270	14.1 (9.9-22.1)[c]	10.3 (8.0-11.8)[a]	2.1 (2.0-2.2)[a]	21.1% (16.4-26.5)[a]	19 (7%)	38 (14.1%)	47 (17.4%)	131 (48.5%)	35 (13.0%)	NR (1.6+ to 15.6+)[c]	
	Chemotherapy	272	14.1 (9.9-22.1)[c]	7.4 (6.1-8.3)[a]	3.3 (2.3-3.5)[a]	11.4% (7.9-15.8)[a]	9 (3.3%)	22 (8.1%)	91 (33.5%)	90 (33.1%)	60 (22.1%)	4.3 (1.4+ to 15.4+)[c]	
Renal cell cancer													
Motzer 2015 (26)	Nivolumab 3 mg/kg	410	NA	25.0 (21.8-NR)[a]	4.6 (3.7-5.4)[a]	25%	4 (1%)	99 (24%)	141 (34%)	143 (35%)	23 (6%)	12.0 (0 to 27.6)[c]	
	Everolimus 10 mg	411	NA	19.6 (17.6-23.1)[a]	4.4 (3.7-5.5)[a]	5%	2 (1%)	20 (5%)	227 (55%)	114 (28%)	48 (12%)	12.0 (0 to 22.2)[c]	
Motzer 2015 (25)	Nivolumab 0.3 mg/kg	60	NA	18.2 (16.2-24.0)[b]	2.7 (1.9-3.0)[b]	20% (13.4-28.2)[b]	1 (2%)	11 (18%)	22 (37%)	24 (40%)	2 (3%)	NR (NR to NR)[b]	
	Nivolumab 2 mg/kg	54	NA	25.5 (19.8-28.8)[b]	4.0 (2.8-4.2)[b]	22% (15.0-31.1)[b]	1 (2%)	11 (20%)	23 (43%)	18 (33%)	1 (2%)	NR (4.2 to NR)[b]	
	Nivolumab 10mg/kg	54	NA	24.7 (15.3-26.0)[b]	4.2 (2.8-5.5)[b]	20% (13.4-29.1)[b]	0 (0%)	11 (20%)	24 (44%)	17 (32%)	2 (4%)	22.3 (4.8 to NR)[b]	
Choueiri 2016 (24)	All patients	91	NA	NA	NA	15% (8.7-24.5)[a]	2 (2%)	12 (13%)	42 (46%)	27 (30%)	8 (9%)	NA	
Previously treated group	Nivolumab 0.3 mg/kg	22	NA	16.4 (10.1-NR)[a]	NA	9% (1.1-29.2)[a]	0 (0%)	2 (9%)	8 (36%)	9 (41%)	3 (14%)	NA	
	Nivolumab 2 mg/kg	22	NA	NR	NA	18% (5.2-40.3)[a]	0 (0%)	4 (18%)	10 (46%)	5 (23%)	3 (14%)	NA	
	Nivolumab 10 mg/kg	23	NA	25.2 (12.0-NR)[a]	NA	22% (7.5-43.7)[a]	0 (0%)	5 (22%)	11 (48%)	6 (26%)	1 (4%)	NA	
Treatment naive group	Nivolumab 10 mg/kg	24	NA	NR	NA	13% (2.7-32.4)[a]	2 (8%)	1 (4%)	13 (54%)	7 (29%)	1 (4%)	NA	
Prostate cancer													**PSA RR (CI)[a]**
Beer 2017 (27)	Ipilimumab	400	24-48	28.7 (24.5-32.5)[a]	5.6 (5.3-6.3)[a]	NA	NA	NA	NA	NA	NA	NA	23% (19-27)[a]
	Placebo	202	24-48	29.7 (26.1-34.2)[a]	3.8 (2.8-4.1)[a]	NA	NA	NA	NA	NA	NA	NA	8% (5-13)[a]
Kwon 2014 (28)	Radiotherapy with ipilimumab	399	9.9 (4.3-16.7)[d]	11.2 (9.5- 12.7)[a]	4.0 (3.6-4.3)[a]	NA	NA	NA	NA	NA	NA	NA	13.1% (9.5-17.5)[a]
	Radiotherapy with placebo	400	9.3 (5.4-14.6)[d]	10.0 (8.3-11.0)[a]	3.1 (2.9-3.4)[a]	NA	NA	NA	NA	NA	NA	NA	5.2% (3.0-8.4)[a]

OS, overall survival; PFS, progression free survival; ORR, objective response rate; CR, complete response; PR, partial response; SD, stable disease; PD, progressive disease; NE, not evaluable; PSA RR, PSA response rate; NA, not available; NR, not reached; [a] 95% CI; [b] 80% CI; [c] range; [d] interquartile range.

Table 3. Efficacy of immune checkpoint inhibitors in randomized clinical trials in urological cancer according to tumor PD-L1 expression status.

Study	Assessment of PD-L1 expression	Treatment	PD-L1 expression	Patients (n)	Median OS in months (95% CI)	Median PFS in months (95% CI)	ORR (95% CI)	CR	PR	SD	PD	NE
Urothelial cell cancer												
Bellmunt 2017 (23)	Combined positive score of tumor cells and tumor infiltrating immune cells	Pembrolizumab	All patients	270	10.3 (8.0-11.8)	2.1 (2.0-2.2)	21.1% (16.4-26.5)	19 (7%)	38 (14.1%)	47 (17.4%)	131 (48.5%)	35 (13.0%)
			PD-L1 ≥10%	74	8.0 (5.0-12.3)	NA	21.6% (12.9-32.7)	5 (6.8%)	11 (14.9%)	9 (12.2%)	37 (50%)	12 (16.2%)
		Chemotherapy	All patients	272	7.4 (6.1-8.3)	3.3 (2.3-3.5)	11.4% (7.9-15.8)	9 (3.3%)	22 (8.1%)	91 (33.5%)	90 (33.1%)	60 (22.1%)
			PD-L1 ≥10%	90	5.2 (4.0-7.4)	NA	6.7 (2.5-13.9)	2 (2.2%)	4 (4.4%)	35 (35.6%)	38 (31.1%)	24 (26.7%)
Renal cell cancer												
Motzer 2015 (26)	Tumor membrane expression	Nivolumab	PD-L1 <1%	276	27.4 (21.4-NR)	NA	NA	NA	NA	NA	NA	NA
			PD-L1 ≥1%	94	21.8 (16.5-28.1)	NA	NA	NA	NA	NA	NA	NA
			PD-L1 <5%	326	24.6 (21.4-NR)	NA	NA	NA	NA	NA	NA	NA
			PD-L1 ≥5%	44	21.9 (14.0-NR)	NA	NA	NA	NA	NA	NA	NA
		Everolimus	PD-L1 <1%	299	21.2 (17.7-26.2)	NA	NA	NA	NA	NA	NA	NA
			PD-L1 ≥1%	87	18.8 (11.9-19.9)	NA	NA	NA	NA	NA	NA	NA
			PD-L1 <5%	345	20.0 (17.7-24.7)	NA	NA	NA	NA	NA	NA	NA
			PD-L1 ≥5%	41	18.1 (10.3-NR)	NA	NA	NA	NA	NA	NA	NA
Motzer 2015 (25)	Tumor membrane expression	Nivolumab	≥1 or <5%	78	18.2 (12.7-26.0)	2.9 (2.1-4.2)	18% (10.2-28.3)	NA	NA	NA	NA	NA
		Nivolumab	≥5%	29	NR (13.4-NR)	4.9 (1.4-7.8)	31% (15.3-50.8)	NA	NA	NA	NA	NA
Choueiri 2016 (24)	Not determined											

OS, overall survival; PFS, progression free survival; ORR, objective response rate; CR, complete response; PR, partial response; SD, stable disease; PD, progressive disease; NE, not evaluable; NA, not available; NR, not reached.

Table 4. Treatment-related adverse events in randomized clinical trials on immune checkpoint inhibitors in urological cancer.

	Treatment	Patients (n)	Any grade AEs	Grade 3-4 AEs	Types of grade 3-4 AEs	Grade 3-4 IR AEs	Types of grade 3-4 IR AEs	AEs leading to discontinuation[a]	AEs leading to death[b]
Urothelial cell cancer									
Bellmunt 2017 (23)	Pembrolizumab	270	162 (61%)	40 (15%)	Fatigue (1.1%), diarrhea (1.1%), anemia (0.8%), nausea (0.4%), asthenia (0.4%), decreased neutrophil count (0.4%)	12 (4.5%)	Pneumonitis (2.3%), colitis (1.1%), nephritis (0.8%), severe skin reaction (0.4%), adrenal insufficiency (0.4%)	12 (4.5%)	4 (1.5%)
	Chemotherapy	272	230 (90%)	126 (49%)	Neutropenia (13.3%), decreased neutrophil count (12.2%), anemia (7.8%), fatigue (4.3%), constipation (3.1%), asthenia (2.7%), peripheral sensory neuropathy (2.0%), nausea (1.6%), decreased appetite (1.2%), diarrhea (0.8%), peripheral neuropathy (0.8%), alopecia (0.8%) pruritus (0.4%)	4 (1.6%)	Severe skin reaction (1.2%), myositis (0.4%)	28 (11%)	4 (1.6%)
Renal cell cancer									
Motzer 2015 (26)	Nivolumab	406	319 (79%)	76 (19%)	Fatigue (2%), anemia (2%), diarrhea (1%), dyspnea (1%), pneumonitis (1%), hyperglycemia (1%), decreased appetite (<1%), rash (<1%), nausea (<1%)	NA	NA	31 (8%)	0
	Everolimus	397	349 (88%)	145 (37%)	Anemia (8%), hypertriglyceridemia (5%), hyperglycemia (4%), stomatitis (4%), fatigue (3%), pneumonitis (3%), mucosal inflammation (3%), nausea (1%), diarrhea (1%), decreased appetite (1%), rash (1%), dyspnea (1%), peripheral edema (1%)	NA	NA	52 (13%)	2
Motzer 2015 (25)	Nivolumab 0.3 mg/kg	59	44 (75%)	3 (5%)	Nausea (2%)	NA	Increased AST (2%), increased ALT (2%)	1 (2%)	0
	Nivolumab 2 mg/kg	54	36 (67%)	9 (17%)	Nausea (2%), pruritus (2%)	NA	Pruritus (2%), hypothyroidism (2%), gastrointestinal (2%), increased AST (2%), increased ALT (2%)	6 (11%)	0
	Nivolumab 10mg/kg	54	42 (78%)	7 (13%)	Arthralgia (2%)	NA	0	4 (7%)	0

Table 4. Continued

	Treatment	Patients (n)	Any grade AEs	Grade 3-4 AEs	Types of grade 3-4 AEs	Grade 3-4 IR AEs	Types of grade 3-4 IR AEs	AEs leading to discontinuation[a]	AEs leading to death[b]
Choueri 2016 (24)	Nivolumab 0.3 mg/kg	22	22 (100%)	15 (68%)	Constipation (5%), increased AST (5%), increased ALT (5%), acute renal failure (5%), pneumonitis (5%)	0	0	NA	NA
	Nivolumab 2 mg/kg	22	22 (100%)	8 (36%)	Fatigue (9%), constipation (5%)	0	0	NA	NA
	Nivolumab 10 mg/kg	23	23 (100%)	13 (57%)	Increased AST (9%), colitis (4%), diarrhea (4%), increased ALT (4%), increased blood bilirubin (4%), acute renal failure (4%), pneumonitis (4%), skin (4%)	1 (4%)	Skin (4%)	NA	NA
Treatment naive	Nivolumab 10 mg/kg	24	24 (100%)	12 (50%)	Colitis (8%), fatigue (4%), diarrhea (4%), endocrine (4%), hypersensitivity/infusion reaction (4%), infusion-related reaction (4%)	0	0	NA	NA
Prostate cancer									
Beer 2017 (27)	Ipilimumab	399	325 (82%)	158 (40%)	Diarrhea (15%), rash (3%), fatigue (3%), nausea (2%), decreased appetite (1%), vomiting (1%) pruritus (<1%)	125 (31%)	NA	114 (29%)	9 (2%)
	Placebo	199	98 (49%)	11 (6%)	Fatigue (1%), pruritus (<1%)	3 (2%)	NA	5 (3%)	0
Kwon 2014 (28)	RTx followed by ipilimumab	393	295 (75%)	NA	NA	101 (26%)	NA		4 (1%)
	RTx followed by placebo	396	180 (45%)	NA	NA	11 (3%)	NA		0

AEs, adverse events; IR AE, immune related adverse event; NA, not available; AST, aspartate aminotransferase; ALT, alanine aminotransferase; NA, not available; [a] Treatment related events of any grade leading to treatment discontinuation; [b] Treatment related events of any grade leading to patient death.

DISCUSSION

Principal findings

Although UC and RCC have totally different tumor characteristics, varying from a high mutational load in UC (29) to high vascularization and chemotherapy resistance in RCC (3), immune modulating therapies have a great potential in at least a subgroup of both populations. In patients with advanced UC and RCC, the ICIs pembrolizumab and nivolumab, respectively, have shown proven efficacy as evidenced by survival improvement, as well as a favorable AE profile in randomized comparator controlled trials, thereby changing treatment paradigms in second-line treatment. Immune checkpoint blockade with the anti-CTLA-4 antibody ipilimumab, though, did not show survival benefit combined with a relatively high risk of toxicity in patients with mCRPC.

Efficacy and future perspectives

Urothelial cell cancer

The success of ICIs in UC is likely associated with its high mutational load (29), thereby potentially sensitizing UC to immune checkpoint blockade (30). Based on an almost 3 month OS benefit (23), the U.S. Food and Drug Administration (FDA) has lent priority review for pembrolizumab as second-line treatment of UC, and the file has also been submitted to the European Medicine Agency. Previous phase 2 clinical trials have already resulted in FDA approval of atezolizumab and nivolumab for second-line therapy of UC (Supplementary Tables 1 and 2) (31, 32). Meanwhile, after obtaining approval in second-line treatment of UC, ICIs are currently moving towards earlier treatment lines and disease stages.

In a recent phase 2 study, cisplatin-ineligible patients with advanced UC were treated with first-line atezolizumab (1200 mg intravenously every 3 weeks), resulting in an ORR of 23% (9% complete response rate) and median OS of 15.9 months (Supplementary Tables 1 and 2) (30). Similar results from a phase 2 study with pembrolizumab showed a comparable ORR in this patient population (33). Since the median OS in patients unfit for cisplatin, who receive mostly carboplatin–gemcitabine as first-line chemotherapy, is around 9 months at best (34), the extrapolated median OS of more than 12 months in these studies seem encouraging for ICIs, having prompted applications for the additional indication as first-line treatment in the frail cisplatin-unfit patient population. In addition, several phase 3 studies are currently evaluating the efficacy of ICIs as first-line treatment in cisplatin-eligible patients. In several ongoing first-line RCTs, immune checkpoint blockade (monotherapy, in combination with platinum-based chemotherapy, or combination of anti-PD-1 and anti-CTLA-4) is compared with conventional platinum-based chemotherapy (35, 36). Likewise, studies addressing the use of ICIs in the adjuvant setting are in progress in patients at high risk for disease progression following radical

cystectomy (35). BCG-unresponsive high-risk NMIBC has high recurrence rates and also a significant risk of progression to muscle-invasive disease. At present, radical cystectomy is the only available treatment option for BCG-unresponsive NMIBC (37). The use of ICIs as a treatment strategy and potential means to avoid bladder cancer surgery would be of great potential. This is further supported by the observation that PD-L1 expression seems to be higher following BCG treatment (38) and that, like in muscle-invasive disease, a high mutational load is present in BCG-unresponsive NMIBC (39). An ongoing international multicenter phase II clinical trial explores the efficacy of pembrolizumab in BCG-unresponsive NMIBC (35).

Renal cell cancer

With an almost 6 months OS benefit (26), nivolumab has been approved by the FDA, thereby replacing everolimus as second-line treatment of advanced clear cell RCC. Cost per responder analysis of the CheckMate025 trial showed that nivolumab is also cost effective compared with everolimus, with a monthly cost per responder of $54 315 for nivolumab compared with $224 711 for everolimus (40). However, large studies on the efficacy of ICIs for non-clear cell RCC are still lacking. Furthermore, the place of nivolumab as second-line treatment of clear cell RCC is currently shared with cabozantinib, since this tyrosine kinase inhibitor has been approved more recently as another second-line treatment option (41, 42).

In resemblance with UC, immune checkpoint blockade is also moving toward earlier treatment lines and disease stages of RCC, including the neoadjuvant and adjuvant settings. Current clinical trials mainly focus on several combination strategies, including the combination nivolumab–ipilimumab (35). From an historical perspective, combining immune checkpoint blockade with antiangiogenic therapy is a logical step in the treatment of RCC. It has been shown that bevacizumab increases the migration of cytotoxic T cells into RCC, thereby potentially enhancing the local immune response induced by atezolizumab (43). At present, several clinical trials have been initiated in which ICIs are combined with the monoclonal antibody bevacizumab or a tyrosine kinase inhibitor such as axitinib (35).

Prostate cancer

In contrast with UC and RCC, data on the efficacy of ICIs in mCRPC are limited. Although the phase 3 trials did not show benefit for ipilimumab in patients with mCRPC (27, 28), immune checkpoint blockade may still play a role in a subset of patients with mCRPC. In patients with mCRPC who are enzalutamide-resistant, early phase 2 studies have shown efficacy of pembrolizumab when added to enzalutamide (44). The survival benefit conferred by sipuleucel-T also indicates that immunotherapy-boosting T-cell activity can exert effects in patients with PC (4). In order to enhance T-cell activity in mCRPC, several combination strategies are currently under development, including ICIs combined with anticancer vaccination, PARP inhibition, radium-223, chemotherapy, or enzalutamide (35).

Tumor PD-L1 expression as a predictive marker for efficacy

Overall, the results on the value of PD-L1 expression in UC and RCC are somewhat conflicting. In the phase 3 trial in patients with advanced UC, the beneficial effect of pembrolizumab over chemotherapy was observed irrespective of PD-L1 expression, which is underscored by the results of previous phase 2 trials with either atezolizumab or nivolumab as second-line treatment in UC (31, 32). However, high PD-L1 expression, defined as a combined positive score of ≥10%, was associated with shorter OS in both chemotherapy- and pembrolizumab-treated patients with UC (23). In advanced RCC, high PD-L1 expression (≥1%), determined as the percentage of PD-L1–positive tumor cells relative to the total number of tumor cells, was also associated with an unfavorable outcome in both nivolumab- and everolimus-treated patients. These findings suggest that higher PD-L1 expression may be associated with more aggressive tumor behavior (38) and may be a prognostic instead of a predictive marker.

Conflicting results on PD-L1 status in different studies may be related to different targets of the administered agents (PD-1 and PD-L1) and different methods to determine PD-L1 expression including differences in assays, measurements, definition of PD-L1 expression (tumor cells, tumor-infiltrating immune cells, or combined), semiquantitative analyses, and cutoffs. In addition, archival tissue from primary tumors, often collected years prior to metastatic disease, was mostly used to determine PD-L1 expression, whereas PD-L1 expression is a dynamic marker that may change during several disease stages and sequential therapies. To better understand PD-L1 dynamics, future studies will focus on fresh biopsies from metastatic lesions sequentially obtained during treatment with ICIs. In clinical practice, tools are needed to select patients for immune checkpoint blockade. In particular, stratification for combination strategies is required, as a number of patients have already benefited from monotherapy and may not benefit from an additional therapy with regard to antitumor effect and higher risk of toxicity. Alternative tools to stratify patients may include genomic subtype, interferon-γ gene expression signature, chemokine expression signature, and mutational load. In addition, positron emission tomography (PET) using 89Zr-labeled ICIs may be valuable, as this noninvasive technique enables drug uptake measurements in tumors, thereby revealing intertumor heterogeneity (45). Future studies will show whether PET using 89Zr-labeled ICIs may be useful to select patients for treatment with ICIs.

Safety

In UC and RCC, anti-PD-1 therapy with pembrolizumab and nivolumab, respectively, was associated not only with fewer AEs (23, 26), but also with better quality of life than the comparator treatment, that is, chemotherapy and everolimus, respectively (46, 47). However, ipilimumab was associated with a high risk of grade 3–4 toxicity in approximately 40% of patients with mCRPC (28), which is specifically associated with inhibition of CTLA-4 signaling. Although blockade of PD-1 and PD-L1 signaling is associated with less toxicity, awareness and expertise for immune-related toxicity such as colitis, endocrinopathies (eg, hypothyroidism, type 1 diabetes), nephritis, and pneumonitis are required as immune-related toxicities can develop rapidly and severely, and, although rare, can even be fatal. In addition, immune-related toxicities can even develop after discontinuation of treatment. Early recognition and treatment are necessary, as these toxicities can be treated adequately with immune-suppressive agents, including high-dose steroids, tumor necrosis factor-alpha blockers (eg, infliximab), and, in case of endocrinopathies, hormone replacement therapy (48). Although combination strategies with ICIs may enhance efficacy, they are also associated with a higher risk of toxicity.

In rare cases, rapid disease progression is observed after the initiation of ICIs, indicating that ICIs may be harmful for some patients. Hyperprogressive disease during ICIs develops independently of tumor histology and is associated with a poorer OS. So far, no predictive markers for hyperprogressive disease have been identified (49).

For optimal patient selection and counseling, there is a need for tools to identify patients with a high risk of severe toxicity. Since antitumor activity of ICIs has also been observed at low dosages (25) and may even last after early discontinuation of treatment, further optimization of dosage and administration schedules is required, potentially reducing toxicity and costs. To reduce the economic burden of ICIs, future studies should focus on the optimal treatment duration, value of treatment beyond disease progression (50), and development of predictive tools for both tumor response and toxicity.

Strengths and limitations of review

The strengths of this review are the prespecified and systematic literature search, selecting only published RCTs. As a result, only high-quality studies were selected. However, an important limitation is the lack of unpublished results from other phase 3 studies. To overcome this limitation, potential landmark studies, which are not published yet, are mentioned in the Discussion section. In addition, early phase 1 and 2 studies, including those potentially leading to FDA approval, and phase 3 studies are mentioned in the Discussion section and presented in Supplementary Tables 1 and 2.

CONCLUSIONS

In conclusion, ICIs show superior efficacy and safety outcomes compared with conventional second-line treatment in patients with advanced UC and RCC. To date, treatment paradigms with ICIs have not shown clinical benefit in patients with mCRPC. Ongoing studies, also assessing novel combination strategies with ICIs, may further enhance efficacy in earlier treatment lines and disease stages of urological cancers. Since PD-L1 expression thus far seems to be inconclusive as a predictive marker, future research needs to focus on alternative markers.

2

REFERENCES

1. Carosella ED, Ploussard G, LeMaoult J, Desgrandchamps F. A systematic review of immunotherapy in urologic cancer: evolving roles for targeting of CTLA-4, PD-1/PD-L1, and HLA-G. Eur Urol 2015;68:267–79.
2. Malmstrom PU, Sylvester RJ, Crawford DE, et al. An individual patient data meta-analysis of the long-term outcome of randomized studies comparing intravesical mitomycin C versus bacillus Calmette–Guerin for non-muscle-invasive bladder cancer. Eur Urol 2009;56:247–56.
3. Motzer RJ, Rini BI, Bukowski RM, et al. Sunitinib in patients with metastatic renal cell carcinoma. JAMA 2006;295:2516–24.
4. KantoffPW, Higano CS, Shore ND, et al. Sipuleucel-T immunotherapy for castration-resistant prostate cancer. N Engl J Med 2010;363:411–22.
5. Logothetis CJ, Dexeus FH, Finn L, et al. A prospective randomized trial comparing MVAC and CISCA chemotherapy for patients with metastatic urothelial tumors. J Clin Oncol 1990;8:1050–5.
6. Von der Maase H, Sengelov L, Roberts JT, et al. Long-term survival results of a randomized trial comparing gemcitabine plus cisplatin, with methotrexate, vinblastine, doxorubicin, plus cisplatin in patients with bladder cancer. J Clin Oncol 2005;23:4602–8.
7. Galsky MD, Hahn NM, Rosenberg J, et al. A consensus definition of patients with metastatic urothelial carcinoma who are unfit for cisplatin-based chemotherapy. Lancet Oncol 2011;12:211–4.
8. Raggi D, Miceli R, Sonpavde G, et al. Second-line single-agent versus doublet chemotherapy as salvage therapy for metastatic urothelial cancer: a systematic review and meta-analysis. Ann Oncol 2016;27:49–61.
9. Escudier B, Porta C, Schmidinger M, et al. Renal cell carcinoma: ESMO clinical practice guidelines for diagnosis, treatment and follow-up. Ann Oncol 2016;27:v58–68.
10. Ko JJ, XieW, Kroeger N, et al. The International Metastatic Renal Cell Carcinoma Database Consortium model as a prognostic tool in patients with metastatic renal cell carcinoma previously treated with first-line targeted therapy: a population-based study. Lancet Oncol 2015;16:293–300.
11. Horwich A, Hugosson J, De Reijke T, et al. Prostate cancer: ESMO Consensus Conference Guidelines 2012. Ann Oncol 2013;24:1141–62.
12. Berthold DR, Pond GR, Soban F, De Wit R, Eisenberger M, Tannock IF. Docetaxel plus prednisone or mitoxantrone plus prednisone for advanced prostate cancer: updated survival in the TAX 327 study. J Clin Oncol 2008;26:242–5.
13. De Bono JS, Oudard S, Ozguroglu M, et al. Prednisone plus cabazitaxel or mitoxantrone for metastatic castration-resistant prostate cancer progressing after docetaxel treatment: a randomised openlabel trial. Lancet 2010;376:1147–54.
14. Ryan CJ, Smith MR, Fizazi K, et al. Abiraterone acetate plus prednisone versus placebo plus prednisone in chemotherapy-naive men with metastatic castration-resistant prostate cancer (COU-AA-302): final overall survival analysis of a randomised, double-blind, placebo-controlled phase 3 study. Lancet Oncol 2015;16:152–60.
15. Scher HI, Fizazi K, Saad F, et al. Increased survival with enzalutamide in prostate cancer after chemotherapy. N Engl J Med 2012;367:1187–97.
16. Parker C, Nilsson S, Heinrich D, et al. Alpha emitter radium-223 and survival in metastatic prostate cancer. N Engl J Med 2013;369:213–23.
17. Pardoll DM. The blockade of immune checkpoints in cancer immunotherapy. Nat Rev Cancer 2012;12:252–64.
18. Brahmer JR, Tykodi SS, Chow LQ, et al. Safety and activity of anti-PD-L1 antibody in patients with advanced cancer. N Engl J Med 2012;366:2455–65.
19. Topalian SL, Hodi FS, Brahmer JR, et al. Safety, activity, and immune correlates of anti-PD-1 antibody in cancer. N Engl J Med 2012;366:2443–54.
20. Powles T, Eder JP, Fine GD, et al. MPDL3280A (anti-PD-L1) treatment leads to clinical activity in metastatic bladder cancer. Nature 2014;515:558–62.
21. Moher D, Liberati A, Tetzlaff J, Altman DG, PRISMA Group. Preferred reporting items for systematic reviews and meta-analyses: the PRISMA statement. PLoS Med 2009;6:e1000097.
22. Eisenhauer EA, Therasse P, Bogaerts J, et al. New response evaluation criteria in solid tumours: revised RECIST guideline (version 1.1). Eur J Cancer 2009;45:228–47.
23. Bellmunt J, De Wit R, Vaughn DJ, et al. Pembrolizumab as second line therapy for advanced urothelial carcinoma. N Engl J Med 2017;376:1015–26.
24. Choueiri TK, Fishman MN, Escudier B, et al. Immunomodulatory activity of nivolumab in metastatic renal cell carcinoma. Clin Cancer Res 2016;22:5461–71.
25. Motzer RJ, Rini BI, McDermott DF, et al. Nivolumab for metastatic renal cell carcinoma: results of a randomized phase II trial. J Clin Oncol 2015;33:1430–7.
26. Motzer RJ, Escudier B, McDermott DF, et al. Nivolumab versus everolimus in advanced renal-cell carcinoma. N Engl J Med 2015;373:1803–13.
27. Beer TM, Kwon ED, Drake CG, et al. Randomized, double-blind, phase III trial of ipilimumab versus placebo in asymptomatic orminimally symptomatic patients with metastatic chemotherapy-naïve castration-resistant prostate cancer. J Clin Oncol 2017;35:40–7.
28. Kwon ED, Drake CG, Scher HI, et al. Ipilimumab versus placebo after radiotherapy in patients with metastatic castration-resistant prostate cancer that had progressed after docetaxel chemotherapy (CA184-043): a multicentre, randomised, double-blind, phase 3 trial. Lancet Oncol 2014;15:700–12.
29. Alexandrov LB, Nik-Zainal S, Wedge DC, et al. Signatures of mutational processes in human cancer. Nature 2013;500:415–21.
30. Balar AV, Galsky MD, Rosenberg JE, et al. Atezolizumab as first-line treatment in cisplatin-ineligible patients with locally advanced and metastatic urothelial carcinoma: a single-arm, multicentre, phase 2 trial. Lancet 2017;389:67–76.
31. Rosenberg JE, Hoffman-Censits J, Powles T, et al. Atezolizumab in patients with locally advanced and metastatic urothelial carcinoma who have progressed following treatment with platinum-based chemotherapy: a single-arm, multicentre, phase 2 trial. Lancet 2016;387:1909–20.
32. Sharma P, Retz M, Siefker-Radtke A, et al. Nivolumab in metastatic urothelial carcinoma after platinum therapy (CheckMate 275): a multicentre, single-arm,phase 2 trial. LancetOncol 2017;18:312–22.
33. Balar AV, Castellano DE, O'Donnell PH, et al. Pembrolizumab as first-line therapy in cisplatin-ineligible advanced urothelial cancer: results from the total KEYNOTE-052 study population. Genitourinary Cancers Symposium (ASCO-GU) 2017.
34. De Santis M, Bellmunt J, Mead G, et al. Randomized phase II/III trial assessing gemcitabine/carboplatin and methotrexate/carboplatin/vinblastine in patients with advanced urothelial cancer who are unfit for cisplatin-based chemotherapy: EORTC study 30986. J Clin Oncol 2012;30:191–9.
35. ClinicalTrials.gov. https://clinicaltrials.gov/.
36. Powles T, Smith K, Stenzl A, Bedke J. Immune checkpoint inhibition in metastatic urothelial cancer. Eur Urol. In press. http://dx.doi.org/10.1016/j.eururo.2017.03.047.
37. Kamat AM, Sylvester RJ, Bohle A, et al. Definitions, end points, and clinical trial designs for non-muscle-invasive bladder cancer: recommendations from the International Bladder Cancer Group. J Clin Oncol 2016;34:1935–44.
38. Boorjian SA, Sheinin Y, Crispen PL, et al. T-cell coregulatory molecule expression in urothelial cell carcinoma: clinicopathologic correlations and association with survival. Clin Cancer Res 2008;14:4800–8.
39. Hedegaard J, Lamy P, Nordentoft I, et al. Comprehensive transcriptional analysis of early-stage urothelial carcinoma. Cancer Cell 2016;30:27–42.
40. Liu JS, Bell J, Sumati R. Cost per responder analysis from the Checkmate 025 phase III trial of nivolumab versus everolimus in previously treated patients with advanced renal cell carcinoma. Value Health 2016;19:A145.
41. Choueiri TK, Escudier B, Powles T, et al. Cabozantinib versus everolimus in advanced renal cell carcinoma (METEOR): final results from a randomised, open-label, phase 3 trial. Lancet Oncol 2016;17:917–27.
42. Joseph RW, Chatta G, Vaishampayan U. Nivolumab treatment for advanced renal cell carcinoma: considerations for clinical practice. Urol Oncol 2017;35:142–8.
43. Wallin JJ, Bendell JC, Funke R, et al. Atezolizumab in combination with bevacizumab enhances antigen-specific T-cell migration in metastatic renal cell carcinoma. Nat Commun 2016;7:12624.
44. Graff JN, Alumkal JJ, Drake CG, et al. Early evidence of anti-PD-1 activity in enzalutamide-resistant prostate cancer. Oncotarget 2016;7:52810–7.
45. Bensch F, Van der Veen E, Jorritsma A, et al. First-in-human PET imaging with the PD-L1 antibody 89Zr-atezolizumab. AACR 2017, April 2017.
46. Cella D, Grunwald V, Nathan P, et al. Quality of life in patients with advanced renal cell carcinoma given nivolumab versus everolimus in CheckMate 025: a randomised, open-label, phase 3 trial. Lancet Oncol 2016;17:994–1003.
47. Vaughn DJ, De Wit R, Fradet T, et al. Health-related quality of life (HRQoL) in the KEYNOTE-045 study of pembrolizumab versus investigator-choice chemotherapy for previously treated advanced urothelial cancer. Genitourinary Cancers Symposium (ASCO-GU) 2017.
48. Champiat S, Lambotte O, Barreau E, et al. Management of immune checkpoint blockade dysimmune toxicities: a collaborative position paper. Ann Oncol 2016;27:559–74.
49. Champiat S, Dercle L, Ammari S, et al. Hyperprogressive disease is a new pattern of progression in cancer patients treated by anti-PD-1/PD-L1. Clin Cancer Res 2017;23:1920–8.
50. Kourie HR, Awada G, Awada AH. Learning from the "tsunami" of immune checkpoint inhibitors in 2015. Crit Rev Oncol Hematol 2016;101:213–20.

Supplementary Table 1. Characteristics of randomized and non-randomized clinical trials on immune checkpoint inhibitors in urological cancer.

	Trial	Study design	Population	Patients (n)	Histology subgroups	Line	Previous therapy	Experimental arm	Comparator
Urothelial cell cancer									
Bellmunt 2017 (1)*	Keynote-045 NCT02256436	Phase 3	Advanced UC	542	Predominant transitional cell features	2nd	Platinum-based chemotherapy	200 mg pembrolizumab IV, every 3 weeks	Investigator's choice of chemotherapy
Plimack 2017 (2)	Keynote-012 NCT01848834	Phase 1b	Locally advanced or metastatic UC	27	Transitional and non-transitional cell features	2nd	Chemotherapy	10 mg/kg pembrolizumab IV, every 2 weeks	NA
Sharma 2017 (3)	CheckMate275 NCT02387996	Phase 2	Locally advanced or metastatic UC	265	NA	2nd	Platinum-based chemotherapy	3 mg/kg nivolumab IV, every 2 weeks	NA
Balar 2016 (4)	Imvigor 210 (cohort 1) NCT02108652	Phase 2	Locally advanced or metastatic UC	119	NA	1st	Cisplatin ineligible patients, no previous systemic therapy	1200mg atezolizumab IV, every 3 weeks	NA
Rosenberg 2016 (5)	Imvigor 210 (cohort 2) NCT02108652	Phase 2	Locally advanced or metastatic UC	310	NA	2nd	Platinum-based chemotherapy	1200mg atezolizumab IV, every 3 weeks	NA
Massard 2016 (6)	NCT01693562	Phase 1/2	Locally advanced or metastatic UC	61	Transitional cell features	2nd	Not specified	10 mg/kg durvalumab IV, every 2 weeks	NA
Sharma 2016 (7)	CheckMate032 NCT01928394	Phase 1/2	Locally advanced or metastatic UC	78	NA	2nd	Platinum-based chemotherapy	3 mg/kg nivolumab IV, every 2 weeks	NA
Powles 2014 (8)	NCT01375842	Phase 1	Incurable or metastatic solid tumor, including UC	67	NA	2nd	Platinum-based chemotherapy	15 mg/kg atezolizumab IV, every 3 weeks	NA
Renal cell cancer									
Motzer 2015 (9)*	CheckMate025 NCT01668784	Phase 3	Advanced and metastatic RCC	821	Clear cell RCC	2nd	Anti-angiogenic therapy	3 mg/kg nivolumab intravenously every 2 weeks	10 mg everolimus, tablet orally once daily
Escudier 2017 (10)	CheckMate025 subgroup analysis of (9)*	Phase 3	Advanced and metastatic RCC	821	Clear cell RCC	2nd	Anti-angiogenic therapy	3 mg/kg nivolumab IV, every 2 weeks	10 mg everolimus, tablet orally once daily
Motzer 2015 (11)*	NCT01354431	Phase 2	Metastatic RCC	168	Clear cell RCC	2nd	Anti-angiogenic therapy	0.3, 2 or 10 mg/kg nivolumab IV, every 3 weeks	Other experimental arms
George 2016 (12)	NCT01354431 subgroup analysis of (11)*	Phase 2	Metastatic RCC	128	Clear cell RCC	2nd	Anti-angiogenic therapy	0.3, 2 or 10 mg/kg nivolumab IV, every 3 weeks	Other experimental arms
Choueiri 2016 (13)*	NCT01358721	Phase 1b	Metastatic RCC	91	Clear cell RCC	1st, 2nd	Systemic therapy, not specified	0.3, 2 or 10 mg/kg nivolumab, every 3 weeks	Other experimental arms

Supplementary Table 1. Continued

	Trial	Study design	Population	Patients (n)	Histology subgroups	Line	Previous therapy	Experimental arm	Comparator
McDermott 2016 (14)	NCT01375842	Phase 1a	Metastatic RCC	70	Clear-cell and non-clear cell	2nd	VEGF-inhibitor, mTOR-inhibtor or interleukin-2	Dose expansion study: 10, 15 or 20 mg/kg atezolizumab IV, every 3 weeks for 16 cycles	NA
McDermott 2015 (15)	NCT0730639	Phase 1	Advanced RCC	34	NA	2nd	Anti-angiogenic therapy, immune modulating therapy, mTOR inhibitor	10 mg/kg nivolumab IV, every 2 weeks, followed by an expansion cohort at 1 mg/kg	NA
Brahmer 2012 (16)	NCT00729664	Phase 1	Mixed patient population, including advanced RCC	17 (RCC)	NA	2nd	Not specified	Dose escalation study: 0.3, 1, 3 or 10 mg/kg BMS-936559 IV, every 2 weeks, up to 16 cycles	NA
Yang 2007 (17)	NA	Phase 2	Metastatic RCC	61	NA	2nd	Not specified	Cohort A, loading dose 3 mg/kg ipilimumab, subsequent doses 1 mg/kg every 3 weeks; Cohort B, 3 mg/kg ipilimumab every 3 weeks	NA
Prostate cancer									
Beer 2017 (18)*	NCT01057810	Phase 3	mCRPC	602	NA	2nd	Anti-androgenic, no chemotherapy	10 mg/kg ipilimumab IV, every 3 weeks for up to 4 doses, followed by maintenance treatment every 12 weeks	Placebo IV, every 3 weeks for up to 4 doses, followed by maintenance treatment every 12 weeks
Kwon 2014 (19)*	NCT00861614	Phase 3	mCRPC	799	Adenocarcinoma	2nd	Anti-androgenic therapy, docetaxel-based chemotherapy for mCRPC	Single-dose bone-directed radiotherapy (8 Gy) followed by 10 mg/kg ipilimumab IV, every 3 weeks for up to 4 doses	Single-dose bone-directed radiotherapy (8 Gy) followed by placebo IV, every 3 weeks for up to 4 doses
Graff 2016 (20)	NCT02312557	Phase 2	mCRPC	10	Adenocarcinoma	2nd	Anti-androgenic therapy, docetaxel-based chemotherapy, sipuleucel-T	80-160 mg enzalutamide orally, daily with 200 mg pembrolizumab IV, every 3 weeks	NA

Supplementary Table 1. Continued

	Trial	Study design	Population	Patients (n)	Histology subgroups	Line	Previous therapy	Experimental arm	Comparator
Slovin 2013 (21)	NCT00323882	Phase 1/2	mCRPC	30	Adenocarcinoma	2nd	Anti-androgenic therapy, chemotherapy	Dose escalation study: 3, 5 or 10 mg/kg ipilimumab IV, every 3 weeks, up to 4 doses	Dose escalation study: 3 or 10 mg/kg ipilimumab with external beam radiotherapy
Small 2007 (22)	NA	Pilot trial	mCRPC	14	Adenocarcinoma	2nd	Anti-angiogenic therapy	Anti-androgenic therapy with a single dose of 3 mg/kg ipilimumab IV	NA

*randomized clinical trial; UC, urothelial cell cancer; RCC, renal cell cancer; mCRPC, metastatic castration resistant prostate cancer; NA, not available; IV, intravenously

Supplementary Table 2. Efficacy of immune checkpoint inhibitors in randomized and non-randomized clinical trials in urological cancer.

	Treatment	Patients (n)	Median follow up in months (CI)	Median OS months (CI)	Median PFS months (CI)	ORR (CI)	CR	PR	SD	PD	NE	Median duration of response in months (CI)	Other
Urothelial carcinoma													
Bellmunt 2017 (1)*	Pembrolizumab 200 mg	270	14.1 (9.9-22.1)[c]	10.3 (8.0-11.8)[a]	2.1 (2.0-2.2)[a]	21.1% (16.4-26.5)[a]	19 (7%)	38 (14.1%)	47 (17.4%)	131 (48.5%)	35 (13.0%)	NR (1.6+ to 15.6+)[c]	
	Chemotherapy	272	14.1 (9.9-22.1)[c]	7.4 (6.1-8.3)[a]	3.3 (2.3-3.5)[a]	11.4% (7.9-15.8)[a]	9 (3.3%)	22 (8.1%)	91 (33.5%)	90 (33.1%)	60 (22.1%)	4.3 (1.4+ to 15.4+)[c]	
Plimack 2017 (2)	Pembrolizumab 10 mg/kg	33	13 (1-26)[c]	13 (5-20)[a]	2 (2-4)[a]	26% (11-46)[a]	3 (11%)	4 (15%)	4 (15%)	14 (52%)	2 (7%)	10 (4-22+)[c]	
Sharma 2017 (3)	Nivolumab 3 mg/kg	270	7.0 (2.96-8.77)[d]	8.74 (6.05-NR)[a]	2.00 (1.87-2.63)[a]	19.6% (15.0-24.9)[a]	6 (2%)	46 (17%)	60 (23%)	104 (39%)	49 (18%)	NR (7.43-NR)[d]	
Balar 2016 (4)	Atezolizumab 1200 mg	119	17.2 (0.2-23.5)[c]	15.9 (10.4-NR)[a]	2.7 (2.1-4.2)[a]	23% (16-31)[a]	11 (9%)	16 (13%)	29 (24%)	43 (36%)	NA	NR (14.1-NR)[a]	
Rosenberg 2016 (5)	Atezolizumab 1200 mg	310	11.7 (11.4-2.2)[a]	7.9 (6.6-9.3)[a]	2.1 (2.1-2.1)[a]	15% (11-19)[a]	15 (5%)	30 (10%)	59 (19%)	159 (51%)	NA	NR (2.0-13.7)[c]	
Massard 2016 (6)	Durvalumab 10 mg/kg	61	6.5 (0.8-14.8)[c]	NA	NA	31.0% (17.6-47.1)[a]	NA	NA	NA	NA	NA	NR (4.1+ to 49.3+)[c]	
Sharma 2016 (7)	Nivolumab 3 mg/kg	78	15.2 (12.9-16.8)[d]	9.7 (7.3-16.2)[a]	2.8 (1.5-5.9)[a]	24.4% (15.3-35.4)[a]	5 (6%)	14 (18%)	22 (28%)	30 (38%)	7 (9%)	9.4 (5.7-12.5)[d]	
Powles 2014 (8)	Anti-PD-L1 15 mg/kg	67	NA	NA	NA	17 (26%)	2 (3%)	NA	21 (32%)	21 (32%)	NA	NA	
Renal cell cancer													
Motzer 2015 (9)*	Nivolumab 3 mg/kg	410	18.3 (11.6-22.8)[d]	25.0 (21.8-NR)[a]	4.6 (3.7-5.4)[a]	25% (3.68-9.72)[a]	4 (1%)	99 (24%)	141 (34%)	143 (35%)	23 (6%)	12.0 (0 to 27.6)[c]	
	Everolimus 10 mg	411	17.2 (7.2-21.4)[d]	19.6 (17.6-23.1)[a]	4.4 (3.7-5.5)[a]	5%	2 (<1%)	20 (5%)	227 (55%)	114 (28%)	48 (12%)	12.0 (0 to 22.2)[c]	

Supplementary Table 2. Continued

	Treatment	Patients (n)	Median follow up in months (CI)	Median OS months (CI)	Median PFS months (CI)	ORR (CI)	CR	PR	SD	PD	NE	Median duration of response in months (CI)	Other
Escudier 2017 (10)	Nivolumab 3 mg/kg	410	Subgroup analyses										
	Everolimus 10 mg	411											
Motzer 2015 (11)*	Nivolumab 0.3 mg/kg	60	NA	18.2 (16.2-24.0)[b]	2.7 (1.9-3.0)[b]	20% (13.4-28.2)[b]	1 (2%)	11 (18%)	22 (37%)	24 (40%)	2 (3%)	NA	
	Nivolumab 2 mg/kg	54	NA	25.5 (19.8-28.8)[b]	4.0 (2.8-4.2)[b]	22% (15.0-31.1)[b]	1 (2%)	11 (20%)	23 (43%)	18 (33%)	1 (2%)	NA	
	Nivolumab 10mg/kg	54	NA	24.7 (15.3-26.0)[b]	4.2 (2.8-5.5)[b]	20% (13.3-29.1)[b]	0 (0%)	11 (20%)	24 (44%)	17 (32%)	2 (4%)	22.3 (4.8 to NR)[b]	
George 2016 (12)	Nivolumab, treated beyond progression	36	NA	22.5 (12.3-31.3)[a]	4.2 (2.8-5.5)[a]	14% (5-30)[a]	0 (0%)	5 (14%)	21 (58%)	9 (25%)	1 (3%)	NA	
	Nivolumab, not treated beyond progression	92	NA	12.3 (8.0-17.1)[a]	2.6 (1.5-3.9)[a]	16% (9-26)[a]	1 (1%)	14 (15%)	35 (38%)	38 (41%)	4 (4%)	NA	
Choueiri 2016 (13)*	All patients	91	NA	NA	NA	15% (8.7-24.5)[a]	2 (2%)	12 (13%)	42 (46%)	27 (30%)	8 (9%)	NA	
Previously treated group	Nivolumab 0.3 mg/kg	NA	NA	16.4 (10.1-NR)[a]	NA	9% (1.1-29.2)[a]	0	2 (9%)	8 (36%)	9 (41%)	3 (14%)	NA	
	Nivolumab 2 mg/kg	NA	NA	NA	NA	18% (5.2-40.3)[a]	0	4 (18%)	10 (46%)	5 (23%)	3 (14%)	NA	
	Nivolumab 10 mg/kg	NA	NA	25.2 (12.0-NR)[a]	NA	22% (7.5-43.7)[a]	0	5 (22%)	11 (48%)	6 (26%)	1 (4%)	NA	
Treatment naive group	Nivolumab 10 mg/kg	24	NA	NA	NA	13% (7.5-32.4)[a]	2 (8%)	12 (13%)	42 (46%)	27 (30%)	8 (9%)	NA	
McDermott 2016 (14)	Atezolizumab 3 mg/kg	70	23.9 (16.1-29.2)[a]	28.9 (20.0-NR)[a]	5.6 (3.9-8.2)[a]	15% (7-26)[a]	NA	NA	NA	NA	NA	17.4 (7.6-26.9+)[c]	

Supplementary Table 2. Continued

	Treatment	Patients (n)	Median follow up in months (CI)	Median OS months (CI)	Median PFS months (CI)	ORR (CI)	CR	PR	SD	PD	NE	Median duration of response in months (CI)	Other
McDermott 2015 (15)	All patients	34	45.2 (25.9-7.9)[c]	22.4 (12.5-NR)[a]	7.3 (3.6-10.9)[a]	29.4% (15.1-47.5)[a]	NA	NA	NA	NA	NA	12.9 (8.4-29.1+)[c]	
	Nivolumab 1 mg/kg	18	NA	29.3 (11.5-NR)[a]	4.7 (1.9-10.9)[a]	27.8% (9.7-53.3)[a]	NA	NA	NA	NA	NA	12.9 (9.2-17.5+)[c]	
	Nivolumab 10 mg/kg	16	NA	18.8 (11.4-NR)[a]	8.0 (1.7-14.0)[a]	31.3% (11.0-58.7)[a]	NA	NA	NA	NA	NA	12.9 (8.4-29.1+)[c]	
Brahmer 2012 (16)	Anti PD-L1 (BMS-936559) 10 mg/kg	17	NA	NA	NA	12% (2-36)[a]	NA	NA	NA	NA	NA	17.4	
Yang 2007 (17)	Ipilimumab 1 mg/kg	21	NA	NA	NA	NA	0 (0%)	1 (5%)	NA	NA	NA	NA	
	Ipilimumab 3 mg/kg	40	NA	NA	NA	12.5%	0 (0%)	5 (12.5%)	NA	NA	NA	NA	
Prostate cancer													**PSA RR (CI)[a]**
Beer 2017 (18)*	Ipilimumab	400	24-48	28.7 (26.1-34.2)[a]	5.6 (5.3-6.3)[a]	NA	NA	NA	NA	NA	NA	NA	23% (19-27)[a]
	Placebo	202	24-48	29.7 (26.1-34.1)[a]	3.8 (2.8-4.1)[a]	NA	NA	NA	NA	NA	NA	NA	8% (5-13)[a]
Kwon 2014 (19)*	Radiotherapy with ipilimumab	399	9.9 (4.3-16.7)[d]	11.2 (9.5- 12.7)[a]	4.0 (3.6-4.3)[a]	NA	NA	NA	NA	NA	NA	NA	13.1% (9.5-17.5)[a]
	Radiotherapy with placebo	400	9.3 (5.4-14.6)[d]	10.0 (8.3-11.0)[a]	3.1 (2.9-3.4)[a]	NA	NA	NA	NA	NA	NA	NA	5.2% (3.0-8.4)[a]

Supplementary Table 2. Continued

	Treatment	Patients (n)	Median follow up in months (CI)	Median OS months (CI)	Median PFS months (CI)	ORR (CI)	CR	PR	SD	PD	NE	Median duration of response in months (CI)	Other
Graff 2016 (20)	Pembrolizumab 200 mg	10	30 weeks (16-55)[c]	NA	NA	NA	0	2	3	4	1	NA	3
Slovin 2013 (21)	Ipilimumab 3 mg/kg	8	NA	NA	NA	NA	0	0	1	0	7	NA	2
	Ipilimumab 3 mg/kg with radiotherapy	7	NA	NA	NA	NA	0	0	1	1	5	NA	2
	Ipilimumab 5 mg/kg	6	NA	NA	NA	NA	0	0	1	0	5	NA	1
	Ipilimumab 10 mg/kg	16	NA	NA	NA	NA	1	0	1	3	11	NA	4
	Ipilimumab 10 mg/kg with radiotherapy	34	NA	NA	NA	NA	0	0	5	5	24	NA	4
Small 2007 (22)	Ipilimumab 3 mg/kg 1 dose	14	NA	NA	NA	NA	NA	NA	NA	NA	NA	NA	10

*randomized clinical trial; CI, confidence interval; OS, overall survival; PFS, progression free survival; ORR, objective response rate; CR, complete response; PR, partial response; SD, stable disease; PD, progressive disease; NE, not evaluable; PSA RR, PSA response rate; NA, not available; NR, not reached; a 95% CI; b 80% CI; c range; d interquartile range.

Supplementary Table 3. Detailed patient characteristics in randomized clinical trials on immune checkpoint inhibitors in urological cancer.

	Study treatment	Patients (n)	Median age (range)	Sex (male/ female)	Performance score	Visceral metastasis	Prior systemic therapy	Drugs
Urothelial cell cancer								
Bellmunt 2017 (23)	Pembrolizumab	270	67 (29-88)	200/70	ECOG 0: 44% 1: 53% 2: <1%	88.9% in total 33.7% liver	(neo)adjuvant 11.5% First-line 67.8% Second-line 20.4%	Cisplatin: 73.3% Carboplatin: 25.9% Oxaliplatin or nedaplatin: <1%
	Chemotherapy	272	65 (26-84)	202/70	ECOG 0: 39% 1: 58% 2: 1.5%	85.7% in total 34.9% liver	(neo)adjuvant 19.5% First-line 57.7% Second-line 22.1%	Cisplatin: 78.3% Carboplatin: 20.6% Oxaliplatin or nedaplatin: <1%
Renal cell carcinoma								
Motzer 2015 (26)	Nivolumab	410	62 (23-88)	315/95	Karnofsky <70: <1% 70-90: 32% 90-100: 67%	19% bone 24% liver 68% lung	No of previous treatments 1: 72% 2: 28%	Sunitinib: 60% Pazopanib: 29% Axitinib: 12%
	Everolimus	411	62 (18-86)	304/107	<70: <1% 70-90: 35% 90-100: 64%	17% bone 21% liver 66% lung	No of previous treatments 1: 72% 2: 28%	Sunitinib: 59% Pazopanib: 32% Axitinib: 12%
Motzer 2015 (25)	All patients	168	61	121/47	Karnofsky 70-90: 46% 90-100: 54%	74% lung 58% lymph node 28% liver 24% skin 22% adrenal	No of previous treatments 1: 30% 2: 37% ≥3: 33%	Sunitinib: 74% Everolimus: 34% Pazopanib: 27% Interleukin-2: 23% Sorafenib: 19%
	Nivolumab 0.3 mg/kg	60	61	41/19	Karnofsky 70-90: 37% 90-100: 63%	77% lung 48% lymph node 25% liver 30% skin 13% adrenal	No of previous treatments 1: 27% 2: 33% ≥3: 40%	Sunitinib: 77%, Everolimus: 35% Pazopanib: 25% Interleukin-2: 25% Sorafenib: 22%
	Nivolumab 2 mg/kg	54	61	40/14	Karnofsky 70-90: 56% 90-100: 44%	72% lung 65% lymph node 24% liver 20% skin 35% adrenal	No of previous treatments 1: 30% 2: 35% ≥3: 35%	Sunitinib: 78% Everolimus: 33% Pazopanib: 33% Interleukin-2: 20% Sorafenib: 15%

Supplementary Table 3. Continued

	Study treatment	Patients (n)	Median age (range)	Sex (male/ female)	Performance score	Visceral metastasis	Prior systemic therapy	Drugs
	Nivolumab 10mg/ kg	54	61	40/14	Karnofsky 70-90: 46% 90-100: 52%	72% lung 63% lymph node 35% liver 20% skin 19% adrenal	No of previous treatments 1: 33% 2: 43% >3: 24%	Sunitinib: 69% Everolimus: 33% Pazopanib: 24% Interleukin-2: 22% Sorafenib: 19%
Choueiri 2016 (24)	All patients	91	61	61/30	NA	NA	NA	NA
	Previously treated patients	67	61	46/21	NA	NA	Metastatic: 90% Adjuvant: 7% Neoadjuvant: 7%	NA
	Treatment-naive patients	24	63.5	15/9	NA	NA	None	NA
Prostate cancer								
Beer 2017 (27)	Ipilimumab	400	70 (44-91)	Not relevant	ECOG 0: 75% 1: 25% 2: <1%	No visceral metastases 78% bone	NA	NA
	Placebo	202	69 (42-92)	Not relevant	ECOG 0: 75% 1: 25% 2: 0%	No visceral metastases 79% bone	NA	NA
Kwon 2014 (28)	Radiotherapy with ipilimumab	399	69 (47-86)	Not relevant	ECOG 0: 42% 1: 54% 2: 1%	28% visceral metastases All at least 1 bone metastasis	NA	NA
	Radiotherapy with placebo	400	67.5 (45-86)	Not relevant	ECOG 0: 43% 1: 55% 2: 0	29% visceral metastases All at least 1 bone metastasis	NA	NA

ECOG, Eastern Cooperative Oncology Group performance status score; NA, not available.

Initial literature search strategy for Embase including Medline

('pembrolizumab'/exp OR 'pembrolizumab' OR 'atezolizumab'/exp OR 'atezolizumab' OR 'nivolumab'/exp OR 'nivolumab' OR 'avelumab'/exp OR 'avelumab' OR 'durvalumab'/exp OR 'durvalumab' OR 'tremelimumab'/exp OR 'tremelimumab' OR 'ipilimumab'/exp OR 'ipilimumab' OR 'programmed death 1 receptor'/exp OR 'programmed death 1 receptor' OR 'programmed death 1 ligand 1'/exp OR 'programmed death 1 ligand 1' OR 'programmed death 1 ligand 2/de' OR 'cytotoxic t lymphocyte antigen 4'/exp OR 'cytotoxic t lymphocyte antigen 4' OR (checkpoint NEXT/1 inhibitor*):ab,ti OR pembrolizumab*:ab,ti OR atezolizumab*:ab,ti OR nivolumab*:ab,ti OR avelumab*:ab,ti OR durvalumab*:ab,ti OR tremelimumab*:ab,ti OR ipilimumab*:ab,ti OR (programmed NEAR/3 death NEAR/3 (receptor* OR ligand*)):ab,ti OR pd1:ab,ti OR 'pd 1':ab,ti OR pdcd1:ab,ti OR 'ctla-4':ab,ti OR pdl1:ab,ti OR 'pd l1':ab,ti OR 'pd l2':ab,ti OR pdl2:ab,ti OR pdcd1lg1:ab,ti OR pdcd1lg2:ab,ti OR ((cd273 OR cd279 OR cd274 OR cd152) NEAR/3 antigen*):ab,ti OR (cytotoxic NEXT/1 't lymphocyte' NEAR/3 antigen*):ab,ti AND ('urinary tract cancer'/mj/exp OR 'urinary tract cancer' OR 'prostate cancer'/mj/exp OR 'prostate cancer' OR ((bladder OR urothelial OR urolog* OR uret* OR vesical OR urinary OR kidney* OR renal* OR prostat*) NEAR/3 (cancer* OR carcino* OR neoplas* OR metasta*)):ab,ti) NOT ((animals)/lim NOT (humans)/lim) NOT ('Conference Abstract').

2

SUPPLEMENTARY REFERENCES

1. Bellmunt J, De Wit R, Vaughn DJ, Fradet Y, Lee JL, Fong L, et al. Pembrolizumab as second-line therapy for advanced urothelial carcinoma. N Engl J Med 2017;376:1015-26.
2. Plimack ER, Bellmunt J, Gupta S, Berger R, Chow LQM, Juco J, et al. Safety and activity of pembrolizumab in patients with locally advanced or metastatic urothelial cancer (KEYNOTE-012): a non-randomised, open-label, phase 1b study. Lancet Oncol. 2017;18:212-20.
3. Sharma P, Retz M, Siefker-Radtke A, Baron A, Necchi A, Bedke J, et al. Nivolumab in metastatic urothelial carcinoma after platinum therapy (CheckMate 275): a multicentre, single-arm, phase 2 trial. Lancet Oncol. 2017;18:312-22.
4. Balar AV, Galsky MD, Rosenberg JE, Powles T, Petrylak DP, Bellmunt J, et al. Atezolizumab as first-line treatment in cisplatin-ineligible patients with locally advanced and metastatic urothelial carcinoma: a single-arm, multicentre, phase 2 trial. Lancet. 2017;389:67-76.
5. Rosenberg JE, Hoffman-Censits J, Powles T, Van der Heijden MS, Balar AV, Necchi A, et al. Atezolizumab in patients with locally advanced and metastatic urothelial carcinoma who have progressed following treatment with platinum-based chemotherapy: a single-arm, multicentre, phase 2 trial. Lancet. 2016;387:1909-20.
6. Massard C, Gordon MS, Sharma S, Rafii S, Wainberg ZA, Luke J, et al. Safety and efficacy of durvalumab (MEDI4736), an anti-programmed cell death ligand-1 immune checkpoint inhibitor, in patients with advanced urothelial bladder cancer. J Clin Oncol. 2016;34:3119-25.
7. Sharma P, Callahan MK, Bono P, Kim J, Spiliopoulou P, Calvo E, et al. Nivolumab monotherapy in recurrent metastatic urothelial carcinoma (CheckMate 032): a multicentre, open-label, two-stage, multi-arm, phase 1/2 trial. Lancet Oncol. 2016;17:1590-8.
8. Powles T, Eder JP, Fine GD, Braiteh FS, Loriot Y, Cruz C, et al. MPDL3280A (anti-PD-L1) treatment leads to clinical activity in metastatic bladder cancer. Nature. 2014;515:558-62.
9. Motzer RJ, Escudier B, McDermott DF, George S, Hammers HJ, Srinivas S, et al. Nivolumab versus everolimus in advanced renal-cell carcinoma. N Engl J Med. 2015;373:1803-13.
10. Escudier B, Sharma P, McDermott DF, George S, Hammers HJ, Srinivas S, et al. CheckMate 025 randomized phase 3 study: outcomes by key baseline factors and prior therapy for nivolumab versus everolimus in advanced renal cell carcinoma. Eur Urol. 2017.
11. Motzer RJ, Rini BI, McDermott DF, Redman BG, Kuzel TM, Harrison MR, et al. Nivolumab for metastatic renal cell carcinoma: results of a randomized phase II Trial. J Clin Oncol. 2015;33:1430-7.
12. George S, Motzer RJ, Hammers HJ, Redman BG, Kuzel TM, Tykodi SS, et al. Safety and efficacy of nivolumab in patients with metastatic renal cell carcinoma treated beyond progression: a subgroup analysis of a randomized clinical trial. JAMA Oncol. 2016;2:1179-86.
13. Choueiri TK, Fishman MN, Escudier B, McDermott DF, Drake CG, Kluger H, et al. Immunomodulatory activity of nivolumab in metastatic renal cell carcinoma. Clin Cancer Res. 2016;22:5461-71.
14. McDermott DF, Sosman JA, Sznol M, Massard C, Gordon MS, Hamid O, et al. Atezolizumab, an anti-programmed death-ligand 1 antibody, in metastatic renal cell carcinoma: long-term safety, clinical activity, and immune correlates from a phase Ia study. J Clin Oncol. 2016;34:833-42.
15. McDermott DF, Choueiri TK, Puzanov I, Hodi S, Drake CG, Brahmer JR, et al. Survival, durable response, and long-term safety in patients with previously treated advanced renal cell carcinoma receiving nivolumab. J Clin Oncol. 2015;33:2013-20.
16. Brahmer JR, Tykodi SS, Chow LQ, Hwu WJ, Topalian SL, Hwu P, et al. Safety and activity of anti-PD-L1 antibody in patients with advanced cancer. N Engl J Med. 2012;366:2455-65.
17. Yang JC, Hughes M, Kammula U, Royal R, Sherry RM, Topalian SL, et al. Ipilimumab (anti-CTLA4 antibody) causes regression of metastatic renal cell cancer associated with enteritis and hypophysitis. J Immunother. 2007;30:825-30.
18. Beer TM, Kwon ED, Drake CG, Fizazi K, Logothetis C, Gravis G, et al. Randomized, double-blind, phase III trial of ipilimumab versus placebo in asymptomatic or minimally symptomatic patients with metastatic chemotherapy-naive castration-resistant prostate cancer. J Clin Oncol. 2017;35:40-7.
19. Kwon ED, Drake CG, Scher HI, Fizazi K, Bossi A, Van den Eertwegh AJM, et al. Ipilimumab versus placebo after radiotherapy in patients with metastatic castration-resistant prostate cancer that had progressed after docetaxel chemotherapy (CA184-043): A multicentre, randomised, double-blind, phase 3 trial. Lancet Oncol. 2014;15:700-12.
20. Graff JN, Alumkal JJ, Drake CG, Thomas GV, Redmond WL, Farhad M, et al. Early evidence of anti-PD-1 activity in enzalutamide-resistant prostate cancer. Oncotarget. 2016;7:52810-7.
21. Slovin SF, Higano CS, Hamid O, Tejwani S, Harzstark A, Alumkal JJ, et al. Ipilimumab alone or in combination with radiotherapy in metastatic castration-resistant prostate cancer: Results from an open-label, multicenter phase i/ii study. Ann Oncol. 2013;24:1813-21.
22. Small EJ, Tchekmedyian NS, Rini BI, Fong L, Lowy I, Allison JP. A pilot trial of CTLA-4 blockade with human anti-CTLA-4 in patients with hormone-refractory prostate cancer. Clin Cancer Res. 2007;13:1810-5.

CHAPTER 3

PD-L1 antibody comparison in urothelial carcinoma

Maud Rijnders
Astrid A.M. van der Veldt
Tahlita C.M. Zuiverloon
Katrien Grünberg
Erik Thunnissen
Ronald de Wit
Geert J.L.H. van Leenders

Full text thesis version
Published in short as letter in European Urology, 2019 Mar;75(3):538-540

ABSTRACT

Background

PD-L1 expression is commonly applied as an inclusion criterion or stratification factor in clinical trials with immune checkpoint inhibitors (ICIs). To date, conflicting results have been published regarding the predictive and prognostic value of PD-L1 in metastatic urothelial cancer (mUC), which might be explained by the use of different PD-L1 companion diagnostics. The objective of this study was therefore to accurately compare PD-L1 expression by five commercially available PD-L1 antibodies in patients with UC.

Methods

Tissue microarrays (TMA) containing samples from 139 patients with muscle-invasive UC were stained with PD-L1 antibodies 22C3 (pembrolizumab), 28-8 (nivolumab), SP142 (atezolizumab), SP263 (durvalumab) and E1L3N (research antibody) on the Ventana Benchmark (SP142, SP263) and DAKO platforms (22C3, 28-8, E1L3N). PD-L1 expression was manually scored on tumor cells and infiltrating immune cells, and subsequently PD-L1 status was determined according to the corresponding assay specifications used in clinical trials in mUC.

Results

PD-L1 expression was generally higher on tumor cells than on immune cells using antibodies 22C3, 28-8, SP263 and E1L3N, while SP142 demonstrated less PD-L1 expression on tumor cells. PD-L1 status was positive in 20-48% of patients. The agreement in PD-L1 status between individual antibody clones i) varied from 60-90% (Kappa concordance 0.185-0.708), ii) was better when based on a higher cutoff value for 22C3 (≥10%) and 28-8 (≥5%), and iii) was lowest for E1L3N and SP142. PD-L1 status was identical for all five PD-L1 assays in 89 out of 139 patients (64%; Krippendorff's alpha for overall inter-assay agreement 0.513). Agreement in PD-L1 status improved when only companion diagnostic assays were considered; 109 out of 139 patients (78%) displayed similar PD-L1 status by all four antibodies (Krippendorff's alpha 0.630).

Conclusions

We found that there was substantial concordance in PD-L1 status between the four companion diagnostics. In the majority of cases the PD-L1 status was similar, implying that these tests may be interchangeable in clinical practice. Therefore, the application of different PD-L1 companion diagnostics may have limited implications on therapeutic decision making in ICI treatment.

INTRODUCTION

For decades, platinum-based chemotherapy has been the standard treatment for patients with advanced and metastatic urothelial cancer (mUC). Since May 2016 several immune checkpoint inhibitors (ICIs) have been approved for second-line treatment of advanced and metastatic UC, including atezolizumab, nivolumab, durvalumab, avelumab, and pembrolizumab. Moreover, atezolizumab and pembrolizumab have been approved for first-line treatment of patients with UC who are cisplatin-ineligible.

Although ICIs may result in durable responses (1-5), only 20-30% of patients obtain an objective tumor response (6, 7). As adequate patient selection is required, PD-L1 expression has extensively been evaluated as a biomarker to predict therapeutic response to ICI treatment. In non-small cell lung cancer (NSCLC), patient selection for ICI therapy is strictly confined to PD-L1 expression, as the efficacy of ICIs has been shown to be superior in NSCLC patients with high PD-L1 expression (8). For patients with mUC, clinical trials have shown conflicting results on the prognostic and predictive value of PD-L1. In the phase 2 trials with first- and second-line atezolizumab, response rates to atezolizumab were higher for patients with ≥5% PD-L1 expression (9, 10). Based on these results, randomization in the phase III trial comparing second-line atezolizumab to chemotherapy, was stratified based on PD-L1 expression (<5% versus ≥5% expression on tumor infiltrating immune cells) and the primary endpoint of the study was overall survival in PD-L1 positive patients. Also in this trial, the response rate to atezolizumab was higher for patients with ≥5% PD-L1 expression. However, there was no overall survival benefit for patients treated with atezolizumab compared to chemotherapy, both in PD-L1 positive patients as well as the total study population (2). In the phase III trial comparing second-line pembrolizumab with chemotherapy, randomization was not stratified on PD-L1 expression. Here, the median overall survival was significantly longer for patients treated with pembrolizumab compared to chemotherapy, both in the total study population and for PD-L1 positive patients. However, the response rate to pembrolizumab was similar for patients with ≥10% PD-L1 expression compared to the total study population (objective response rate of 21.1% and 21.6% respectively) (1). For this reason, PD-L1 testing is not required for second-line pembrolizumab treatment in patients with mUC.

The U.S. Food and Drug Administration (FDA) also approved atezolizumab and pembrolizumab for first-line treatment of cisplatin-ineligible patients. Preliminary data from two ongoing trials studying combination therapy of ICIs with chemotherapy demonstrated that patients receiving single agent pembrolizumab or atezolizumab with low PD-L1 expression had inferior overall survival as compared to patients allocated to receiving chemotherapy (11, 12). Therefore, PD-L1 testing is now required for

selection of patients with mUC who are cisplatin-ineligible for first-line treatment with pembrolizumab and atezolizumab (13, 14).

Clinical ICI trials have used different FDA approved companion diagnostic PD-L1 tests including distinct PD-L1 antibodies, staining platforms and scoring algorithms on a range of available archival tissue specimens (Table 1). This considerable variability in PD-L1 testing may explain the conflicting results on the prognostic and predictive value of PD-L1 in previous trials. Four companion diagnostic PD-L1 tests have been applied in clinical trials on ICIs in patients with mUC, while some pathology laboratories might also use specific laboratory developed tests (LDTs). In order to facilitate widespread and reliable PD-L1 testing in clinical practice, it is essential to determine to what extent the different PD-L1 tests are interchangeable. Therefore, the aim of this study was to accurately compare the staining pattern and diagnostic performance of five different PD-L1 tests in a large set of patients with advanced UC.

PATIENTS AND METHODS

Patient characteristics

In total 139 patients with muscle-invasive bladder cancer (MIBC), treated in six Dutch medical centers between 1990-2009, were included in this study. Tissue microarrays (TMAs) were constructed of representative transurethral resection of bladder tumor (TURB; n = 21) or cystectomy specimens (n = 118), consisting of three tissue cores of 1 mm per specimen. The use of tissue samples for scientific purposes was approved by the Medical Research Ethics Committee of the Erasmus MC-Cancer Institute, Rotterdam, The Netherlands (MEC-2014-553). Samples were used in accordance with the "Code for Proper Secondary Use of Human Tissue in The Netherlands" as developed by the Dutch Federation of Medical Scientific Societies (FMWV, version 2002, update 2011).

PD-L1 immunohistochemistry and scoring

Four µm tissue slides were stained with five primary PD-L1 antibodies strictly according to the applicable manufacturer's guidelines for clinical use. Antibodies 22C3 and 28-8 were stained at a DAKO platform (VU Medical Center, Amsterdam); SP142 and SP263 at the Ventana Benchmark ULTRA platform (Erasmus MC, Rotterdam); and E1L3N at a DAKO platform (Radboud University Medical Center, Nijmegen). All TMA punches were scored by an expert genitourinary pathologist (GvL) with expertise in PD-L1 scoring. For each tissue core, the percentage of tumor cells and the percentage of tumor infiltrating immune cells with PD-L1 expression was estimated. The mean PD-L1 expression on tumor and immune cells was calculated for each patient. PD-L1 status was determined based on the corresponding predefined scoring algorithms and cutoff values as applied in clinical

ICI trials in mUC. Details on PD-L1 immunohistochemistry, scoring methodology and cutoffs are provided in Table 1. Since no predefined cutoff has previously been determined for the research antibody E1L3N, we used ≥25% PD-L1 expression on tumor and/or immune cells; this cutoff resulted in a similar percentage of PD-L1 positive and negative cases as the mean of the other four antibodies (Table 2).

Statistical analysis

The correlation of PD-L1 expression as continuous value on tumor cells and infiltrating immune cells between individual assays was assessed using the intra-class correlation coefficient (ICC). The agreement of categorical PD-L1 status between individual assays was determined by Cohen's Kappa concordance coefficient. Overall concordance between the used assays was determined by Krippendorff's alpha coefficient. Concordance values indicate poor, 0.01-0.20 slight, 0.21-0.40 fair, 0.41-0.60 moderate, 0.61-0.80 substantial, and 0.81-1 almost perfect agreement (15). All statistical analyses were performed using SPSS Statistics 21 software (IBM; Chicago Illinois, USA) and using the R package 'irr'.

RESULTS

Patient cohort

Patient characteristics are described in Supplementary Table 1. In total, 292 tissue cores from 139 patients with MIBC were analyzed. PD-L1 expression could be assessed in 132 (22C3), 130 (28-8), 135 (SP142), 137 (SP263) and 130 (E1L3N) patients, respectively. Minor variability in assessable numbers was caused by drop out of specific tissue cores or absence of invasive tumor at deeper TMA levels. In 117 patients all five antibodies could be evaluated.

PD-L1 expression

For all antibodies, PD-L1 expression was generally higher on tumor cells than on infiltrating immune cells (Figure 1). Tumor cell expression was most common for E1L3N and lowest for SP142, while the frequency of PD-L1 expression by 22C3, 28-8 and SP263 was comparable (Figure 1B, left graph). The pairwise agreement for PD-L1 expression on tumor cells was lowest for SP142 (ICC 0.07-0.252) and E1L3N (ICC 0.07-0.505) (Supplementary Table 2). Less variability was observed for immune cell staining, with 22C3 showing slightly more frequent expression (Figure 1B, right graph). The pairwise agreement of immune cell staining of all antibodies was moderate to substantial (ICC 0.409-0.656) (Supplementary Table 2).

Concordance of PD-L1 status

The PD-L1 status was determined in accordance with previous clinical ICI trials in

patients with mUC (Table 1). A positive PD-L1 status was found in 20-48% of patient samples dependent on the antibody and cutoff used (Table 2). In clinical trials two different cutoffs have been used for 28-8 (≥1% and ≥5%) and 22C3 (≥1% and ≥10%). For both antibodies, application of the highest cutoff value resulted in better agreement between tests (Table 3). Therefore, in further analyses, cutoff values of ≥5% and ≥10% were applied for 28-8 and 22C3, respectively. In general, pairwise concordant PD-L1 status was found in 60-90% of cases (Kappa 0.185-0.707). Mutual pairwise concordance of PD-L1 status was 88-90% for antibodies 22C3, 28-8 and SP263 (Kappa 0.657-0.708, substantial concordance). Agreement of PD-L1 status by E1L3N with the other four antibodies was generally slight to moderate (Kappa 0.185-0.435), while agreement of SP142 with other antibodies was overall fair to substantial (Kappa 0.334-0.697).

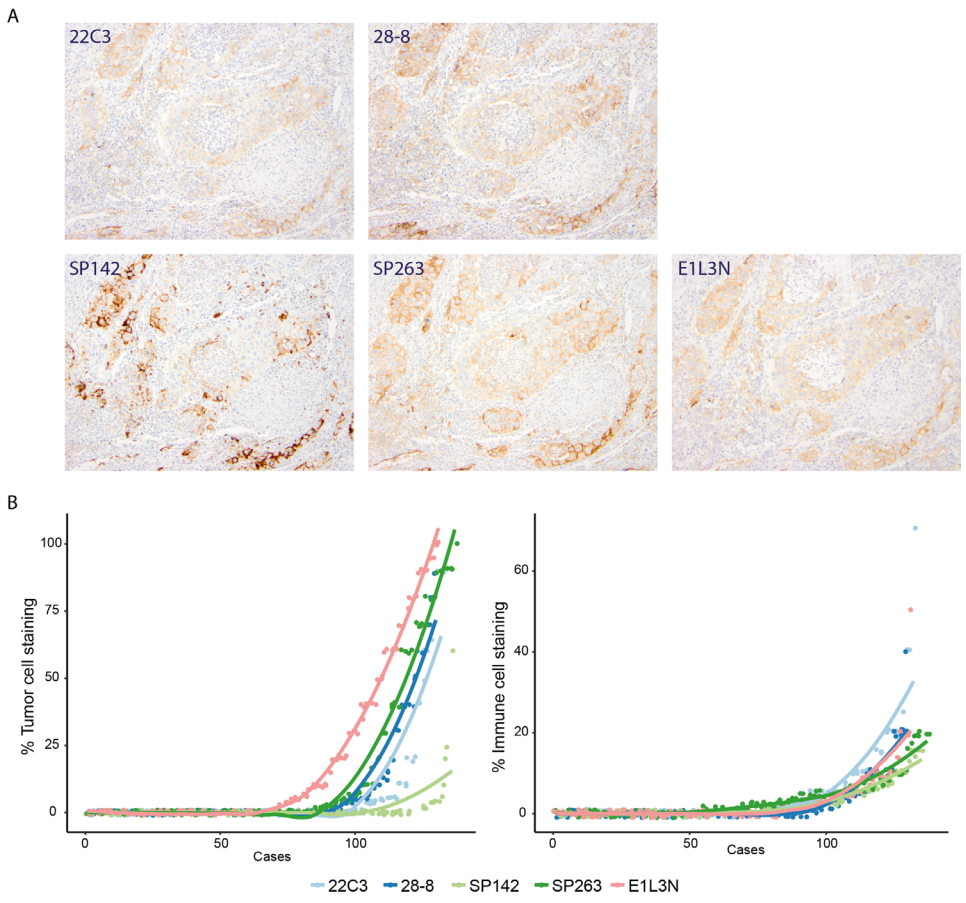

Figure 1. Distribution of PD-L1 expression on tumor cells and infiltrating immune cells.
A. Representative examples of PD-L1 staining of primary MIBC tissue by five different PD-L1 assays. **B.** PD-L1 expression level was manually scored on tumor cells and infiltrating immune cells. Each dot represents the mean PD-L1 expression score from 1-3 tissue cores from the same tumor. Colored lines display the "best fit" curve per antibody clone to aid comparison of expression scores between anti-PD-L1 antibodies.

Table 1. Detailed summary of anti-PD-L1 IHC assays

	Pembrolizumab (1, 11)	Nivolumab (3)	Atezolizumab (2,9,10)	Durvalumab (5)	Lab developed test
Drug target	PD-1	PD-1	PD-L1	PD-L1	Not applicable
Antibody clone	22C3	28-8	SP142	SP263	E1L3N
Target domain	Extracellular	Extracellular	Intracellular	Extracellular	Intracellular
Therapeutic developer	Merck	Bristol-Myers Squibb	Genentech	Ventana	Not applicable
Platform	Autostainer Link 48 (DAKO)	Autostainer Link 48 (DAKO)	Benchmark ULTRA	Benchmark ULTRA	Any
Cutoff for positivity	TC and IC ≥1% or ≥10%	TC ≥1% or ≥5%	IC ≥5%	TC or IC ≥25%	Not defined

Table 2. PD-L1 status determined by the specific cutoff for positivity per test

	22C3 (N = 132)		28-8 (N = 130)		SP142 (N = 135)	SP263 (N = 137)	E1L3N (N =130)
Cutoff for positivity	≥1%	≥10%	≥1%	≥5%	≥5%	≥25%	≥25%
PD-L1 positive – no. (%)	63 (47.7)	35 (26.5)	42 (32.3)	30 (23.3)	28 (20.7)	28 (20.4)	35 (26.9)

Table 3. Concordance in PD-L1 status between antibody clones determined by Cohen's Kappa concordance coefficient.

	28-8 ≥ 1%	28-8 ≥ 5%	SP142 ≥ 5%	263 ≥ 25%	E1L3N ≥ 25%
22C3 ≥ 1%	76% 0.523 (0.384-0.662)		73% 0.437 (0.306-0.568)	72% 0.416 (0.287-0.545)	60% 0.185 (0.026-0.344)
22C3 ≥ 10%		88% 0.685 (0.538-0.832)	89% 0.697 (0.550-0.844)	88% 0.657 (0.504-0.810)	75% 0.366 (0.184-0.548)
28-8 ≥ 1%			77% 0.421 (0.250-0.592)	85% 0.631 (0.486-0.776)	67% 0.217 (0.072-0.397)
28-8 ≥ 5%			80% 0.419 (0.229-0.609)	90% 0.708 (0.559-0.857)	72% 0.255 (0.067-0.443)
SP142 ≥ 5%				86% 0.582 (0.410-0.754)	75% 0.334 (0.150-0.518)
SP263 ≥ 25%					79% 0.435 (0.257-0.613)

Poor agreement — Excellent agreement

Values are displayed as percentage agreement, Cohen's Kappa concordance coefficient, 95% confidence interval. Concordance values indicate poor, 0.01-0.20 slight, 0.21-0.40 fair, 0.41-0.60 moderate, 0.61-0.80 substantial, and 0.81-1 almost perfect agreement (15).

Clinical impact of PD-L1 concordance

Overall agreement of the five antibodies was moderate (Krippendorff's α 0.513). Identical PD-L1 status was found for all five antibodies in 72 patients (61%; Figure 2). In 30 patients (26%) one antibody demonstrated dissimilar outcome and in 15 patients (13%) two antibodies. If there was disagreement in PD-L1 status by one antibody, in the majority of cases (19 patients, 63%) classification according to antibody E1L3N was different. When only the four companion diagnostics were analyzed, overall agreement increased to substantial (Krippendorff's α 0.630). 91 patients (78%) showed similar PD-L1 assay outcome. In 13 tumor samples (11%) one antibody led to a dissimilar PD-L1 score and in another 13 samples two antibodies gave another outcome. If one companion assay gave a discordant outcome, this was observed in 5 cases for SP142 (38%), 5 for 28-8 (38%), 2 for SP263 (16%) and one for 22C3 (8%).

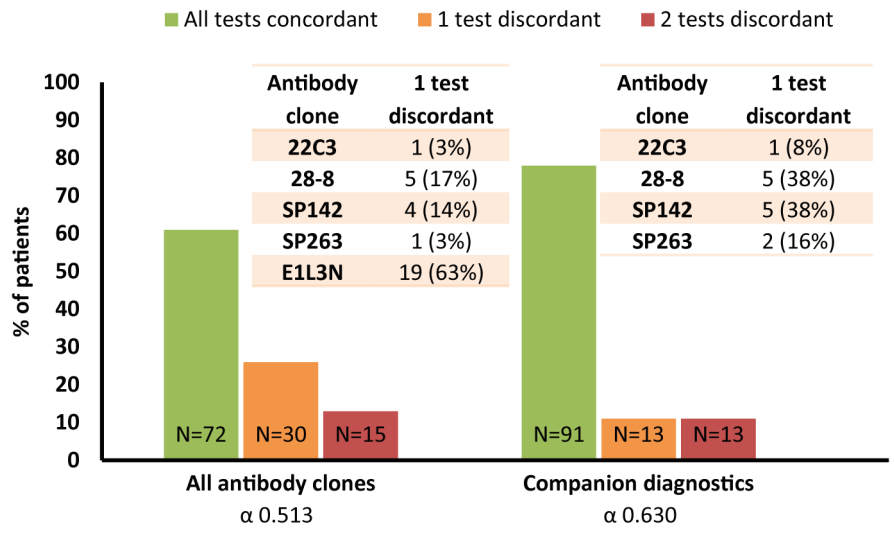

Antibody clone	1 test discordant
22C3	1 (3%)
28-8	5 (17%)
SP142	4 (14%)
SP263	1 (3%)
E1L3N	19 (63%)

Antibody clone	1 test discordant
22C3	1 (8%)
28-8	5 (38%)
SP142	5 (38%)
SP263	2 (16%)

Figure 2. Agreement in PD-L1 status between all five antibody clones or companion diagnostic antibodies (22C3, 28-8, SP142, and SP263) only.
PD-L1 status was determined based on the predefined cutoff value per assay (≥10% for 22C3 and ≥5% for 28-8). Bar graphs: proportion of patients for which PD-L1 status was concordant for all tests and proportion of patients for which 1 or 2 tests were discordant. Tables: specification of which antibody clone displayed a different PD-L1 status in case one test was discordant.

DISCUSSION

In order to improve our knowledge regarding the available PD-L1 assays and assist in the interpretation of test results for patients with mUC, we compared five PD-L1 antibodies including four companion diagnostic assays (22C3, 28-8, SP142, SP263) and one research antibody (E1L3N) in MIBC samples of 139 patients. Agreement of PD-L1 status was substantial among companion antibodies 22C3, 28-8 and SP263, fair for SP142 and poor for E1L3N. In case of 22C3 and 28-8, where two different cutoffs have been applied in clinical trials, the highest cutoff showed best agreement with the other tests. If the four companion diagnostic PD-L1 tests are considered, alternative decisions on ICI treatment would be taken in 30 out of 139 (22%) patients based on dissimilar PD-L1 assay outcome.

Our results are in line with previously published studies in mUC (16, 17) and NSCLC (18, 19), which also observed best concordance among 22C3, 28-8 and SP263 antibodies. However, these studies did not consider the cutoff values used in mUC trials. Research antibody E1L3N displayed markedly more PD-L1 expression on tumor cells as compared to the companion diagnostics. Previous studies did report acceptable concordance of PD-L1 expression on TCs and ICs determined by the E1L3N antibody compared with companion diagnostic antibodies in patients with mUC, with ICC values of 0.500-0.949 on tumor cells and 0.300-0.866 on immune cells (16, 17). Since E1L3N has not been used in clinical mUC trials, no predefined cutoff value has been determined, which may at least partially explain the poor concordance we observed for this test. Atezolizumab companion diagnostic antibody SP142 displayed lower PD-L1 expression on tumor cells and does therefore, as only companion diagnostic test, not take tumor cell staining into account in the scoring algorithm. This might therefore have resulted in the more frequent dissimilar PD-L1 status by the SP142 test. Previous studies also reported lower inter-observer concordance for PD-L1 expression on immune cells as compared to tumor cells for multiple PD-L1 antibodies (18, 19). A complete explanation for staining differences between antibodies is not readily available but is likely related to location and accessibility of target epitopes (20-22).

PD-L1 testing has recently been implemented for selection of patients with mUC who are cisplatin-ineligible using the companion diagnostic assays for pembrolizumab (22C3) and atezolizumab (SP142). The definitive role of PD-L1 testing in second-line ICI treatment decision making for patients with mUC remains to be established since previous trials have shown contradictory results regarding the predictive value of different PD-L1 assays in patient outcome. In all previous clinical trials, PD-L1 status has been determined on available archival UC specimens, which varied significantly from TURB specimens obtained months or even years before initiation of ICI therapy, to biopsies from metastases obtained shortly before treatment. Little is known to what

extent tumor specimen (TURB, cystectomy, lymph node or visceral site), surgical type (biopsy, resection), age of specimen (fresh or archival tissue), previous (neo)adjuvant therapies, tumor heterogeneity, and scoring algorithm affect PD-L1 assessment and impact (17, 23, 24). Fresh tumor biopsies seem most representative since it is known that PD-L1 expression is dynamic and can be influenced by different therapeutic regimens. However, biopsy specimens might underestimate real PD-L1 expression in some cases, as compared with tumor resection specimens. For instance, Rosenberg et al. found that biopsies from metastatic sites were PD-L1 (SP142) positive in 8% of cases while 28% of metastatic excision specimens revealed PD-L1 expression (9). Furthermore, PD-L1 positive lymphocytes physiologically reside in lymph nodes, making assessment of tumor-associated PD-L1 expression in immune cells ambiguous at this site.

To resemble clinical practice of PD-L1 assessment, all PD-L1 assays were technically established and scored according to manufacturers' specified protocols applied in clinical studies. A limitation of this study, however, is the use of TMA's for PD-L1 assessment, as PD-L1 status is frequently determined on whole tissue slides of available archival tissue specimens or biopsies specifically obtained for determination of PD-L1 status. Due to heterogeneity in larger tissue slides, we expect that concordance between assays will be lower than on small TMA tumor samples. Discordances in PD-L1 expression by the SP142 antibody between tumor biopsy samples and subsequent surgical resection specimens have been reported in NSCLC when PD-L1 expression was scored on tumor cells and infiltrating immune cells (25). However, in another NSCLC trial no differences in PD-L1 expression levels were observed for the SP142 assay when only scoring of tumor cell expression was performed (26). Another limitation of our study is that none of the patients were treated with ICIs. Although we were able to assess concordance between PD-L1 assays, we cannot conclude whether the different assays provide the same predictive value per type of ICI.

In conclusion, we show superior concordance in PD-L1 status as assessed by companion diagnostic tests 22C3, 28-8, SP263 and SP142 than E1L3N. Furthermore, higher cutoff values for 22C3 and 28-8 (□10% and □5%, respectively) resulted in better assay agreement and led to complete agreement of the four companion diagnostics in 78% of patients, implying that these tests may be interchangeable in clinical practice. Therefore, the impact of factors such as specimen type, method of acquisition and effects of previous (neo) adjuvant therapies might be more relevant for the predictive value of PD-L1 tests than companion diagnostic assay differences.

REFERENCES

1. Bellmunt J, de Wit R, Vaughn DJ, Fradet Y, Lee JL, Fong L, et al. Pembrolizumab as Second-Line Therapy for Advanced Urothelial Carcinoma. N Engl J Med. 2017;376(11):1015-26.
2. Powles T, Durán I, van der Heijden MS, Loriot Y, Vogelzang NJ, De Giorgi U, et al. Atezolizumab versus chemotherapy in patients with platinum-treated locally advanced or metastatic urothelial carcinoma (IMvigor211): a multicentre, open-label, phase 3 randomised controlled trial. The Lancet.391(10122):748-57.
3. Sharma P, Retz M, Siefker-Radtke A, Baron A, Necchi A, Bedke J, et al. Nivolumab in metastatic urothelial carcinoma after platinum therapy (CheckMate 275): a multicentre, single-arm, phase 2 trial. Lancet Oncol. 2017;18(3):312-22.
4. Andrea BA, John Allan E, Jeffrey RI, Manish A, Michael SG, Raid A, et al. Updated efficacy and safety of avelumab in metastatic urothelial carcinoma (mUC): Pooled analysis from 2 cohorts of the phase 1b Javelin solid tumor study. Journal of Clinical Oncology. 2017;35(15_suppl):4528-.
5. Christophe M, Michael SG, Sunil S, Saeed R, Zev AW, Jason L, et al. Safety and Efficacy of Durvalumab (MEDI4736), an Anti–Programmed Cell Death Ligand-1 Immune Checkpoint Inhibitor, in Patients With Advanced Urothelial Bladder Cancer. Journal of Clinical Oncology. 2016;34(26):3119-25.
6. Rijnders M, de Wit R, Boormans JL, Lolkema MPJ, van der Veldt AAM. Systematic Review of Immune Checkpoint Inhibition in Urological Cancers. European Urology. 2017;72(3):411-23.
7. Powles T, Necchi A, Rosen G, Hariharan S, Apolo AB. Anti–Programmed Cell Death 1/Ligand 1 (PD-1/PD-L1) Antibodies for the Treatment of Urothelial Carcinoma: State of the Art and Future Development. Clinical Genitourinary Cancer. 2018;16(2):117-29.
8. Pakkala S, Owonikoko TK. Immune checkpoint inhibitors in small cell lung cancer. J Thorac Dis. 2018;10(Suppl 3):S460-S7.
9. Rosenberg JE, Hoffman-Censits J, Powles T, van der Heijden MS, Balar AV, Necchi A, et al. Atezolizumab in patients with locally advanced and metastatic urothelial carcinoma who have progressed following treatment with platinum-based chemotherapy: a single-arm, multicentre, phase 2 trial. Lancet. 2016;387(10031):1909-20.
10. Balar AV, Galsky MD, Rosenberg JE, Powles T, Petrylak DP, Bellmunt J, et al. Atezolizumab as first-line treatment in cisplatin-ineligible patients with locally advanced and metastatic urothelial carcinoma: a single-arm, multicentre, phase 2 trial. Lancet. 2017;389(10064):67-76.
11. Thomas P, Juergen EG, Yohann L, Joaquim B, Lajos G, Christof V, et al. Phase 3 KEYNOTE-361 trial: Pembrolizumab (pembro) with or without chemotherapy versus chemotherapy alone in advanced urothelial cancer. Journal of Clinical Oncology. 2017;35(15_suppl):TPS4590-TPS.
12. Matt DG, Enrique G, Ian DD, Maria De S, Jose Angel Arranz A, Eiji K, et al. IMvigor130: A randomized, phase III study evaluating first-line (1L) atezolizumab (atezo) as monotherapy and in combination with platinum-based chemotherapy (chemo) in patients (pts) with locally advanced or metastatic urothelial carcinoma (mUC). Journal of Clinical Oncology. 2018;36(15_suppl):TPS4589-TPS.
13. EMA restricts use of Keytruda and Tecentriq in bladder cancer 2018 (updated 01-06-2018. Available from: http://www.ema.europa.eu/ema/index.jsp?curl=pages/news_and_events/news/2018/05/news_detail_002964.jsp&mid=WC0b01ac058004d5c1.
14. FDA Alerts Health Care Professionals and Oncology Clinical Investigators about an Efficacy Issue Identified in Clinical Trials for Some Patients Taking Keytruda (pembrolizumab) or Tecentriq (atezolizumab) as Monotherapy to Treat Urothelial Cancer with Low Expression of PD-L1 (updated 20-06-2018. Available from: https://www.fda.gov/Drugs/DrugSafety/ucm608075.htm.
15. Landis JR, Koch GG. The measurement of observer agreement for categorical data. Biometrics. 1977;33(1):159-74.
16. Hodgson A, Slodkowska E, Jungbluth A, Liu SK, Vesprini D, Enepekides D, et al. PD-L1 Immunohistochemistry Assay Concordance in Urothelial Carcinoma of the Bladder and Hypopharyngeal Squamous Cell Carcinoma. Am J Surg Pathol. 2018.
17. Tretiakova M, Fulton R, Kocherginsky M, Long T, Ussakli C, Antic T, et al. Concordance study of PD-L1 expression in primary and metastatic bladder carcinomas: comparison of four commonly used antibodies and RNA expression. Mod Pathol. 2018;31(4):623-32.
18. Hirsch FR, McElhinny A, Stanforth D, Ranger-Moore J, Jansson M, Kulangara K, et al. PD-L1 Immunohistochemistry Assays for Lung Cancer: Results from Phase 1 of the Blueprint PD-L1 IHC Assay Comparison Project. J Thorac Oncol. 2017;12(2):208-22.
19. Tsao MS, Kerr KM, Kockx M, Beasley MB, Borczuk AC, Botling J, et al. PD-L1 immunohistochemistry comparability study in real-life clinical samples: results of Blueprint phase 2 project. J Thorac Oncol. 2018.
20. Mahoney KM, Sun H, Liao X, Hua P, Callea M, Greenfield EA, et al. Antibodies to the cytoplasmic domain of PD-L1 most clearly delineate cell membranes in immunohistochemical staining. Cancer immunology research. 2015;3(12):1308-15.
21. Kelly S, Emily AVV, Dorien S, Ingrid De M, Mark K. Epitope mapping of PD-L1 primary antibodies (28-8, SP142, SP263, E1L3N). Journal of Clinical Oncology. 2017;35(15_suppl):3028-.
22. Gaule P, Smithy JW, Toki M, Rehman J, Patell-Socha F, Cougot D, et al. A Quantitative Comparison of Antibodies to

Programmed Cell Death 1 Ligand 1. JAMA Oncol. 2016.
23. Pichler R, Heidegger I, Fritz J, Danzl M, Sprung S, Zelger B, et al. PD-L1 expression in bladder cancer and metastasis and its influence on oncologic outcome after cystectomy. Oncotarget. 2017;8(40):66849-64.
24. Mukherji D, Jabbour MN, Saroufim M, Temraz S, Nasr R, Charafeddine M, et al. Programmed Death-Ligand 1 Expression in Muscle-Invasive Bladder Cancer Cystectomy Specimens and Lymph Node Metastasis: A Reliable Treatment Selection Biomarker? Clin Genitourin Cancer. 2016;14(2):183-7.
25. Ilie M, Long-Mira E, Bence C, Butori C, Lassalle S, Bouhlel L, et al. Comparative study of the PD-L1 status between surgically resected specimens and matched biopsies of NSCLC patients reveal major discordances: a potential issue for anti-PD-L1 therapeutic strategies. Ann Oncol. 2016;27(1):147-53.
26. Gradecki SE, Grange JS, Stelow EB. Concordance of PD-L1 Expression Between Core Biopsy and Resection Specimens of Non-Small Cell Lung Cancer. Am J Surg Pathol. 2018.

SUPPLEMENTARY TABLES

Supplementary Table 1. Clinicopathological features of the study population.

		All patients (n = 139)
Age at diagnosis – median (range)		68 (33-91)
Gender – no. (%)	Male	113 (81.3)
	Female	26 (18.7)
Tissue type – no. (%)	Cystectomy	118 (84.9)
	TURB	21 (15.1)
Tumor Grade – no. (%)	G1	1 (0.7)
	G2	9 (6.5)
	G3	129 (92.8)
Tumor stage – no. (%)	T2	62 (44.6)
	T3	61 (43.9)
	T4	16 (11.5)
Nodal status – no. (%)	Positive	32 (23.0)
	Negative	73 (52.5)
	Unknown	34 (24.5)
Visceral metastasis – no. (%)	Yes	9 (6.5)
	No	113 (81.3)
	Unknown	17 (12.2)

Supplementary Table 2. Values are displayed as intra-class correlation coefficient (ICC), with 95% confidence interval.

Correlation of PD-L1 expression on tumor cells between assays

	22C3	28-8	SP142	SP263	E1L3N
22C3		0.709 (0.611-0.786)	0.252 (0.088-0.404)	0.632 (0.471-0.744)	0.334 (0.145-0.494)
28-8			0.213 (0.047-0.369)	0.647 (0.506-0.749)	0.316 (0.141-0.470)
SP142				0.134 (0-0.286)	0.07 (0-0.212)
SP263					0.505 (0.365-0.623)
E1L3N					

Correlation of PD-L1 expression on immune cells between assays

	22C3	28-8	SP142	SP263	E1L3N
22C3		0.659 (0.524-0.757)	0.409 (0.250-0.546)	0.538 (0.404-0.649)	0.603 (0.462-0.711)
28-8			0.429 (0.274-0.562)	0.656 (0.529-0.751)	0.501 (0.356-0.622)
SP142				0.623 (0.480-0.729)	0.641 (0.525-0.733)
SP263					0.550 (0.418-0.660)
E1L3N					

Low ICC — High ICC

CHAPTER 4

Comprehensive molecular characterization reveals genomic and transcriptomic subtypes of metastatic urothelial carcinoma

J. Alberto Nakauma-González‡
Maud Rijnders‡
Job van Riet
Michiel S. van der Heijden
Jens Voortman
Edwin Cuppen
Niven Mehra
Sandra van Wilpe
Sjoukje F. Oosting
L. Lucia Rijstenberg
Hans M. Westgeest
Ellen C. Zwarthoff
Ronald de Wit
Astrid A.M. van der Veldt
Harmen J.G. van de Werken‡
Martijn P.J. Lolkema‡
Joost L. Boormans‡

‡contributed equally

Published in European Urology, 2022 Apr;81(4):331-336

ABSTRACT

Recent molecular characterization of primary urothelial carcinoma (UC) may guide future clinical decision-making. For metastatic UC (mUC), a comprehensive molecular characterization is still lacking. We analyzed whole-genome DNA and RNA sequencing data for fresh-frozen metastatic tumor biopsies from 116 patients with mUC who were scheduled for palliative systemic treatment within the context of a clinical trial (NCT01855477 and NCT02925234). Hierarchical clustering for mutational signatures revealed two major genomic subtypes: GenS1 (67%), which was APOBEC-driven; and GenS2 (24%), which had a high fraction of *de novo* mutational signatures related to reactive oxygen species and is putatively clock-like. Significantly mutated genes (SMGs) did not differ between the genomic subtypes. Transcriptomic analysis revealed five mUC subtypes: luminal-a and luminal-b (40%), stroma-rich (24%), basal/squamous (23%), and a nonspecified subtype (12%). These subtypes differed regarding expression of key genes, SMGs, oncogenic pathway activity, and immune cell infiltration. We integrated the genomic and transcriptomic data to propose potential therapeutic options by transcriptomic subtype and for individual patients. This in-depth analysis of a large cohort of patients with mUC may serve as a reference for subtype-oriented and patient-specific research on the etiology of mUC and for novel drug development.

BRIEF CORRESPONDENCE

Urothelial cancer (UC) is a molecularly and clinically heterogeneous disease. Comprehensive molecular profiling has been restricted to primary UC (1,2), and a multi-omics characterization of metastatic UC (mUC) is still lacking in the literature. Because of the lethality of mUC, with few therapeutic options available for patients, a multi-omics characterization of mUC could aid in improving patient selection for new and existing therapies. To unravel the molecular landscape of mUC, we conducted a comprehensive genomic and transcriptomic analysis of freshly obtained metastatic biopsies from 116 patients with mUC (Supplementary Tables 1 and 2; see the Supplementary material for methods).

Analysis of whole-genome sequencing (WGS) data was performed on tissue samples from liver, lymph node, bone, and other metastatic sites. A stratification based on the proposed etiology of single-base substitution (SBS) COSMIC signatures (3) (Supplementary Table 3) using unsupervised consensus clustering revealed two major genomic subtypes. GenS1 (67%; Figure 1) was APOBEC-driven with a large contribution from APOBEC-associated SBS2 and SBS13 signatures (median 54%). GenS2 (24%) predominantly comprised tumors with low APOBEC mutagenesis and was characterized by COSMIC signatures of unknown etiology.

To further examine the etiology of these tumors, deconvolution of SBS patterns was performed to identify *de novo* mutational signatures (Supplementary Figure 1). This confirmed that GenS1 is APOBEC-driven, whereas GenS2 is dominated by *de novo* mutational signatures associated with reactive oxygen species (SigF; 0.91 cosine similarity with SBS18) and is putatively clock-like (SigG; 0.90 cosine similarity with SBS5). GenS1 and GenS2 have also previously been identified as the two major genomic subtypes in primary UC (4). GenS1 was characterized by a higher number of SBS than GenS2, whereas GenS2 had more small insertions and deletions (indels) than GenS1 (Supplementary Figure 2). Tumors with predicted homologous recombination deficiency were of subtype GenS2 (Fisher's exact test, $p = 0.02$).

The genes most frequently affected by structural variants (SVs) were *CCSER1* (13%) and *AHR* (12%). We identified 71 promoters that were frequently mutated (Supplementary Table 4) of which the promoters of *TERT* (64%), *LEPROTL1* (20%), and *GSTA4* (14%) had the highest mutation rate. *TERT* and *LEPROTL1* were predominantly affected by hotspot mutations. When considering coding and promoter alterations, *TERT* was mutated in 74% of cases. Mutations in the *LEPROTL1* promoter were more frequent in GenS1 than in GenS2 (Fisher's exact test, $p = 0.03$). Significantly mutated genes (SMGs; Supplementary Tables 5 and 6) resembled those reported in primary UC (2) and did not correspond with the genomic subtypes.

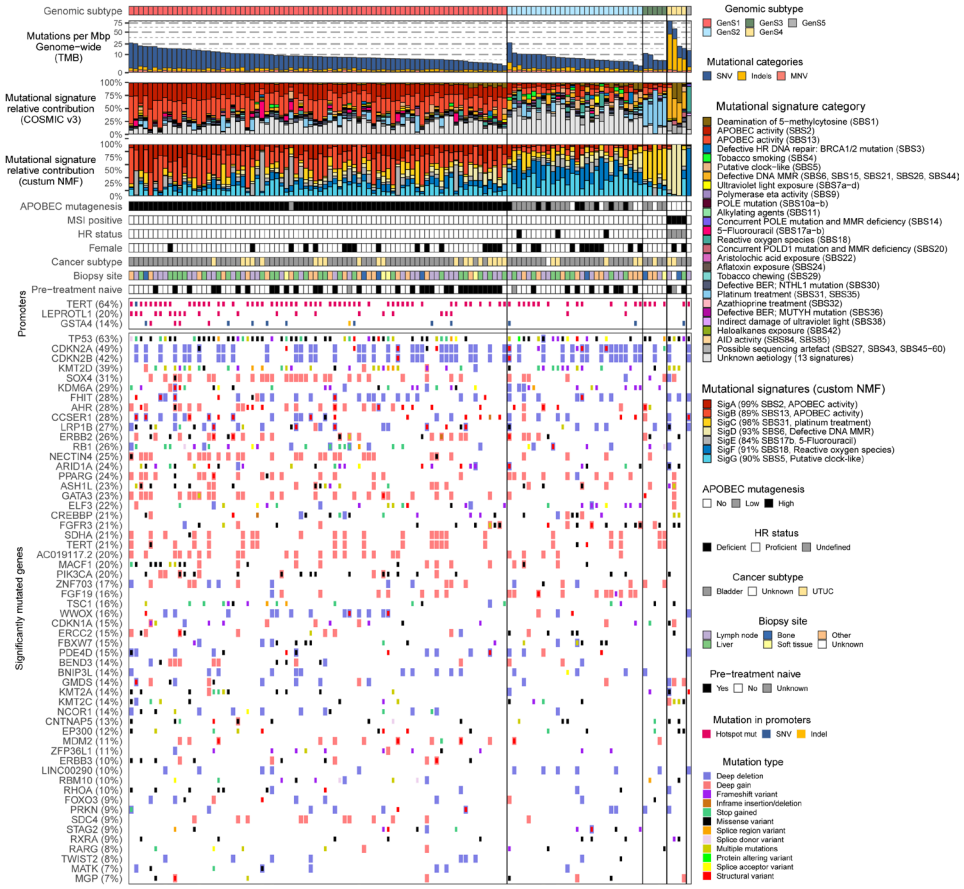

Figure 1. Genomic landscape for 116 metastatic urothelial carcinomas stratified by genomic subtype. The analysis was performed on whole-genome DNA sequencing data for freshly obtained biopsy samples from metastatic sites that were centrally reviewed to confirm the diagnosis of metastatic urothelial carcinoma. Tumor samples were classified into genomic subtypes via hierarchical consensus clustering of the relative contribution of COSMIC v3 mutational signatures (3) grouped by etiology. The genomic features are displayed from top to bottom as follows: genomic subtype (GenS1–5); genome-wide tumor mutational burden (TMB) as mutations per Mbp; mutational signatures grouped by etiology (MMR = mismatch repair); relative contribution of seven *de novo* (custom) mutational signatures via deconvolution of single-nucleotide variants (SNVs) in the 96 trinucleotide context with non-negative matrix factorization (NMF); APOBEC enrichment analysis showing tumors with no, low, and high APOBEC mutagenesis; tumors with microsatellite instability (MSI); homologous recombination (HR) status; female patients; site of origin of the primary tumor (UTUC = upper tract urothelial carcinoma); metastatic site from which a biopsy was obtained; systemic treatment-naïve patients; mutations in the promoter of genes present in >10% of samples; and overview of significantly mutated genes.

Clinical characteristics such as sex, primary cancer subtype, and pretreatment status did not differ between the subtypes. Response to treatment was better among patients with GenS1 in comparison to those with GenS2 tumors (Supplementary Figure 3). The less prevalent genomic subtypes (9%) were related to the platinum treatment signature (GenS3), the defective DNA mismatch repair signature and microsatellite instability (GenS4), and the reactive oxygen species signature (GenS5).

In conclusion, WGS analyses identified two major genomic subtypes of mUC that correlated with response to treatment. These subtypes resembled different mutagenic processes leading to the development of mUC, although both subtypes showed similar SMG profiles.

A consensus transcriptomic classifier was recently developed for primary UC (5). However, this classifier does not consider transcriptomic differences inherited from the metastatic site for mUC samples (Figure 2A) and therefore cannot be applied directly to the present metastatic cohort (6). Furthermore, transcriptomic subtyping of mUC has not been reported thus far. To identify mUC transcriptomic subtypes, we performed *de novo* subtyping of RNA sequencing (RNA-seq) data. Hierarchical consensus clustering was applied to organ-corrected paired RNA-seq data for 90 of the 116 patients with mUC (Supplementary Table 7) and revealed five transcriptomic subtypes (Figure 2B and Supplementary Table 8). The phenotypes of the five subtypes were established according to phenotypic signature scores (Supplementary Figure 4A).

We identified two luminal subtypes (40%) that exhibited high expression of the genes *PPARG*, *GATA3*, and *FGFR3* (Supplementary Figure 4). The luminal-a subtype had high expression of *PPARGC1B* and *MYCN*, low tumor purity, and a high fraction of natural killer (NK) cells. *NECTIN4* was amplified in 61% of these tumors (Fisher's exact test, $p < 0.001$) and expression of *NECTIN4* was high (Supplementary Figure 4). The luminal-b subtype had high tumor purity, a low number of SVs, a low fraction of NK cells, high expression of *MYC*, high Myc and RTK-RAS pathway activity (Supplementary Figures 4 and 5), and a higher proportion of *ELF3* (56%) and *FGFR3* (50%) DNA alterations (Fisher's exact test, $p = 0.002$ and $p = 0.005$) than the other subtypes.

Stroma-rich tumors (24%) showed high expression of *DDR2*, *PDGFRA*, collagens (Supplementary Table 9), and genes associated with stromal content and cancer-associated fibroblasts (*THBS4*, *CNTN1*, *CXCL14* and *BOC*) (7-9). Furthermore, these tumors had low tumor purity, a high signature score for epithelial-to-mesenchymal transition, high TGF-β pathway activity (Supplementary Figures 4 and 5), and a higher rate of *TSC1* DNA alterations than other subtypes (45%; Fisher's exact test, $p < 0.001$).

The basal/squamous subtype (23%) had high expression of basal and squamous markers (*DSG3*, *KRT5*, *KRT6A*, and *S100A7*), was enriched among females (52%; Fisher's exact test, p = 0.004), had a large fraction of M1 macrophages, and was associated with the poorest outcomes (Supplementary Figure 3). TGF-β and Myc pathway activity and expression levels of *TGFBR1*, *MYC*, *CD274* (PD-L1), and *MSLN*—a tumor-associated antigen—were high. Amplification of *NECTIN4* was absent (Fisher's exact test, p = 0.001) and *NECTIN4* expression was low.

The nonspecified subtype (12%) did not clearly overexpress any of the phenotypic markers associated with a basal, squamous, luminal, stromal, or neuroendocrine phenotype, but had a high score for claudin markers, high numbers of indels and SVs, high expression of *APOBEC3B*, high cell-cycle pathway activity, and low p53 pathway activity (Supplementary Figures 4 and 5). This subtype was enriched among patients who were previously treated with chemotherapy (Fisher's exact test, p = 0.023).

Next, we assessed the clinical relevance of genomic alterations and identified potential targetable mutations in 114 of 116 patients with mUC, including on- and off-label treatment modalities for UC as well as therapies approved for other tumor types (Supplementary Figure 6A). In addition, the transcriptomic subtypes may guide the identification of potential therapeutic targets (Supplementary Figure 6B; the Supplementary material describes the rationale for therapeutic options for patients with mUC). Tumors of the luminal-a subtype could benefit from NK cell enhancers and FGFR or PPARγ inhibitors, whereas the luminal-b subtype might be susceptible to FGFR, BET, and RAS pathway inhibitors. The stroma-rich subtype could be sensitive to immune checkpoint inhibitors (ICIs) combined with TGF-β inhibitors. The basal/squamous subtype could benefit from mesothelin-targeted therapy, BET inhibitors, or ICIs plus a TGF-β inhibitor. Individualized targeted therapy should be prioritized in patients with tumors of the nonspecified subtype.

Limitations of the study include the lack of matched primary tumor samples, the heterogeneity of the study population, and the lack of pathology-based data. Despite these limitations, the study defined for the first time the molecular subtypes of mUC on the basis of whole-genome and transcriptome analyses of metastatic biopsies from 116 patients with mUC. The findings improve our understanding of the molecular landscape of mUC and may serve as a reference for future drug development in this disease setting.

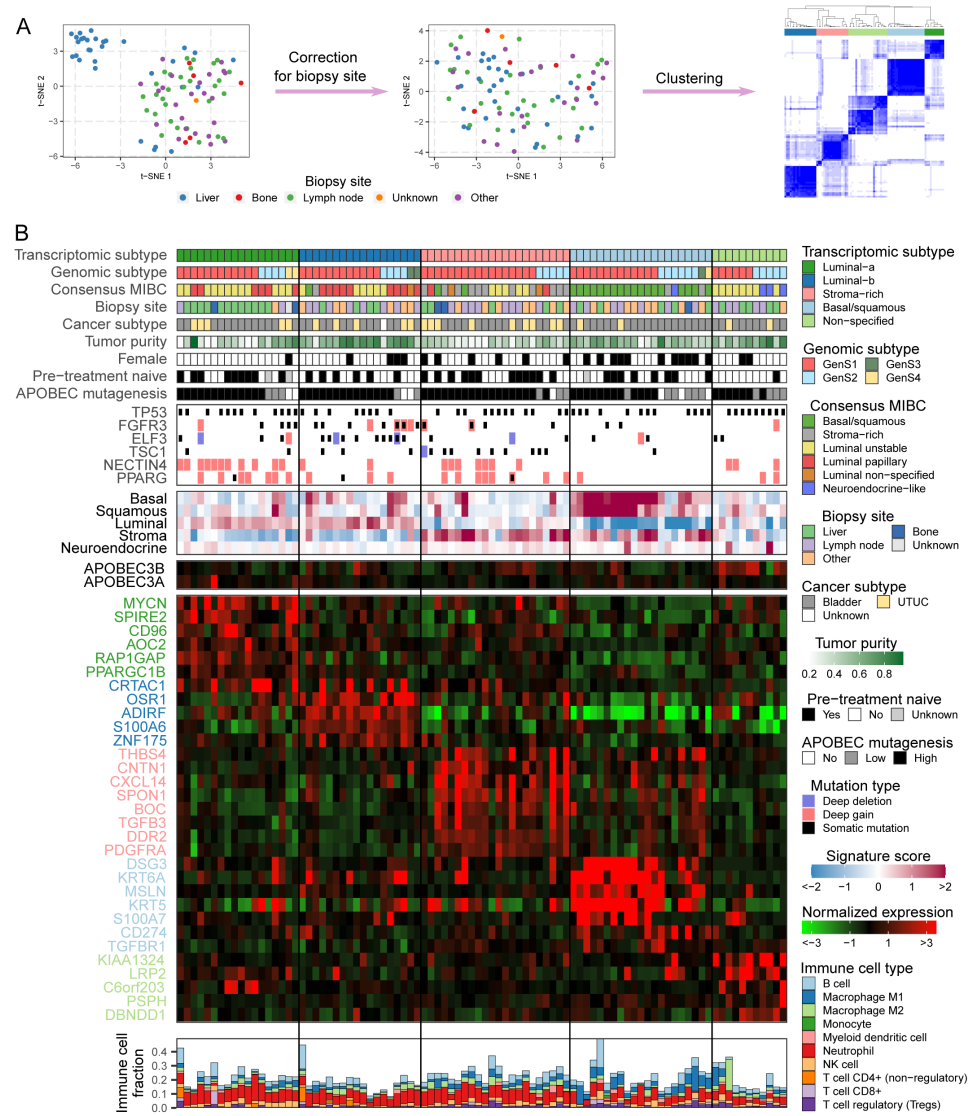

Figure 2. Genomic and transcriptomic characteristics of metastatic urothelial carcinoma stratified by transcriptomic subtype.
A. Strategy in the present study to identify transcriptomic subtypes from tissue samples derived from different metastatic biopsy sites for 90 patients with metastatic urothelial carcinoma. Hierarchical consensus clustering was applied on transcriptomic profiles corrected for biopsy site (see the Supplementary material for details). **B.** Five transcriptomic subtypes were identified: luminal-a, luminal-b, stroma-rich, basal/squamous, and nonspecified. Features per sample are displayed from top to bottom as follows: transcriptomic subtype; genomic subtype (GenS1–4); transcriptomic subtype according to the consensus classifier for primary muscle-invasive bladder cancer (MIBC) (5); metastatic site from which a biopsy was obtained; site of origin of the primary tumor (UTUC = upper tract urothelial carcinoma); estimated tumor cell percentage; female patients; systemic pretreatment-naïve patients; APOBEC enrichment analysis showing tumors with no, low, and high APOBEC mutagenesis; tumors with genomic alterations in selected genes; signature score (mean expression of genes related to each phenotype) for basal, squamous, luminal, stroma, and neuroendocrine markers; *APOBEC3B* and *APOBEC3A* expression; top overexpressed genes; and immune cell fractions.

REFERENCES

1. Lindskrog SV, Prip F, Lamy P, et al. An integrated multi-omics analysis identifies prognostic molecular subtypes of non-muscle-invasive bladder cancer. Nat Commun 2021;12:2301.
2. Robertson AG, Kim J, Al-Ahmadie H, et al. Comprehensive Molecular Characterization of Muscle-Invasive Bladder Cancer. Cell 2017;171:540-556.e25.
3. Tate JG, Bamford S, Jubb HC, et al. COSMIC: The Catalogue Of Somatic Mutations In Cancer. Nucleic Acids Res 2019;47:D941–7.
4. Taber A, Christensen E, Lamy P, et al. Molecular correlates of cisplatin-based chemotherapy response in muscle invasive bladder cancer by integrated multi-omics analysis. Nat Commun 2020;11:1–15.
5. Kamoun A, Reyniès A de, Allory Y, et al. A Consensus Molecular Classification of Muscle-invasive Bladder Cancer. Eur Urol 2019;77:420–33.
6. Williams SB, Black PC, Dyrskjøt L, et al. Re: Aurélie Kamoun, Aurélien de Reyniès, Yves Allory, et al. A Consensus Molecular Classification of Muscle-invasive Bladder Cancer. Eur Urol 2020;77:420–33: A Statement from the International Bladder Cancer Network. Eur Urol 2020;77:e105–6.
7. Kuroda K, Yashiro M, Sera T, et al. The clinicopathological significance of Thrombospondin-4 expression in the tumor microenvironment of gastric cancer. PLoS One 2019;14:e0224727.
8. Gu Y, Li T, Kapoor A, Major P, Tang D. Contactin 1: An important and emerging oncogenic protein promoting cancer progression and metastasis. Genes (Basel) 2020;11:1–22.
9. Mathew E, Zhang Y, Holtz AM, et al. Dosage-dependent regulation of pancreatic cancer growth and angiogenesis by Hedgehog signaling. Cell Rep 2014;9:484–94.

SUPPLEMENTARY DATA

Rationale on therapeutic options for patients with mUC

In a previous study (1), the genomic landscape of 85 (72 re-analyzed here) patients with mUC was compared with that of other metastatic tumor types. This pan-cancer study concluded that mUC was characterized by high TMB, with no difference between mUC and primary UC, high CNAs, the highest number of driver genes among all cancer types analyzed, and actionable targets in 75% of the patients. In the present study, we identified a potential targetable alteration in the genome of 98% of the 116 patients (Supplementary Figure 5A, Supplementary Table 9). In line with Priestley et al., 2019, we found that 41% of patients could benefit from on-label therapies, and 63% from therapies approved by the US Food and Drug Administration for other tumor types. Additionally, we identified targets for therapies under investigation in clinical trials including basket trials in 109 of 116 patients. We identified four patients with MSI-high tumors that are potentially sensitive to immune checkpoint inhibitors (2). HR deficiency, observed in three patients, is a potential target for treatment with poly-ADP ribose polymerase inhibitors and/or double-stranded DNA break-inducing chemotherapy. At the RNA level, targetable FGFR3 and NTRK2 gene fusions were identified in eight patients.

In a previous study, the antibody-drug conjugate enfortumab vedotin targeting NECTIN4 induced objective clinical responses in 44% of patients with mUC who experienced disease progression following chemotherapy and anti-PD1/L1 therapy (3). Currently, preselection for this treatment is not required. However, we found significant variation in the expression of NECTIN4, suggesting that patients with tumors of the basal/squamous subtype may be less likely to experience clinical benefit of enfortumab vedotin, as no NECTIN4 amplifications were detected, and NECTIN4 expression levels were low. The 23 patients with HER2 aberrations may be sensitive to HER2 targeting agents; especially some of the newer antibody-drug conjugates with DNA damaging payloads could represent an effective treatment (4, 5).

Based on the identified transcriptomic subtypes, we suggested potential therapeutic targets per subtype. The luminal-a subtype was characterized by PPARGC1B overexpression and PPARG amplification/overexpression. In pre-clinical studies, PPARγ-inhibitor downregulated the expression levels of PPARG, and this inhibitor had an antiproliferative effect on tumor cells (6). PPARγ is essential in normal tissue and only a partial inhibition of PPARG could be considered for this subtype. FGFR3 was mutated and highly expressed in this subtype, which could benefit patients with FGFR inhibition. The immune cell compartment of tumors of the luminal-a subtype was found to be enriched for NK cells, which could be explained by the large fraction of liver biopsies, as the liver is enriched for NK cells (7). Thus, other potential treatment strategies comprise

of cytokine-mediated stimulation of NK cells and TLR agonists (8).

The luminal-b subtype showed high expression of MYC and high myc pathway activity for which treatment with a BET-inhibitor could be considered (9). Enrichment for FGFR3 mutations and high expression of FGFR3 was also observed, suggesting that this subtype may be susceptible to treatment with FGFR inhibitors. This subtype may also be sensitive to RAS pathway inhibitors as the RTK-RAS pathway activity was high (10).

Compared with the other subtypes, the stroma-rich subtype displayed the highest TGF-β pathway activity and overexpression of different collagens. Previous studies showed that TGF-β stimulated cancer-associated fibroblasts to produce collagens (11, 12). Other studies found that TGF-β expression was associated with resistance to immune checkpoint inhibition in UC (13, 14). Results from pre-clinical studies in mUC suggest that addition of a TGF-β inhibitor may improve anti-PD1 efficacy (15).

The basal/squamous subtype was associated with high immune cell infiltration (significantly more M1 macrophages) and overexpression of PD-L1, which suggests that patients with tumors of this subtype are likely to benefit from immunotherapy (16). Since TGF-β pathway activity was also high in this subtype, combination therapy with a TGF-β inhibitor could be of added value. Treatment with BET inhibition could also be considered as high expression of MYC and high myc pathway activity was observed in this subtype. Furthermore, this subtype was characterized by overexpression of mesothelin, a known tumor antigen that is being investigated as a target for antibody-based, vaccine and CAR-T cell therapies in several tumor types (17).

Methods

Data and code availability

All code and scripts are available at https://github.com/hartwigmedical/ and at https://bitbucket.org/ccbc/dr31_hmf_muc/.

Pre-processed WGS data, RNA-seq data and corresponding clinical data have been requested from the Hartwig Medical Foundation (HMF) and were provided under data request number DR-031. All data are freely available for academic use from the HMF through standardized procedures. Request forms can be found at https://www.hartwigmedicalfoundation.nl.

Patient cohort and study procedures

Between 07 June 2012 up to and including 28 February 2019, patients with advanced or mUC (n = 210) from 23 Dutch hospitals who were scheduled for 1st or 2nd line palliative systemic treatment were included in the Dutch nationwide study of the Center for Personalized Cancer Treatment (CPCT) consortium (CPCT-02 Biopsy Protocol, NCT01855477 (1)) and the Drug Rediscovery Protocol (DRUP Trial, NCT02925234), which aimed to analyze the cancer genome and transcriptome of patients with advanced cancer. The CPCT-02 and DRUP study protocols were approved by the medical ethics review board of the University Medical Center Utrecht and the Netherlands Cancer Institute, respectively. Patients eligible for inclusion were those aged ≥18 years old, with locally advanced or mUC, from whom a histological tumor biopsy could be safely obtained, and whom had an indication for initiation of a new line of systemic treatment with anti-cancer agents. Written informed consent was obtained from all participants prior to inclusion in the trial; the studies comply with all relevant ethical regulations. Tumor biopsies, matched normal blood samples and the associated clinical data were collected following standardized procedures (18). Biopsies were obtained from a safely accessible site, including lymph nodes, liver, bone and other organs. In five patients, a tumor biopsy was obtained from the primary bladder or upper urinary tract tumor as no safely accessible metastatic lesion was present. In two patients, a biopsy was obtained from a local recurrence after cystectomy and nephroureterectomy, respectively. WGS was successfully performed on DNA from 116 out of 210 patients with mUC, and matched RNA-seq was available for 90 out of 116 patients. This study extends the pan-cancer analysis of Priestley et al., 2019, in which WGS (but not RNA-seq) data of 72 patients with mUC included in the current cohort were previously analyzed. Best overall survival (BOR), as reported on the 6th of February 2020, were available for 85 patients. Treatment response was measured according to response evaluation criteria in solid tumors (RECIST) v1.1. Responders were considered those patients with a complete response (CR) or a partial response (PR) and non-responders as those with stable disease (SD) or progressive disease (PD). The proportion of responders was 42% (36 out of 85 patients). The median time to BOR was 69 days (range: 22-335 days).

Whole-genome sequencing and analysis

Whole-genome DNA sequencing, alignment and data processing

Sufficient amount of DNA was extracted from fresh-frozen tumor tissue and blood samples following standard protocols from Qiagen. Between 50-200 ng of DNA was fragmented by sonication for NGS TruSeq library preparation and sequenced paired-end reads of 2x150 bases with the Illumina HiSeqX platform. Alignment, somatic alterations, ploidy, sample purity and copy number estimations were performed as previously described (1). WGS was aligned to the human reference genome GRCH37 with BWA-mem v.0.7.5a (19), and duplicate reads were marked for filtering. Indels were realigned using GATK IndelRealigner v3.4.46 (20). Recalibration of base qualities for single nucleotide variants (SNVs) and small insertions and deletions (Indels) was performed with GATK BQSR (21), and SNV and Indel variants were evaluated with Strelka v.1.0.14 (22) using matched blood WGS as normal reference. Somatic mutations were further annotated with Ensembl Variant Effect Predictor (VEP, v99, cache 99_GRCh37) (23) using

GENCODE v33 in combinations with the dbNSFP plugin v3.5 hg19 (24) for gnomAD (25) population frequencies. SNVs, Indels and multiple nucleotide variants (MNVs) variants were removed if the following filters were not passed: default Strelka filters (PASS-only), gnomAD exome (ALL) allele frequency <0.001, gnomAD genome (ALL) <0.005 and number of reads <3. In addition, structural variants (SVs) and copy number changes were estimated using GRIDSS, PURPLE and LINX suit v2.25 (26). SVs that passed the default QC filters (PASS-only) and Tumor Allele Frequency (TAF) ≥0.1 were annotated as "somatic SVs" if there was overlap with coding region. Mean read coverages of tumor and reference samples were estimated using Picard Tools v1.141 (CollectWgsMetrics) based on GRCh37 (https://broadinstitute.github.io/picard/). The median WGS coverage for tumor and normal tissue were 104x and 38x, respectively. Description of quality control and the bioinformatics pipeline have been previously reported (1). To estimate the number of mutations per mega-base pair (Mbp), the total number of somatic mutations in the whole genome was divided by 2,858.67.

APOBEC enrichment and mutagenesis

For each sample, the total number of C>T or C>G (G>A or G>C) mutations was calculated ($C^{mut\ (C>T,C>G)}$). From these mutations, the total number of APOBEC mutations was estimated by counting all mutations in TCW (WGA) context (TCW^{Cmut}), where W = A or T. The total number of TCW (WGA) motifs and total C (G) nucleotides in the hg19 reference genome were also estimated ($TCW^{context}$ and $C^{context}$, respectively). Using this information and following Roberts *et al.*, 2013 , a contingency table was constructed; one-sided Fisher's exact test was applied to calculate the overrepresentation of APOBEC mutations. P-values were Benjamini-Hochberg corrected. Tumors with adjusted p-values lower than 0.01 were considered APOBEC enriched.

The magnitude of APOBEC enrichment E was estimated as (27)

$$E = \frac{\mathrm{TCW}^{Cmut} \cdot \mathrm{C}^{context}}{\mathrm{TCW}^{context} \cdot \mathrm{C}^{mut(C>T,C>G)}}. \qquad (1)$$

APOBEC enriched tumors (always $E>1$) were classified as high APOBEC mutagenesis when $E \geq 2$, and as low APOBEC mutagenesis when $E<2$. Tumors without APOBEC enrichment were considered tumors with no APOBEC mutagenesis.

Detection of significantly mutated genes using dN/dS ratios

Cancer driver genes under strong positive selection were detected using a statistical model that combines the ratio of non-synonymous to synonymous mutations and covariates (dNdScv) v0.0.0.9 (28). This model uses 192 mutation rates representing all combinations in trinucleotide context. Mutation rates of each gene were corrected by

the global mutation rate. The ratio of non-synonymous over synonymous mutations was calculated with maximum-likelihood methods, and statistical significance was estimated. Genes with either qglobal_cv ≤0.05 or qallsubs_cv ≤0.05 were considered drivers of mUC.

Detection of recurrent copy number alterations to identify significantly mutated genes
Ploidy and copy number alterations (CNAs) were estimated as described by Priestley et al. 2019; and following the pipeline described by van Dessel et al., 2019. Recurrent focal and broad CNAs were estimated with GISTIC2.0 v2.0.23 (30). CNAs were classified as shallow or deep according to the threshold in GISTIC2 calls. Significant recurrent focal CNAs were identified when q ≤0.05 and annotated with genes overlapping these regions, which were considered drivers.

Detection of mutations in promoters

The promoter region was defined as 1,000 bp upstream the transcription start site. SNVs, Indels and MNVs mutations occurring in this region were analyzed. Hotspot mutations were those occurring more than once in the same position.

Mutational signatures and genomic subtypes

An advantage of using WGS over other next generation sequencing techniques is that mutational signatures can be deconvoluted from all samples as the number of mutations is much higher for WGS. This allowed us to stratify all patients into genomic subtypes.

The mutational pattern of each sample was established by categorizing SNVs according to their 96-trinucleotide context. The contribution of each of the 67 mutational signatures from COSMIC v3 (as deposited in May 2019) (31) was subsequently estimated with MutationalPatterns v1.4.2 (32). To reduce the noise attributed to mutational signatures with very low contribution, mutational signatures were grouped into 26 proposed etiology categories derived from Alexandrov et al., 2020, Petljak et al., 2019, Angus et al., 2019 and Christensen et al., 2019. All 26 proposed etiology contributions were used, and hierarchical clustering was applied on 1-Pearson's correlation coefficient, 80% resampling and 1,000 iterations using ConsensusClusterPlus v1.48.0 (37). Considering average stability of each cluster and the cluster size (favoring large clusters) after each partition, samples were grouped into five distinct clusters.

Independently, mutational patterns were deconvoluted to estimate *de novo* mutational signatures. Non-negative Matrix Factorization from the NMF R package v0.21.0 was used with 1000 iterations (38). Evaluating different metrics provided by the NMF R package (high cophenetic correlation coefficient, high dispersion coefficient, high silhouette consensus, high sparseness basis and low sparseness coefficients), seven *de novo*

signatures were recovered from the mutational patterns. Cosine similarity was applied to compare the *de novo* signatures with mutational signatures from COSMIC v3.

Microsatellite instabilty (MSI) status

As previously described (1), MSI status was determined by estimating the MSI score as the number of indels (length <50 bp) per Mbp occurring in homopolymers of five or more bases, dinucleotide, trinucleotide and tetranucleotide sequences of repeat count above five. Tumors with MSI score >4 were considered MSI positive.

Detection of homologous recombination (HR) deficiency

The Classifier for Homologues Recombination Deficiency (CHORD; v2.0) with default parameters was used to identify tumors with HR proficiency and deficiency (39). Four samples had very high number of indels corresponding with MSI samples and were excluded for the HR deficiency analysis.

Inventory of clinically actionable somatic alterations and putative therapeutic targets

Current clinical relevance of somatic alterations in relation to putative treatment options or resistance mechanisms and trial eligibility was determined based upon the following databases: CiViC (40) (Nov. 2018), OncoKB (41) (Nov. 2018), CGI (42) (Nov. 2018) and the iClusion (Dutch) clinical trial database (Sept. 2019, Rotterdam, the Netherlands). The databases were aggregated and harmonized using the HMF knowledgebase-importer (v1.7; https://github.com/hartwigmedical/hmftools/tree/master/knowledgebase-importer). Subsequently, we curated the linked putative treatments and selected treatments for which level A (biomarker for approved therapy or in guidelines) or level B (biomarker on strong biological evidence or used in clinical trials) evidence was available. Genomic alterations that confer resistance to certain therapies were excluded from the analysis. Treatment strategies including anti-hormonal therapy (as used for breast and prostate cancer), surgical resection, or radioiodine uptake therapy were excluded. Furthermore, closed trials (according to www.clinicaltrials.gov), and trials with only pediatric patients or patients with hematological malignancies were excluded. The data base was complemented with FGFR3 and NTRK2 gene fusions (at RNA level) and patients with MSI high and HR deficient tumors. On-label treatments included chemotherapy (cisplatin, gemcitabine, doxorubicin, mitomycin, and valrubicin) and the FGFR3 inhibitor erdafitinib. Off-label treatments included treatments that are on-label for other tumor types (FDA approved drugs according to the US national cancer institute; https://www.cancer.gov/about-cancer/treatment/drugs/cancer-type), and treatments available in clinical trials or basket trials. When patients had more than one possible treatment, on-label treatment was the preferred treatment, followed by on-label treatments for other tumor types.

Transcriptome sequencing and analysis

RNA-sequencing, alignment and data pre-processing

Total RNA was extracted using the QIAGEN QIAsymphony kit (Qiagen, FRITSCH GmbH, Idar-Oberstein, Germany). Samples with a minimum of 100 ng total RNA were sequenced according to the manufacturer's protocols. Paired-end sequencing of RNA was performed on the Illumina NextSeq 550 platform (2x75bp) and Illumina NovaSeq 6000 platform (2x150bp).

Prior to alignment, samples were visually inspected with FastQC v0.11.5. Sequence adapters (Illumina TruSeq) were trimmed using Trimmomatic v0.39 (43) at the following settings: ILLUMINACLIP:adapters.fa:2:30:10:2:keepBothReads MINLEN:36. The trimmed paired-end reads were aligned to the human reference (GRCh37) using STAR v2.7.1a (44) with genomic annotations from GENCODE hg19 release 30 (45). Multiple lanes and runs per sample were aligned simultaneously and given respective read-group identifiers for use in downstream analysis to produce two BAM files per sample, consisting of genome- and transcriptome-aligned reads respectively.

STAR was performed using the following command:

```
STAR --genomeDir <genome> --readFilesIn <R1> <R2> --readFilesCommand
zcat --outFileNamePrefix <outPrefix> --outSAMtype BAM
SortedByCoordinate --outSAMunmapped Within --chimSegmentMin 12
--chimJunctionOverhangMin 12 --chimOutType WithinBAM --twopassMode
Basic --twopass1readsN -1 --runThreadN 10 --limitBAMsortRAM 10000000000
--quantMode TranscriptomeSAM --outSAMattrRGline <RG>
```

After alignment, duplicate reads were marked, and alignment quality metrics (flagstat) were generated using Sambamba v0.7.1 (46). For each genome-aligned sample, the uniformity of read distributions across transcript lengths was assessed using tin.py v2.6.6 (47) from the RseQC library v3.0.0 (48).

FeatureCounts v1.6.3 (49(was applied to count the number of overlapping reads per gene using genomic annotations from GENCODE (hg19) release 30 (45); only primary (uniquely mapped) reads were counted per exon and summarized per gene:

```
featureCounts -T 50 -t exon -g gene_id --primary -p -s 2 -a <gencode> -o
<output> <genomic BAMs>
```

RSEM v1.3.1 (50) was applied to quantify RNA expression into transcripts per million (TPM) values using transcript annotations from GENCODE (hg19) release 30 (45):

```
rsem-calculate-expression --bam --paired-end --strand-specific --alignments
-p 8 <transcriptome BAM> <RSEM Index> <output>
```

Transcriptomic subtypes: clustering samples by RNA-seq data

Several methods have been proposed to classify bladder cancer into transcriptomic subtypes. In an attempt to standardize the molecular profiling of bladder cancer, a consensus molecular classification was proposed for MIBC based on RNA-seq data from 1750 patients (51). This classifier was developed strictly for MIBC and is not directly applicable to mUC (52). Furthermore, this classifier was developed for samples derived from the same organ carrying transcriptomic contamination of normal urothelial cells. In this study, biopsies were obtained from metastatic sites leading to contamination with normal cells from multiple different organs for which no correction was applied in the consensus classifier. Therefore, it was mandatory to perform *de novo* subtyping in this study, which is described below.

Multiple methods were explored to correct for the bias of biopsy site, including batch-correction with DESeq2 (53), and a tissue-aware correction method developed by the Genotype-Tissue Expression (GTEx) project (54). In both cases, transcripts from liver tissue were very dominant and clustered together in one stable cluster. The tissue-specific transcript removal method described above was successfully able to correct for organ-specific transcripts, and as a result, samples were clustered based on transcriptomic features rather than biopsy site.

Transcripts were normalized using DESeq2 v1.24.0 (53) with variance stabilizing transformation. Only highly expressed mRNA with base mean above 100 was kept. The top 50% most variably expressed genes (6,398 transcripts) were used for clustering. To reduce the 'transcriptomic noise' introduced by normal cells of the tissue from which the biopsy was taken, these transcripts were identified and excluded. Samples were grouped according to their biopsy site: liver (n = 31), lymph node (n = 30), bone (n = 5), other (n = 23) and unknown (n = 1). Differential expression analysis was performed to compare tumors from a specific biopsy site (liver, lymph node and bone) against all other tumors using DESeq2 with Wald test p-value estimation. Tissue-specific transcripts with log2 Fold Change (log2FC) >1.0 and Benjamini-Hochberg corrected p-value <0.05 were considered differentially expressed and identified as tissue-specific. A total of 689 transcripts were tissue-specific and were removed from the data set.

The remaining 5,709 transcripts were grouped by hierarchical clustering with 1-Pearson's correlation coefficient, 80% resampling and 1,000 iterations using ConsensusClusterPlus v1.48.0 (37). The mean cluster consensus value was obtained as a measure of cluster stability. Increasing the number of clusters will increase the stability by creating smaller clusters. Taking this into account, the criteria for selecting five clusters was based on cluster stability and cluster size by not allowing clusters with <5 samples. Patients with primary upper tract tumors did not cluster together as was observed for biopsy sites, instead they were distributed across all different transcriptomic clusters, suggesting that their influence on the clustering was negligible.

To identify transcripts that contribute most to each cluster, we followed the same strategy used to identify tissue-specific transcripts. The top five transcripts with the highest log2FC and with Benjamini-Hochberg adjusted p-values lower than 1x10-5 were identified as the most overexpressed genes per cluster. Other differentially expressed genes were included for their clinical relevance (*PPARGC1B*, *TGFB3*, *DDR2*, *PDGFRA*, *CD274* and *TGFBR1*). All differentially expressed genes per cluster with adjusted p $<1x10^{-5}$ and $\log_2$FC >1 are listed in Supplementary Table 8.

To compare our classification system developed for mUC with the consensus classifier, all samples were classified into one of six molecular classes identified in MIBC. All normalized transcripts (excluding biopsy specific transcripts) were used as input for the consensus classifier of primary MIBC (v1.1.0) (51). Both stratification systems were highly concordant regarding the stroma-rich and basal/squamous subtypes. The luminal subtypes as a whole were also similar, although characteristics of individual mUC luminal subtypes were different from the luminal MIBC subtypes. The non-specified mUC subtype was classified mainly as luminal by the consensus classifier, despite the low signature score for luminal markers (Supplementary Figure 3A).

Phenotypic markers and signature score

Marker genes for basal (*CD44, CDH3, KRT1, KRT14, KRT16, KRT5, KRT6A, KRT6B, KRT6C*), squamous (*DSC1, DSC2, DSC3, DSG1, DSG2, DSG3, S100A7, S100A8*), luminal (*CYP2J2, ERBB2, ERBB3, FGFR3, FOXA1, GATA3, GPX2, KRT18, KRT19, KRT20, KRT7, KRT8, PPARG, XBP1, UPK1A, UPK2*), neuroendocrine (*CHGA, CHGB, SCG2, ENO2, SYP, NCAM1*), cancer-stem cell (*CD44, KRT5, RPSA, ALDH1A1), EMT (ZEB1, ZEB2, VIM, SNAI1, TWIST1, FOXC2, CDH2*) and claudin (*CLDN3, CLDN7, CLDN4, CDH1, SNAI2, VIM, TWIST1, ZEB1, ZEB2)* were used for signature scores (16). Stroma (*FAP*), interferon, and CD8+ effector T cell (*IFNG, CXCL9, CD8A, GZMA, GZMB, CXCL10, PRF1, TBX21*) markers were also included (13). All normalized expression values were median centered, and the mean expression of each group of genes was defined as signature score.

Pathway activity score

Transcriptionally activated genes by the eleven canonical pathways analyzed in this study were used to estimate pathway activity score. All normalized expression values were median centered, and the mean expression of each group of genes was defined as activity score. Activity score was estimated for the TGFβ pathway (*ACTA2, ACTG2, ADAM12, ADAM19, CNN1, COL4A1, CCN2, CTPS1, RFLNB, FSTL3, HSPB1, IGFBP3, PXDC1, SEMA7A, SH3PXD2A, TAGLN, TGFBI, TNS1, TPM1*) (15), cell cycle pathway (*MKI67, CCNE1, BUB1, BUB1B, CCNB2, CDC25C, CDK2, MCM4, MCM6, MCM2*) (13), WNT pathway (*EFNB3, MYC, TCF12, VEGFA*) (15), Notch pathway (*HES1, HES5, HEY1*) (55), PI3K pathway (*AGRP, BCL2L11, BCL6, BNIP3, BTG1, CAT, CAV1, CCND1, CCND2, CCNG2, CDKN1A, CDKN1B, ESR1, FASLG, FBXO32, GADD45A, INSR, MXI1, NOS3, PCK1, POMC, PPARGC1A, PRDX3, RBL2, SOD2, TNFSF10*) (56), hippo pathway (*TAZ, YAP1*) (57), p53 pathway (*CDKN1A, RRM2B, GDF15, SUSD6, BTG2, DDB2, GADD45A, PLK3, TIGAR, RPS27L, TNFRSF10B, TRIAP1, ZMAT3, BAX, BLOC1S2, PGF, POLH, PPM1D, PSTPIP2, SULF2, XPC*) (58), Nrf2 pathway (*GCLM, NQO1, PHGDH, PSAT1, SHMT2*) (59), MYC pathway (*TFAP4, BMP7, CCNB1, CCND2, CCNE1, CDC25A, CDK4, CDT1, E2F1, GATA4, HMGA1, HSP90AA1, JAG2, CDCA7, LDHA, MCL1, NDUFAF2, MTA1, MYCT1, NPM1, ODC1, SPP1, PIN1, PTMA, PRDX3, PRMT5, DNPH1, TFRC, EMP1, PMEL, C1QBP*) (60), RTK-RAS pathway (*SPRY2, SPRY4, ETV4, ETV5, DUSP4, DUSP6, CCND1, EPHA2, EPHA4*) (61) and JAK-STAT pathway (*IRGM, ISG15, GATA3, FCER2, THY1, NFIL3, ARG1, RETNLB, CLEC7A, CHIA, OSM, BCL2L1, CISH, PIM1, SOCS2, GRB10*) (62).

Immune cell infiltration

To quantify immune cell fractions in each sample, we analyzed RSEM read counts of all transcripts with immunedeconv v2.0.3 (63) using the quanTIseq method (64).

Statistical analysis

Two-sided Fisher's exact test was used to compare frequency of categorical variables between two groups. Other statistical tests used are mentioned when describing significance including Wald test for differential expression analysis, Wilcoxon rank-sum test, Kruskal-Wallis test, and tests performed by dNdScv (28) and GISTIC20 (30). In cases of multiple testing, p-values were Benjamini-Hochberg corrected. All statistical analyses were performed using the statistical computing and graphics platform R v3.6.1 (65).

REFERENCES

1. Priestley P, Baber J, Lolkema MP, Steeghs N, de Bruijn E, Shale C, et al. Pan-cancer whole-genome analyses of metastatic solid tumours. Nature 2019;575:210–6.
2. Pivot XB, Bondarenko I, Dvorkin M, Trishkina E, Ahn J-H, Im S-A, et al. A randomized, double-blind, phase III study comparing SB3 (trastuzumab biosimilar) with originator trastuzumab in patients treated by neoadjuvant therapy for HER2-positive early breast cancer. J Clin Oncol 2017;35:509–509.
3. Rosenberg JE, O'Donnell PH, Balar A V., McGregor BA, Heath EI, Yu EY, et al. Pivotal Trial of Enfortumab Vedotin in Urothelial Carcinoma After Platinum and Anti-Programmed Death 1/Programmed Death Ligand 1 Therapy. J Clin Oncol 2019;37:2592–600.
4. Boni V, Sharma MR, Patnaik A. The Resurgence of Antibody Drug Conjugates in Cancer Therapeutics: Novel Targets and Payloads. Am Soc Clin Oncol Educ B 2020;40:e58–74.
5. Sheng X, Yan X, Wang L, Shi Y, Yao X, Luo H, et al. Open-label, Multicenter, Phase II Study of RC48-ADC, a HER2-Targeting Antibody–Drug Conjugate, in Patients with Locally Advanced or Metastatic Urothelial Carcinoma. Clin Cancer Res 2021;27:43–51.
6. Goldstein JT, Berger AC, Shih J, Duke FF, Furst L, Kwiatkowski DJ, et al. Genomic activation of PPARG reveals a candidate therapeutic axis in bladder cancer. Cancer Res 2017;77:6987–98.
7. Peng H, Wisse E, Tian Z. Liver natural killer cells: Subsets and roles in liver immunity. Cell Mol Immunol 2016;13:328–36.
8. Ochoa MC, Minute L, Rodriguez I, Garasa S, Perez-Ruiz E, Inogés S, et al. Antibody- dependent cell cytotoxicity: immunotherapy strategies enhancing effector NK cells. Immunol Cell Biol 2017;95:347–55.
9. Delmore JE, Issa GC, Lemieux ME, Rahl PB, Shi J, Jacobs HM, et al. BET bromodomain inhibition as a therapeutic strategy to target c-Myc. Cell 2011;146:904–17.
10. Moore AR, Rosenberg SC, McCormick F, Malek S. RAS-targeted therapies: is the undruggable drugged? Nat Rev Drug Discov 2020;19:533–52.
11. Meng XM, Nikolic-Paterson DJ, Lan HY. TGF-β: The master regulator of fibrosis. Nat Rev Nephrol 2016;12:325–38.
12. Borthwick LA, Wynn TA, Fisher AJ. Cytokine mediated tissue fibrosis. Biochim Biophys Acta - Mol Basis Dis 2013;1832:1049–60.
13. Powles T, Kockx M, Rodriguez-Vida A, Duran I, Crabb SJ, Van Der Heijden MS, et al. Clinical efficacy and biomarker analysis of neoadjuvant atezolizumab in operable urothelial carcinoma in the ABACUS trial. Nat Med 2019;25:1706–14.
14. van Dijk N, Gil-Jimenez A, Silina K, Hendricksen K, Smit LA, de Feijter JM, et al. Preoperative ipilimumab plus nivolumab in locoregionally advanced urothelial cancer: the NABUCO trial. Nat Med 2020;26:1839–1844.
15. Mariathasan S, Turley SJ, Nickles D, Castiglioni A, Yuen K, Wang Y, et al. TGFβ attenuates tumour response to PD-L1 blockade by contributing to exclusion of T cells. Nature 2018;554:544–8.
16. Robertson AG, Kim J, Al-Ahmadie H, Bellmunt J, Guo G, Cherniack AD, et al. Comprehensive Molecular Characterization of Muscle-Invasive Bladder Cancer. Cell 2017;171:540-556.e25.
17. Lv J, Li P. Mesothelin as a biomarker for targeted therapy. Biomark Res 2019;7:18.
18. Bins S, Cirkel GA, Hooijdonk CGG-V, Weeber F, Numan IJ, Bruggink AH, et al. Implementation of a Multicenter Biobanking Collaboration for Next-Generation Sequencing-Based Biomarker Discovery Based on Fresh Frozen Pretreatment Tumor Tissue Biopsies. Oncologist 2017;22:33–40.
19. Li H, Durbin R. Fast and accurate short read alignment with Burrows-Wheeler transform. Bioinformatics 2009;25:1754–60.
20. McKenna A, Hanna M, Banks E, Sivachenko A, Cibulskis K, Kernytsky A, et al. The genome analysis toolkit: A MapReduce framework for analyzing next-generation DNA sequencing data. Genome Res 2010;20:1297–303.
21. Van der Auwera GA, Carneiro MO, Hartl C, Poplin R, del Angel G, Levy-Moonshine A, et al. From fastQ_data to high-confidence variant calls: The genome analysis toolkit best practices pipeline. Curr Protoc Bioinforma 2013;43:11.10.1-11.10.33.
22. Saunders CT, Wong WSW, Swamy S, Becq J, Murray LJ, Cheetham RK. Strelka: Accurate somatic small-variant calling from sequenced tumor-normal sample pairs. Bioinformatics 2012;28:1811–7.
23. McLaren W, Gil L, Hunt SE, Riat HS, Ritchie GRS, Thormann A, et al. The Ensembl Variant Effect Predictor. Genome Biol 2016;17:122.
24. Liu X, Wu C, Li C, Boerwinkle E. dbNSFP v3.0: A One-Stop Database of Functional Predictions and Annotations for Human Nonsynonymous and Splice-Site SNVs. Hum Mutat 2016;37:235–41.
25. Lek M, Karczewski KJ, Minikel E V., Samocha KE, Banks E, Fennell T, et al. Analysis of protein-coding genetic variation in 60,706 humans. Nature 2016;536:285–91.
26. Cameron D, Baber J, Shale C, Papenfuss A, Valle-Inclan JE, Besselink N, et al. GRIDSS, PURPLE, LINX: Unscrambling the tumor genome via integrated analysis of structural variation and copy number. BioRxiv Prepr 2019:https://doi.org/10.1101/781013.
27. Roberts SA, Lawrence MS, Klimczak LJ, Grimm SA, Fargo D, Stojanov P, et al. An APOBEC cytidine deaminase

mutagenesis pattern is widespread in human cancers. Nat Genet 2013;45:970–6.
28. Martincorena I, Raine KM, Gerstung M, Dawson KJ, Haase K, Van Loo P, et al. Universal Patterns of Selection in Cancer and Somatic Tissues. Cell 2017;171:1029-1041.e21.
29. van Dessel LF, van Riet J, Smits M, Zhu Y, Hamberg P, van der Heijden MS, et al. The genomic landscape of metastatic castration-resistant prostate cancers reveals multiple distinct genotypes with potential clinical impact. Nat Commun 2019;10:1–13.
30. Mermel CH, Schumacher SE, Hill B, Meyerson ML, Beroukhim R, Getz G. GISTIC2.0 facilitates sensitive and confident localization of the targets of focal somatic copy-number alteration in human cancers. Genome Biol 2011;12:R41.
31. Tate JG, Bamford S, Jubb HC, Sondka Z, Beare DM, Bindal N, et al. COSMIC: The Catalogue Of Somatic Mutations In Cancer. Nucleic Acids Res 2019;47:D941–7.
32. Blokzijl F, Janssen R, van Boxtel R, Cuppen E. MutationalPatterns: Comprehensive genome-wide analysis of mutational processes. Genome Med 2018;10:33.
33. Alexandrov LB, Kim J, Haradhvala NJ, Huang MN, Tian Ng AW, Wu Y, et al. The repertoire of mutational signatures in human cancer. Nature 2020;578:94–101.
34. Petljak M, Alexandrov LB, Brammeld JS, Price S, Wedge DC, Grossmann S, et al. Characterizing Mutational Signatures in Human Cancer Cell Lines Reveals Episodic APOBEC Mutagenesis. Cell 2019;176:1282-1294.e20.
35. Angus L, Smid M, Wilting SM, van Riet J, Van Hoeck A, Nguyen L, et al. The genomic landscape of metastatic breast cancer highlights changes in mutation and signature frequencies. Nat Genet 2019;51:1450–8.
36. Christensen S, Van der Roest B, Besselink N, Janssen R, Boymans S, Martens JWM, et al. 5-Fluorouracil treatment induces characteristic T>G mutations in human cancer. Nat Commun 2019;10:1–11.
37. Wilkerson MD, Hayes DN. ConsensusClusterPlus: A class discovery tool with confidence assessments and item tracking. Bioinformatics 2010;26:1572–3.
38. Gaujoux R, Seoighe C. A flexible R package for nonnegative matrix factorization. BMC Bioinformatics 2010;11:367.
39. Nguyen L, Martens J, Hoeck A van, Cuppen E. Pan-cancer landscape of homologous recombination deficiency. Nat Commun 2020;11:5584.
40. Griffith M, Spies NC, Krysiak K, McMichael JF, Coffman AC, Danos AM, et al. CIViC is a community knowledgebase for expert crowdsourcing the clinical interpretation of variants in cancer. Nat Genet 2017;49:170–4.
41. Chakravarty D, Gao J, Phillips S, Kundra R, Zhang H, Wang J, et al. OncoKB: A Precision Oncology Knowledge Base. JCO Precis Oncol 2017;1:1–16.
42. Tamborero D, Rubio-Perez C, Deu-Pons J, Schroeder MP, Vivancos A, Rovira A, et al. Cancer Genome Interpreter annotates the biological and clinical relevance of tumor alterations. Genome Med 2018;10:25.
43. Bolger AM, Lohse M, Usadel B. Trimmomatic: a flexible trimmer for Illumina sequence data. Bioinformatics 2014;30:2114–20.
44. Dobin A, Davis CA, Schlesinger F, Drenkow J, Zaleski C, Jha S, et al. STAR: Ultrafast universal RNA-seq aligner. Bioinformatics 2013;29:15–21.
45. Harrow J, Frankish A, Gonzalez JM, Tapanari E, Diekhans M, Kokocinski F, et al. GENCODE: The reference human genome annotation for the ENCODE project. Genome Res 2012;22:1760–74.
46. Tarasov A, Vilella AJ, Cuppen E, Nijman IJ, Prins P. Sambamba: Fast processing of NGS alignment formats. Bioinformatics 2015;31:2032–4.
47. Wang L, Nie J, Sicotte H, Li Y, Eckel-Passow JE, Dasari S, et al. Measure transcript integrity using RNA-seq data. BMC Bioinformatics 2016;17:58.
48. Wang L, Wang S, Li W. RSeQC: quality control of RNA-seq experiments. Bioinformatics 2012;28:2184–5.
49. Liao Y, Smyth GK, Shi W. FeatureCounts: An efficient general purpose program for assigning sequence reads to genomic features. Bioinformatics 2014;30:923–30.
50. Li B, Dewey CN. RSEM: Accurate transcript quantification from RNA-seq data with or without a reference genome. BMC Bioinformatics 2011;12:323.
51. Kamoun A, Reyniès A de, Allory Y, Sjödahl G, Gordon Robertson A, Seiler R, et al. A Consensus Molecular Classification of Muscle-invasive Bladder Cancer. Eur Urol 2019;77:420- 33.
52. Williams SB, Black PC, Dyrskjøt L, Seiler R, Schmitz-Dräger B, Nawroth R, et al. Re: Aurélie Kamoun, Aurélien de Reyniès, Yves Allory, et al. A Consensus Molecular Classification of Muscle-invasive Bladder Cancer. Eur Urol 2020;77:420–33: A Statement from the International Bladder Cancer Network. Eur Urol 2020;77:e105–6.
53. Love MI, Huber W, Anders S. Moderated estimation of fold change and dispersion for RNA-seq data with DESeq2. Genome Biol 2014;15:550.
54. Paulson JN, Chen CY, Lopes-Ramos CM, Kuijjer ML, Platig J, Sonawane AR, et al. Tissue-aware RNA-Seq processing and normalization for heterogeneous and sparse data. BMC Bioinformatics 2017;18:1–10.
55. Borggrefe T, Oswald F. The Notch signaling pathway: Transcriptional regulation at Notch target genes. Cell Mol Life Sci 2009;66:1631–46.
56. van Ooijen H, Hornsveld M, Dam-de Veen C, Velter R, Dou M, Verhaegh W, et al. Assessment of Functional Phosphatidylinositol 3-Kinase Pathway Activity in Cancer Tissue Using Forkhead Box-O Target Gene Expression in a Knowledge-Based Computational Model. Am J Pathol 2018;188:1956–72.
57. Varelas X. The hippo pathway effectors TAZ and YAP in development, homeostasis and disease. Dev 2014;141:1614–26.
58. Fischer M. Census and evaluation of p53 target genes. Oncogene 2017;36:3943–56.
59. Kitamura H, Motohashi H. NRF2 addiction in cancer cells. Cancer Sci 2018;109:900–11.
60. Hartl M. The quest for targets executing MYC-dependent cell transformation. Front Oncol 2016;6:132.
61. Wagle M-C, Kirouac D, Klijn C, Liu B, Mahajan S, Junttila M, et al. A transcriptional MAPK Pathway Activity Score (MPAS) is a clinically relevant biomarker in multiple cancer types. Npj Precis Oncol 2018;2:1–12.
62. Murray PJ. The JAK-STAT Signaling Pathway: Input and Output Integration. J Immunol 2007;178:2623–9.
63. Sturm G, Finotello F, Petitprez F, Zhang JD, Baumbach J, Fridman WH, et al. Comprehensive evaluation of transcriptome-based cell-type quantification methods for immuno-oncology. Bioinformatics 2019;35:i436–45.
64. Finotello F, Mayer C, Plattner C, Laschober G, Rieder D, Hackl H, et al. Molecular and pharmacological modulators of the tumor immune contexture revealed by deconvolution of RNA-seq data. Genome Med 2019;11:34.
65. R Core Team. R Core Team (2017). R: A language and environment for statistical computing. R Found Stat Comput Vienna, Austria URL Http//WwwR-ProjectOrg/ 2017:R Foundation for Statistical Computing.

SUPPLEMENTARY FIGURES

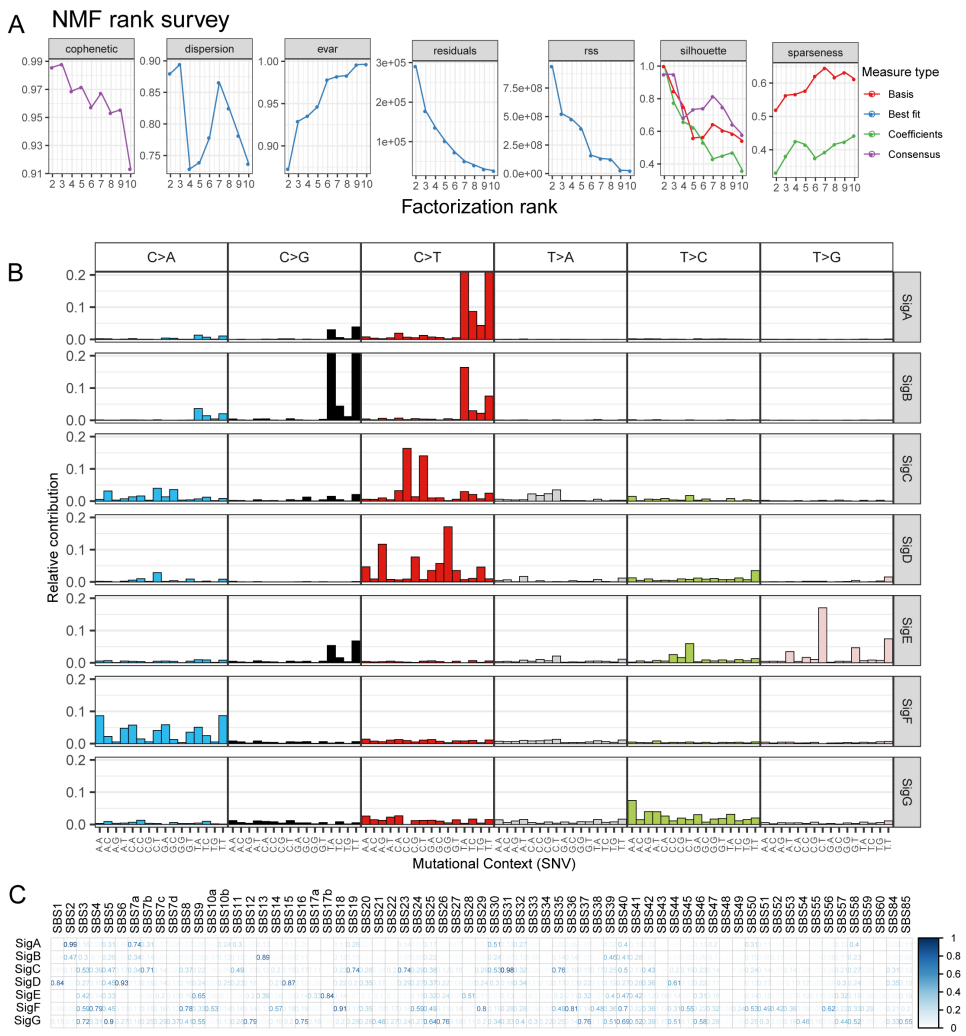

Supplementary Figure 1. *De novo* mutational signatures estimated from all SNVs considering the tri-nucleotide context.
A. Results from non-negative matrix factorization to estimate *de novo* mutational signatures from k = 2 to k = 10. **B.** Mutational profile of seven *de novo* signatures. Mutations are shown in their 96 tri-nucleotide context. **C.** Cosine similarity of *de novo* signatures with all mutational signatures from COSMIC v3. Cosine similarity values are shown for each pairwise comparison and colored in darker blue for higher values.

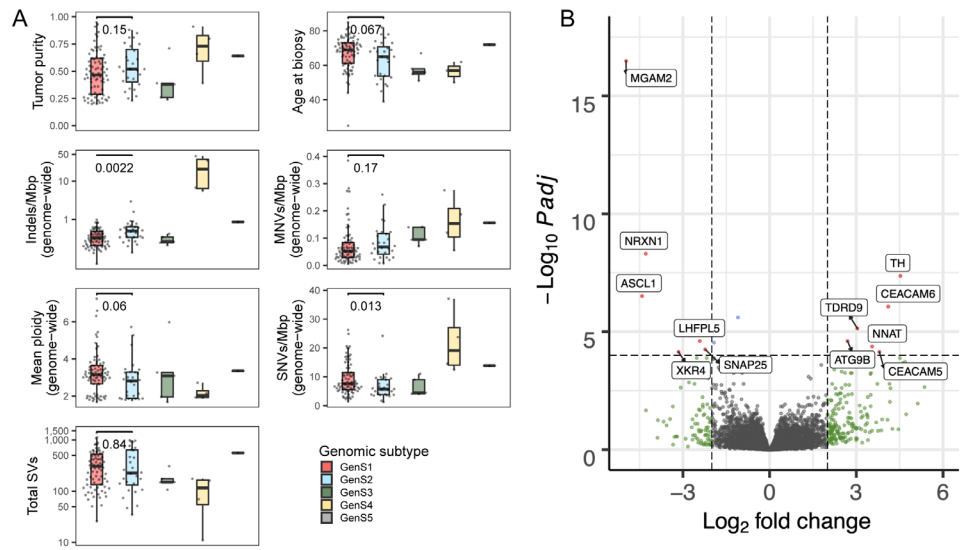

Supplementary Figure 2. Comparing the genomics and transcriptomics features between genomic subtypes.
A. Distribution of some genomic and transcriptomic features among genomic subtypes. Age at biopsy and tumor purity are also shown. Wilcoxon rank-sum test p-values are shown for comparisons of GenS1 with GenS2. **B.** Volcano plot of differential gene expression analysis between GenS1 and GenS2. Fold changes were log2 transformed and represent expression values of genes in GenS1 over GenS2.

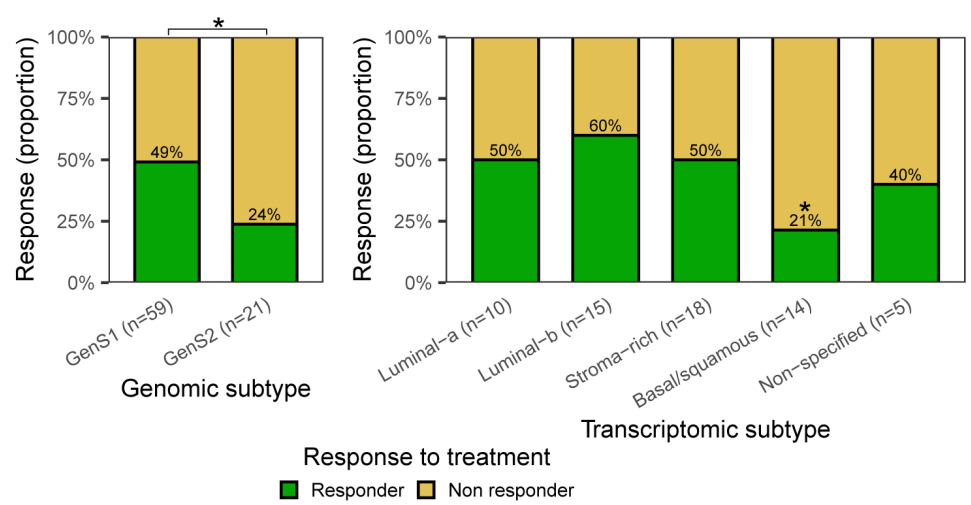

Supplementary Figure 3. Response to treatment.
Patients received different palliative therapies (immune therapy or chemotherapy) as first- or second-line treatment. Best overall response according to response evaluation criteria in solid tumors (RECIST) v1.1 was available for 80 patients with WGS data (GenS1 + GenS2) and for 62 patients with RNA-seq data. Responders were considered those patients with CR or PR and non-responders were those with SD or PD. The star (*) represents p <0:05 for one-sided Fisher's exact test.

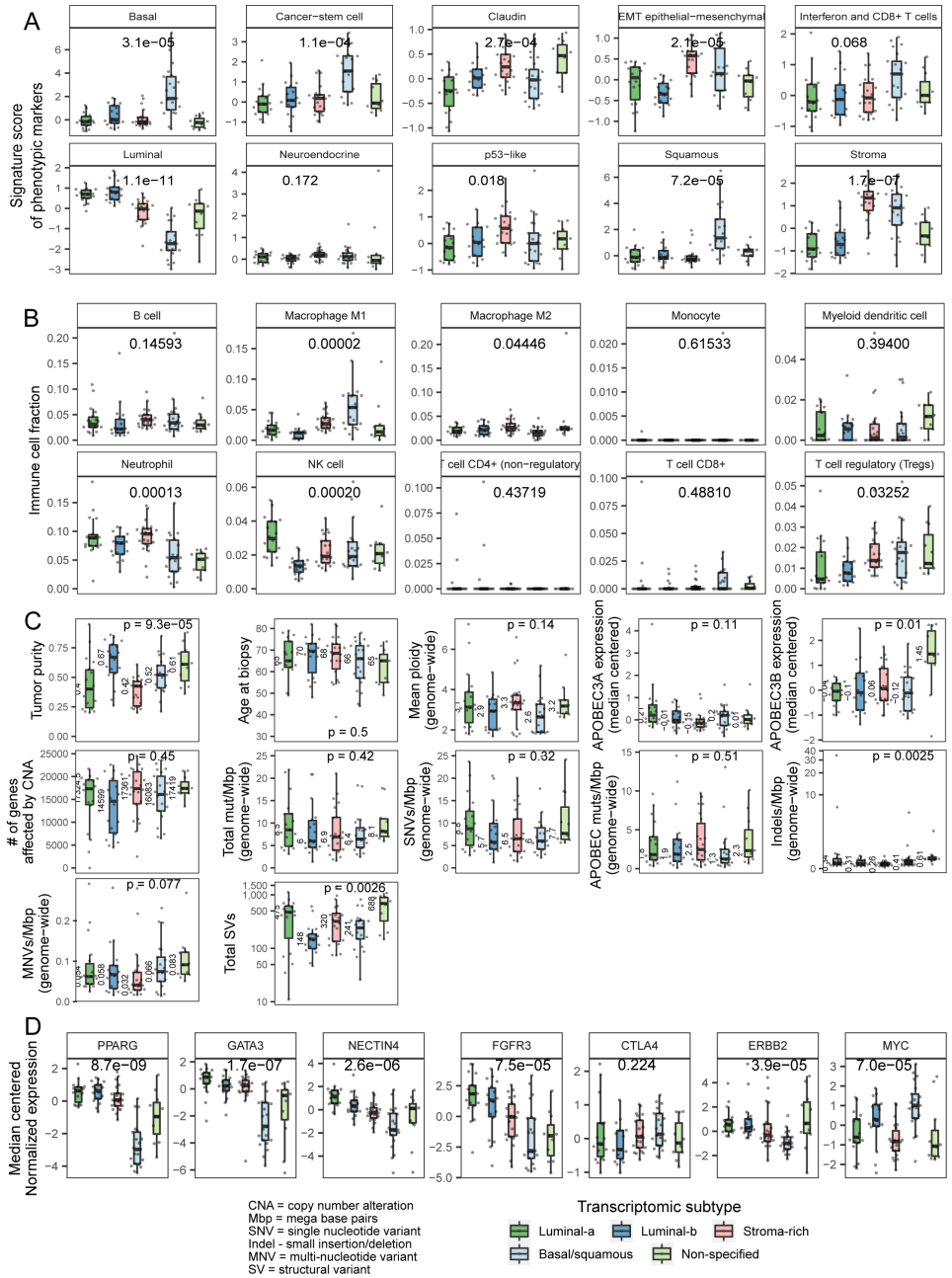

Supplementary Figure 4. Molecular differences between the five transcriptomic subtypes of metastatic urothelial carcinoma.

A. Signature score of phenotypic markers estimated as the mean expression of genes associated with each phenotype. Kruskal-Wallis test p-values were Benjamini-Hochberg (BH) corrected. **B.** Immune cell fractions estimated with immunedeconv (3) using the quanTIseq method (4). Kruskal-Wallis test p-values were BH corrected. **C.** Tumor purity, genomic (mean ploidy, number of genes affected by copy number alterations and mutational load), transcriptomic (APOBEC expression) and clinical data (age at biopsy) were compared. Kruskal-Wallis test p-value for each comparison is shown. **D.** Expression of selected genes. Kruskal-Wallis test p-values were BH corrected.

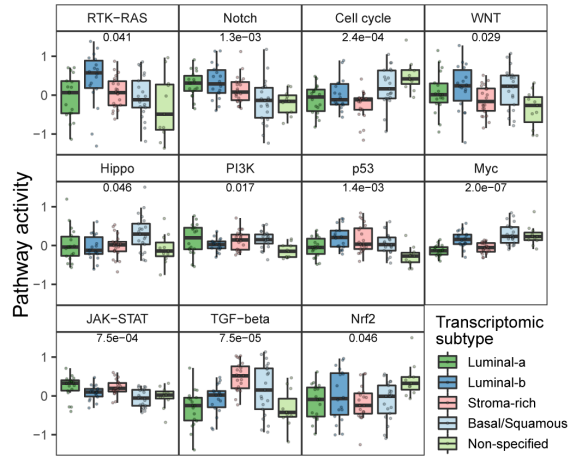

Supplementary Figure 5. Oncogenic pathway activity across mRNA-based subtypes of metastatic urothelial carcinoma.

Pathway activity was estimated as the mean expression of downstream genes targeted by each pathway. Only genes that were transcriptionally activated by these pathways were considered. Kruskal-Wallis test p-values were Benjamini-Hochberg corrected.

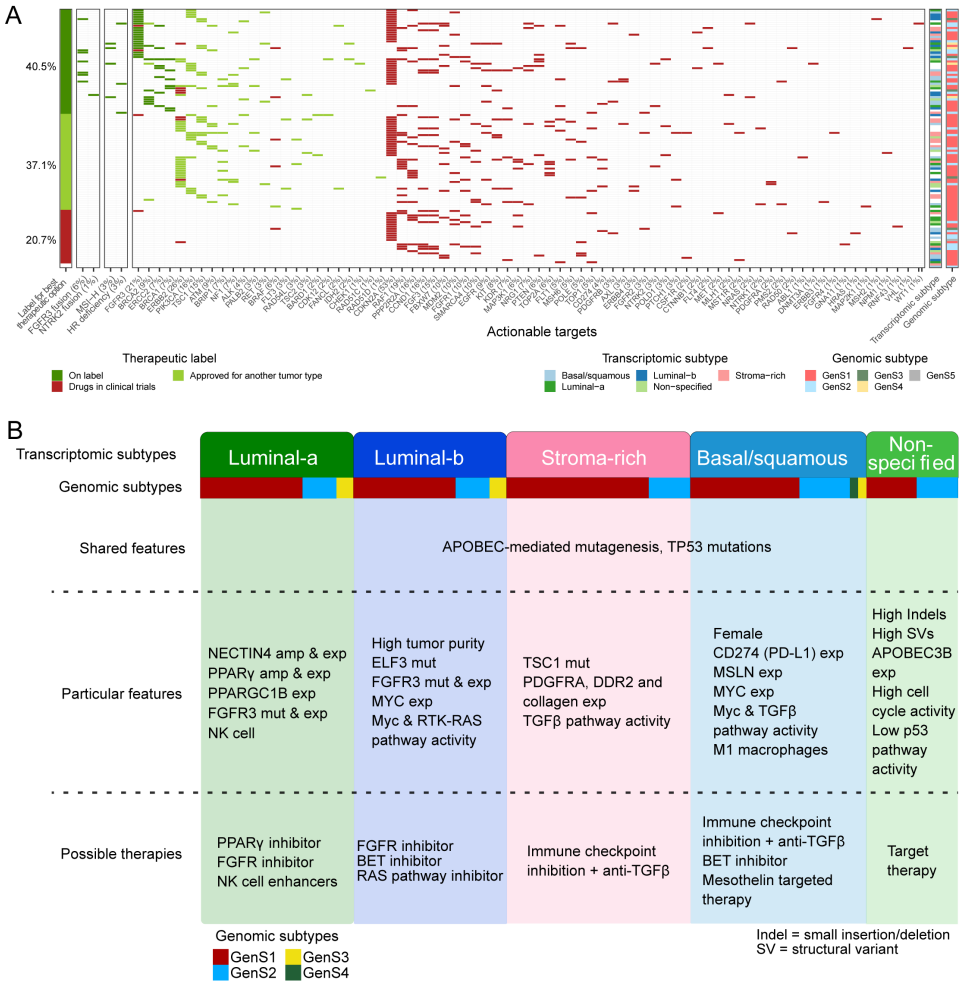

Supplementary Figure 6. Overview of actionable targets and possible treatments per transcriptomic subtype of metastatic urothelial carcinoma.
A. Per patient overview of therapeutic targets based on gene fusions at RNA level estimated with Arriba v2.0.0 (https://github.com/suhrig/arriba; *first column*), tumors with high microsatellite instability (MSI-H) or homologous recombination (HR) deficiency (*second column*), and clinically actionable genomic alterations for on- and off-label therapies for urothelial carcinoma (*third column*). On the left side, the therapeutic label for the best treatment option per patient is shown. Bars on the right depict the genomic and the transcriptomic subtype per patient. **B.** Summary of molecular characteristics found in the present study, and potential therapeutic implications for the treatment of metastatic urothelial carcinoma per transcriptomic subtype. From top to bottom: transcriptomic mUC subtypes, genomic mUC subtypes, shared genomic features among transcriptomic subtypes, unique characteristics per transcriptomic subtype, suggested therapeutic strategies per transcriptomic subtype.

REFERENCES

1. Wilkerson MD, Hayes DN (2010) Consensusclusterplus: a class discovery tool with confidence assessments and item tracking. Bioinformatics 26:1572{1573.
2. Kamoun A, et al. (2020) A consensus molecular classification of muscle-invasive bladder cancer. European Urology 77(4):420{433. Sturm G, et al. (2019) Comprehensive evaluation of transcriptome-based cell-type quantification methods for immuno-oncology. Bioinformatics 35(14):i436{i445.
3. Finotello F, et al. (2019) Molecular and pharmacological modulators of the tumor immune contexture revealed by deconvolution of RNA-seq data. Genome Medicine 11(1):34.

SUPPLEMENTARY TABLES

Supplementary table 1. Patient characteristics.

	Patients (n = 116)
Age (median, range)	68 (25-85)
Male sex	87 (75%)
Primary tumor location	
Bladder	88 (76%)
Upper tract	27 (23%)
Unknown	1 (1%)
Systemic pretreatment	
Yes	71 (61%)
Gemcitabine, cisplatin and/or carboplatin	58 (82%)
Methotrexate, vinblastine, doxorubicin, cisplatin	4 (6%)
Chemotherapy in combination with immunotherapy	3 (4%)
Other [a]	6 (8%)
No	42 (36%)
Unknown	3 (3%)
Radiotherapy pretreatment	
Yes	33 (28%)
No	80 (69%)
Unknown	3 (3%)

[a] Other systemic pretreatments include mitomycin C and randomized trial treatment with nivolumab or placebo.

CHAPTER 5

Anti–PD-1 efficacy in patients with metastatic urothelial cancer associates with intratumoral juxtaposition of T helper-type 1 and CD8+ T-cells

Maud Rijnders
Hayri E. Balcioglu
Debbie G.J. Robbrecht
Astrid A.M. Oostvogels
Rebecca Wijers
Maureen J.B. Aarts
Paul Hamberg
Geert J.L.H. van Leenders
J. Alberto Nakauma-González
Jens Voortman
Hans M. Westgeest
Joost L. Boormans
Ronald de Wit
Martijn P. Lolkema
Astrid A.M. van der Veldt
Reno Debets

Published in Clinical Cancer Research, 2022 Jan 1;28(1):215-226.

ABSTRACT

Purpose

PD-1 inhibition results in durable antitumor responses in a proportion of patients with metastatic urothelial cancer (mUC). The majority of patients, however, do not experience clinical benefit. In this study, we aimed to identify early changes in T-cell subsets that underlie anti–PD-1 efficacy in patients with mUC.

Experimental design

Paired samples were collected from peripheral blood, plasma, and metastatic lesions of 56 patients with mUC at baseline and weeks 6 and 12 after initiating pembrolizumab treatment (200 mg intravenously, every 3 weeks). Samples were analyzed using multiplex flow cytometry, ELISA, and *in situ* stainings, including cellular network analysis. Treatment response was evaluated as best overall response according to RECIST v1.1, and patients were classified as responder (complete or partial response) or non-responder (progressive disease).

Results

In responders, baseline fractions of CD4+ T-cells expressing co-signaling receptors were higher compared with non-responders. The fraction of circulating PD-1+ CD4+ T-cells decreased at weeks 6 and 12, whereas the fraction of 4-1BB+ CD28+ CD4+ T-cells increased at week 12. In metastatic lesions of responders, the baseline density of T helper-type 1 (Th1) cells, defined as T-bet+ CD4+ T-cells, was higher as compared to non-responders. Upon treatment, Th1 cells became localized in close proximity to CD8+ T-cells, CD11b+ myeloid cells, and tumor cells.

Conclusions

A decrease in the fraction of circulating PD-1+ CD4+ T-cells, and juxtaposition of Th1, CD8+, and myeloid cells was associated with response to anti–PD-1 treatment in patients with mUC.

INTRODUCTION

Treatment with antibodies directed against the immune checkpoint programmed cell death protein (PD)-1 or its ligand (PD-L1) leads to robust and durable clinical responses in patients with various tumor types, including melanoma and non–small cell lung cancer (1, 2). In patients with advanced and metastatic urothelial cancer (mUC), first-line treatment with pembrolizumab (i.e., anti–PD-1) and atezolizumab (i.e., anti–PD-L1) has shown promising results in single-arm trials (3, 4). Recently, a randomized trial showed that patients with mUC who received first-line treatment with chemotherapy plus atezolizumab had an improved progression-free survival as compared with patients treated with atezolizumab monotherapy or platinum-based chemotherapy plus placebo (5). Yet, no survival benefit was observed in a phase III trial comparing first-line durvalumab (i.e., anti–PD-L1) and durvalumab plus tremelimumab (i.e., anti–CTLA-4) to chemotherapy in patients with mUC (6). Furthermore, in patients with mUC with progressive disease after platinum-based chemotherapy, second-line treatment with pembrolizumab showed superior efficacy as compared with chemotherapy (objective response rates 21% vs 11%) (7, 8). Despite the limited objective response rate for second-line pembrolizumab, a small proportion of patients with mUC do obtain a durable tumor response (2-year progression-free survival of 12%) (9).

PD-L1 expression in tumor tissue has been investigated extensively as a predictive marker to select patients with mUC for anti–PD-1 treatment (10), but results were conflicting in the second-line setting (11, 12). Currently, the use of PD-L1 expression to select patients for immune checkpoint inhibitors (ICIs) is restricted to the first-line setting for cisplatin-ineligible patients with mUC (13, 14). As treatment with ICIs can be accompanied with severe adverse events and is associated with high costs, new markers are needed to identify patients who will benefit from treatment with ICIs. Furthermore, a better understanding of immune mechanisms that underly response and resistance to ICIs would facilitate the development of improved treatments for patients with mUC.

In a pan-cancer setting, tumor response to ICIs has generally been associated with high mutational burden and expression of signature genes downstream of interferon gamma (IFNγ), a major product of activated T-cells (15, 16). In patients with mUC, tumor response to ICIs has also been correlated with markers of T-cell response, such as enrichment for T-cell receptor clones (17-20). More recently, the number and spatial organization of intratumoral T-cells were observed to associate with survival and tumor response to ICIs in multiple tumor types (21-24), including UC (17, 25). Collectively, these translational studies show that recruitment of T-cells and intratumoral interactions between T-cells and antigen-presenting cells represent prerequisites for optimal antitumor immune responses (26-28).

In the current study, we investigated whether numerical and phenotypical differences in CD4+ and CD8+ T-cell subsets were associated with anti–PD-1 efficacy in patients with mUC. To this end, peripheral blood, plasma, and tumor biopsies were prospectively collected from patients treated with pembrolizumab in a clinical trial. Samples were analyzed using multimodality flow cytometry, ELISA and *in situ* stainings. We observed predominant differences between responders and non-responders regarding CD4+ T-cell subsets. Responders demonstrated enhanced fractions of CD4+ T-cell subsets expressing co-signaling receptors in blood, and fractions of these subsets changed during treatment. Furthermore, in metastatic lesions of responders, anti–PD-1 induced the formation of immune cell niches that are rich in CD4+ T helper-type 1 (Th1) cells, CD8+ T-cells, and CD11b+ myeloid cells.

MATERIALS AND METHODS

Patients and assessment of clinical response

Patients with advanced or metastatic UC were included in a phase II prospective biomarker discovery study (RESPONDER trial, NCT03263039). The study protocol was approved by the medical ethics review board of the Foundation BEBO (Evaluation of Ethics in Biomedical Research). The study was conducted in accordance with the Declaration of Helsinki principles for medical research involving human subjects. Written informed consent was obtained from all subjects before any study procedure. Between September 1, 2017, and December 31, 2019, 56 patients with mUC initiated first- (n = 5) or second-line (n = 51) treatment with pembrolizumab (200 mg intravenously, every 3 weeks). Prior to the start of therapy and every 12 weeks thereafter, tumor response was evaluated using CT. Patients were classified as responders (complete or partial response according to RECIST v1.1, n = 22) and non-responders (progressive disease according to RECIST v1.1, n = 34) according to their best overall response during treatment. Patients with stable disease showed diverse tumor responses varying between limited progressive disease (<20% increase in diameter of target lesions), limited tumor response (<30% decrease in diameter of target lesions), and mixed response. For this patient group, findings are presented per type of biomaterial in Supplementary Figure 8 and Supplementary Table 1. For the current analyses, data cutoff was set at July 1, 2020.

PD-L1 expression was determined on baseline metastatic tumor biopsies using the companion diagnostic assay of pembrolizumab (PD-L1 IHC 22C3 pharmDx, Agilent Technologies), according to the manufacturer's guidelines (DAKO platform, Maastricht University Medical Center, Maastricht, the Netherlands). All tissues were assessed for the PD-L1 CPS by an expert genitourinary pathologist (G.J.L.H. van Leenders) (3, 7). Nine of 14 patients (64%) with a CPS ≥10 obtained a tumor response, compared with 8 of 27 patients (30%) with a CPS <10 (Table 1). Patient characteristics as well as patient numbers per type of biomaterial are provided in Table 1.

Collection and processing of biomaterials

Peripheral blood was collected in EDTA tubes at three timepoints: pretreatment (baseline (Bl)) and prior to the third and fifth administration of pembrolizumab (weeks 6 and 12; see Supplementary Figure 1 for study design and patient numbers). Whole blood was used to enumerate immune cell populations, and PBMCs and plasma were isolated using Ficoll gradient centrifugation. Samples were stored according to standardized protocols and thawed at later timepoints to assess fractions of T-cell subsets (PBMCs) and levels of chemo-attractants (plasma). Tumor biopsies were collected from a safely accessible metastatic lesion at baseline, and from the same lesion after 6 weeks of treatment (see Table 1 for biopsy sites). Tissue specimens for multiplex immunofluorescence stainings were formalin-fixed and paraffin-embedded (FFPE). At baseline, an additional biopsy from the same lesion was snap frozen for RNA sequencing (RNA-seq) according to a standardized procedure (29).

Multiplex flow cytometry of blood samples

Whole blood was stained, lysed to remove red blood cells, and analyzed by multiplex flow cytometry using a BD 3-laser Celesta flow cytometer and FACSDIVA 8.x software. Cell counts of major T-cell populations were determined using Flow-Count Fluorospheres (Beckman Coulter). PBMC samples were stained with a mix of antibodies directed against T-cell markers of maturation, co-inhibition, co-stimulation, or chemotaxis as described previously (30). All antibody panels were optimized and compensated using fluorescence minus one (FMO) controls and measurements were corrected for background fluorescence. Data were gated and analyzed using FlowJo software.

Table 1. Patient characteristics and collection of biomaterials.

		Responder n = 22	Non-responder n = 34
Age (median, range)		71 (49 – 85)	67 (31 – 78)
Sex			
Male		19 (86%)	20 (59%)
Female		3 (14%)	14 (41%)
Metastatic sites			
Lymph node		14 (64%)	23 (68%)
Lymph node only disease		9 (41%)	4 (12%)
Lung		7 (32%)	14 (41%)
Liver		3 (14%)	14 (41%)
Bone		4 (18%)	9 (26%)
Unknown		1 (4.5%)	2 (6%)
Treatment			
First-line		4 (18%)	1 (3%)
Second-line		18 (82%)	33 (97%)
First 4 treatment cycles completed		22 (100%)	12 (35%)[a]
Treatment response (RECIST v1.1)[b]			
Complete response		4 (18%)	0
Partial response		18 (82%)	0
Progressive disease		0	34 (100%)
Biomaterials and PD-L1 score			
Blood samples (PBMC and plasma)		22	34
Metastatic tumor biopsies		18	27
Biopsy sites	Lymph node	8 (44%)	8 (30%)
	Liver	2 (11%)	9 (33%)
		0	5 (18%)
Abdominal mass			
	Soft tissue	3 (17%)	1 (4%)
	Lung	2 (11%)	0
	Other[c]	3 (17%)	4 (15%)
PD-L1	CPS ≥10	9 (50%)	5 (19%)
	CPS <10	8 (44%)	19 (70%)
	Not evaluable	1 (6%)	3 (11%)
RNA		7	11

Note: treatment with pembrolizumab was initiated in 56 patients with mUC. Abbreviations: CPS, combined positivity score according to the companion diagnostic PD-L1 staining of pembrolizumab; PBMC, peripheral blood mononuclear cells. [a] One patient discontinued treatment due to treatment related toxicity (pancreatitis), the other 21 patients discontinued due to disease progression. [b] Patients with stable disease were excluded from the main analyses, please refer to Supplementary Figure 8 and Supplementary Table 1 for an overview of findings in these patients. PBMC and plasma samples were available for all patients, and tumor biopsies were available for 45 out of 56 patients. [c] Other biopsy sites included bladder tumor, colon, omentum, and non-specified.

Clustering and visualization of T-cell subsets in blood

CD4+ T-cell populations were analyzed in Python (Python Software Foundation, v3.6.8) using in-house written scripts. First, data and corresponding background from non-stained samples were normalized for spillover, and logicle transformed (31), after which the median of background was subtracted from each sample for each marker. These data were further processed using a Python adaptation of the self-organizing map algorithm FlowSOM (32). To this end, data were centered and scaled resulting in mean marker intensities of 0 and standard deviations of 1 across all samples. Second, a self-organizing map was trained using 100 nodes, and a minimal spanning tree was built to form 20 meta-clusters. These meta-clusters corresponded to the 20 most abundant CD4+ T-cell subsets according to the set of markers used. A meta-cluster was considered positive or negative for a certain marker if the mean intensity of that marker in the cluster was more than its standard deviation above or below the mean intensity of that marker across all data, respectively. Clusters with equal marker positivity were combined, resulting in 17 to 18 unique clusters per set of markers. Abundances of these T-cell clusters were assessed per patient, and uniform manifold approximation and projections (UMAP) (33) were generated using 200,000 random data points to visualize marker intensities across clusters. Finally, differential abundance of clusters was analyzed between timepoints (baseline, week 6, week 12) and patient groups (responders and non-responders).

Quantification of chemo-attractants in plasma

Levels of chemo-attractants in plasma were determined with the following ELISA kits according to the manufacturer's instructions: CCL3 (Invitrogen), CCL5 (BioLegend ELISA MAX), CXCL9 (Thermo Fisher Scientific), CXCL10 (BioLegend ELISA MAX), and XCL1 (Invitrogen). Different ELISA assays were performed simultaneously to minimize biological variation, and to avoid repeated freeze and thaw cycles of samples.

Multiplex immunofluorescence of tumor tissue

Multiplex immunofluorescence was performed using OPAL reagents (Akoya Biosciences) on 4-µm sections of FFPE tumor biopsies. In brief, stainings were performed in multiple cycles of the following: antigen retrieval (15-minute boiling in antigen retrieval buffer, pH 6 or pH 9 depending on primary antibodies) followed by cooling, blocking, and consecutive staining with primary antibodies, HRP-polymer, and Opal fluorophores. Cycles were repeated until all markers were stained. Finally, nuclei were stained with DAPI. The sequence of antibody stainings was as follows: (i) CD4 (FP1600/EP204, Akoya Biosciences, 1:100) – OPAL540; (ii) CD8 (FP1601/144B, Akoya Biosciences, 1:200) – OPAL690; (iii) CXCR3 (HPA045942, Sigma, 1:100) – OPAL620; (iv) T-bet (4B10, eBioscience, 1:50) – OPAL570; (v) PD-1 (NAT105, ImmunoLogic, 1:50) – OPAL520; (vi) CD11b (EP1345Y, Abcam, 1:200) – OPAL650; (vii) Cytokeratin-Pan (AE1/AE3, Invitrogen, 1:200) – Coumarin (tyramide signal amplification coumarin system, Akoya Biosciences); and (viii) DAPI.

To assess immune cell clusters for the presence of B cells, we additionally stained consecutive tissue sections of responders with the following antibodies: (i) CD3 (SP7, Sigma Aldrich, 1:250) – OPAL520; (ii) CD20 (L26, Cell Marque, 1:1,000) – OPAL620; (iii) CD8 (144B, Cell Marque, 1:400) – OPAL570; (iv) Cytokeratin-Pan (AE1/AE3, Invitrogen, 1:200) – OPAL690; and (v) DAPI.

Digital image analysis of multiplex immunofluorescence stainings

Whole slides were scanned and images were obtained using VECTRA 3.0 (Akoya Biosciences), after which at least four stamps (regions of interest; stamp size: 671 × 500 µm2; resolution: 2 pixels/µm; pixel size: 0.5 × 0.5 µm2) were set in nonnecrotic areas to cover >90% of tissue area. Images were spectrally unmixed using inForm software (Akoya Biosciences) to visualize markers of interest as well as autofluorescence. Subsequently, images were manually analyzed in Python using the following five steps (Tumor Microenvironment Analyzer, H.E. Balcioglu, manuscript in preparation): (i) Foreground selection: images were thresholded using all channels to generate a foreground area that covers regions positive for all signals. (ii) Tissue segmentation: cytokeratin-positive and -negative regions of the foreground were identified as tumor and stroma regions, respectively. For steps i and ii, regions that were deemed too small were excluded. (iii) Nucleus detection: background signal was subtracted from the DAPI signal through a rolling ball filter algorithm, and the nuclear mask was obtained by thresholding. (iv) Nucleus and cell segmentation: clusters of nuclei were segmented by applying a watershed segmentation algorithm to the nuclear mask, where regions that were deemed too small were excluded. Once identified, nuclei were used for cell detection through a Voronoi segmentation algorithm. (v) Phenotyping: fluorescent intensities for the channels that correspond to each marker were analyzed per cell and nucleus (in case of T-bet). Cells were assigned to either tumor or stroma regions according to the location of the center of their nuclei. Spatial orientations of individual cells were assigned according to the center of their area. Cellular densities were calculated by dividing the number of cells with a certain phenotype by the total area of that region (i.e., tumor, stroma, or both), and were averaged per patient across all stamps. Distances from a cell with a certain phenotype to the nearest cell with another phenotype were calculated by nearest neighbor analysis; this was done in the region of interest (i.e., tumor, stroma, or both), and was averaged across all cells, and per patient across all stamps.

Whole-transcriptome sequencing and analysis

Total RNA was extracted from freshly obtained metastatic tumor biopsies using the QIAsymphony Kit (Qiagen). Samples with a minimum of 100 ng total RNA were sequenced by paired-end sequencing on the Illumina NextSeq 550 (2 × 75 bp) and NovaSeq 6000 (2 × 150 bp) platforms. Samples were visually inspected with FastQC (v0.11.5). Sequence adapters (Illumina TruSeq) were trimmed using Trimmomatic v0.39 (34) and paired-end reads were aligned to the human reference genome (GRCh37) using STAR v2.7.1a (35) with genomic annotations from GENCODE hg19 release 30 (36). FeatureCounts v1.6.3 (37) was applied to count the number of overlapping reads per gene; only uniquely mapped reads were counted per exon and summarized per gene. RSEM v1.3.1 (38) was applied to quantify RNA expression into transcripts per million (TPM) values.

To delineate the relative presence of immune cells, RSEM read counts of all transcripts were analyzed with the R package immunedeconv (39) using the quanTIseq method (40). To capture different CD4+ and CD8+ T-cell subsets, we used previously published gene expression signatures (37, 41, 42). In addition, gene expression levels of the chemo-attractants CCL3, CCL5, CXCL9, CXCL10, and XCL1 were assessed. Gene expression values were median centered, and the mean expression of each individual gene or set of genes was displayed as gene or signature scores, respectively.

Statistical analysis

Statistical analysis was performed using R version 3.5.1. Mann–Whitney U test was used to compare continuous variables of two unpaired groups (responders vs. non-responders). Wilcoxon signed rank test was used to compare continuous variables of two paired groups (timepoints). Spearman correlation was used to assess linear relationships between continuous variables. Differences were considered significant when $p < 0.05$. Because of the exploratory nature of this study, no correction for multiple testing was applied.

RESULTS

In responders, the fraction of circulating PD-1+ BTLA+ CD4+ T-cells is higher at baseline, and decreases upon anti–PD-1 treatment

Fresh peripheral blood samples were obtained at baseline (n = 56), and after 6 (n = 43) and 12 weeks (n = 31) of treatment with pembrolizumab (Supplementary Figure 1, see Materials and Methods for details). The numbers of T-cells and their major subsets were measured in blood using Flow-Count Fluorospheres. The numbers of αβ T-cells, γδ T-cells, CD4+ T-cells, and CD8+ T-cells (per µL of blood) were not significantly different between responders and non-responders at baseline, and remained unchanged after 6 and 12 weeks of treatment (Supplementary Figure 2A). T-cells were further classified according to the expression of 20 markers regarding co-signaling, maturation, and chemotaxis using multiplex flow cytometry. In particular, fractions of CD4+ T-cell subsets (Figures 1-3; Supplementary Figures 2 and 3, as described below), and to a lesser extent CD8+ T-cell subsets (Supplementary Table 2), were significantly different between responders and non-responders.

In responders, the fraction of circulating 4-1BB+ CD28+ CD4+ T-cells is higher at baseline, and increases upon anti–PD-1 treatment

In addition to co-inhibitory receptors, CD4+ T-cells were investigated for the expression of the co-stimulatory receptors CD28, ICOS (CD278), CD40L (CD154), 4-1BB (CD137), and/or OX40 (CD134), as well as the maturation/activation markers CD45RA, CCR7 (CD197), CD27, CD69, CD95, and/or CD103 (Figure 2 and Supplementary Figures 2B, 2C, 3B, and 3C). At baseline, the fractions of 4-1BB+ CD4+ T- cells and CD28+ 4-1BB+ CD4+ T-cells were higher in responders compared with non-responders (Figure 2). The fractions of 4-1BB+ CD28+ CD4+ T-cells and 4-1BB+ ICOS+ CD4+ T-cells significantly increased from baseline to week 12 in responders (Figure 2B), whereas an increase in the fraction of 4-1BB+ CD4+ T-cells was only observed at week 6 in non-responders (Figure 2A). In addition, at baseline and week 6, the fraction of effector memory (CD45RA– CCR7–) CD4+ T-cells was higher in responders compared with non-responders. Finally, the baseline fraction of CD4+ T-cells with an activation phenotype (CD95+ CD103+ CD4+ T-cells) was higher in responders compared with non-responders (Supplementary Figure 2C).

Fractions of circulating CD4+ T-cells expressing chemo-attractant receptors remain unchanged upon anti–PD-1 treatment in responders, but not in non-responders

To address T-cell recruitment, CD4+ T-cells were assessed for the expression of the chemo-attractant receptors CCR1 (CD191), CCR4 (CD194), CCR5 (CD195), CXCR3 (CD183), and/or CXCR4 (CD184). Dimensionality reduction and (co-)expression analysis revealed no differences between responders and non-responders at baseline. At week 6, the fraction of CCR1+ CD4+ T-cells was higher in non-responders compared with responders. Notably, treatment-induced changes were only observed in non-responders, where the fraction of CXCR3+ CD4+ T-cells decreased at week 12 (Figure 3A and B; Supplementary Figure 3D). To complement flow cytometry findings, the levels of CCL3 and CCL5 (ligands for CCR1 and CCR5), CXCL9 and CXCL10 (ligands for CXCR3), and XCL1 (ligand for XCR1) were measured in plasma using ELISA. At baseline, plasma levels of CCL5 were lower, whereas levels of CXCL9 were higher in responders compared with non-responders. At weeks 6 and 12, the levels of all chemo-attractants increased in responders, except for CCL5. In non-responders, an increase in the levels of CXCL9 and CXCL10 was also observed during treatment, although to a lesser extent (Figure 3C).

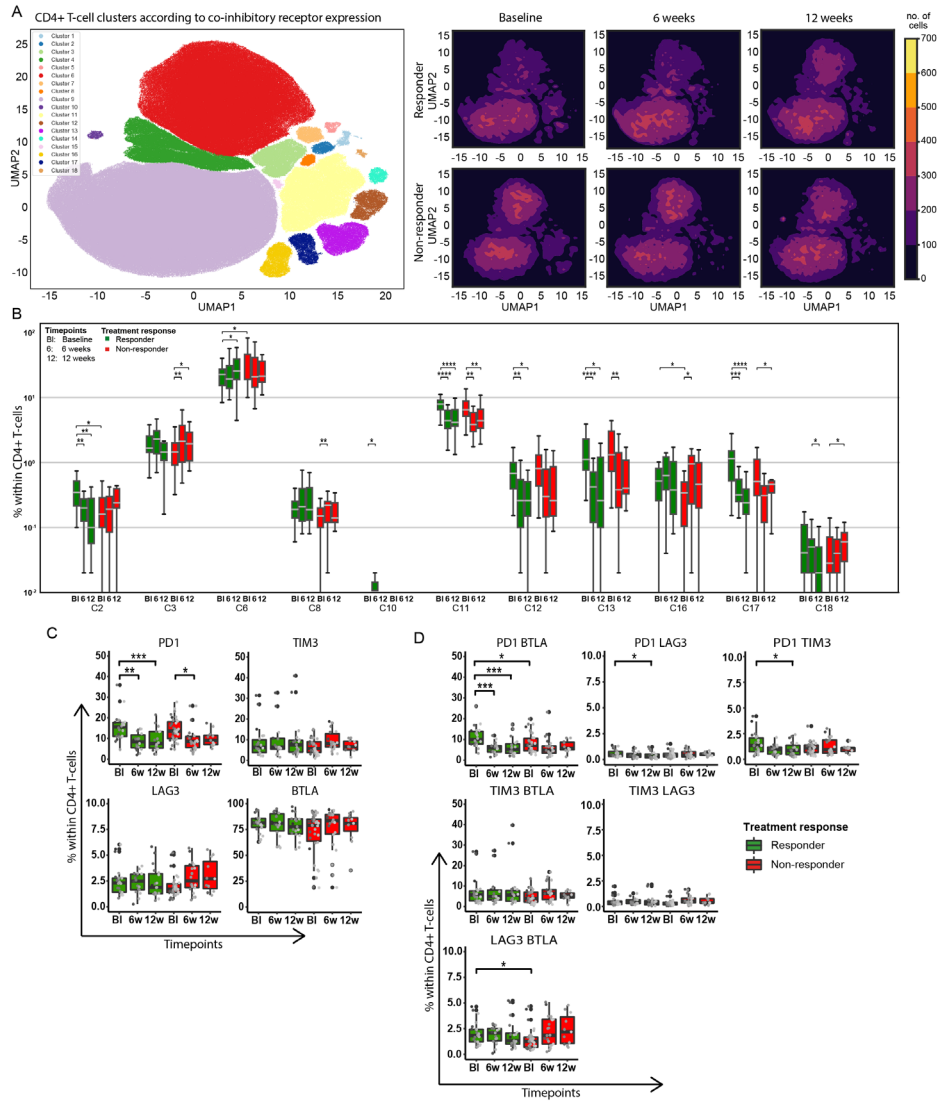

Figure 1. Patients with mUC with a tumor response to anti–PD-1 demonstrate an increased fraction of circulating PD-1+ BTLA+ CD4+ T-cells at baseline, and a decrease in this fraction during therapy.
A. Uniform manifold approximation and projections (UMAP) scatter plot of 200,000 random data points of CD4+ T-cells obtained following flow cytometric staining of PBMCs for (co-)expression of four co-inhibitory receptors (56 patients, 3 timepoints), and split according to treatment response and timepoints. **B.** Differential abundance of self-organizing map clusters between responders and non-responders at different timepoints. **C.** Boxplots display fractions of CD4+ T-cells expressing a single type of co-inhibitory receptor. **D.** Boxplots display fractions of CD4+ T-cells co-expressing two different types of co-inhibitory receptors. Green: responders (n = 22), red: non-responders (n = 34). Timepoints: baseline (Bl), 6 w (6 weeks of treatment), 12 w (12 weeks of treatment); see Supplementary Figure 1 for details. Statistically significant differences between responders and non-responders were determined using the Mann–Whitney U test; differences between timepoints were determined for paired samples using the Wilcoxon signed rank test. * $p < 0.05$; ** $p < 0.01$; *** $p < 0.001$; **** $p < 0.0001$.

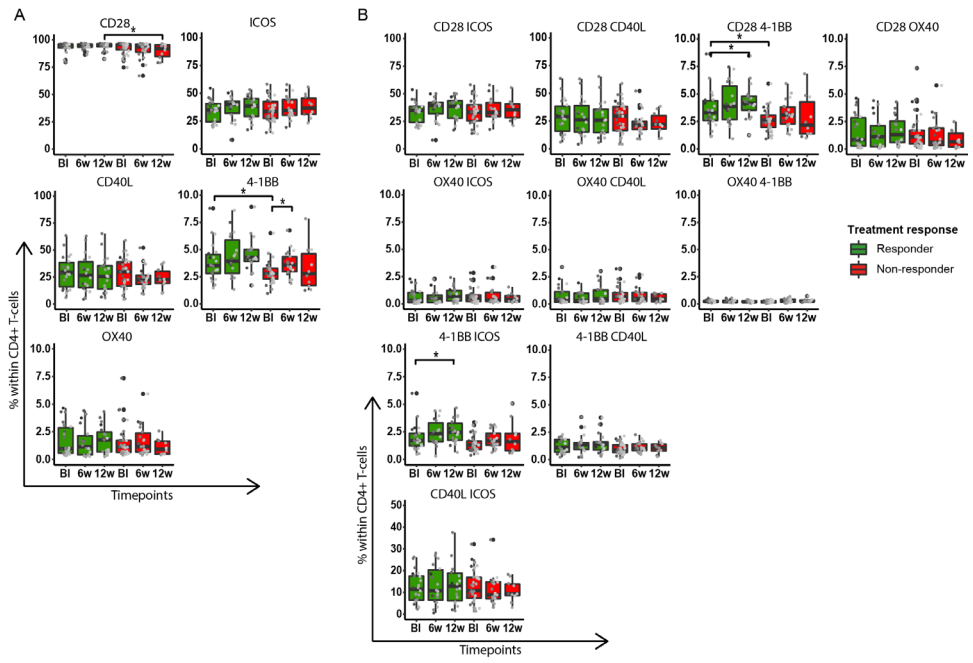

Figure 2. Patients with mUC with a tumor response to anti–PD-1 demonstrate an increased fraction of circulating 4-1BB+ CD28+ CD4+ T-cells at baseline, and an increase in this fraction during therapy. **A.** Boxplots display fractions of CD4+ T-cells expressing a single type of co-stimulatory receptor. **B.** Boxplots display fractions of CD4+ T-cells co-expressing two different types of co-stimulatory receptors. Green: responders (n = 22), red: non-responders (n = 34). Timepoints: baseline (Bl), 6 w (6 weeks of treatment), 12 w (12 weeks of treatment). See legend of Figure 1 for details on statistics.

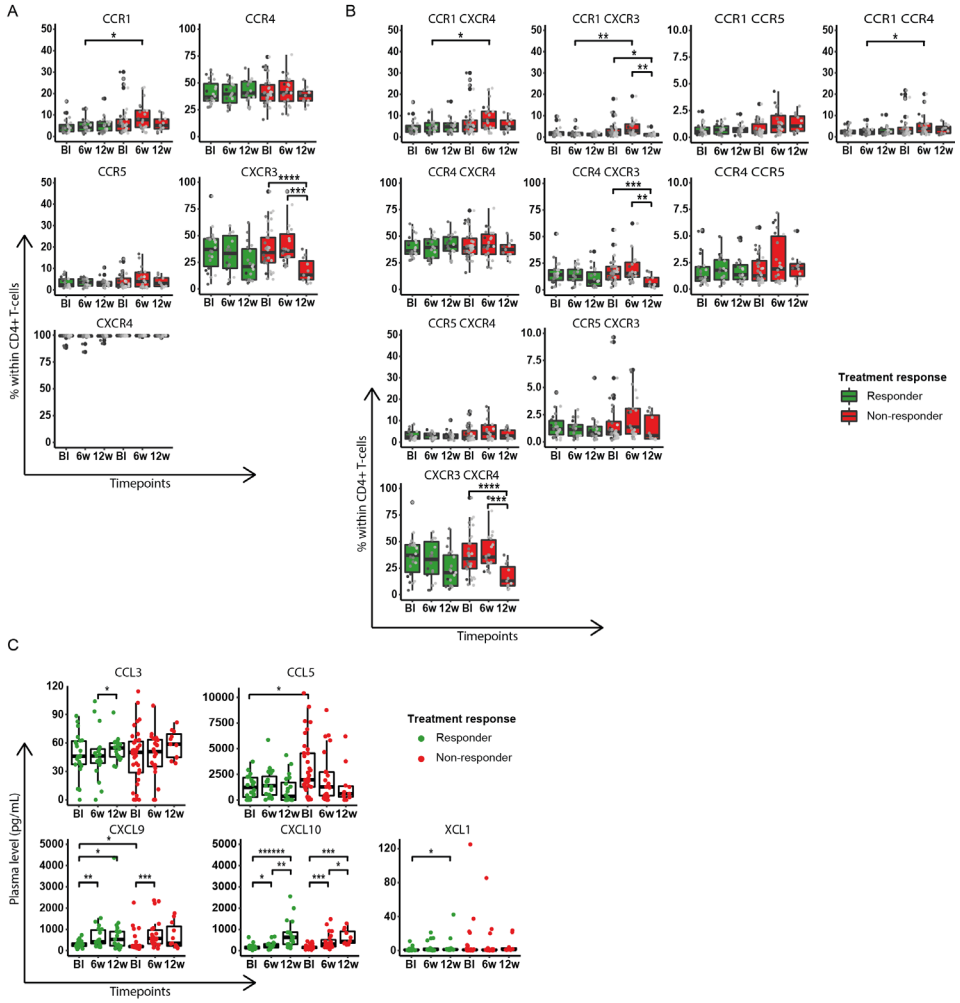

Figure 3. Patients with mUC without a tumor response to anti–PD-1 demonstrate a decrease in the fraction of circulating CXCR3+ CD4+ T-cells during treatment.
A. Boxplots display fractions of CD4+ T-cells expressing a single type of chemo-attractant receptor. **B.** Boxplots display fractions of CD4+ T-cells co-expressing two different types of chemo-attractant receptors. **C.** Levels of CCL3, CCL5, CXCL9, CXCL10, and XCL1 in plasma (pg/mL) as measured by ELISA. Green: responders (n = 22), red: non-responders (n = 34). Timepoints: baseline (Bl), 6 w (6 weeks of treatment), 12 w (12 weeks of treatment). See legend of Figure 1 for details on statistics.

Responders show high intratumoral densities of T-bet+ CD4+ T-cells at baseline

To obtain a better understanding of differences observed in blood, the presence of CD4+ T-cells, CD8+ T-cells, and CD11b+ myeloid cells was assessed in metastatic lesions using multiplex immunofluorescence (Figure 4A; see Materials and Methods for details). Tumor biopsies were available for 45 of 56 patients (Supplementary Figure 1; n = 18 responders, n = 27 non-responders), and were obtained from different metastatic sites, including lymph node, liver, and lung (Table 1). Baseline and on-treatment biopsies were obtained from the same metastatic lesion. CD4+ and CD8+ T-cells were further assessed for expression of PD-1 and CXCR3, whereas the expression of T-bet, a transcription factor typical for IFNγ-producing Th1 cells, was assessed specifically for CD4+ T-cells. The vast majority of all immune cells was present in the stroma (i.e., cytokeratin-negative area), therefore tumor (i.e., cytokeratin-positive area) and stroma areas were not distinguished in further image analysis (Supplementary Figure 4A-C). The intratumoral densities (calculated as the number of cells per mm^2) of CD4+ T-cells, CD8+ T-cells, and CD11b+ myeloid cells were similar among responders and non-responders at baseline, and remained unchanged during therapy (Figure 4B, left). Principal component analysis demonstrated that biopsy site did not affect intratumoral immune cell densities (Supplementary Figure 4D). In line with the observations in peripheral blood, most differences between responders and non-responders were observed in CD4+ T-cell subsets (Figure 4B, middle) rather than CD8+ T-cell or CD11b+ myeloid cell subsets (Figure 4B, right). At baseline, the density of T-bet+ CD4+ T-cells (i.e., Th1 cells) was significantly higher in responders compared with non-responders (Figure 4A and B). When focusing on Th1 subsets, responders had significantly higher baseline densities of PD-1+ Th1, and PD-1+ CXCR3+ Th1 cells (Figure 4B, middle). Interestingly, the intratumoral density of Th1 cells correlated positively with the intratumoral density of CD8+ T-cells (Supplementary Figure 5). Upon treatment, no changes in the density of CD4+ T-cell subsets were observed.

To further assess the contribution of CD4+ T-cell subsets, we interrogated RNA-seq data of the same lesions for the relative presence of immune cells and for different CD4+ and CD8+ T-cell subsets using reported signatures (n = 18 patients; see Materials and Methods section and Table 1 for details). We observed a higher total immune cell fraction in responders compared with non-responders. In addition, the scores for CD4+ T-cell subset signatures, specifically those capturing activated, cytotoxic, Th1, or T follicular helper cells, were higher in responders. These comparisons did not reach statistical significance due to the limited number of patients. Intratumoral gene expression of most chemo-attractants, particularly CXCL10, was also higher in responders, and it is noteworthy that high chemo-attractant expression was associated with high T-cell signature scores (Supplementary Figure 6).

Upon anti–PD-1 treatment, intratumoral Th1 cells become part of niches rich in CD8+ T-cells and CD11b+ myeloid cells in responders

Intratumoral networks between CD4+, CD8+, and CD11b+ cells were assessed by measuring distances between these cells using nearest neighbor analyses (see Materials and Methods for details). At baseline, the distance between tumor cells (cytokeratin+) and myeloid cells, and tumor cells and Th1 cells were smaller in responders compared with non/responders (Figure 5A and B), and the latter correlated positively with plasma levels of CCL5 (Supplementary Figure 5). Distances from Th1 cells to either CD8+ T-cells or CD11b+ myeloid cells did not differ between responders and non-responders at baseline. Upon treatment, distances between immune cell subsets generally became smaller and showed less variance in responders, but not in non-responders. Particularly, the distances between Th1 and CD8+ T-cells, Th1 and CD11b+ cells, and Th1 and tumor cells decreased upon treatment in responders, and were smaller compared with non-responders at week 6 (Figure 5B-D). Furthermore, distances between CD11b+ cells and CD4+ and CD8+ cells expressing CXCR3 decreased in responders upon treatment (Figure 5C). To study whether the clusters of immune cells are related to tertiary lymphoid structures (TLS), we performed CD20 stainings on consecutive tissue sections. We observed co-occurrence of B cells in immune cell clusters in the majority of responders (Supplementary Figure 7A), as well as a decrease in distance between CD20+ cells and CD8+ cells (Supplementary Figure 7B). Collectively, the smaller distances between Th1 cells, CD8+ T-cells, myeloid cells, and B cells upon anti–PD-1 treatment in responders reflect the formation of intratumoral immune cell niches (Figure 5A, left).

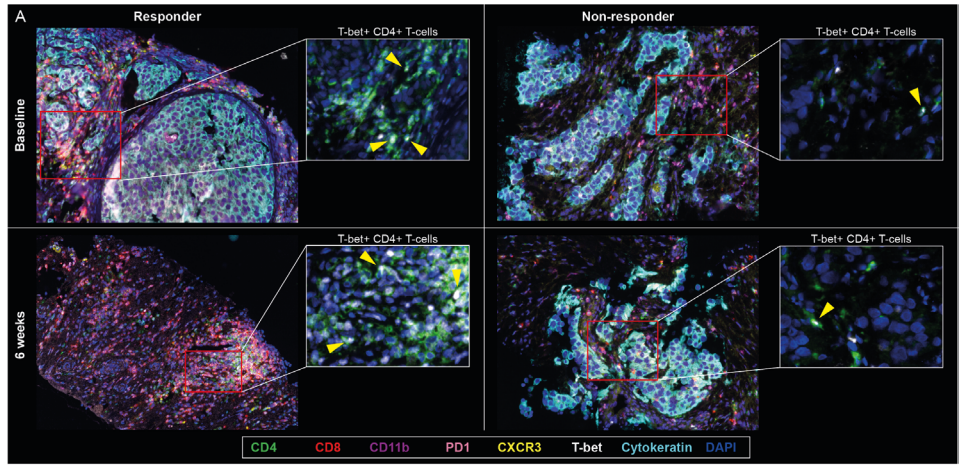

Figure 4. Prior to treatment, the intratumoral density of T-bet+ CD4+ T-cells was higher in patients with mUC with a tumor response to anti–PD-1.

A. Representative multiplex immunofluorescence images of a lymph node metastasis from a responder, and an intra-abdominal metastasis from a non-responder at baseline and week 6. Tissue sections were stained for CD4, CD8, CD11b, PD-1, CXCR3, T-bet, cytokeratin, and DAPI (see Materials and Methods for details). Red squares show regions at higher magnification, and display CD4+ T-cells (green) expressing T-bet (white). **B.** Circle plots show mean densities (cells/mm²) of: CD4+, CD8+, and CD11b+ immune cells (left); CD4+ subsets according to T-bet, PD-1, and/or CXCR3 expression (middle); and CD8+ and CD11b+ subsets according to PD-1 and/or CXCR3 expression (right). The density of CD8+ T-cells was not significantly different between responders and non-responders, or between timepoints due to variation between patients (not shown, $p = 0.47$ and $p = 0.063$, respectively). Each panel compares responders (R; $n = 18$) and non-responders (NR; $n = 27$) at baseline and week 6. Above each panel, colored circles with descending sizes are shown that reflect different numerical densities. Statistically significant differences between responders and non-responders were determined using the Mann–Whitney U test. * $p < 0.05$; ** $p < 0.01$.

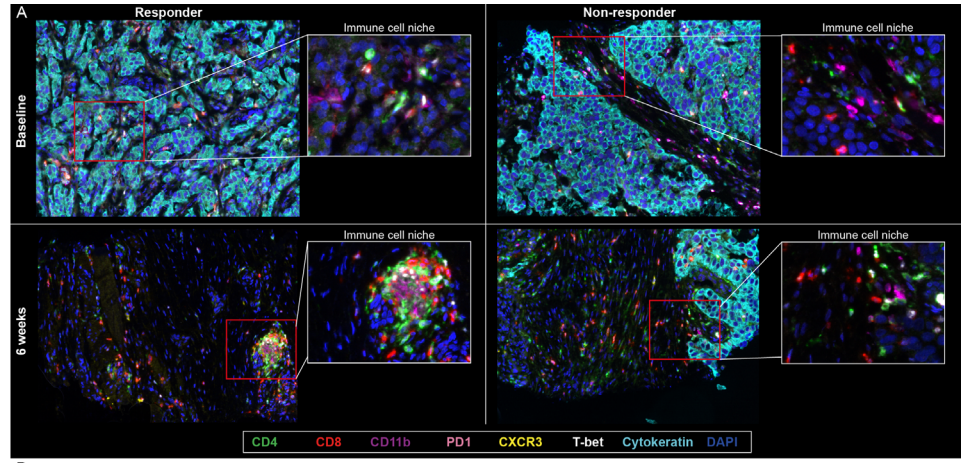

Figure 5. Treatment-induced juxtaposition of intratumoral T-cells and myeloid cells in patients with mUC with a tumor response to anti–PD-1.

A. Representative multiplex immunofluorescence images of an abdominal wall metastasis from a responder, and an intra-abdominal metastasis from a non-responder at baseline and week 6. Tissue sections were stained for CD4, CD8, CD11b, PD-1, CXCR3, T-bet, cytokeratin, and DAPI (see Materials and

Methods for details). Red squares show regions at higher magnification, and display stainings for CD4, CD8, CD11b, T-bet, and DAPI. **B-D.** Histograms show mean distance in µm (x-axis) from CD4+ T-cell subsets to CD8+ T-cell subsets (**B**); distance from CD11b+ cells to CD4+ and CD8+ T-cell subsets (**C**); and distance from tumor cells (cytokeratin+, CK) to immune cells (**D**). Green: responders (n = 18), red: non-responders (n = 27). Timepoints: baseline (Bl) and 6 weeks of treatment (6 w). Statistically significant differences between responders and non-responders were determined using the Mann–Whitney U test. * $p < 0.05$; ** $p < 0.01$; *** $p < 0.001$.

DISCUSSION

In this study, prospectively collected paired sets of blood, plasma, and tumor samples from patients with mUC treated with pembrolizumab were analyzed for peripheral blood fractions and tissue localizations of T-cell subsets. In particular, pretreatment fractions and treatment-induced changes in circulating CD4+ T-cell subsets were different between responders and non-responders. Responders displayed higher fractions of circulating CD4+ T-cells expressing co-signaling receptors (i.e., PD-1+ BTLA+ and 4-1BB+ CD28+) at baseline, and showed durable changes in these fractions during treatment. Prior to treatment, responders also had high intratumoral densities of Th1 cells, which became part of niches containing immune effector cells upon treatment. These findings are summarized in Supplementary Figure 9 and suggest that the mechanism of action of anti–PD-1 therapy in patients with mUC relies heavily on activation of CD4+ T-cells, and intratumoral clustering of Th1 cells.

Most studies investigating ICI-induced antitumor immune responses have focused on CD8+ T-cells (43, 44). For example, distinctive frequencies and localizations of CD8+ T-cells were shown in patients with melanoma (23) and non–small cell lung cancer who obtained a tumor response to anti–PD-1 (45, 46). We report that patients with mUC with a tumor response to anti–PD-1 were predominantly characterized by presence and phenotype of CD4+ T-cell subsets, suggesting that the contribution of CD4+ and CD8+ T-cell subsets to anti–PD-1 efficacy may vary per tumor type. In line with our findings, preclinical studies in mouse models of UC and non–muscle invasive bladder cancer showed that the efficacy of anti–PD-L1 treatment depends on the presence of CD4+ T-cells (47) and that efficacy of anti-PD-1 treatment is lost after CD4+ T-cell depletion (48). Furthermore, Oh and colleagues recently demonstrated that primary bladder tumors from treatment-naïve patients contained different CD4+ T-cell subsets, including a cytotoxic CD4+ T-cell subset that was able to recognize and kill tumor cells in a major histocompatibility complex (MHC) class II–dependent manner in vitro. A gene signature related to these cytotoxic CD4+ T-cells correlated with response to anti–PD-L1 in patients with mUC (42), and higher scores of this signature were also observed in responders in our cohort. It may be that the CD4+ T-cell dominance that we observed is a consequence of downregulated MHC class I expression by urothelial cancer cells (49),

which is a well-known immune escape mechanism resulting in the inability of CD8+ T-cells to recognize tumor antigens.

Responders were characterized by a higher baseline fraction of circulating CD4+ T-cells that express co-signaling receptors, and that had a more differentiated phenotype. These findings suggest that peripheral CD4+ T-cells have an antigen-experienced phenotype in responders prior to anti–PD-1 treatment, which may reflect an earlier antitumor immune response that has become prematurely halted. Up until 12 weeks of anti–PD-1 treatment, the fraction of circulating PD-1+ CD4+ T-cells decreased and the fraction of 4-1BB+ CD4+ T-cells increased in responders, most likely as a result of renewed activation of CD4+ T-cells in tumor lesions. Along these lines, the fraction of activated CD4+ T-cells (CD95+, CD103+) correlated positively with the fraction of 4-1BB+ CD4+ T-cells (Supplementary Figure 5). The changes in fractions of CD4+ T-cells expressing co-signaling receptors in non-responders were not long-lasting, which most likely mirrors an insufficient antitumor immune response in these patients. Our findings extend earlier observations that T-cell co-stimulation, which can be provided by 4-1BB, is required to rescue T-cells via anti–PD-1 treatment (50). Therefore, non-responders may benefit from combination therapy with agonistic antibodies targeting co-stimulatory receptors, to compensate for the lack of co-signaling during treatment.

When assessing T-cell recruitment to tumor tissues, we observed that treatment-induced changes in circulating CD4+ T-cells expressing chemo-attractant receptors occurred exclusively in non-responders. In fact, there was a sharp decrease in the fraction of CXCR3+ CD4+ T-cells in non-responders, which may be in line with recent studies in which repression of CXCR3 or loss of chemo-attractant expression led to abrogation of the efficacy of anti-PD-(L)1 treatment (51-53). In extension to flow cytometry, we assessed levels of chemo-attractants in tumors and plasma. At baseline, intratumoral gene expression levels of *CCL5*, *CXCL9*, *CXCL10*, and *XCL1* were higher in responders compared with non-responders, and this was generally associated with higher scores of T-cell signatures. Interestingly, baseline plasma levels of CCL5 were lower in responders, and correlated with lower intratumoral distances between Th1 cells and tumor cells. This may suggest that local production of CCL5 supports interactions between Th1 cells and tumor cells. In responders, plasma and intratumoral CXCL9 levels were higher at baseline. These findings extend earlier reports in which CXCL9 was related to effective antitumor immune responses and survival in several tumor types (54, 55), and favorable response to anti-PD-(L)1 therapy in patients with mUC (17, 19). During treatment, plasma levels of both CXCL9 and CXCL10 significantly increased in responders and to a lesser extent in non-responders. This may reflect a positive feedback loop to recruit more T-cells to the tumor site, yet we cannot exclude this to reflect a general systemic treatment effect as we did not observe a correlation between intratumoral and plasma chemo-attractant levels.

In metastatic lesions, responders displayed a 2-fold higher density of Th1 cells at baseline. Immune cell densities remained unchanged upon treatment; however, distances between Th1 cells, CD8+ T-cells, and CD11b+ myeloid cells significantly reduced in responders, suggestive of active clustering of these cells into immune cell niches. Notably, when studying the treatment response of the biopsied lesions, the baseline density of Th1 cells was higher, and distances between Th1, CD8+, and CD11b+ cells were lower in lesions with a decrease in diameter (≥30%, according to RECIST v1.1 criteria) compared with lesions with an increase in diameter (≥20%) after 12 weeks of treatment ($p = 0.078$ and $p < 0.05$, respectively). Mechanistically, pembrolizumab most likely enhances IFNγ production by Th1 cells, resulting in activation of nearby antigen presenting CD11b+ cells, such as dendritic cells, which subsequently initiate the formation of immune cell niches. Interestingly, dendritic cells express XCR1 and are a major target for XCL1 (56), a chemo-attractant that increased in plasma of responders during treatment. The niches we detected also contained B cells, and resemble TLS, which generally contain CD4+ T-cells, B cells, and other antigen presenting cells, and to a lesser extent CD8+ T-cells. Intratumoral presence of TLS has been observed in several cancer types and has previously been associated with response to ICI therapy (57–60).

It is noteworthy that the immune parameters that distinguish responders from non-responders (Supplementary Figure 9) are partly shared by patients with stable disease and are partly unique to responders (Supplementary Figure 8 and Supplementary Table 2). Particularly, responders were similar to patients with stable disease regarding fractions of PD-1+, and PD-1+ BTLA+ CD4+ T-cells in blood, as well as plasma levels of CCL5 and CXCL9. In contrast, responders deviated from patients with either stable disease or non-response regarding fractions of 4-1BB+, CD28+ 4-1BB+, and CXCR3+ CD4+ T-cells in blood. Importantly, the increased density of T-bet+ CD4+ T-cells at baseline, and shortened distances between immune cells at 6 weeks, also represented unique immune characteristics of responders.

In this study, the majority of patients received pembrolizumab as second-line treatment. PD-L1 expression, mostly assessed on archival tumor tissue, did not have predictive value for treatment response in the registration trial (7). In our study, the predictive value of PD-L1 expression was also limited, as high PD-L1 expression was observed in half of the responders, and a third of the non-responders. The intratumoral presence of CD4+ T-cell subsets at baseline, and the dynamic changes in co-signaling receptor-expressing CD4+ T-cells in blood, may provide new and early predictive markers for response to anti–PD-1. Particularly, the observations in blood can be measured in routine diagnostic laboratories at relatively low cost. Before clinical implementation, our results require validation in larger cohorts of anti–PD-1–treated patients with mUC. Furthermore, the long-term evolution of CD4+ and CD8+ T-cell responses in patients with durable responses to anti–PD-1 should be assessed in follow-up studies. With respect to limitations of the study, tumor biopsies from a single metastatic lesion have precluded the assessment of intratumoral and intertumoral heterogeneity, both of which are recognized for their impacts on ICI response (61, 62). Finally, as our study is limited by (in part) correlative analyses, studies in preclinical models of mUC are recommended towards a more defined understanding of the mechanism of action of anti–PD-1 treatment in patients with mUC.

In conclusion, we showed that efficacy of anti–PD-1 treatment in patients with mUC is accompanied by dynamic changes in the fractions of peripheral CD4+ T-cells expressing co-signaling receptors, and juxtaposition of Th1 and immune effector cells at metastatic lesions.

REFERENCES

1. Callahan Margaret K, Postow Michael A, Wolchok Jedd D. Targeting T Cell Co-receptors for Cancer Therapy. Immunity. 2016;44(5):1069-78.
2. Darvin P, Toor SM, Sasidharan Nair V, Elkord E. Immune checkpoint inhibitors: recent progress and potential biomarkers. Experimental & Molecular Medicine. 2018;50(12):165.
3. Balar AV, Castellano D, O'Donnell PH, Grivas P, Vuky J, Powles T, et al. First-line pembrolizumab in cisplatin-ineligible patients with locally advanced and unresectable or metastatic urothelial cancer (KEYNOTE-052): a multicentre, single-arm, phase 2 study. The Lancet Oncology. 2017;18(11):1483-92.
4. Balar AV, Galsky MD, Rosenberg JE, Powles T, Petrylak DP, Bellmunt J, et al. Atezolizumab as first-line treatment in cisplatin-ineligible patients with locally advanced and metastatic urothelial carcinoma: a single-arm, multicentre, phase 2 trial. Lancet. 2017;389(10064):67-76.
5. Galsky MD, Arija JÁ A, Bamias A, Davis ID, De Santis M, Kikuchi E, et al. Atezolizumab with or without chemotherapy in metastatic urothelial cancer (IMvigor130): a multicentre, randomised, placebo-controlled phase 3 trial. Lancet. 2020;395(10236):1547-57.
6. AstraZeneca. Update on Phase III DANUBE trial for Imfinzi and tremelimumab in unresectable, Stage IV bladder cancer. (News release). 2020 (updated March 6, 2020. Available from: https://bit.ly/2THDTAm.
7. Bellmunt J, de Wit R, Vaughn DJ, Fradet Y, Lee JL, Fong L, et al. Pembrolizumab as Second-Line Therapy for Advanced Urothelial Carcinoma. N Engl J Med. 2017;376(11):1015-26.
8. Rijnders M, de Wit R, Boormans JL, Lolkema MPJ, van der Veldt AAM. Systematic Review of Immune Checkpoint Inhibition in Urological Cancers. Eur Urol. 2017;72(3):411-23.
9. Fradet Y, Bellmunt J, Vaughn DJ, Lee JL, Fong L, Vogelzang NJ, et al. Randomized phase III KEYNOTE-045 trial of pembrolizumab versus paclitaxel, docetaxel, or vinflunine in recurrent advanced urothelial cancer: results of >2 years of follow-up. Ann Oncol. 2019;30(6):970-6.
10. Rijnders M, van der Veldt AAM, Zuiverloon TCM, Grünberg K, Thunnissen E, de Wit R, et al. PD-L1 Antibody Comparison in Urothelial Carcinoma. Eur Urol. 2019;75(3):538-40.
11. Ghate K, Amir E, Kuksis M, Hernandez-Barajas D, Rodriguez-Romo L, Booth CM, et al. PD-L1 expression and clinical outcomes in patients with advanced urothelial carcinoma treated with checkpoint inhibitors: A meta-analysis. Cancer Treatment Reviews. 2019;76:51-6.
12. Powles T, Walker J, Andrew Williams J, Bellmunt J. The evolving role of PD-L1 testing in patients with metastatic urothelial carcinoma. Cancer Treat Rev. 2020;82:101925.
13. FDA Alerts Health Care Professionals and Oncology Clinical Investigators about an Efficacy Issue Identified in Clinical Trials for Some Patients Taking Keytruda (pembrolizumab) or Tecentriq (atezolizumab) as Monotherapy to Treat Urothelial Cancer with Low Expression of PD-L1 2018 (updated 20-06-2018. Available from: https://www.fda.gov/Drugs/DrugSafety/ucm608075.htm.
14. EMA restricts use of Keytruda and Tecentriq in bladder cancer 2018 (updated 01-06-2018. Available from: http://www.ema.europa.eu/ema/index.jsp?curl=pages/news_and_events/news/2018/05/news_detail_002964.jsp&mid=WC0b01ac058004d5c1.
15. Ayers M, Lunceford J, Nebozhyn M, Murphy E, Loboda A, Kaufman DR, et al. IFN-gamma-related mRNA profile predicts clinical response to PD-1 blockade. J Clin Invest. 2017;127(8):2930-40.
16. Cristescu R, Mogg R, Ayers M, Albright A, Murphy E, Yearley J, et al. Pan-tumor genomic biomarkers for PD-1 checkpoint blockade-based immunotherapy. Science. 2018;362(6411).
17. Rosenberg JE, Hoffman-Censits J, Powles T, van der Heijden MS, Balar AV, Necchi A, et al. Atezolizumab in patients with locally advanced and metastatic urothelial carcinoma who have progressed following treatment with platinum-based chemotherapy: a single-arm, multicentre, phase 2 trial. The Lancet. 2016;387(10031):1909-20.
18. M.D. Galsky AS, P.M. Szabo, A. Azrilevich, C. Horak, A. Lambert, A. Siefker-Radtke, A. Necchi, P. Sharma. Impact of Tumor Mutation Burden on Nivolumab Efficacy in Second-Line Urothelial Carcinoma Patients: Exploratory Analysis of the Phase II CheckMate 275 Study. Annals of Oncology. 2017(28:v295–329).
19. Sharma P, Retz M, Siefker-Radtke A, Baron A, Necchi A, Bedke J, et al. Nivolumab in metastatic urothelial carcinoma after platinum therapy (CheckMate 275): a multicentre, single-arm, phase 2 trial. The Lancet Oncology. 2017;18(3):312-22.
20. Snyder A, Nathanson T, Funt SA, Ahuja A, Buros Novik J, Hellmann MD, et al. Contribution of systemic and somatic factors to clinical response and resistance to PD-L1 blockade in urothelial cancer: An exploratory multi-omic analysis. PLoS medicine. 2017;14(5):e1002309.
21. Al-Shibli KI, Donnem T, Al-Saad S, Persson M, Bremnes RM, Busund L-T. Prognostic Effect of Epithelial and Stromal Lymphocyte Infiltration in Non–Small Cell Lung Cancer. Clinical Cancer Research. 2008;14(16):5220-7.
22. Fridman WH, Pagès F, Sautès-Fridman C, Galon J. The immune contexture in human tumours: impact on clinical outcome. Nature Reviews Cancer. 2012;12(4):298-306.
23. Tumeh PC, Harview CL, Yearley JH, Shintaku IP, Taylor EJ, Robert L, et al. PD-1 blockade induces responses by inhibiting adaptive immune resistance. Nature. 2014;515(7528):568-71.

24. Galon J, Costes A, Sanchez-Cabo F, Kirilovsky A, Mlecnik B, Lagorce-Pagès C, et al. Type, Density, and Location of Immune Cells Within Human Colorectal Tumors Predict Clinical Outcome. Science. 2006;313(5795):1960-4.
25. Sharma P, Shen Y, Wen S, Yamada S, Jungbluth AA, Gnjatic S, et al. CD8 tumor-infiltrating lymphocytes are predictive of survival in muscle-invasive urothelial carcinoma. Proceedings of the National Academy of Sciences. 2007;104(10):3967-72.
26. Laidlaw BJ, Craft JE, Kaech SM. The multifaceted role of CD4(+) T cells in CD8(+) T cell memory. Nat Rev Immunol. 2016;16(2):102-11.
27. Eickhoff S, Brewitz A, Gerner MY, Klauschen F, Komander K, Hemmi H, et al. Robust Anti-viral Immunity Requires Multiple Distinct T Cell-Dendritic Cell Interactions. Cell. 2015;162(6):1322-37.
28. Hor JL, Whitney PG, Zaid A, Brooks AG, Heath WR, Mueller SN. Spatiotemporally Distinct Interactions with Dendritic Cell Subsets Facilitates CD4+ and CD8+ T Cell Activation to Localized Viral Infection. Immunity. 2015;43(3):554-65.
29. Bellmunt J, de Wit R, Vaughn DJ, Fradet Y, Lee JL, Fong L, et al. Pembrolizumab as Second-Line Therapy for Advanced Urothelial Carcinoma. The New England journal of medicine. 2017;376(11):1015-26.
30. Priestley P, Baber J, Lolkema MP, Steeghs N, de Bruijn E, Shale C, et al. Pan-cancer whole-genome analyses of metastatic solid tumours. Nature. 2019;575(7781):210-6.
31. Kunert A, Basak EA, Hurkmans DP, Balcioglu HE, Klaver Y, van Brakel M, et al. CD45RA(+)CCR7(-) CD8 T cells lacking co-stimulatory receptors demonstrate enhanced frequency in peripheral blood of NSCLC patients responding to nivolumab. Journal for immunotherapy of cancer. 2019;7(1):149.
32. Parks DR, Roederer M, Moore WA. A new "Logicle" display method avoids deceptive effects of logarithmic scaling for low signals and compensated data. Cytometry Part A. 2006;69A(6):541-51.
33. Van Gassen S, Callebaut B, Van Helden MJ, Lambrecht BN, Demeester P, Dhaene T, et al. FlowSOM: Using self-organizing maps for visualization and interpretation of cytometry data. Cytometry Part A. 2015;87(7):636-45.
34. McInnes L, Healy J, Melville J. UMAP: Uniform Manifold Approximation and Projection for Dimension Reduction. arXiv e-prints (Internet). 2018 February 01, 2018:(arXiv:1802.03426 p.). Available from: https://ui.adsabs.harvard.edu/abs/2018arXiv180203426M.
35. Bolger AM, Lohse M, Usadel B. Trimmomatic: a flexible trimmer for Illumina sequence data. Bioinformatics. 2014;30(15):2114-20.
36. Dobin A, Davis CA, Schlesinger F, Drenkow J, Zaleski C, Jha S, et al. STAR: ultrafast universal RNA-seq aligner. Bioinformatics. 2012;29(1):15-21.
37. Harrow J, Frankish A, Gonzalez JM, Tapanari E, Diekhans M, Kokocinski F, et al. GENCODE: the reference human genome annotation for The ENCODE Project. Genome Res. 2012;22(9):1760-74.
38. Li B, Dewey CN. RSEM: accurate transcript quantification from RNA-Seq data with or without a reference genome. BMC Bioinformatics. 2011;12(1):323.
39. Sturm G, Finotello F, Petitprez F, Zhang JD, Baumbach J, Fridman WH, et al. Comprehensive evaluation of transcriptome-based cell-type quantification methods for immuno-oncology. Bioinformatics. 2019;35(14):i436-i45.
40. Finotello F, Mayer C, Plattner C, Laschober G, Rieder D, Hackl H, et al. Molecular and pharmacological modulators of the tumor immune contexture revealed by deconvolution of RNA-seq data. Genome Medicine. 2019;11(1):34.
41. Spranger S, Bao R, Gajewski TF. Melanoma-intrinsic β-catenin signalling prevents anti-tumour immunity. Nature. 2015;523(7559):231-5.
42. Charoentong P, Finotello F, Angelova M, Mayer C, Efremova M, Rieder D, et al. Pan-cancer Immunogenomic Analyses Reveal Genotype-Immunophenotype Relationships and Predictors of Response to Checkpoint Blockade. Cell reports. 2017;18(1):248-62.
43. Oh DY, Kwek SS, Raju SS, Li T, McCarthy E, Chow E, et al. Intratumoral CD4+ T Cells Mediate Anti-tumor Cytotoxicity in Human Bladder Cancer. Cell. 2020.
44. Angell HK, Bruni D, Barrett JC, Herbst R, Galon J. The Immunoscore: Colon Cancer and Beyond. Clinical Cancer Research. 2020;26(2):332-9.
45. van der Leun AM, Thommen DS, Schumacher TN. CD8(+) T cell states in human cancer: insights from single-cell analysis. Nature reviews Cancer. 2020;20(4):218-32.
46. Donnem T, Hald SM, Paulsen EE, Richardsen E, Al-Saad S, Kilvaer TK, et al. Stromal CD8+ T-cell Density-A Promising Supplement to TNM Staging in Non-Small Cell Lung Cancer. Clin Cancer Res. 2015;21(11):2635-43.
47. Han J, Duan J, Bai H, Wang Y, Wan R, Wang X, et al. TCR Repertoire Diversity of Peripheral PD-1+ CD8+ T Cells Predicts Clinical Outcomes after Immunotherapy in Patients with Non–Small Cell Lung Cancer. Cancer Immunology Research. 2020;8(1):146-54.
48. Vandeveer AJ, Fallon JK, Tighe R, Sabzevari H, Schlom J, Greiner JW. Systemic Immunotherapy of Non-Muscle Invasive Mouse Bladder Cancer with Avelumab, an Anti-PD-L1 Immune Checkpoint Inhibitor. Cancer immunology research. 2016;4(5):452-62.
49. Sato Y, Bolzenius JK, Eteleeb AM, Su X, Maher CA, Sehn JK, et al. CD4+ T cells induce rejection of urothelial tumors after immune checkpoint blockade. JCI insight. 2018;3(23).
50. Oh DY, Kwek SS, Raju SS, Li T, McCarthy E, Chow E, et al. Intratumoral CD4+ T Cells Mediate Anti-tumor Cytotoxicity in Human Bladder Cancer. Cell. 2020;181(7):1612-25.e13.
51. Romero JM, Jiménez P, Cabrera T, Cózar JM, Pedrinaci S, Tallada M, et al. Coordinated downregulation of the

antigen presentation machinery and HLA class I/β2-microglobulin complex is responsible for HLA-ABC loss in bladder cancer. International Journal of Cancer. 2005;113(4):605-10.
52. Kamphorst AO, Wieland A, Nasti T, Yang S, Zhang R, Barber DL, et al. Rescue of exhausted CD8 T cells by PD-1-targeted therapies is CD28-dependent. Science. 2017;355(6332):1423-7.
53. Dangaj D, Bruand M, Grimm AJ, Ronet C, Barras D, Duttagupta PA, et al. Cooperation between Constitutive and Inducible Chemokines Enables T Cell Engraftment and Immune Attack in Solid Tumors. Cancer Cell. 2019;35(6):885-900 e10.
54. Chow MT, Ozga AJ, Servis RL, Frederick DT, Lo JA, Fisher DE, et al. Intratumoral Activity of the CXCR3 Chemokine System Is Required for the Efficacy of Anti-PD-1 Therapy. Immunity. 2019;50(6):1498-512 e5.
55. House IG, Savas P, Lai J, Chen AXY, Oliver AJ, Teo ZL, et al. Macrophage-Derived CXCL9 and CXCL10 Are Required for Antitumor Immune Responses Following Immune Checkpoint Blockade. Clinical cancer research : an official journal of the American Association for Cancer Research. 2020;26(2):487-504.
56. Bedognetti D, Spivey TL, Zhao Y, Uccellini L, Tomei S, Dudley ME, et al. CXCR3/CCR5 pathways in metastatic melanoma patients treated with adoptive therapy and interleukin-2. British journal of cancer. 2013;109(9):2412-23.
57. Straetemans T, Berrevoets C, Coccoris M, Treffers-Westerlaken E, Wijers R, Cole DK, et al. Recurrence of melanoma following T cell treatment: continued antigen expression in a tumor that evades T cell recruitment. Mol Ther. 2015;23(2):396-406.
58. Dorner BG, Dorner MB, Zhou X, Opitz C, Mora A, Güttler S, et al. Selective Expression of the Chemokine Receptor XCR1 on Cross-presenting Dendritic Cells Determines Cooperation with CD8⁺ T Cells. Immunity. 2009;31(5):823-33.
59. Messina JL, Fenstermacher DA, Eschrich S, Qu X, Berglund AE, Lloyd MC, et al. 12-Chemokine gene signature identifies lymph node-like structures in melanoma: potential for patient selection for immunotherapy? Scientific reports. 2012;2:765.
60. Cabrita R, Lauss M, Sanna A, Donia M, Skaarup Larsen M, Mitra S, et al. Tertiary lymphoid structures improve immunotherapy and survival in melanoma. Nature. 2020.
61. Helmink BA, Reddy SM, Gao J, Zhang S, Basar R, Thakur R, et al. B cells and tertiary lymphoid structures promote immunotherapy response. Nature. 2020.
62. Petitprez F, de Reyniès A, Keung EZ, Chen TW-W, Sun C-M, Calderaro J, et al. B cells are associated with survival and immunotherapy response in sarcoma. Nature. 2020.
63. Marusyk A, Janiszewska M, Polyak K. Intratumor Heterogeneity: The Rosetta Stone of Therapy Resistance. Cancer Cell. 2020;37(4):471-84.
64. Sidaway P. Tracing evolution reveals new biomarkers. Nature Reviews Clinical Oncology. 2020;17(1):5-.

SUPPLEMENTARY DATA

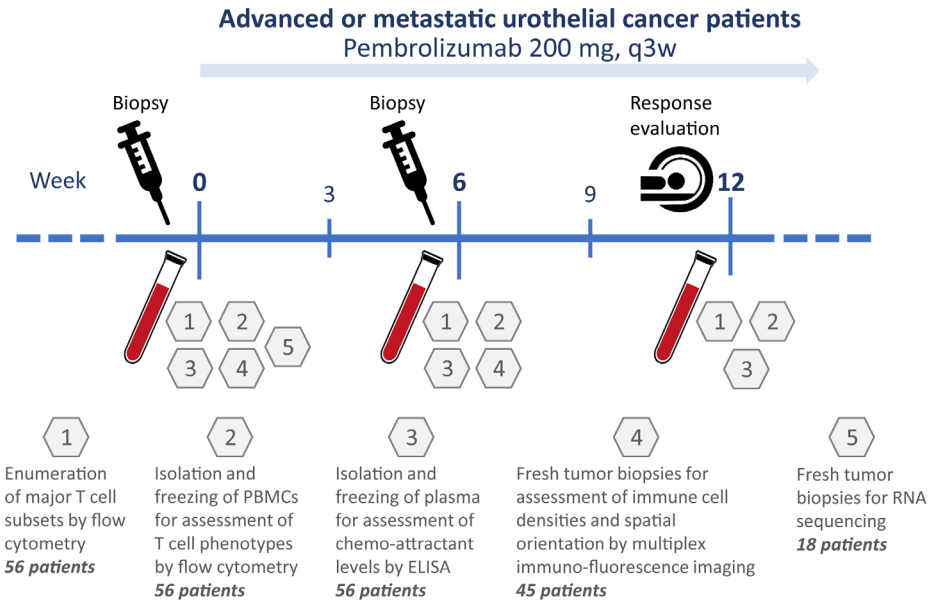

Supplementary Figure 1. Study design.
The design of the study is depicted schematically, including timeline, sample collection, and radiological imaging (see Materials and Methods for details). Handlings and analyses of different biomaterials were numbered 1 to 5. **(1)** Twenty mL of peripheral blood was collected at 3 timepoints: prior to start of treatment (0), and after 6 and 12 weeks of treatment (6 and 12). Cell counts of 4 major T-cell subsets were determined at 3 timepoints. **(2)** PBMCs were isolated and cryopreserved, stained for 20 markers and analyzed by flow cytometry at 3 timepoints. **(3)** Plasma was isolated and frozen, and chemo-attractant levels were measured by ELISA at baseline and weeks 6 and 12. **(4)** Fresh tumor biopsies were obtained from safely accessible metastatic lesions, and analyzed by multiplex immunofluorescence imaging at baseline and week 6. **(5)** Fresh tumor biopsies were analyzed by RNA sequencing at baseline. Immune phenotyping of blood, plasma and tissue was correlated with tumor response (i.e., complete and partial response) and non-response (i.e., progressive disease) based on best overall response according to RECIST v1.1.

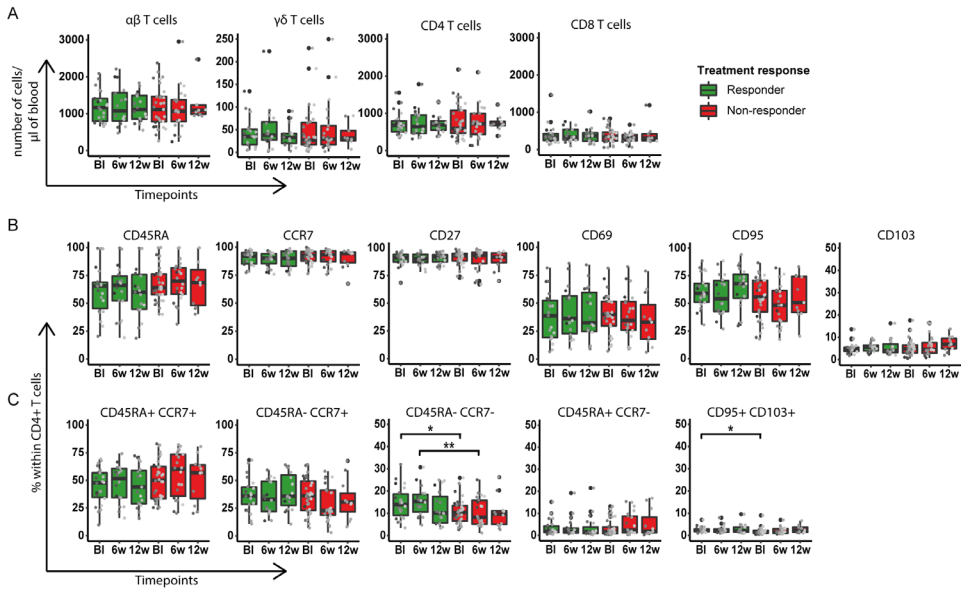

Supplementary Figure 2. Numbers of major T-cell subsets in peripheral blood and expression of T-cell maturation/activation markers on CD4+ T-cells.
A. Blood samples were obtained from 56 patients with mUC at baseline, week 6 and week 12, and were stained, ery-lysed and subsequently analyzed by multi-color flow cytometry to measure the absolute numbers of 4 major T-cell subsets (see Materials and Methods for details). **B.** Boxplots display fractions of CD4+ T-cells expressing a single type of marker of T-cell maturation/activation. **C.** Boxplots display fractions of CD4+ T-cells co-expressing two different types of markers of T-cell maturation/activation. Green: responders (n = 22), red: non-responders (n = 34). Timepoints: baseline (Bl), 6w (6 weeks of treatment), 12w (12 weeks of treatment). See legend to Figure 1 for details on statistics.

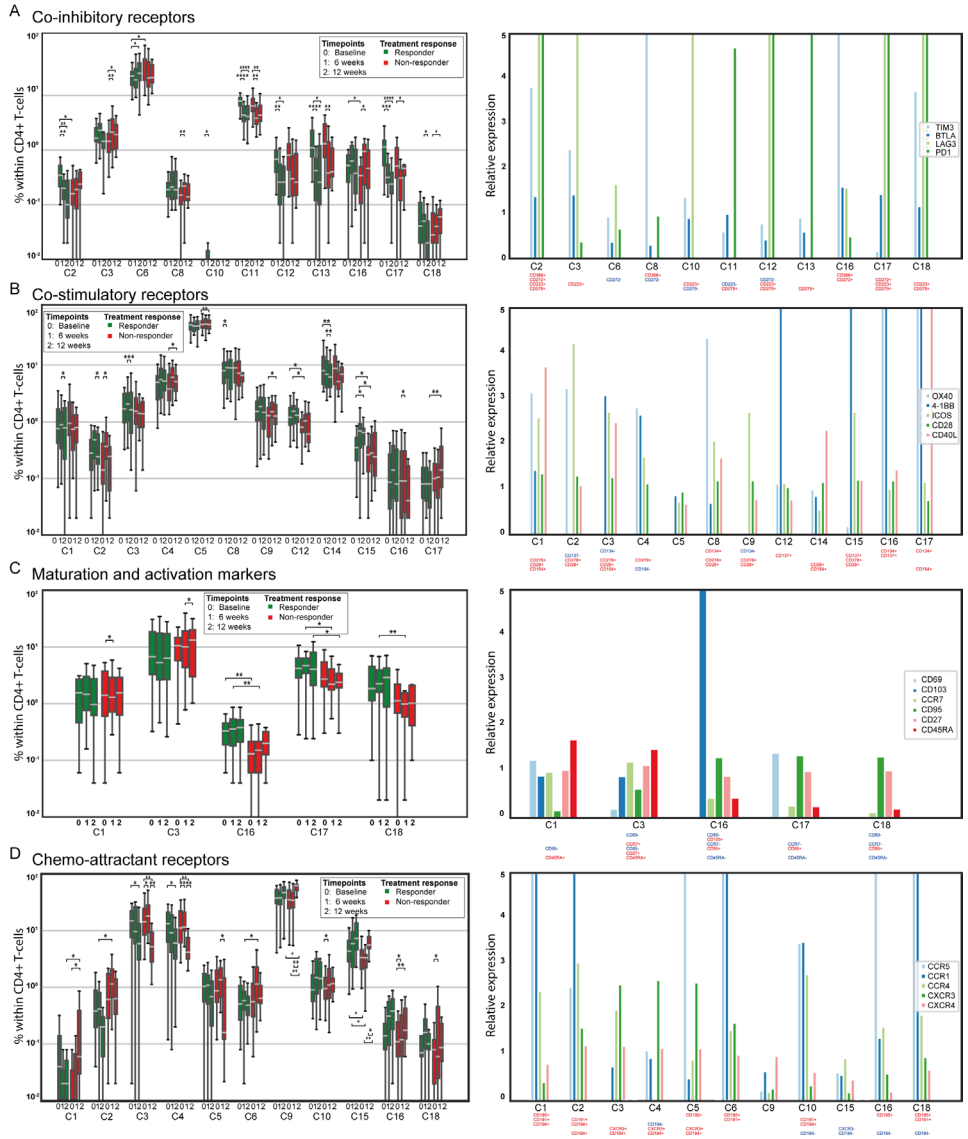

Supplementary Figure 3. Clusters of peripheral blood CD4+ T-cell subsets in patients with mUC with and without a tumor response to anti-PD-1.
Differential abundance of self-organizing map clusters of CD4+ T-cell subsets between responders and non-responders at different timepoints according to **A.** co-inhibitory receptors, **B.** co-stimulatory receptors, **C.** maturation/activation markers, and **D.** chemo-attractant receptors (left panels). Relative expressions of these sets of markers within differentially abundant clusters are displayed in the right panels in **A-D**. Timepoints: 0 (baseline), 1 (6 weeks of treatment), 2 (12 weeks of treatment). Green: responders (n = 22), red: non-responders (n = 34). See legend to Figure 1 for details on panels as well as statistics.

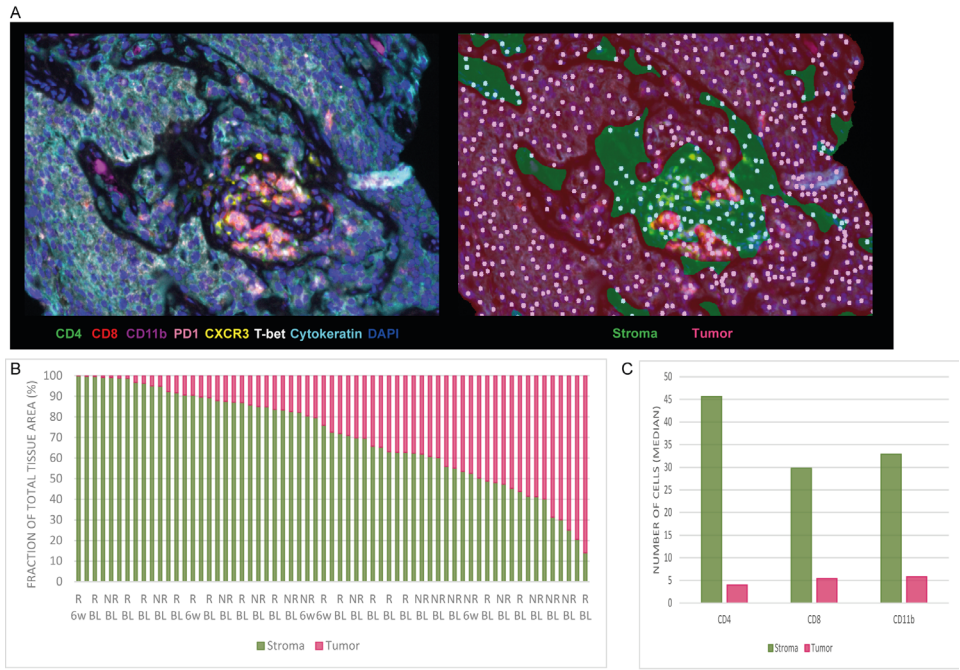

Supplementary Figure 4. Immune cells were mainly present in stroma areas of metastatic lesions of patients with mUC.
A. Representative multiplex immunofluorescence image of a lung metastasis (left image, see Materials and Methods for details) with corresponding tissue segmentation (right image; green: stroma; pink: tumor). **B.** Fraction (%) of tumor and stroma areas per specimen of responders (R; n = 18) and non-responders (NR; n = 27) at baseline (Bl) and week 6 (6w). Tumor and stroma areas were not different between responders and non-responders **C.** Median number of CD4+, CD8+, and CD11b+ immune cells in tumor and stroma areas for all patients at all timepoints (not split according to treatment response or timepoint). **D.** Principal component analysis (PCA) of intra-tumoral immune cell densities for all patient samples at baseline and week 6 stratified by biopsy site.

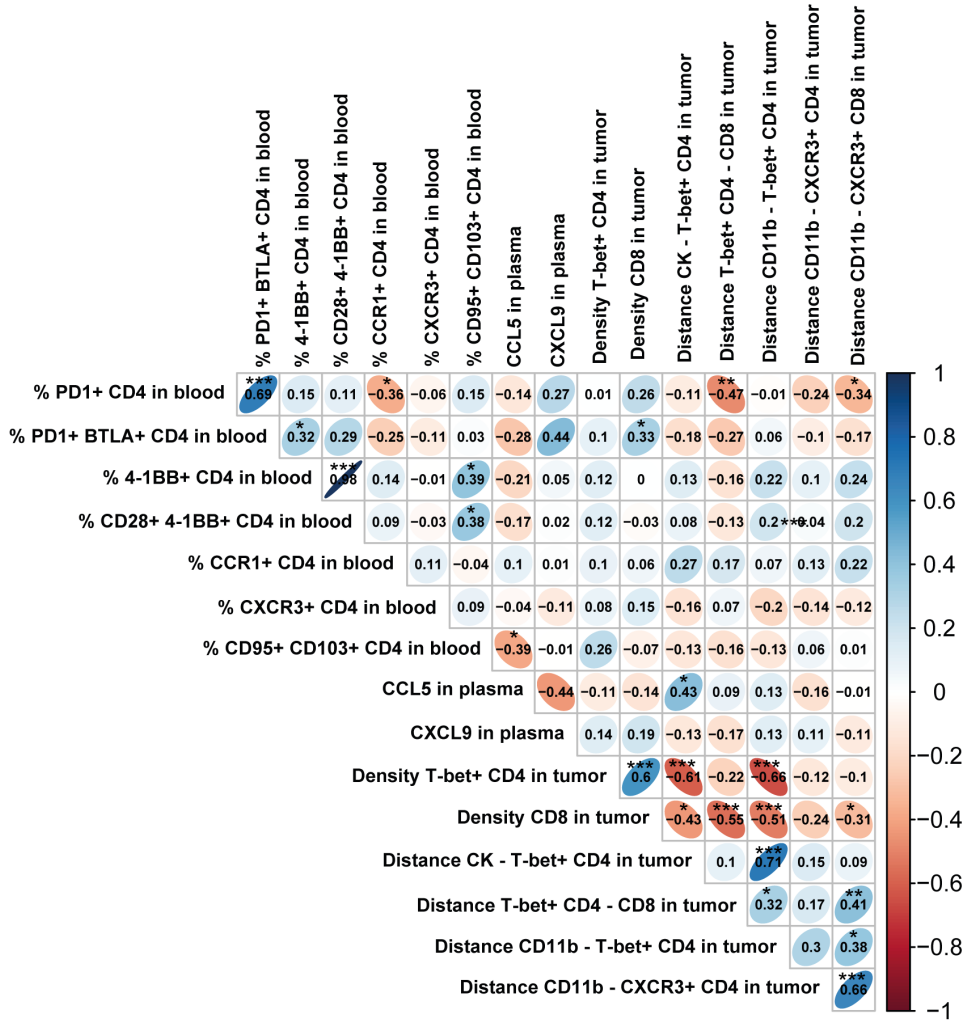

Supplementary Figure 5. Correlations between immune parameters in blood, plasma and tumor tissue.
Matrix of Spearman correlation coefficients between selected immune cell subsets in blood (%), levels of chemo-attractants in plasma (pg/ml), densities of immune cells in tumor (cells/mm²), and distances between immune cells in tumor (µm) at baseline. Paired measurements were available for 42 patients. * $p < 0.05$; ** $p < 0.01$; *** $p < 0.001$.

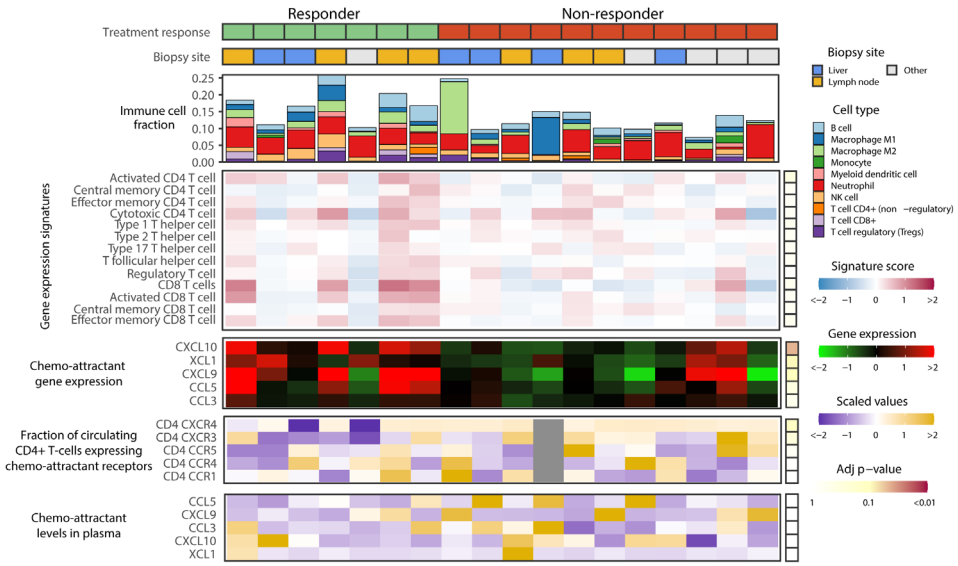

Supplementary Figure 6. Transcriptomic analysis of immune cell fractions, T-cell subsets, and chemo-attractants of baseline metastatic tumor biopsies from patients with mUC.
Patients were stratified according to best overall response to treatment (n = 7 responders; n = 11 non-responders). From top to bottom: type of metastatic lesion; immune cell fractions estimated using quanTIseq; scores for CD4+ and CD8+ T-cell gene expression signatures (41-43); intra-tumoral gene expression of chemo-attractants; scaled fractions of CD4+ T-cells that express chemo-attractant receptors in blood; scaled levels of chemo-attractants in plasma.

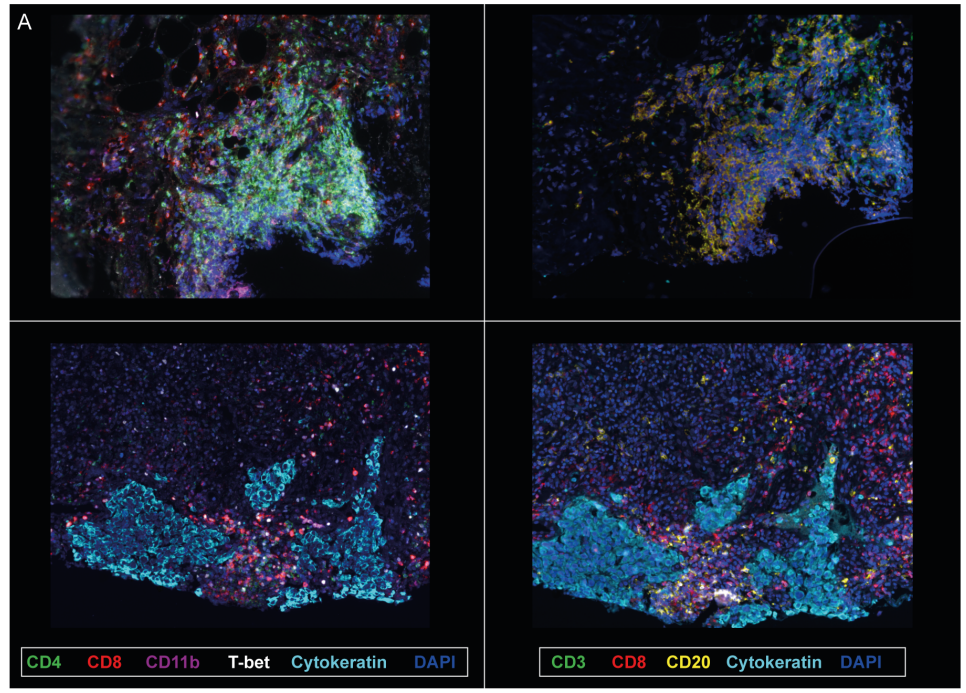

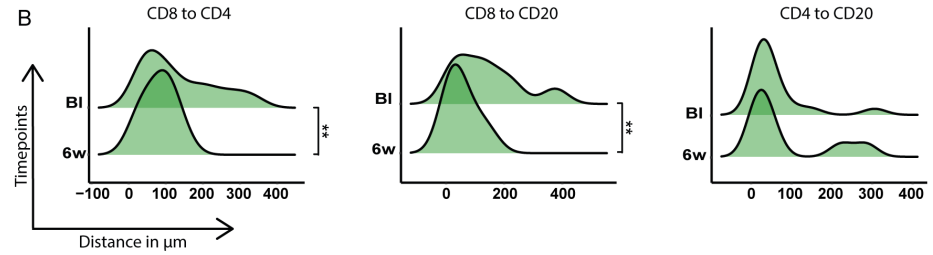

Supplementary Figure 7. CD20+ B cells are present in immune cell niches in lesions of responders upon anti-PD-1 treatment.
A. Representative multiplex immunofluorescence images of a lung metastasis (upper panels) and a lymph node metastasis (lower panels) from responders at week 6. Consecutive tissue sections were stained for CD4, CD8, CD11b, T-bet, cytokeratin, and DAPI (left panels), and for CD3, CD8, CD20, cytokeratin, and DAPI (right panels; see Materials and Methods for details). **B.** Histograms show mean distance in µm (x-axis) from CD8+ to CD4+ cells (defined as CD3+ CD8- cells), CD8+ to CD20+ cells, and CD4+ to CD20+ cells. Green: responders (n = 18). Timepoints: baseline (Bl) and 6 weeks of treatment (6w). Statistically significant differences between baseline and week 6 were determined for paired samples using the Wilcoxon signed rank test. * $p < 0.05$; ** $p < 0.01$.

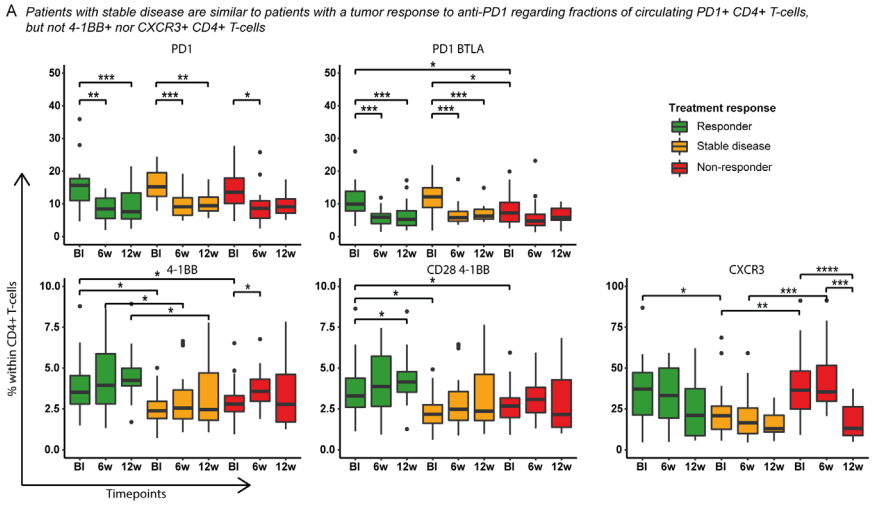

Supplementary Figure 8. Highlighted immune parameters in blood, plasma and tumor tissue from patients with mUC with stable disease as best overall response to anti-PD-1.
Numerical, phenotypical and immune contextual features of CD4+ T-cells that characterize responders are displayed for patients with mUC with stable disease. **A.** Boxplots display fractions of CD4+ T-cells (co-)expressing one or two different types of co-inhibitory receptors, co-stimulatory receptors, or chemo-attractant receptors. **B.** Levels of CCL5 and CXCL9 in plasma (pg/mL) as measured by ELISA. **C.** Circle plot showing mean densities (cells/mm²) of T-bet+ CD4+ T-cells in responders (R), patients with

stable disease (SD), and non-responders (NR), at baseline and week 6. Next to the figure, colored circles with descending sizes are shown that reflect different numerical densities. **D.** Histograms show mean distances between intra-tumoral immune cell subsets and/or tumor cells (CK) in µm (x-axis). Treatment response was determined according to best overall response, green: responder (n = 18-22); orange: stable disease (n = 14-17), red: non-responder (n = 27-34). Statistically significant differences between SD, R and NR were determined using the Mann-Whitney U test, differences between timepoints were determined for paired samples using the Wilcoxon signed rank test. * $p < 0.05$; ** $p < 0.01$; *** $p < 0.001$; **** $p < 0.0001$. Supplementary Table 1 provides an overview of all statistically significant differences between SD, R and NR, at baseline and week 6 and 12.

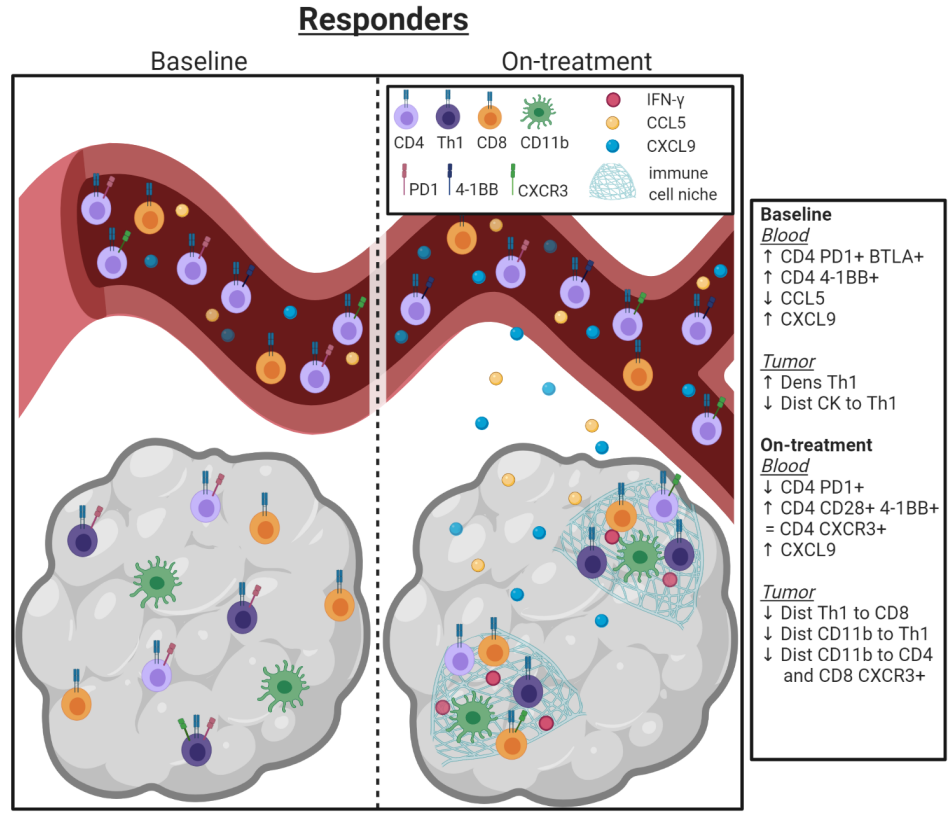

Supplementary Figure 9. Proposed mechanism of action of pembrolizumab in patients with mUC.
Schematic overview of numerical, phenotypical and immune contextual features of CD4+ T-cells and other immune cells in patients with mUc with a tumor response to anti-PD-1. See discussion section for details. Created with BioRender.

Supplementary Table 1. Immune parameters in blood, plasma and tumor tissue from patients with mUC with stable disease as best overall response to anti-PD-1

	Blood	Plasma	Tumor tissue
Baseline			
	Compared to non-responder		
	↑ % LAG3+ CD4+ * ↑ % BTLA+ CD4+ * ↑ % LAG3+ BTLA+ CD4+ ** ↑ % LAG3+ PD1+ CD4+ ** ↑ % PD1+ BTLA+ CD4+ * ↓ % 4-1BB+ OX40+ ** ↓ % CXCR3+ CD4+ ** ↓ % CXCR3+ CXCR4+ CD4+ ** ↓ % CXCR3+ CCR4+ CD4+ **	↓ CCL5 * ↑ CXCL9 ***** ↑ CXCL10 ***	↑ Dens CD8+ * ↓ Dens CXCR3+ CD8+ * ↓ Dens CXCR3+ PD1+ CD8+ ** ↓ Dist CD4+ to CD8+ ** ↓ Dist T-bet+ CD4+ to CD8+ * ↓ Dist CXCR3+ CD4+ to CD8+ ** ↓ Dist C11b+ to CD8+ * ↓ Dist CK+ to CD8+ *
On treatment			
	Compared to non-responder		
	6w ↑ % CD28+ CD4+ * 6w, 12w ↓ % 4-1BB+ OX40+ CD4+ **/**** 6w ↓ % CXCR3+ CD4+ *** 6w ↓ % CXCR3+ CCR1+ CD4+ *** 6w ↓ % CXCR3+ CCR4+ CD4+ ** 6w ↓ % CXCR3+ CCR5+ CD4+ * 6w ↓ % CXCR3+ CXCR4+ CD4+ *** 12w ↓ % CCR1+ CCR5+ CD4+ *	6w, 12w ↑ CXCL9 *****/*** 6w ↑ CXCL10 *	↑ Dens CD8 * ↑ Dens CD11b * ↓ Dens CXCR3+ PD1+ CD4+ * ↓ Dens CXCR3+ PD1+ CD8+ *
	Compared to baseline		
	6w, 12w ↓ % PD1+ CD4+ ***/** 6w, 12w ↓ % PD1+ BTLA+ CD4+ ***/*** 12w ↓ % PD1+ LAG3+ CD4+ **	6w, 12w ↑ CXCL9 ***/*** 6w, 12w ↑ CXCL10 ***/***	No differences

Overview of observed differences in immune parameters in blood, plasma, and tumor tissue for patients with stable disease (n = 14-17) compared to non-responders (n = 27-34), and comparing differences between baseline, week 6 (6w), and week 12 (12w). Treatment response was determined according to best overall response. Statistically significant differences between patients with stable disease and non-responders were determined using the Mann-Whitney U test, differences between timepoints were determined for paired samples using the Wilcoxon signed rank test. * $p < 0.05$; ** $p < 0.01$; *** $p < 0.001$; **** $p < 0.0001$; ***** $p < 0.00001$.

Supplementary Table 2. Fractions of circulating CD8+ T-cell subsets in patients with mUC with and without a tumor response to anti-PD-1.

	Responder	Non-responder
Baseline	*Compared to non-responder* • ↑ % BTLA+ * • ↑ % BTLA+ LAG3+ *** • ↑ % BTLA+ PD1+ ** • ↑ % CD28+ 4-1BB+ * • ↓ % CXCR4+ *	
On-treatment	*Compared to non-responder* • ↑ % CD28+ ** • ↑ % CD28+ 4-1BB+ * • ↓ % CCR1+ CXCR4+ * • ↓ % CCR1+ CXCR3+ * *Compared to baseline* • 6w ↓ % CXCR4+ *	*Compared to baseline* • 6w, 12w ↑ % TIM3+ * • 12w ↑ % LAG3+ * • 6w ↑ % 4-1BB+ * • 12w ↓ % CXCR3+ **** • 12w ↓ % CCR1+ CXCR3+ *****

Summary of peripheral CD8+ T-cells subsets with differential fractions in blood in responders (n = 22) and non-responders (n = 34) at baseline, week 6 (6w), and week 12 (12w).

CHAPTER 7

A blood-based immune marker for resistance to pembrolizumab in patients with metastatic urothelial cancer

Maud Rijnders
Debbie G.J. Robbrecht
Astrid A.M. Oostvogels
Mandy van Brakel
Joost L. Boormans
Maureen J.B. Aarts
Hayri E. Balcioglu
Paul Hamberg
Jens Voortman
Hans M. Westgeest
Martijn P. Lolkema
Ronald de Wit
Astrid A.M. van der Veldt
Reno Debets

Published in Cancer Immunology, Immunotherapy, 2022 Aug 17

ABSTRACT

PD1 inhibition is effective in patients with metastatic urothelial cancer (mUC), yet a large fraction of patients does not respond. In this study, we aimed to identify a blood-based immune marker associated with non-response to facilitate patient selection for anti-PD1. To this end, we quantified 18 immune cell populations using multiplex flow cytometry in blood samples from 71 patients with mUC (as part of a biomarker discovery trial; NCT03263039, registration date 28-08-2017). Patients were classified as responder (ongoing complete or partial response, or stable disease; n = 25) or non-responder (progressive disease; n = 46) according to RECIST v1.1 at 6 months of treatment with pembrolizumab. We observed no differences in numbers of lymphocytes, T-cells, granulocytes, monocytes or their subsets between responders and non-responders at baseline. In contrast, analysis of ratios of immune cell populations revealed that a high mature neutrophil-to-T-cell ratio (MNTR) exclusively identified non-responders. In addition, the survival of patients with high versus low MNTR was poor: median overall survival (OS) 2.2 vs 8.9 months (hazard ratio (HR) 6.6; $p < 0.00001$), and median progression-free survival (PFS) 1.5 vs 5.2 months (HR 5.6; $p < 0.0001$). The associations with therapy response, OS, and PFS for the MNTR were stronger than for the classical neutrophil-to-lymphocyte ratio (HR for OS 3.5, and PFS 3) and the PD-L1 combined positivity score (HR for OS 1.9, and PFS 2.1). In conclusion, the MNTR distinctly and uniquely identified non-responders to treatment and may represent a novel pre-treatment blood-based immune metric to select patients with mUC for treatment with pembrolizumab.

INTRODUCTION

The therapeutic landscape of metastatic urothelial cancer (mUC) has changed since immune checkpoint inhibitors (ICI) directed against programmed cell death protein (PD)1 or its ligand (PD-L1) were introduced. ICIs are approved in the first- (1, 2) and second-line setting (3, 4) for mUC, as maintenance therapy for patients who had a response to chemotherapy (5), and for treatment of Bacillus Calmette-Guérin-unresponsive carcinoma in situ of the bladder (6). Overall, response rates of ICIs in mUC are modest, and given the high costs and accompanying toxicities (7) pre-treatment selection of patients is critical.

Currently, PD-L1 expression in tumor tissue is the only approved biomarker that is used for selection of cisplatin-ineligible patients for ICIs in the first-line setting (8, 9). In the second-line setting, PD-L1 expression does not have predictive value (3), and no biomarkers are applied yet for patient selection. In an effort to identify new selection markers, previous studies have revealed that numbers of circulating T-cells at baseline, and dynamic changes in particular T-cell subsets during treatment, are associated with response to ICIs (10,11,12,13). Furthermore, a relationship between the neutrophil-to-lymphocyte ratio (NLR) and clinical outcome of patients has been observed in multiple tumor types, including UC (14,15,16,17). However, these studies generally have shortcomings, such as lack of predictive value, use of immune cell fractions rather than numbers, and focus on on-treatment rather than baseline predictors. In the current study, we have enumerated 18 immune cell populations in blood of 71 patients with mUC by multiparameter flow cytometry, to study whether individual immune cell populations or ratios thereof identify patients with mUC who do or do not respond to pembrolizumab.

MATERIALS AND METHODS

Patients and assessment of clinical response

Patients with locally advanced or mUC of the bladder or upper urinary tract with an indication for pembrolizumab were included in a phase II prospective biomarker discovery study (NCT03263039), and treated as described previously (pembrolizumab, 200 mg intravenously, 3-weekly (18)). Patients were classified as responder (ongoing complete or partial response, or stable disease) or non-responder (progressive disease) at 6 months after treatment initiation according to response evaluation criteria in solid tumors (RECIST) v1.1. Overall survival (OS) was defined as the time from start of pembrolizumab to date of death; progression-free survival (PFS) was defined as the time from start of pembrolizumab to clinical or radiological disease progression.

Multiplex flow cytometry of blood samples

Peripheral blood was prospectively collected in EDTA tubes at baseline, and weeks 6 and 12 of treatment. Whole blood was stained and analyzed by multiplex flow cytometry to quantify 18 immune cell populations as described previously (19), antibody specifications are listed in Supplementary Table 1. In short, lymphocyte, T-cell, granulocyte, and monocytes populations were gated separately in a scatter plot of CD45+staining versus side scatter. Immune cell populations were further defined using the following markers for B cells: CD3- CD19+; natural killer (NK) cells: CD3- CD56+CD16±; T-cells: CD3+; γδ T-cells: CD3+TCRγδ+; CD4 or CD8 T-cells: CD3+TCRγδ- CD4+or CD8+; eosinophils: CD15+CD16-; mature neutrophils: CD15high CD16high; immature neutrophils: CD15+CD16+; classical monocytes: CD14+CD16-; intermediate monocytes: CD14+CD16+; non-classical monocytes: CD14- CD16+; dendritic cells (DC): CD14- CD16- CD11c+; and myeloid derived suppressor cells (MDSC): CD14+CD16- CD11b+HLA-DRlow. Besides quantitation of immune cell populations for individual timepoints, we performed normalization of data to more specifically assess longitudinal changes in numbers of immune cell populations. To this end, the measured numbers were normalized per patient by subtracting the patients' mean number for a given population from the individual measurement, followed by addition of the overall mean number of that particular population.

PD-L1 immunohistochemistry and scoring

The PD-L1 combined positivity score (CPS) was determined on fresh metastatic tumor biopsies obtained prior to start of therapy (n=46), or archival tumor tissue (n=25), using the companion diagnostic assay of pembrolizumab (PD-L1 IHC 22C3 pharmDx, Agilent Technologies, Carpinteria, CA, USA).

Multiplex immunofluorescence of tumor tissue

Multiplex immunofluorescence was performed using OPAL reagents (Akoya Biosciences, Marlborough, MA, USA) on 4-µm sections of FFPE tumor biopsies as described previously (18). The sequence of antibody stainings was as follows: 1. CD4 (FP1600/EP204, Akoya Biosciences, 1:100) – OPAL520; 2. CD8 (FP1601/144B, Akoya Biosciences, 1:200) – OPAL690; 3. CD66b (80H3, Sanbio, 1:100) – OPAL570; 4. Cytokeratin-Pan (AE1/AE3, Invitrogen, 1:500) – Opal 620; and 5. DAPI. Digital image analysis was also performed as described previously (18). Cellular densities were calculated by dividing the number of cells with a certain phenotype by the total area of that region and were averaged per patient across all regions of interest. Distances from a cell with a certain phenotype to the nearest cell with another phenotype were calculated by nearest neighbor analysis; this was averaged across all cells, and per patient across all regions of interest.

Statistical analysis

Statistical analysis was performed using R version 3.5.1. Use of the Mann–Whitney U, Wilcoxon signed rank, or Fisher's exact test is specified in figure legends. The optimal cut-off level for dichotomous analysis of immune markers was determined using receiver operating characteristic (ROC) curves. OS and PFS were estimated using Kaplan–Meier estimates, patients who were alive or without disease progression were censored at last date the patient was known to be alive, or at last date of tumor assessment. Hazard ratios (HR) were calculated using univariate Cox regression models. Multivariate Cox regression analysis was performed for known risk factors: performance status, hemoglobin concentration, presence of liver metastases, and time since completion of previous treatment. Correction for multiple testing was performed using the Holm-Bonferroni method.

RESULTS

Patient cohort

In this study, 71 patients with mUC received first- (n=9) or second-line (n=62) treatment with pembrolizumab. Non-responders were younger than responders and had a lower albumin concentration in blood (Table 1). For patients who received first-line pembrolizumab a PD-L1 CPS of ≥10 was required; five of these patients were responders. In the second-line setting, 55% of responders versus 29% of non-responders had a positive PD-L1 CPS (Table 1).

No differential numbers of immune cell populations in blood of non-responders versus responders to pembrolizumab at baseline.

Fresh blood samples were available for 71 patients at baseline (n=26 responders, n=45 non-responders), for 55 patients at week 6 (n=21 responders, n=34 non-responders), and for 38 patients at week 12 (n=22 responders, n=16 non-responders). At baseline, no differences were observed between responders and non-responders in the numbers (number of cells per µl blood) of lymphocytes and their subsets (B cells, NK cells, and CD16+NK cells; Figure 1a), T-cells and their subsets (T-cells, γδ T-cells, CD4+T-cells, and CD8+T-cells; Figure 1b), granulocytes and their subsets (eosinophils, immature neutrophils, and mature neutrophils; Figure 1c), nor monocytes and their subsets (classical monocytes, intermediate monocytes, non-classical monocytes, MDSC, and DC; Figure 1d). Also at weeks 6 and 12 of therapy, the numbers of all 18 immune cell populations in blood remained non-different between responders and non-responders (Figure 1a–d). To specifically assess therapy-induced changes, numbers of immune cell populations were normalized per patient (see methods section). We did not observe on-treatment changes in any of the immune cell populations either in responders or non-responders (Supplementary Figure 1).

Table 1. Patient characteristics of 71 patients with metastatic urothelial cancer.

	Responders n = 25	Non-responders n = 46	p-value
Age - median (range) ‡	72 (41-85)	67 (29-78)	**0.03**
Male gender - no. (%)§	21 (84%)	30 (65%)	0.09
Primary tumor location - no. (%)§			
Bladder	18 (72%)	26 (57%)	0.31
Upper urinary tract	4 (16%)	17 (37%)	0.10
Both	3 (12%)	3 (7%)	0.66
Prognostic factors - no. (%)§			
ECOG performance score of 1[1]	16 (64%)	29 (63%)	1.0
Lymph node-only disease	9 (36%)	9 (20%)	0.15
Liver metastases	4 (16%)	16 (35%)	0.10
Lactate dehydrogenase concentration >248 U/L	6 (24%)	13 (28%)	0.79
Hemoglobin concentration <10 g/dL	19 (76%)	40 (87%)	0.32
Albumin concentration <35 mg/L	0	7 (15%)	**0.047**
Treatment-free interval <3 months from previous chemotherapy	4 (20%)	14 (33%)	0.38
Treatment line - no. (%)§			
First-line	5 (20%)	4 (9%)	0.262
Second-line	20 (80%)	42 (91%)	
PD-L1 combined positivity score[2] - no. (%)§			
Positive (≥10) in first-line patients	5 (100%)	4 (100%)	1.0
Positive (≥10) in second-line patients	11 (55%)	12 (29%)	0.054

Patients were stratified according to response to pembrolizumab at 6 months of therapy (responders: ongoing complete or partial response, or stable disease; non-responders: progressive disease). 1Eastern cooperative oncology group performance status, score of 0 or 1 was required. 2PD-L1 expression in tumor tissue according to the companion diagnostic assay of pembrolizumab. ‡ Mann-Whitney U test, §Fisher's Exact test.

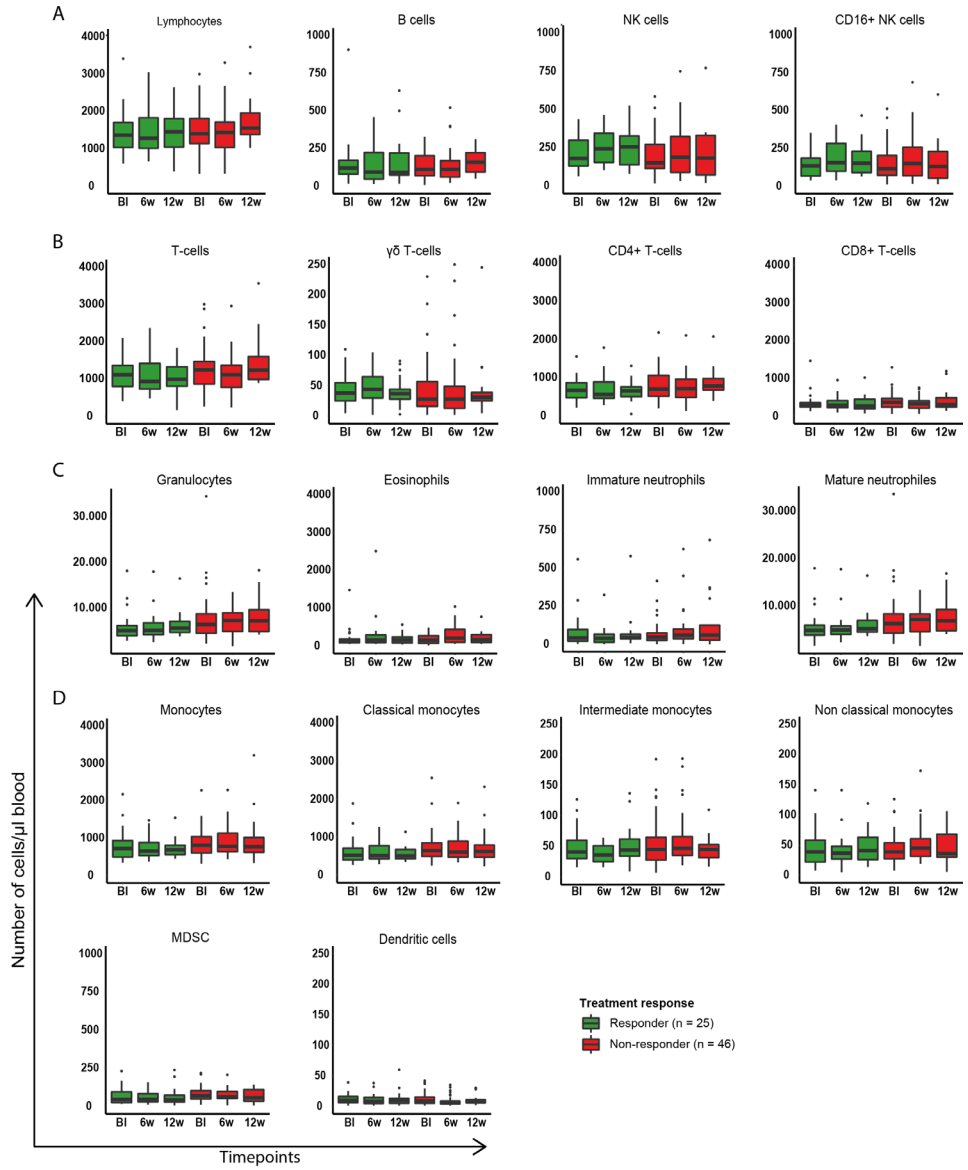

Figure 1. Responders to pembrolizumab had lower numbers of mature neutrophils and intermediate monocytes in blood compared to non-responders after 6 weeks.
Boxplots display the number of cells belonging to subsets of: **A**. lymphocytes; **B**. T-cells; **C**. granulocytes; and **D**. monocytes per microliter blood. Immune markers per subset are provided in the methods section. Timepoints: baseline (Bl), 6w, 12w (6, 12 weeks of treatment). Differences between responders and non-responders were determined using the Mann-Whitney U test, and differences between timepoints were determined for paired samples using the Wilcoxon signed rank test, p-values were corrected for multiple testing using the Holm-Bonferroni method.

The mature neutrophil-to-T-cell ratio at baseline exclusively identifies non-responders to pembrolizumab

Since numbers of individual immune cell populations were not distinctive between responders and non-responders at baseline, we systematically interrogated ratios of granulocyte, monocyte and lymphocyte subsets, and assessed their association with OS and PFS at their respective optimal cut-off levels (Figure 2). We assessed the classical NLR, defined as the quotient of the sum of mature and immature neutrophil counts and the sum of total lymphocyte and T-cell counts, and the PD-L1 CPS, as references. For granulocyte subsets, the ratio of mature neutrophils to lymphocytes showed similar associations with OS and PFS as the classical NLR, whereas no associations were observed for immature neutrophils or eosinophils. For monocyte subsets, the ratio of monocytes to lymphocytes was associated with OS and PFS. For lymphocyte subsets, the strongest association with OS and PFS was observed for the ratio of mature neutrophils to T-cells (MNTR), which was mostly attributed to CD4+ and not CD8+ T-cells. The median value of the MNTR was not different between responders and non-responders (Figure 3A, left graph). When using an optimal cut-off level of 11.5 (Figure 3A, middle graph), this ratio exclusively identified non-responders (n = 9; Figure 3A, right graph). The positive predictive value (PPV) of a high MNTR for non-response to therapy was 100%, with a specificity of 100% and sensitivity of 19%. Thereby the MNTR outperforms the classical NLR (PPV 91%, specificity 96%, sensitivity 22%) and the PD-L1 CPS in the total cohort (PPV 50%, specificity 36%, sensitivity 35%). Patients with a high versus low MNTR had a significantly shorter OS (median 2.2 vs 8.9 months; HR 6.6; p = 5.6x10-6) and PFS (median 1.5 vs 5.2 months; HR 5.6; p = 2x10-5; Figure 3B). This association with survival was stronger compared to the classical NLR (Figure 3C) and PD-L1 CPS (Figure 3D). Finally, multivariate cox regression analysis revealed that MNTR was the strongest factor associated with OS (p < 0.0001) and PFS (p < 0.0001), and a weaker association was observed for presence of liver metastases (p = 0.02 for OS, and not significant for PFS), and a treatment-free interval of less than three months from previous chemotherapy (p = 0.021 for OS, and p = 0.03 for PFS).

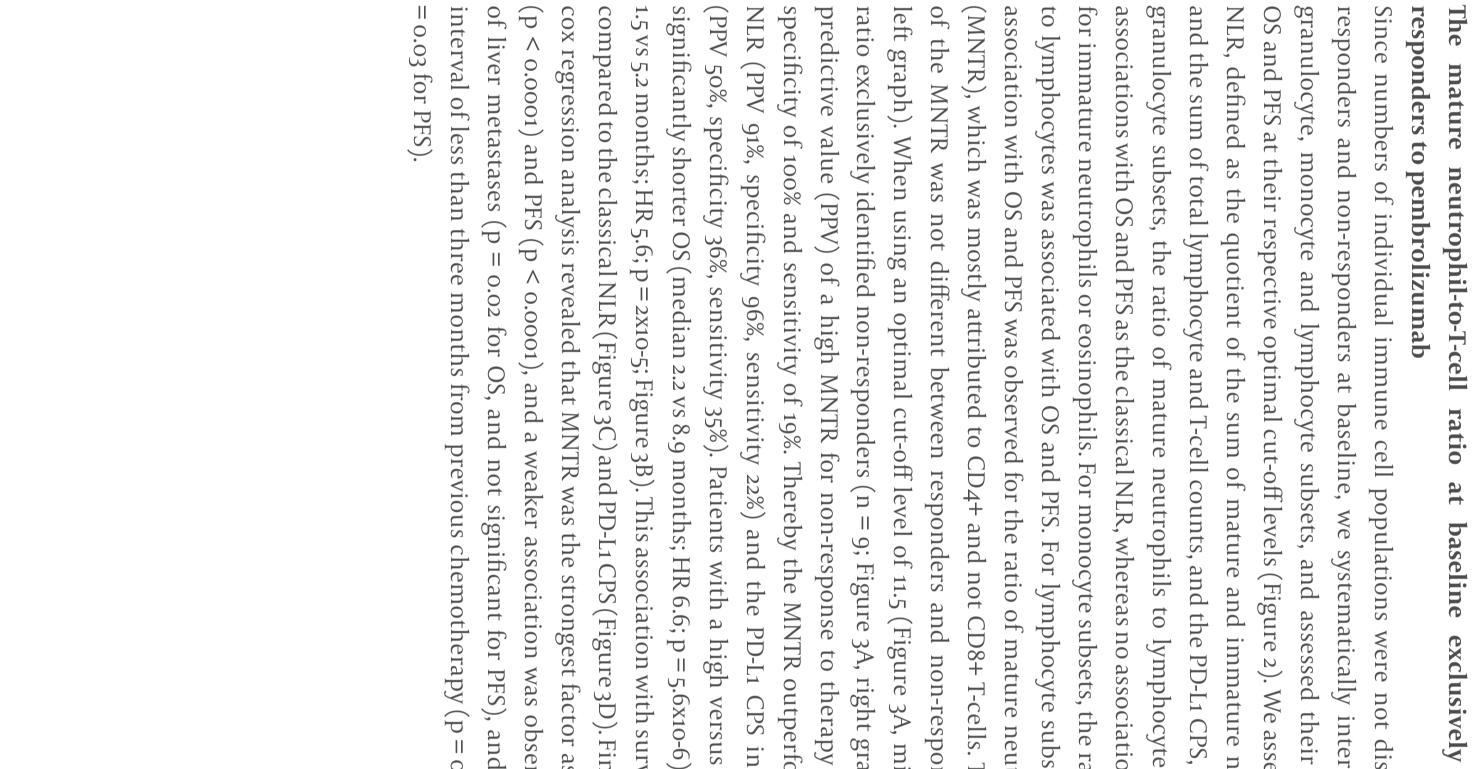

Figure 2. Testing ratios of granulocyte, monocyte and lymphocyte subsets demonstrated that the mature neutrophil-to-T-cell ratio was most strongly associated with overall and progression-free survival.

Forest plots displaying hazard ratios (HR) for overall (OS; left) and progression-free survival (PFS; right) for ratios of immune cell populations. The classical neutrophil-to-lymphocyte ratio and PD-L1 combined positivity score (CPS; bottom two rows) were used as references. Plot displays from left to right: the optimal cut-off level for survival analyses based on receiver operating characteristics (ROC); the area under the curve (AUC); and adjusted p-values for OS and PFS. P-values were corrected for multiple testing using the Holm-Bonferroni method. No significant associations with OS and PFS were observed when a median split was used for survival analyses.

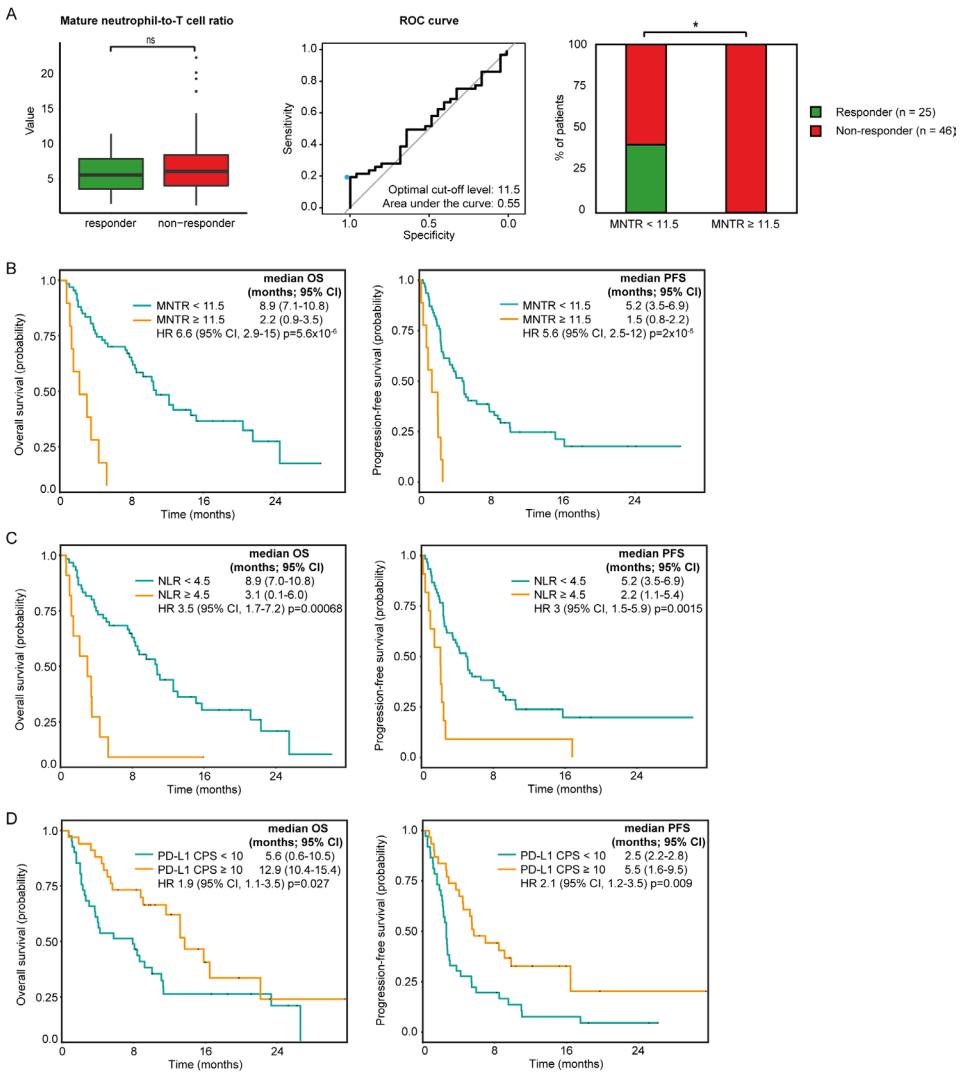

Figure 3. High mature neutrophil-to-T-cell ratio at baseline distinctly identified non-responders to pembrolizumab.
A. Left graph: boxplot displaying the mature neutrophil-to-T-cell ratio (MNTR) in responders and non-responders at baseline. Middle graph: receiver operating characteristic (ROC) curve for MNTR. Right graph: fraction of responders and non-responders in patients with MNTR <11.5 (n = 62) and ≥11.5 (n = 9). **B**. Kaplan-Meier estimation of overall survival (OS; left graph) and progression-free survival (PFS; right graph) for patients with MNTR <11.5 and ≥11.5. **C**. Kaplan-Meier estimation of OS (left graph) and PFS (right graph) for patients with NLR <4.5 and ≥4.5. **D**. Kaplan-Meier estimation of OS (left graph) and PFS (right graph) for patients with PD-L1 combined positivity score (CPS) <10 (n = 39) and ≥10 (n = 32). CI: confidence interval. HR: hazard ratio.

DISCUSSION

In this study, we enumerated 18 immune cell populations in prospectively collected fresh blood samples from 71 patients with mUC treated with pembrolizumab and demonstrated that a high MNTR prior to treatment is associated with therapy resistance. These data introduce a new blood-based immune marker that can be measured easily and non-invasively, and that has the potential to identify patients with mUC who will not benefit from pembrolizumab before treatment initiation.

The presented data extend our previous study on the frequency of T-cell subsets in blood samples of 56 out of these 71 patients with mUC (18). In this earlier study we demonstrated that responders harbor higher frequencies of CD4+ T-cells that express PD1 and 4-1BB when compared to non-responders at baseline, and responders showed changes in frequencies of these subsets during treatment. In the current study, we analyzed numbers of 14 additional immune cell populations in blood. We did not identify differences between responders and non-responders for any of the 18 T-cell, lymphocyte, granulocyte or monocyte populations at baseline nor at weeks 6 and 12 of treatment. Moreover, we did not identify longitudinal changes during therapy for any of these immune cell populations in responders or non-responders. In line with previous studies (14-17), we did show that the classical NLR is related to OS and PFS. Extending our analyses to novel ratios of immune cell populations, revealed that the quotient of mature neutrophils and T-cells outperformed the classical NLR and PD-L1 CPS, and was superior among all ratios regarding its potency to discriminate non-responders from responders, and regarding its association with Os and PFS.

From a mechanistic point of view, the negative predictive value of the MNTR may be in line with earlier reports showing that tumor-infiltrating neutrophils form a barrier around tumor cells, and as such prevent adequate contact between tumor cells and T-cells (20). When studying paired tumor biopsies from patients with a high versus low MNTR, however, we did not observe differences in densities of CD4+ T-cells, CD8+ T-cells or CD66b+ neutrophils, nor differences in distances among these cells (Supplementary Figure 2A-D). In other words, we cannot support a direct relationship between a high MNTR in blood with tumor cell-entrapment by neutrophils in tumor tissue. Previously, we showed that a lack of CD4+ T helper type 1 (Th1) cells in the tumor at baseline, and their inability to cluster with CD8+ T-cells and myeloid cells upon treatment, were associated with resistance to pembrolizumab (18). Also, in case of the MNTR, it appeared that lack of CD4+ rather than CD8+ T-cells was predominantly associated with non-response and limited survival. Exclusion of CD8+ T-cells from the MNTR, however, reduced its association with survival, suggesting that involvement of CD8+ T-cells in this metric is not negligible. Future studies in patient blood and tumor specimens are

required to identify the underlying mechanism of action.

The MNTR can be measured non-invasively by a commonly used technique (flowcytometry) that comes with a low cost burden. Identification of patients with a high MNTR may prevent patients with mUC from receiving potentially toxic and ineffective treatment with pembrolizumab. The optimal cut-off level for MNTR was determined specifically for this study and may therefore overestimate survival associations. Along this line, maximally selected rank statistics (20) were employed as an alternative approach to determine the optimal cut-off levels, and yielded similar results (data not shown). Our results require validation in an independent cohort of patients with mUC treated with an ICI, however, to the best of our knowledge, a homogeneous cohort of patients with thorough measurements of numbers of immune cell populations in blood, is currently not available.

In conclusion, we showed that a high MNTR at baseline is associated with treatment resistance and poor OS and PFS. This new blood-based marker potentially enables stratification of patients with mUC for treatment with pembrolizumab, thereby improving clinical outcomes and quality of life while reducing costs of care.

REFERENCES

1. Balar AV, Castellano D, O'Donnell PH, Grivas P, Vuky J, Powles T, et al. First-line pembrolizumab in cisplatin-ineligible patients with locally advanced and unresectable or metastatic urothelial cancer (KEYNOTE-052): a multicentre, single-arm, phase 2 study. The Lancet Oncology. 2017;18(11):1483-92.
2. Balar AV, Galsky MD, Rosenberg JE, Powles T, Petrylak DP, Bellmunt J, et al. Atezolizumab as first-line treatment in cisplatin-ineligible patients with locally advanced and metastatic urothelial carcinoma: a single-arm, multicentre, phase 2 trial. Lancet. 2017;389(10064):67-76.
3. Bellmunt J, de Wit R, Vaughn DJ, Fradet Y, Lee JL, Fong L, et al. Pembrolizumab as Second-Line Therapy for Advanced Urothelial Carcinoma. N Engl J Med. 2017;376(11):1015-26.
4. Fradet Y, Bellmunt J, Vaughn DJ, Lee JL, Fong L, Vogelzang NJ, et al. Randomized phase III KEYNOTE-045 trial of pembrolizumab versus paclitaxel, docetaxel, or vinflunine in recurrent advanced urothelial cancer: results of >2 years of follow-up. Ann Oncol. 2019;30(6):970-6.
5. Powles T, Park SH, Voog E, Caserta C, Valderrama BP, Gurney H, et al. Avelumab Maintenance Therapy for Advanced or Metastatic Urothelial Carcinoma. N Engl J Med. 2020;383(13):1218-30.
6. Balar AV, Kamat AM, Kulkarni GS, Uchio EM, Boormans JL, Roumiguié M, et al. Pembrolizumab monotherapy for the treatment of high-risk non-muscle-invasive bladder cancer unresponsive to BCG (KEYNOTE-057): an open-label, single-arm, multicentre, phase 2 study. The Lancet Oncology. 2021;22(7):919-30.
7. Rijnders M, de Wit R, Boormans JL, Lolkema MPJ, van der Veldt AAM. Systematic Review of Immune Checkpoint Inhibition in Urological Cancers. Eur Urol. 2017;72(3):411-23.
8. FDA Alerts Health Care Professionals and Oncology Clinical Investigators about an Efficacy Issue Identified in Clinical Trials for Some Patients Taking Keytruda (pembrolizumab) or Tecentriq (atezolizumab) as Monotherapy to Treat Urothelial Cancer with Low Expression of PD-L1 2018 (updated 20-06-2018. Available from: https://www.fda.gov/Drugs/DrugSafety/ucm608075.htm.
9. EMA restricts use of Keytruda and Tecentriq in bladder cancer 2018 (updated 01-06-2018. Available from: http://www.ema.europa.eu/ema/index.jsp?curl=pages/news_and_events/news/2018/05/news_detail_002964.jsp&mid=WC0b01ac058004d5c1.
10. Mazzaschi G, Facchinetti F, Missale G, Canetti D, Madeddu D, Zecca A, et al. The circulating pool of functionally competent NK and CD8+ cells predicts the outcome of anti-PD1 treatment in advanced NSCLC. Lung Cancer. 2019;127:153-63.
11. Nabet BY, Esfahani MS, Moding EJ, Hamilton EG, Chabon JJ, Rizvi H, et al. Noninvasive Early Identification of Therapeutic Benefit from Immune Checkpoint Inhibition. Cell. 2020;183(2):363-76.e13.
12. Kamphorst AO, Pillai RN, Yang S, Nasti TH, Akondy RS, Wieland A, et al. Proliferation of PD-1+ CD8 T cells in peripheral blood after PD-1–targeted therapy in lung cancer patients. Proceedings of the National Academy of Sciences. 2017;114(19):4993-8.
13. Huang AC, Postow MA, Orlowski RJ, Mick R, Bengsch B, Manne S, et al. T-cell invigoration to tumour burden ratio associated with anti-PD-1 response. Nature. 2017;545(7652):60-5.
14. Marchioni M, Primiceri G, Ingrosso M, Filograna R, Castellan P, De Francesco P, et al. The Clinical Use of the Neutrophil to Lymphocyte Ratio (NLR) in Urothelial Cancer: A Systematic Review. Clinical Genitourinary Cancer. 2016;14(6):473-84.
15. Ogihara K, Kikuchi E, Okabe T, Hattori S, Yamashita R, Yoshimine S, et al. Neutrophil-to-lymphocyte ratio is a useful biomarker for predicting worse clinical outcome in chemo-resistant urothelial carcinoma patients treated with pembrolizumab. Annals of Oncology. 2019;30:ix74.
16. Powles T, Jin C, Zheng Y, Baverel P, Narwal R, Mukhopadhyay P, et al. Tumor shrinkage and increased overall survival are associated with improved albumin, neutrophil lymphocyte ratio (NLR) and decreased durvalumab clearance in NSCLC and UC patients receiving durvalumab. Journal of Clinical Oncology. 2017;35(15_suppl):3035-.
17. Sonpavde G, Manitz J, Gao C, Tayama D, Kaiser C, Hennessy D, et al. Five-Factor Prognostic Model for Survival of Post-Platinum Patients with Metastatic Urothelial Carcinoma Receiving PD-L1 Inhibitors. J Urol. 2020;204(6):1173-9.
18. Rijnders M, Balcioglu HE, Robbrecht DGJ, Oostvogels AAM, Wijers R, Aarts MJB, et al. Anti-PD1 efficacy in metastatic urothelial cancer patients associates with intratumoral juxtaposition of T helper-type 1 and CD8+ T-cells. Clinical Cancer Research. In press.
19. Kunert A, Basak EA, Hurkmans DP, Balcioglu HE, Klaver Y, van Brakel M, et al. CD45RA(+)CCR7(-) CD8 T cells lacking co-stimulatory receptors demonstrate enhanced frequency in peripheral blood of NSCLC patients responding to nivolumab. Journal for immunotherapy of cancer. 2019;7(1):149.
20. Müller J, Hothorn T. Maximally selected two-sample statistics as a new tool for the identification and assessment of habitat factors with an application to breeding-bird communities in oak forests. European Journal of Forest Research. 2004;123(3):219-28.

SUPPLEMENTARY TABLES

Supplementary Table 1. Overview of antibodies used for flow cytometry.

Antibody	Clone	Supplier	Dilution
CD3-PB	UCHT1	BD Biosciences	1:50
CD4-V500	RPA-T4	BD Biosciences	1:50
CD8-APC-Cy7	SK1	BD Biosciences	1:200
CD11b-APC	D12	BD Biosciences	1:40
CD11c-APC-eF780	BU15	eBioscience	1:50
CD14-FITC	M φP9	BD Biosciences	1:20
CD15-PE	HI98	BD Biosciences	1:20
CD16-PE-Cy7	3G8	BD Biosciences	1:400
CD19-V500	HIB19	BD Biosciences	1:50
CD45-PerCP	2D1	BD Biosciences	1:50
CD56-APC	TULY56	eBioscience	1:40
HLA-DR-BV786	G46-6	BD Biosciences	1:80
TCRgd-FITC	11F2	BD Biosciences	1:20

SUPPLEMENTARY FIGURES

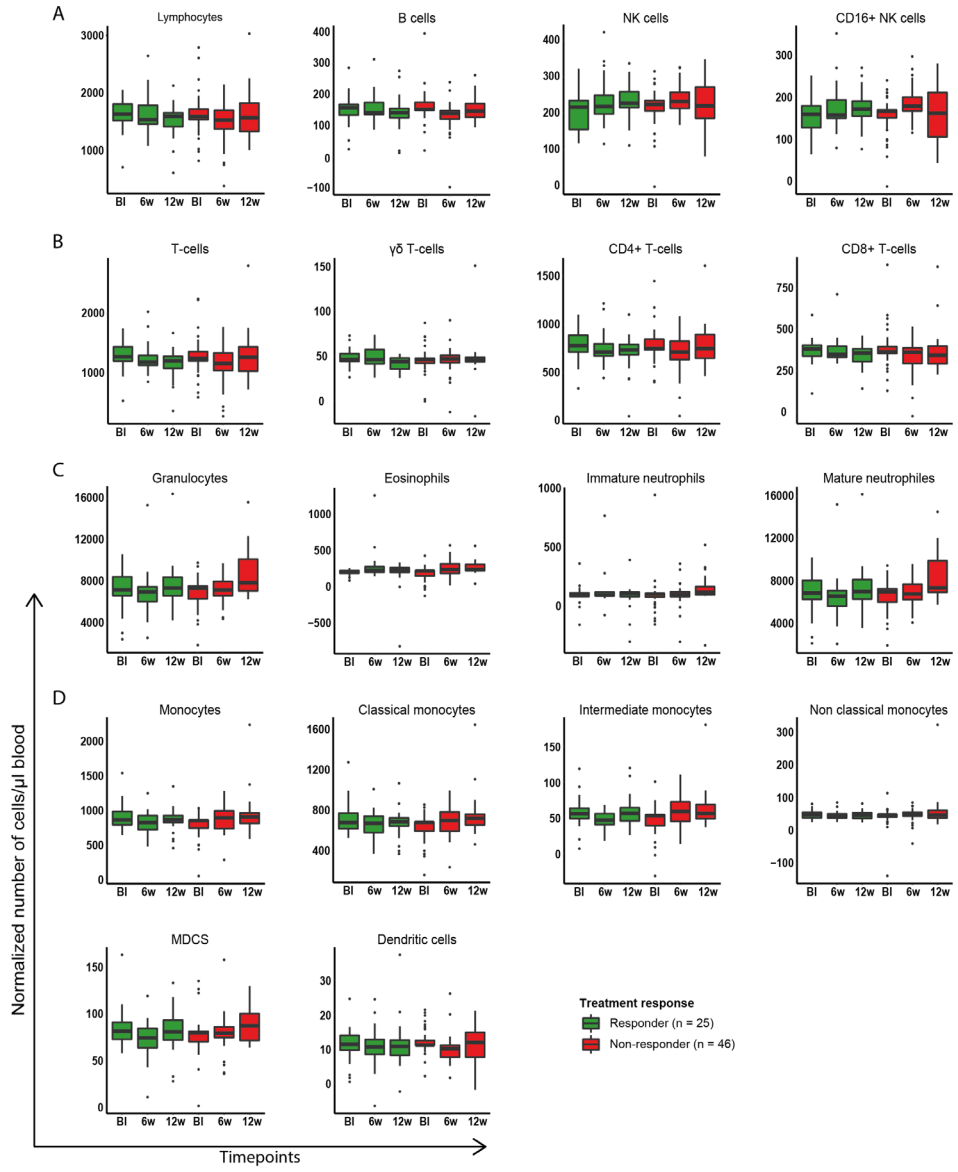

Supplementary Figure 1. Responders and non-responders to pembrolizumab do not demonstrate longitudinal changes in normalized numbers of immune cell populations in blood.
Boxplots display the normalized number of cells belonging to subsets of: **A**. lymphocytes; **B**. T-cells; **C**. granulocytes; and **D**. monocytes per microliter blood (see Methods section for details on normalization and staining methods). Timepoints: baseline (BI), 6w, 12w (6, 12 weeks of treatment). Differences between timepoints were determined for paired samples using the Wilcoxon signed rank test and p-values were corrected for multiple testing using the Holm-Bonferroni method.

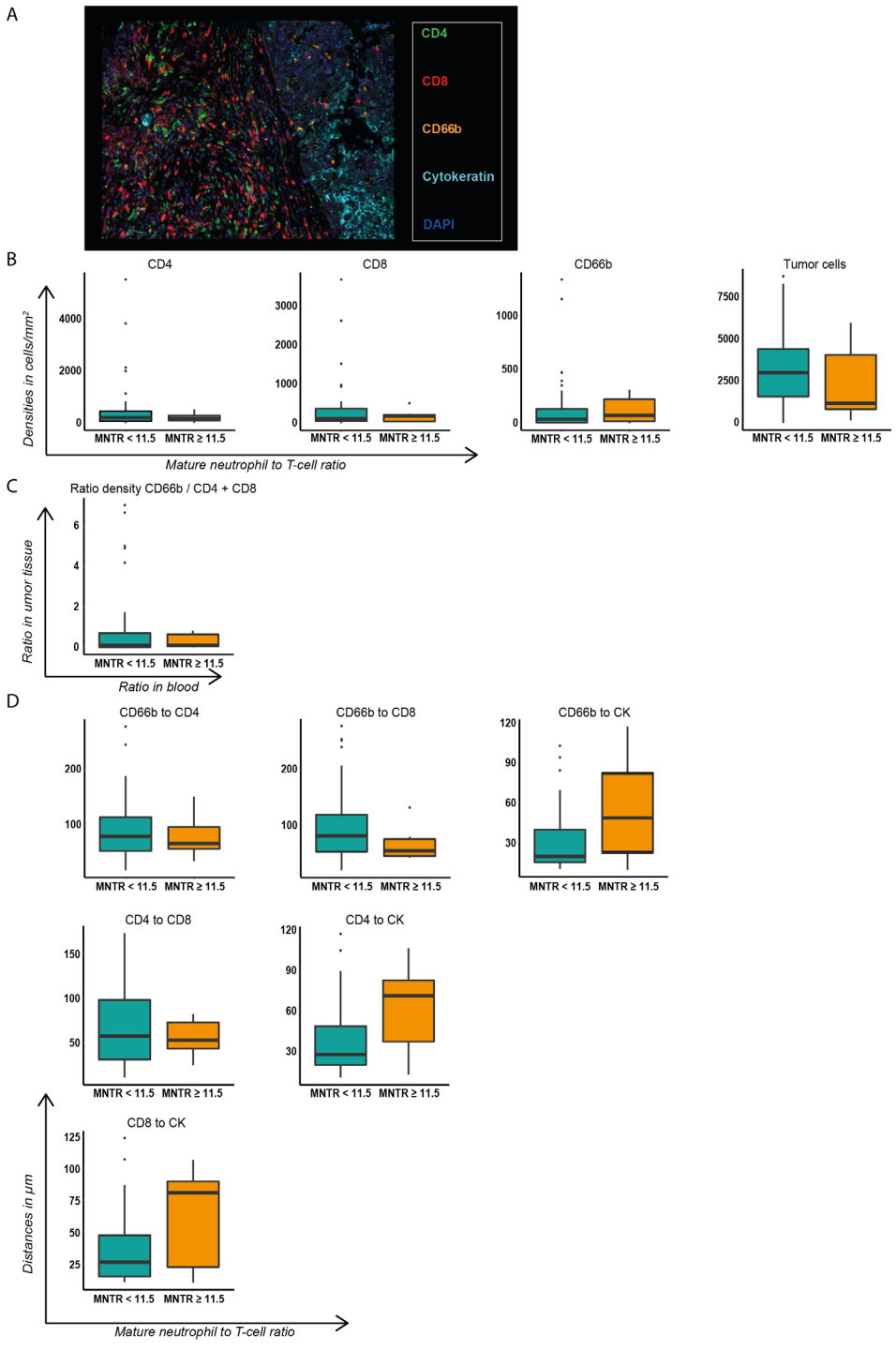

Supplementary Figure 2. Patients with low versus high mature neutrophil-to-T-cell ratio in blood do not show differences in tissue contexture of neutrophils and T-cells at baseline.
A. Representative multiplex immunofluorescence image of a lymph node metastasis. Tissue sections were stained for CD4+ T-cells (green), CD8+ T-cells (red), CD66b+ neutrophils (orange), and pan-cytokeratin (CK) positive tumor cells (cyan; see Methods section for details). **B**. Densities (cells/mm2) as well as **C**. ratios of densities and **D**. distances (in µm) among CD4+ T-cells, CD8+ T-cells, CD66b+ neutrophils, and CK+ tumor cells were displayed for patients with a low (<11.5) versus high mature neutrophil-to-T-cell ratio (MNTR ≥1.5). None of the differences were statistically significant (Mann–Whitney U test; p-values were corrected for multiple testing using the Holm-Bonferroni method).

CHAPTER 8

General discussion

This thesis focuses on the efficacy of immune checkpoint inhibitors (ICIs), in particular pembrolizumab (anti-PD1), in patients with metastatic urothelial cancer (mUC). The first aim was to identify potential biomarkers for response to ICIs to improve patient selection for a more individualized treatment approach for patients with mUC. The second aim was to uncover mechanisms that drive both sensitivity and resistance to treatment with ICIs. Part 1 of this chapter discusses the genomic and transcriptomic characteristics of mUC. In part 2, these genomic and transcriptomic characteristics, as well as immunological characteristics, are described in relation to ICI efficacy in patients with mUC. In addition, novel predictive markers discovered in this thesis are listed and described in relation to existing predictors for response to ICIs. In part 3, our findings on potential mechanisms related to treatment resistance are discussed. Finally, part 4 summarizes challenges and limitations of our studies, and future studies are proposed to validate and clinically test new biomarkers and therapeutic strategies to enhance ICI efficacy.

PART 1. DNA AND RNA PROFILE OF MUC

Understanding the genomic basis of (metastatic) UC is imperative to comprehend the efficacy of current therapies, develop new therapies, and personalize treatment regimens for patients. UC is a heterogeneous disease both at clinical and molecular level, and shows different genomic characteristics at different disease stages. As described in Chapter 4, at DNA level mUC is characterized by a high tumor mutational burden (TMB) (1, 2). Two major genomic subtypes (GenS) were identified; GenS1 (67% of samples) was related to APOBEC (Apolipoprotein B mRNA Editing Catalytic Polypeptide-like) mutagenesis, and GenS2 (24% of samples) was characterized by de novo mutational signatures related to reactive oxygen species and is putatively clock-like. In general, patients with tumors of subtype GenS1 had a more favorable response to different types of treatment (chemo- and immunotherapy) compared to those with tumors of subtype GenS2.

At RNA level, multiple subtyping methods have been described for non-metastatic UC (4-12). Therefore, in 2017 a consensus molecular classifier was established for primary muscle invasive bladder cancer (MIBC) (13). Several reports have shown enrichment of response to chemotherapy and immunotherapy in certain subtypes of MIBC (7, 14-19). It is important to realize, however, that the consensus classifier was developed strictly for MIBC, and is not directly applicable to mUC. Biopsy samples from metastatic tumor lesions contain organ-specific transcripts that disrupt sample classification according to the consensus classifier. To address this issue, we performed *de novo* subtyping on our mUC cohort after removal of organ-specific transcripts. This resulted in the identification of five transcriptomic subtypes: a stroma-rich and a basal/squamous subtype that were both highly similar to the corresponding subtypes of the consensus classifier for MIBC, and two luminal subtypes (a and b), together showing overlapping characteristics with the three luminal subtypes of the consensus classifier. Finally, a non-specified subtype was identified that did not reflect any of the subtypes of the consensus classifier. A neuro-endocrine subtype, present in the classifier for MIBC, was not found in our mUC cohort. Based on the genomic and transcriptomic characteristics of each subtype potential therapeutic strategies were proposed. The luminal-a subtype was characterized by high expression of *PPARG* and a large fraction of NK cells, and may therefore be sensitive to PPARγ-inhibitors, or NK cell directed therapies. *FGFR3* alterations were common in the luminal-b subtype, potentially sensitizing these tumors to FGFR inhibitors. Furthermore, inhibitors of the RAS pathway may be effective due to high RTK-RAS pathway activity in the luminal-b subtype. Previous studies showed sensitivity to ICIs in patients with stroma-rich and basal/squamous tumors. Potentially the efficacy of ICIs can be enhanced in these two subtypes by inhibiting the highly active TGF-β pathway in these tumors. Patients with tumors of the basal/squamous subtype may also benefit from mesothelin-targeted therapy and BET inhibitors. Individualized targeted therapy is suggested for patients

with tumors of the non-specified subtype. Before clinical implementation, validation of our newly defined transcriptomic subtypes of mUC is required in an independent cohort. Furthermore, future (pre-)clinical investigations are needed to test efficacy of proposed subtype-specific interventions. Collectively, our comprehensive description of the genomic and transcriptomic landscape of mUC serves as a valuable repository to accelerate future development of personalized treatments for patients with mUC.

Box 1. Major findings regarding the genomic and transcriptomic landscape of mUC

- Two major genomic subtypes of mUC were identified: one related to APOBEC mutagenesis, and one which had a high fraction of de novo mutational signatures related to reactive oxygen species and which is putatively clock-like. Response to chemo- and immunotherapy was generally better in patients with APOBEC-driven tumors.
- Transcriptomic analysis revealed five mRNA-based subtypes: two luminal subtypes, and a stroma-rich, basal/squamous, and non-specified subtype.
- Potential novel therapeutic means were proposed for each transcriptomic subtype based on their genomic and transcriptomic characteristics.

PART 2. SENSITIVITY TO ICIS IN MUC AND HOW TO STRATIFY PATIENTS

Gene, transcript and immune markers that are associated with ICI response in mUC
Next, we studied genomic, transcriptomic and immunological characteristics of blood and tumor specimens from patients with mUC who were included in the RESPONDER trial, to study which characteristics were related to response to pembrolizumab (Figure 1). These findings resulted in the identification of a number of novel markers that can potentially be of use for selection of patients for ICI therapy (Figure 2).

Immunophenotyping of blood and tumor samples showed that response to pembrolizumab was primarily associated with presence and phenotype of CD4+ rather than CD8+ T cells (Chapter 5). This may suggest that major histocompatibility complex (MHC) I antigens are downregulated in UC cells to escape CD8+ T cell recognition. With respect to CD4+ T cells in blood we observed that the fraction of PD-1+ CD4+ T cells decreased upon treatment, whereas the fraction of 4-1BB+ CD4+ T cells increased specifically in responders. Fractions of CD4+ T cells expressing chemo-attractant receptors did not change in responders during treatment. However, baseline plasma CXCL9 levels and intra-tumoral chemo-attractant gene expression were higher in responders and correlated with higher T cell signature expression scores. Together, these findings point to the systemic occurrence of activated T cells, possibly reflecting T cell activation in tumor tissue. In tumor tissue, we observed higher densities of CD4+ T

helper-type 1 (Th1) cells, but not CD8+ T cells, in responders compared to non-responders prior to treatment. Upon treatment, distances between Th1 cells, CD8+ T cells, and CD11b+ myeloid cells decreased in responders, suggestive of formation of immune cell niches in the tumor microenvironment (TME). These immune cell niches also contained B cells, and likely resemble so-called tertiary lymphoid structures (TLS), which have been associated with response to ICI therapy in several tumor types (20-23). In UC specifically, the number of TLS increased during treatment in patients with a complete response to neoadjuvant treatment with ipilimumab plus nivolumab (24).

Looking into characteristics of the TME at DNA level revealed that high TMB and high APOBEC mutagenesis were associated with response to pembrolizumab (Chapter 6). In both cases, many somatic mutations were present in the tumor which can potentially give rise to neoantigens that can be recognized by T cells (25). The genomic subtypes described in Chapter 4 and individual driver gene alterations were not associated with response to treatment. The newly identified transcriptomic subtypes of mUC were also not related to response to pembrolizumab in our patient cohort. Differential expression analysis of immune-related genes revealed on the one hand upregulated genes in responders that were part of pathways involved in chemokine receptor-ligand interactions, interferon gamma (IFN-γ) signaling, and interactions between lymphoid and non-lymphoid cells. On the other hand, downregulated genes in responders belonged to pathways involved in extracellular matrix organization and collagen formation. Further building on these pathways, we selected previously published gene expression signatures and performed hierarchical clustering analysis. This analysis revealed three clusters of patients that were related to therapy response, and led to the identification of the T cell to-stroma-enrichment (TSE) score. This metric compares the expression scores of T cell and stromal cell-related gene signatures, and showed a significantly higher predictive value for response to pembrolizumab than the individual gene signatures alone. The majority of patients with a positive TSE score had a tumor response to pembrolizumab, whereas none of the patients with a negative TSE score obtained a response to pembrolizumab. These findings will be discussed in more detail in Part 3 of this chapter.

Collectively, our findings suggest that responders to pembrolizumab have tumors that show signs of T cell infiltration and activation prior to treatment (Figure 1) (31, 32). This may be the result of an earlier anti-tumor T cell response that was terminated prematurely, which is supported by the higher abundance of CD4+ T cells with an antigen-experienced phenotype in peripheral blood. This hypothesis is further substantiated by our finding that baseline tumor immunogenicity appeared higher in responders versus non-responders to pembrolizumab, as exemplified by a higher TMB, higher plasma CXCL9 levels, higher intra-tumoral Th1 cell density, and higher T cell signature scores. We hypothesized that pre-existing T cells, mainly CD4+ Th1 cells that

are positioned in close proximity to (CD11b+) antigen-presenting cells (APCs) or tumor cells, become re-activated upon pembrolizumab and start producing IFN-γ. This leads to activation of APCs, potentially dendritic cells, which subsequently produce chemo-attractants to enhance recruitment and activation of other immune cells, and initiates formation of immune cell niches. It appears that interaction between CD4+ Th1 cells, CD8+ T cells and myeloid cells is required for a proper anti-tumor immune response upon pembrolizumab. In this setting, a pre-requisite for response seems to be the absence of an active stromal compartment, which has been associated with an immune excluded phenotype and non-response to therapy (Chapter 6; discussed below).

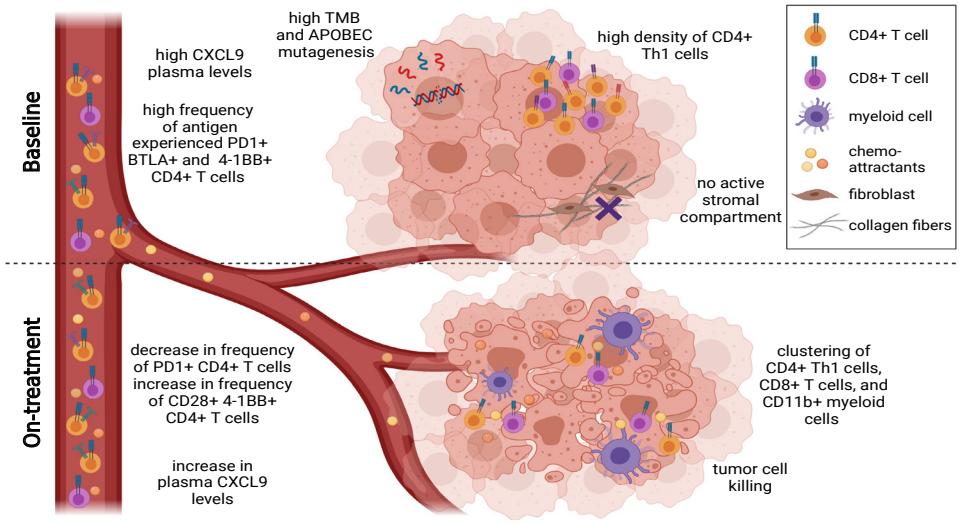

Figure 1. Overview of findings at DNA, RNA and protein level that are associated with response to pembrolizumab in patients with mUC

Predictive markers for response to pembrolizumab identified in the RESPONDER trial

Studies of the DNA, RNA and immune profiles of samples from the RESPONDER trial (as described in 2.1) enabled the discovery of novel predictive markers for response to pembrolizumab in patients with mUC. These predictors are subdivided at blood and tissue level, discussed below, and illustrated in Figure 2.

Markers is blood

Mature neutrophil-to-T cell ratio

Numbers of individual immune cell populations were determined by multiparameter flowcytometry of freshly obtained blood samples (Chapter 7). Baseline numbers of

individual immune cell populations were not related to therapy response. However, a high mature neutrophil-to-T cell ratio (MNTR) was associated with poor overall and progression-free survival (Figure 2). Furthermore, none of the patients with a high MNTR had an ongoing therapy response at 6 months after treatment initiation. Thereby, the MNTR outperformed classical predictors such as the neutrophil-to-lymphocyte ratio (NLR) and the PD-L1 combined positivity score (CPS) with respect to its predictive value for therapy response.

CD4 T cell subsets

Although numbers of T cells in blood at baseline were not different between responders and non-responders to pembrolizumab (Chapter5 and 7), detailed flow cytometric investigation of T cell phenotypes did reveal differences, specifically for CD4+ T cells (Chapter 5, summarized in Figure 1). Previous reports suggest that dynamic changes in immune cells may provide better associations with ICI response compared to pre-treatment assessments (30, 33-36). Given that the phenotype of T cells can be measured in blood easily, such measurements have potential to develop into markers for on-treatment monitoring of therapy efficacy. For instance, our finding of a sharp decrease in the frequency of CXCR3 expressing CD4+ T cells may predict non-response to treatment. Such early identification of disease progression may warrant a timely switch to a subsequent line of therapy, before the patients' clinical condition deteriorates to such an extent that successive therapy is no longer feasible.

Markers in tumor tissue

PD-L1 expression

PD-L1 expression in tumor tissue was the first biomarker used for patient selection for ICI treatment in clinical practice (Figure 2). However, as described extensively in this thesis, the predictive value of PD-L1 expression is limited in mUC. Testing of PD-L1 expression is currently restricted to selection of cisplatin-ineligible patients for first-line pembrolizumab and atezolizumab, and has no place in the second-line setting. In line with this, we did not observe a relationship between PD-L1 CPS on fresh tumor biopsies or archival tumor tissue and treatment outcome in platinum-refractory patients receiving pembrolizumab in the RESPONDER trial. The number of chemotherapy-naïve patients was too small (9 patients) to perform a formal sub-analysis (Chapter 5 and 6).

Interpretation of PD-L1 stainings is complicated by the use of different antibody clones and scoring algorithms per companion diagnostic assay. These algorithms either only take PD-L1 expression on tumor or immune cells, or their combined expression into account. Although conflicting results have been published, it appears that PD-L1 expression on tumor-resident immune cells is long-lasting and associated with a better prognosis, whereas PD-L1 expression on tumor cells seems to be more transient and linked to worse prognosis (37). We showed substantial concordance between the four

companion diagnostic assays for pembrolizumab (clone 22C3), nivolumab (clone 28-8), atezolizumab (clone SP142), and durvalumab (clone SP263). However, we could not draw definitive conclusions on the interchangeability of assays for patient selection in clinical practice as the staining results could not be related to treatment response per type of ICI (Chapter 3). Studies that directly compare the different companion diagnostics in the setting of multiple ICIs are needed to draw a final conclusion on interchangeability of antibodies, or to determine the most optimal antibody for patient stratification.

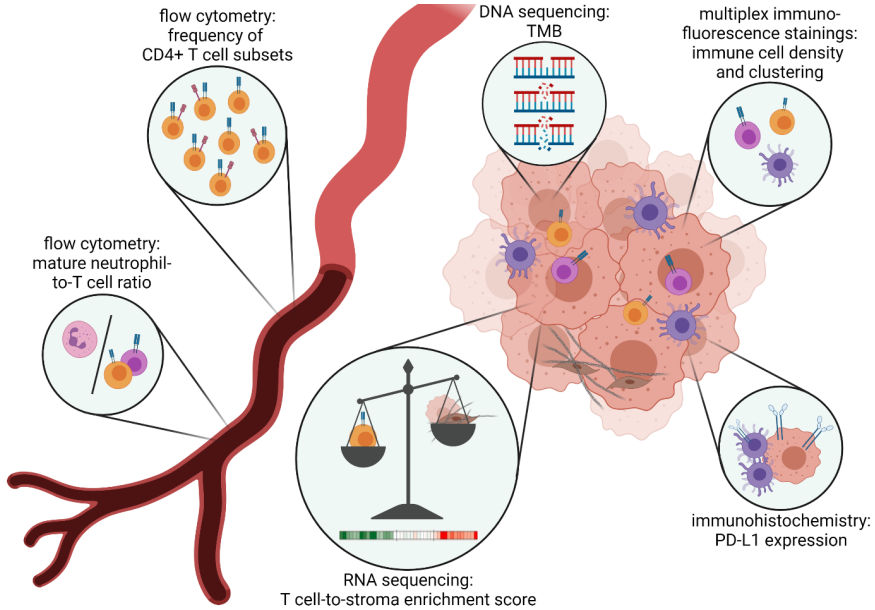

Figure 2. Discovery of predictive markers, and the required tools, for response to pembrolizumab in blood and tumor samples from patients with mUC included in the RESPONDER trial

Tumor mutational burden

Another predictive biomarker that is currently in use in clinical practice is the tumor mutational burden (TMB; Figure 2). Pembrolizumab is now approved by the United States Food and Drug Administration (FDA) for patients with any type of previously treated advanced solid tumor with a high TMB (≥10 mutations/Mbp). This is mainly relevant for patients with variant histologies of UC, as pembrolizumab is already approved for all chemotherapy-refractory, and a subset of chemotherapy-naïve patients with mUC. Associations of high TMB and ICI response in mUC have previously been shown for first- and second-line atezolizumab (14, 18, 38), second-line nivolumab (39), and for pembrolizumab in a study across 22 tumor types (40). In the RESPONDER trial,

TMB was assessed by whole genome sequencing and a similar association was found. However, the positive predictive value of a high TMB was limited (47% were responders), and clinical benefit was also observed in 19% of patients with a low TMB (Chapter 6).

Intra-tumoral presence of T cells and myeloid cells

Intra-tumoral presence of immune cell populations, and specifically T cells, has previously been associated with response to ICIs (14, 26, 31, 41). We investigated the abundance of various immune cell populations in metastatic tumor biopsies by multiplex immunofluorescence stainings and observed that the baseline density of CD4+ Th1 cells was higher in patients with a complete or partial response as their best overall response to therapy compared to patients with progressive disease (as described in section 2.1 of this chapter and in Chapter 5). In an exploratory analysis, patients with a positive versus negative TSE score showed higher densities of CD4+ Th1 cells, CD8+ T cells and B cells, although not formally statistically significant (Chapter 6). Determination of the presence of Th1 cells by immunofluorescence or even by less complex immunohistochemistry prior to treatment may be useful for patient stratification (Figure 2). The formation of clusters of Th1 cells, CD8+ T cells and CD11b+ myeloid cells upon treatment was also associated with therapy response, however, this assessment requires a second biopsy, making this measurement less feasible as a biomarker for patient stratification in clinical practice.

T cell-to-stroma enrichment score

Expression of individual genes (e.g. *CXCL9*, *IFN-γ*) and gene signatures have been associated with response to ICIs (14, 16, 17, 40, 42, 43). In our study, the TSE score captured the difference in expression between signatures related to T cells (e.g. T cell inflammation (42), and T cell cytotoxicity (16)) and stromal cells and their products (e.g. TGF-β pathway (16), and EMT/stroma genes (44)). The TSE score had a strong association with clinical benefit from pembrolizumab (Chapter 6; Figure 2). A positive score was associated with response to pembrolizumab at 6 months of therapy (67% of patients responded), and patients had a significantly better overall and progression-free survival compared to patients with a negative or neutral TSE score. Notably, none of the patients with a negative TSE score had a response to treatment. Furthermore, the predictive value of the TSE score was confirmed in two independent patient cohorts; patients with mUC treated with first-line atezolizumab (IMvigor210 trial), and patients with MIBC treated with neo-adjuvant atezolizumab (ABACUS trial).

Most promising biomarkers identified in the RESPONDER trial

The most promising blood-based biomarker to predict response prior to treatment initiation is the MNTR (Chapter 7). The advantage of a biomarker that can be measured in blood is that a blood sample can be obtained non-invasively, and measurements can be performed relatively easy, uniformly and fast, enabling repeated measurements at serial

time points. The MNTR can be determined by routine flowcytometric analysis and can therefore be determined at relatively low cost. Furthermore, blood-based biomarkers have the potential to provide a reflection of a systemic biological process rather than a small part of a tumor or metastasis.

In tumor tissue, the TSE score is the most promising biomarker to predict response to pembrolizumab (Chapter 6). This novel score showed the strongest association with therapy response and overall and progression-free survival in the RESPONDER trial, and thereby outperformed the TMB and PD-L1 CPS. Moreover, the TSE score was validated for its predictive value in two independent cohorts of patients with mUC. Similar relationships between response to anti-PD(L)1 and expression of T cell and stroma-related genes in UC have been reported before (16, 19, 44). In our study, however, we were able to capture both parameters in a single clinically applicable metric. In a pan-cancer study, four TME subtypes were identified that were highly similar to the TSE subtypes identified in our study (45). In the pan-cancer study, most responses to anti-PDL1 were observed in patients with mUC with an immune-enriched, non-fibrotic tumor, which is similar to TSE score positive tumors. Patients with a fibrotic TME subtype, comparable to patients with a negative TSE score, showed the least responses to anti-PDL1 and had the worst overall survival probability. These observations underscore the robustness of the TSE score that we identified in patients with mUC. Taken together, the TSE score is a promising and broadly applicable marker with strong predictive value both in the primary and metastatic setting. Therefore, it is a potential candidate to improve patient selection for anti-PD(L)1 in clinical practice.

PART 3. RESISTANCE TO ICIS AND HOW TO OVERCOME IT

Mechanisms of resistance to pembrolizumab

The predictors described above aid the identification of patients who respond to pembrolizumab. For patients who do not respond, monotherapy is not sufficient to provoke tumor regression. Our translational studies provided clues on mechanisms underlying this resistance to therapy as well as actionable targets to potentially sensitize resistant tumors to ICI treatment (Figure 3).

Lack of intra-tumoral T cell numbers

In contrast to responders, in non-responders we observed low expression scores for T cell-related gene signatures and high scores for stroma-related signatures (Chapter 6). The presence of an excessive stromal compartment in the TME can impede an efficient influx as well as response of anti-tumor T cells. Transforming growth factor β (TGF-β)-induced genes are part of our stroma-related gene signatures. These genes are

related to excessive stroma, and induce epithelial-to-mesenchymal transition (EMT), extracellular matrix remodeling, fibroblast activation and desmoplasia (46-48). Analysis of pre-treatment tumor samples from the IMvigor210 trial on atezolizumab in patients with mUC revealed that treatment resistance was associated with TGF-β signaling in fibroblasts, and that in these tumors CD8+ T cells were located in tumor surrounding stroma that was rich in fibroblasts and collagens (16). Also, in primary and metastatic UC it was shown that resistance to ICI (combination) therapy was associated with TGF-β signaling, fibroblast activation (24), EMT and an immune excluded phenotype (19)(44). Finally, in large pan-cancer studies it was shown that an active stromal compartment may hamper anti-tumor immune responses and lead to ICI therapy resistance (40, 45). Collectively, these findings point towards a central role for TGF-β signaling and/or (TGF-β induced) EMT in ICI resistance in UC and other tumor types.

A second observation linked to the relevance of intra-tumoral T cell numbers is the lower baseline CXCL9 level in plasma of non-responders. This observation is potentially the result of limited activation of antigen-presenting cells (such as dendritic cells), which are considered a primary source of this chemo-attractant. Furthermore, a sharp on-treatment drop in the frequency of CXCR3+ CD4+ T cells in blood was observed in non-responders (Chapter 5). Multiple studies pointed out that anti-PD(L)1 efficacy is lost in the absence of CXCR3 or chemo-attractant expression in the TME (49-51). In addition, although not a direct outcome of our studies, T cell infiltration into the tumor may also be hampered by a lack of or dysfunction of intra-tumoral blood vessels, or by a lack of expression of adhesion molecules on endothelial cells in these vessels (52, 53).

Lack of T cell clustering

In non-responders, we observed lower intra-tumoral densities of CD4+ Th1 and CD8+ T cells compared to responders, and no immune cell niche formation upon treatment. Absence of T cells, but also tumor-intrinsic defects in IFN-γ signaling, may abrogate the IFN-γ signaling cascade in non-responders, and may also hamper the formation of immune cell niches upon treatment. Furthermore, there was a lack of evidence for an earlier anti-tumor immune response in non-responders given the lower fractions of CD4+ T cells with an activated phenotype (PD1+ BTLA+ and 4-1BB+) in blood, which may reflect lower numbers of such T cells within tumors. In addition, a durable increase in the frequency of CD4+ T cells that express co-stimulatory receptors during treatment, as was observed in responders and shown to be required for anti-PD1 mediated T cell rescue (96), was lacking (Chapter 5). This may be the result of a lower tumor-intrinsic antigenicity (e.g. low TMB), or from defects in antigen presentation by tumor cells and APCs. In UC, it was shown that downregulated expression of members of the antigen processing machinery, such as HLA-ABC and β2-microglobulin, represents a key event that contributes to loss of MHC class I expression (54). Loss of MHC class I expression in turn may be a way to escape CD8+ T cell

recognition and could explain why we observed that CD4+ T cell numbers and phenotypes were related to treatment response. We can also not exclude that expression of tumor-specific antigens is lost as a result of clonal selection or epigenetic silencing (55, 56).

Finally, in non-responders the anti-tumor immune response may be further repressed by the presence of immune-suppressive cells in the TME, such as M2 macrophages, myeloid-derived suppressor cells, regulatory T cells, and neutrophils. In our study we did not identify a clear role for the first three immune cell populations in therapy resistance. We did find that a higher mature neutrophil-to-T cell ratio in blood was associated with a lack of response to pembrolizumab, however we did not observe differences in intra-tumoral densities of neutrophils between responders and non-responders (Chapter 7).

Actionable targets to reverse resistance to ICI

Lack of intra-tumoral T cell numbers

Several interventions to increase immune cell infiltration, and to turn so called 'cold' tumors into 'hot' tumors have been proposed. Along this line, the effects of interference with TGF-β signaling have already been a topic of research. In an immune excluded breast cancer mouse model, for instance, it was shown that addition of a TGF-β inhibitor to anti-PD-L1 therapy led to increased immune cell infiltration, positioning of T cells in the tumor center rather than stromal border, and significant tumor regression (16). So far, clinical development of TGF-β blocking therapies has been limited by the occurrence of severe cardiotoxicities. In a mouse model, it was shown that selective inhibition of TGF-β1 also resulted in induction of intra-tumoral T cell infiltration, in the absence of cardiotoxicities, providing a window for clinical implementation of antibodies directed against TGF-β1 (57). Cancer associated fibroblasts (CAFs) likely contribute to TGF-β-induced immune cell exclusion via production of collagen fibers and extracellular matrix components that create a physical barrier for T cells to infiltrate into the tumor. Induction of angiogenesis and abnormal vascularization by CAFs may further enhance immune cell exclusion in the TME (58). Therefore, therapeutic strategies targeting CAFs, for instance via elimination or reprogramming of CAFs, may also be of value in mUC (58).

Other interventions to turn 'cold' tumors into 'hot' tumors are aimed to induce local proliferation of lymphoid cells via IL-2. The IL-2 pathway agonist bempegaldesleukin provides selective signaling through the IL-2βγ receptor pathway, by which proliferation of CD8+ T cells and NK cells, but not regulatory T cells, is stimulated in the TME. Combination treatment of bempegaldesleukin with anti-PD1 led to impressive responses in patients with metastatic melanoma, renal cell carcinoma, and non-small cell lung cancer (59), and may also be considered for patients with mUC.

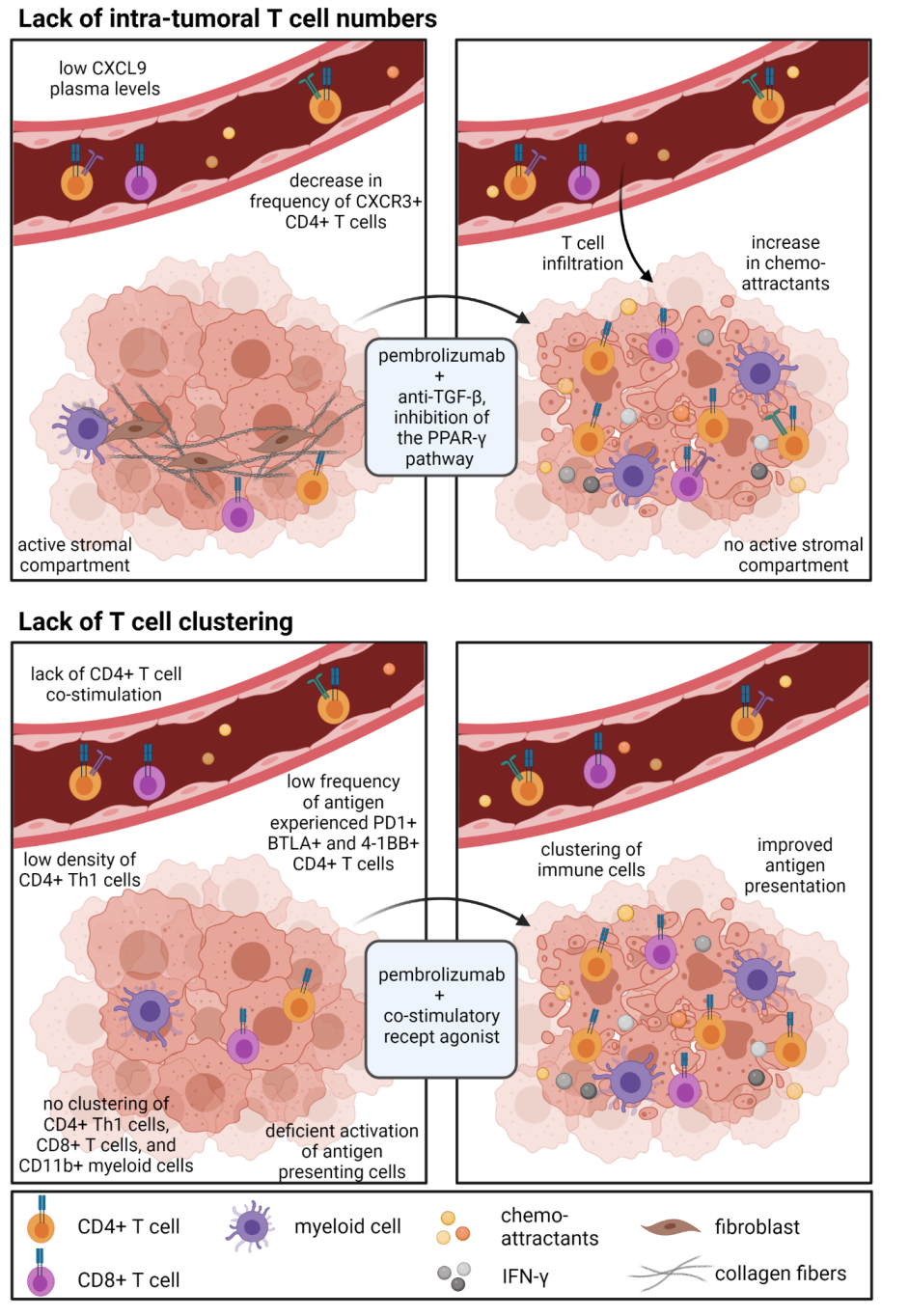

Figure 3. Putative mechanisms of resistance identified in the RESPONDER trial in patients with mUC and potential interventions to re-sensitize tumors to pembrolizumab

Lack of T cell clustering

Our study revealed that a lack of T cell co-stimulation was related to T cell disfunction, lack of T cell clustering and therapy resistance. Possibly, therapy efficacy can be rescued in these patients by co-administration of an agonistic antibody for co-stimulatory receptors (e.g. 4-1BB). In an aggressive UC mouse model, it was shown that the addition of a CD40 co-stimulatory receptor agonist to anti-PD1 therapy resulted in APC activation, CD8+ T cell recruitment, and prolonged survival of the mice (61). Production of chemo-attractants by APCs could also be stimulated in a UC mouse model by inhibition of the PPAR-γ pathway (63).

Non-ICI therapies to treat mUC

A proportion of patients with mUC is probably not responsive to any form of (combination) treatment with ICIs, or experiences disease progression after an initial tumor response. For these patients other (targeted) therapies may be beneficial. In Chapter 4, potential actionable targets for therapy were discovered based on genomic alterations for almost all patients, ranging from therapies that are on-label for UC to therapies that are approved by the FDA for other tumor types, and therapies under investigation in clinical trials including basket trials. These observations hold promise for future expansion of the treatment armamentarium for patients with mUC. Further investigation of the most optimal actionable targets and efficacy in clinical practice is still needed, as some trials on targeted therapies failed to meet their primary efficacy endpoints (83, 84).

An example of a trial that was successful, is a phase II trial with the pan-FGFR inhibitor erdafinitib. This drug is now approved by the FDA for patients with mUC harboring an *FGFR* alteration and who experienced disease progression during or following chemotherapy. The objective response rate (ORR) was 40%. A subset of 22 patients had received ICIs prior to trial inclusion, of whom only one patient obtained a response, suggesting that there may be a negative association between *FGFR* alterations and ICI response. Yet, 59% of these patients achieved a response to erdafitinib (85). The optimal sequence for targeted treatment of patients with *FGFR* alterations is currently undefined and under study in prospective trials. Another example of a successfully developed drug is the antibody-drug conjugate enfortumab vedotin targeting Nectin-4. After promising results were obtained in phase I and II trials (86, 87), the efficacy of enfortumab vedotin was compared to investigator's choice of chemotherapy in 608 patients with mUC who were previously treated with chemotherapy or ICIs (88). The ORR was 41% for enfortumab vedotin treated patients versus 18% in chemotherapy treated patients. Also, the median overall and progression-free survival were significantly longer for patients who received enfortumab vedotin. Efficacy was also shown in cisplatin-ineligible patients who experienced progressive disease upon first-line ICI therapy (ORR 52%) (89), and in the

first-line setting in combination with pembrolizumab (ORR 73%) (90). A final example is sacituzumab govitecan, another antibody-drug conjugate that targets Trop-2. Efficacy of this drug was studied in 113 patients with mUC with progressive disease after chemo- and ICI therapy. This revealed an ORR of 27% and led to approval for clinical use by the FDA (91).

PART 4. PROPOSED FUTURE TRANSLATIONAL AND CLINICAL STUDIES BASED ON OUTCOMES FROM THE RESPONDER TRIAL

Introduction of ICIs as treatment for patients with UC has drastically changed the treatment paradigm, however, current overall response rates are still limited. Therefore, personalizing treatment for patients with mUC is essential to improve patient outcomes and quality of life, prevent exposure to toxic therapies in patients who do not benefit, and improve cost-efficiency rates.

Challenges and limitations of the RESPONDER trial

With respect to challenges and limitations of the study we must consider that both chemotherapy-naïve and chemotherapy-refractory patients were included in the RESPONDER trial at an unequal ratio. This could affect the predictive value of identified markers in both treatment settings. Furthermore, the timing of blood and tissue collection, but also the timing of response evaluation (response at 6 months or best overall response) may affect our findings. The strength of our correlative analyses is further limited by the number of patients from whom both genomic, transcriptomic and immunophenotypic data is available. Samples may be missing due to unavailability of a safely accessible metastatic lesion for biopsies, or due to drop-out of the study as a result of early disease progression (within 6 to 12 weeks after treatment initiation). Data may also be missing due to insufficient quality. Finally, the use of single metastatic tumor biopsies from different sites in the body, ranging from lymph nodes to liver, and soft tissue metastases may affect our observations on the composition of the TME per patient. Analysis of relatively small biopsy specimens also impeded the evaluation of intra-tumoral and inter-tumoral heterogeneity.

Future directions

The most promising biomarkers identified in the RESPONDER trial are the mature neutrophil-to-T cell ratio in blood, and the T cell-to-stroma enrichment score and immune cell clustering in tumor tissue. These findings require validation in an independent patient cohort as scores and cutoffs were specifically developed within the RESPONDER trial. To achieve this, a follow-up study is needed, in which more patients with mUC who will be treated with first- or second-line ICIs are included. Fresh metastatic tumor

biopsies and blood samples for whole genome DNA and RNA sequencing, and immune profiling should be collected. When available, also (archival) samples from the primary tumor of these patients should be included in the study. These can be used to evaluate whether the predictive value of biomarkers is indeed stronger in fresh compared to archival or primary tumor tissue, as was suggested in **Chapter 6**. Furthermore, comparison of the primary tumor to metastatic lesions could inform us on tumor evolution, and processes involved in disease progression and formation of metastases. To further explore mechanisms of primary and acquired resistance to therapy, DNA and RNA sequencing should also be performed on biopsies obtained during therapy, as not only baseline characteristics but also dynamic changes in the TME, such as the clustering of Th1 cells, were found to be associated with therapy response. This is specifically relevant for patients with an initial response to therapy, as such additional biopsies can provide crucial information on mechanisms underlying acquired therapy resistance. In the current study, it turned out to be challenging to obtain tumor tissues from patients at time of disease progression, as patients' clinical condition often rapidly declined, impeding any further study handlings. In addition to analyses performed in the current study, additional biopsies for single-cell RNA sequencing should be collected to obtain an even more detailed view on the composition of the TME. These data are expected to shed light on the exact stromal contributors to a negative TSE score. Furthermore, focused analyses on the identification of long-term responders to therapy should also be performed. A-priori identification of these patients can prevent exposure to unnecessary and potentially toxic combination therapies. In fact, early discontinuation of monotherapy may be feasible and safe in these patients.

When the proposed new biomarkers for patient stratification or combination therapies are validated, these should be prospectively tested within the context of a clinical trial. Trials exploring combination therapy with chemotherapy had negative results, and also the biomarker-directed BISCAY trial failed to show efficacy of multiple combination therapies despite pre-treatment selection of patients with mUC (83). Possibly this may have been caused by the design of the study, as multiple treatment arms were compared, resulting in variable and limited patient populations per arm, decreasing the study power. Validation trials should therefore be carefully designed and address a well-defined research question.

REFERENCES

1. Alexandrov, L.B., et al., *Signatures of mutational processes in human cancer.* Nature, 2013. **500**(7463): p. 415-421.
2. Priestley, P., et al., *Pan-cancer whole-genome analyses of metastatic solid tumours.* Nature, 2019. **575**(7781): p. 210-216.
3. *Comprehensive molecular characterization of urothelial bladder carcinoma.* Nature, 2014. **507**(7492): p. 315-22.
4. Robertson, A.G., et al., *Comprehensive Molecular Characterization of Muscle-Invasive Bladder Cancer.* Cell, 2018. **174**(4): p. 1033.
5. Damrauer, J.S., et al., *Intrinsic subtypes of high-grade bladder cancer reflect the hallmarks of breast cancer biology.* Proceedings of the National Academy of Sciences, 2014. **111**(8): p. 3110-3115.
6. Rebouissou, S., et al., *EGFR as a potential therapeutic target for a subset of muscle-invasive bladder cancers presenting a basal-like phenotype.* Science Translational Medicine, 2014. **6**(244): p. 244ra91-244ra91.
7. Choi, W., et al., *Identification of distinct basal and luminal subtypes of muscle-invasive bladder cancer with different sensitivities to frontline chemotherapy.* Cancer Cell, 2014. **25**(2): p. 152-65.
8. Marzouka, N.A., et al., *A validation and extended description of the Lund taxonomy for urothelial carcinoma using the TCGA cohort.* Sci Rep, 2018. **8**(1): p. 3737.
9. Mo, Q., et al., *Prognostic Power of a Tumor Differentiation Gene Signature for Bladder Urothelial Carcinomas.* JNCI: Journal of the National Cancer Institute, 2018. **110**(5): p. 448-459.
10. Hedegaard, J., et al., *Comprehensive Transcriptional Analysis of Early-Stage Urothelial Carcinoma.* Cancer Cell, 2016. **30**(1): p. 27-42.
11. Hurst, C.D., et al., *Genomic Subtypes of Non-invasive Bladder Cancer with Distinct Metabolic Profile and Female Gender Bias in KDM6A Mutation Frequency.* Cancer Cell, 2017. **32**(5): p. 701-715.e7.
12. Sjödahl, G., et al., *A molecular taxonomy for urothelial carcinoma.* Clin Cancer Res, 2012. **18**(12): p. 3377-86.
13. Kamoun, A., et al., *A Consensus Molecular Classification of Muscle-invasive Bladder Cancer.* Eur Urol, 2020. **77**(4): p. 420-433.
14. Rosenberg, J.E., et al., *Atezolizumab in patients with locally advanced and metastatic urothelial carcinoma who have progressed following treatment with platinum-based chemotherapy: A single-arm, multicentre, phase 2 trial.* Lancet, 2016. **387**(10031): p. 1909-1920.
15. Seiler, R., et al., *Impact of Molecular Subtypes in Muscle-invasive Bladder Cancer on Predicting Response and Survival after Neoadjuvant Chemotherapy.* European Urology, 2017. **72**(4): p. 544-554.
16. Mariathasan, S., et al., *TGFβ attenuates tumour response to PD-L1 blockade by contributing to exclusion of T cells.* Nature, 2018. **554**(7693): p. 544-548.
17. Sharma, P., et al., *Nivolumab in metastatic urothelial carcinoma after platinum therapy (CheckMate 275): a multicentre, single-arm, phase 2 trial.* Lancet Oncol, 2017. **18**(3): p. 312-322.
18. Balar, A.V., et al., *Atezolizumab as first-line treatment in cisplatin-ineligible patients with locally advanced and metastatic urothelial carcinoma: a single-arm, multicentre, phase 2 trial.* Lancet, 2017. **389**(10064): p. 67-76.
19. Powles, T., et al., *Clinical efficacy and biomarker analysis of neoadjuvant atezolizumab in operable urothelial carcinoma in the ABACUS trial.* Nat Med, 2019. **25**(11): p. 1706-1714.
20. Messina, J.L., et al., *12-Chemokine gene signature identifies lymph node-like structures in melanoma: potential for patient selection for immunotherapy?* Sci Rep, 2012. **2**: p. 765.
21. Cabrita, R., et al., *Tertiary lymphoid structures improve immunotherapy and survival in melanoma.* Nature, 2020.
22. Helmink, B.A., et al., *B cells and tertiary lymphoid structures promote immunotherapy response.* Nature, 2020.
23. Petitprez, F., et al., *B cells are associated with survival and immunotherapy response in sarcoma.* Nature, 2020.
24. van Dijk, N., et al., *Preoperative ipilimumab plus nivolumab in locoregionally advanced urothelial cancer: the NABUCCO trial.* Nat Med, 2020. **26**(12): p. 1839-1844.
25. Savage, P.A., *Tumor antigenicity revealed.* Trends in immunology, 2014. **35**(2): p. 47-48.
26. Tumeh, P.C., et al., *PD-1 blockade induces responses by inhibiting adaptive immune resistance.* Nature, 2014. **515**(7528): p. 568-71.
27. Roh, W., et al., *Integrated molecular analysis of tumor biopsies on sequential CTLA-4 and PD-1 blockade reveals markers of response and resistance.* Science Translational Medicine, 2017. **9**(379): p. eaah3560.
28. Forde, P.M., et al., *Neoadjuvant PD-1 Blockade in Resectable Lung Cancer.* N Engl J Med, 2018. **378**(21): p. 1976-1986.
29. Inoue, H., et al., *Intratumoral expression levels of PD-L1, GZMA, and HLA-A along with oligoclonal T cell expansion associate with response to nivolumab in metastatic melanoma.* Oncoimmunology, 2016. **5**(9): p. e1204507.
30. Riaz, N., et al., *Tumor and Microenvironment Evolution during Immunotherapy with Nivolumab.* Cell, 2017. **171**(4): p. 934-949.e16.
31. Galon, J., et al., *Type, density, and location of immune cells within human colorectal tumors predict clinical outcome.* Science, 2006. **313**(5795): p. 1960-4.
32. Gruosso, T., et al., *Spatially distinct tumor immune microenvironments stratify triple-negative breast cancers.* J Clin Invest, 2019. **129**(4): p. 1785-1800.
33. Huang, A.C., et al., *T-cell invigoration to tumour burden ratio associated with anti-PD-1 response.* Nature, 2017. **545**(7652): p. 60-65.

34. Zappasodi, R., et al., *Non-conventional Inhibitory CD4(+)Foxp3(-)PD-1(hi) T Cells as a Biomarker of Immune Checkpoint Blockade Activity.* Cancer Cell, 2018. **33**(6): p. 1017-1032.e7.
35. Huang, A.C., et al., *A single dose of neoadjuvant PD-1 blockade predicts clinical outcomes in resectable melanoma.* Nat Med, 2019. **25**(3): p. 454-461.
36. Chen, P.L., et al., *Analysis of Immune Signatures in Longitudinal Tumor Samples Yields Insight into Biomarkers of Response and Mechanisms of Resistance to Immune Checkpoint Blockade.* Cancer Discov, 2016. **6**(8): p. 827-37.
37. Powles, T., et al., *The evolving role of PD-L1 testing in patients with metastatic urothelial carcinoma.* Cancer Treat Rev, 2020. **82**: p. 101925.
38. Powles, T., et al., *Atezolizumab versus chemotherapy in patients with platinum-treated locally advanced or metastatic urothelial carcinoma (IMvigor211): a multicentre, open-label, phase 3 randomised controlled trial.* Lancet, 2018. **391**(10122): p. 748-757.
39. Galsky, M.D., et al., *Impact of zumor mutation burden on nivolumab efficacy in second-line urothelial carcinoma patients: Exploratory analysis of the phase ii checkmate 275 study.* Annals of Oncology, 2017. **28**: p. v296-v297.
40. Cristescu, R., et al., *Pan-tumor genomic biomarkers for PD-1 checkpoint blockade-based immunotherapy.* Science, 2018. **362**(6411).
41. Al-Shibli, K.I., et al., *Prognostic effect of epithelial and stromal lymphocyte infiltration in non-small cell lung cancer.* Clin Cancer Res, 2008. **14**(16): p. 5220-7.
42. Ayers, M., et al., *IFN-γ-related mRNA profile predicts clinical response to PD-1 blockade.* J Clin Invest, 2017. **127**(8): p. 2930-2940.
43. Litchfield, K., et al., *Meta-analysis of tumor- and T cell-intrinsic mechanisms of sensitization to checkpoint inhibition.* Cell, 2021. **184**(3): p. 596-614.e14.
44. Wang, L., et al., *EMT- and stroma-related gene expression and resistance to PD-1 blockade in urothelial cancer.* Nature Communications, 2018. **9**(1): p. 3503.
45. Bagaev, A., et al., *Conserved pan-cancer microenvironment subtypes predict response to immunotherapy.* Cancer Cell, 2021. **39**(6): p. 845-865.e7.
46. Massagué, J., *TGFbeta in Cancer.* Cell, 2008. **134**(2): p. 215-30.
47. Lebrun, J.J., *The Dual Role of TGFβ in Human Cancer: From Tumor Suppression to Cancer Metastasis.* ISRN Mol Biol, 2012. **2012**: p. 381428.
48. Flavell, R.A., et al., *The polarization of immune cells in the tumour environment by TGFbeta.* Nat Rev Immunol, 2010. **10**(8): p. 554-67.
49. Chow, M.T., et al., *Intratumoral Activity of the CXCR3 Chemokine System Is Required for the Efficacy of Anti-PD-1 Therapy.* Immunity, 2019. **50**(6): p. 1498-1512 e5.
50. House, I.G., et al., *Macrophage-Derived CXCL9 and CXCL10 Are Required for Antitumor Immune Responses Following Immune Checkpoint Blockade.* Clinical Cancer Research, 2020. **26**(2): p. 487-504.
51. Dangaj, D., et al., *Cooperation between Constitutive and Inducible Chemokines Enables T Cell Engraftment and Immune Attack in Solid Tumors.* Cancer Cell, 2019. **35**(6): p. 885-900.e10.
52. Martinet, L., et al., *Human Solid Tumors Contain High Endothelial Venules: Association with T- and B-Lymphocyte Infiltration and Favorable Prognosis in Breast Cancer.* Cancer Research, 2011. **71**(17): p. 5678-5687.
53. Ager, A. and M.J. May, *Understanding high endothelial venules: Lessons for cancer immunology.* Oncoimmunology, 2015. **4**(6): p. e1008791.
54. Romero, J.M., et al., *Coordinated downregulation of the antigen presentation machinery and HLA class I/beta2-microglobulin complex is responsible for HLA-ABC loss in bladder cancer.* Int J Cancer, 2005. **113**(4): p. 605-10.
55. Rosenthal, R., et al., *Neoantigen-directed immune escape in lung cancer evolution.* Nature, 2019. **567**(7749): p. 479-485.
56. Landsberg, J., et al., *Melanomas resist T-cell therapy through inflammation-induced reversible dedifferentiation.* Nature, 2012. **490**(7420): p. 412-6.
57. Martin, C.J., et al., *Selective inhibition of TGFβ1 activation overcomes primary resistance to checkpoint blockade therapy by altering tumor immune landscape.* Sci Transl Med, 2020. **12**(536).
58. Desbois, M. and Y. Wang, *Cancer-associated fibroblasts: Key players in shaping the tumor immune microenvironment.* Immunol Rev, 2021. **302**(1): p. 241-258.
59. Diab, A., et al., *Bempegaldesleukin (NKTR-214) plus Nivolumab in Patients with Advanced Solid Tumors: Phase I Dose-Escalation Study of Safety, Efficacy, and Immune Activation (PIVOT-02).* Cancer Discovery, 2020. **10**(8): p. 1158-1173.
60. Ribas, A., et al., *SD-101 in Combination with Pembrolizumab in Advanced Melanoma: Results of a Phase Ib, Multicenter Study.* Cancer Discov, 2018. **8**(10): p. 1250-1257.
61. Leblond, M.M., et al., *CD40 Agonist Restores the Antitumor Efficacy of Anti-PD1 Therapy in Muscle-Invasive Bladder Cancer in an IFN I/II-Mediated Manner.* Cancer Immunology Research, 2020. **8**(9): p. 1180-1192.
62. Ishizuka, J.J., et al., *Loss of ADAR1 in tumours overcomes resistance to immune checkpoint blockade.* Nature, 2019. **565**(7737): p. 43-48.
63. Korpal, M., et al., *Evasion of immunosurveillance by genomic alterations of PPARγ/RXRα in bladder cancer.* Nature Communications, 2017. **8**(1): p. 103.
64. Sapkota, B., C.E. Hill, and B.P. Pollack, *Vemurafenib enhances MHC induction in BRAFV600E homozygous melanoma cells.* OncoImmunology, 2013. **2**(1): p. e22890.
65. Boni, A., et al., *Selective BRAF^{V600E} Inhibition Enhances T-Cell Recognition of Melanoma without Affecting Lymphocyte Function.* Cancer Research, 2010. **70**(13): p. 5213-5219.
66. Frederick, D.T., et al., *BRAF Inhibition Is Associated with Enhanced Melanoma Antigen Expression and a More Favorable Tumor Microenvironment in Patients with Metastatic Melanoma.* Clinical Cancer Research, 2013. **19**(5): p. 1225-1231.
67. Wilmott, J.S., et al., *Selective BRAF Inhibitors Induce Marked T-cell Infiltration into Human Metastatic Melanoma.* Clinical Cancer Research, 2012. **18**(5): p. 1386-1394.
68. Adeegbe, D.O., et al., *Synergistic Immunostimulatory Effects and Therapeutic Benefit of Combined Histone Deacetylase and Bromodomain Inhibition in Non-Small Cell Lung Cancer.* Cancer Discov, 2017. **7**(8): p. 852-867.
69. Tomita, Y., et al., *The interplay of epigenetic therapy and immunity in locally recurrent or metastatic estrogen receptor-positive breast cancer: Correlative analysis of ENCORE 301, a randomized, placebo-controlled phase II trial of exemestane with or without entinostat.* Oncoimmunology, 2016. **5**(11): p. e1219008.
70. Hammerl, D., et al., *Adoptive T Cell Therapy: New Avenues Leading to Safe Targets and Powerful Allies.* Trends in Immunology, 2018. **39**(11): p. 921-936.
71. Jensen, M.C. and S.R. Riddell, *Designing chimeric antigen receptors to effectively and safely target tumors.* Curr Opin Immunol, 2015. **33**: p. 9-15.
72. Rezvani, K., et al., *Engineering Natural Killer Cells for Cancer Immunotherapy.* Mol Ther, 2017. **25**(8): p. 1769-1781.
73. Yuen, K.C., et al., *High systemic and tumor-associated IL-8 correlates with reduced clinical benefit of PD-L1 blockade.* Nat Med, 2020. **26**(5): p. 693-698.
74. Kroemer, G., et al., *Immunogenic cell death in cancer therapy.* Annu Rev Immunol, 2013. **31**: p. 51-72.
75. Weichselbaum, R.R., et al., *Radiotherapy and immunotherapy: a beneficial liaison?* Nat Rev Clin Oncol, 2017. **14**(6): p. 365-379.
76. Kaufman, H.L., F.J. Kohlhapp, and A. Zloza, *Oncolytic viruses: a new class of immunotherapy drugs.* Nature Reviews Drug Discovery, 2015. **14**(9): p. 642-662.
77. Galsky, M.D., et al., *Atezolizumab with or without chemotherapy in metastatic urothelial cancer (IMvigor130): a multicentre, randomised, placebo-controlled phase 3 trial.* Lancet, 2020. **395**(10236): p. 1547-1557.
78. Powles, T., et al., *Pembrolizumab alone or combined with chemotherapy versus chemotherapy as first-line therapy for advanced urothelial carcinoma (KEYNOTE-361): a randomised, open-label, phase 3 trial.* Lancet Oncol, 2021. **22**(7): p. 931-945.
79. Ribas, A., et al., *Oncolytic Virotherapy Promotes Intratumoral T Cell Infiltration and Improves Anti-PD-1 Immunotherapy.* Cell, 2017. **170**(6): p. 1109-1119.e10.
80. Nadal, R., et al., *Current Therapy for Metastatic Urothelial Carcinoma.* Hematol Oncol Clin North Am, 2021. **35**(3): p. 469-493.
81. Galsky, M.D., et al., *Society for Immunotherapy of Cancer (SITC) clinical practice guideline on immunotherapy for the treatment of urothelial cancer.* Journal for immunotherapy of cancer, 2021. **9**(7): p. e002552.
82. Alifrangis, C., et al., *Molecular and histopathology directed therapy for advanced bladder cancer.* Nat Rev Urol, 2019. **16**(8): p. 465-483.
83. Powles, T., et al., *An adaptive, biomarker-directed platform study of durvalumab in combination with targeted therapies in advanced urothelial cancer.* Nat Med, 2021. **27**(5): p. 793-801.
84. Grivas, P., et al., *Rucaparib for recurrent, locally advanced, or metastatic urothelial carcinoma (mUC): Results from ATLAS, a phase II open-label trial.* Journal of Clinical Oncology, 2020. **38**(6_suppl): p. 440-440.
85. Loriot, Y., et al., *Erdafitinib in Locally Advanced or Metastatic Urothelial Carcinoma.* N Engl J Med, 2019. **381**(4): p. 338-348.
86. Jonathan, R., et al., *EV-101: A Phase I Study of Single-Agent Enfortumab Vedotin in Patients With Nectin-4–Positive Solid Tumors, Including Metastatic Urothelial Carcinoma.* Journal of Clinical Oncology. **0**(0): p. JCO.19.02044.
87. Rosenberg, J.E., et al., *Pivotal Trial of Enfortumab Vedotin in Urothelial Carcinoma After Platinum and Anti-Programmed Death 1/Programmed Death Ligand 1 Therapy.* J Clin Oncol, 2019. **37**(29): p. 2592-2600.
88. Powles, T., et al., *Enfortumab Vedotin in Previously Treated Advanced Urothelial Carcinoma.* New England Journal of Medicine, 2021. **384**(12): p. 1125-1135.
89. Yu, E.Y., et al., *Enfortumab vedotin after PD-1 or PD-L1 inhibitors in cisplatin-ineligible patients with advanced urothelial carcinoma (EV-201): a multicentre, single-arm, phase 2 trial.* Lancet Oncol, 2021. **22**(6): p. 872-882.
90. Rosenberg, J.E., et al., *Study EV-103: Durability results of enfortumab vedotin plus pembrolizumab for locally advanced or metastatic urothelial carcinoma.* Journal of Clinical Oncology, 2020. **38**(15_suppl): p. 5044-5044.
91. Tagawa, S.T., et al., *TROPHY-U-01: A Phase II Open-Label Study of Sacituzumab Govitecan in Patients With Metastatic Urothelial Carcinoma Progressing After Platinum-Based Chemotherapy and Checkpoint Inhibitors.* J Clin Oncol, 2021. **39**(22): p. 2474-2485.

APPENDICES &

Summary
Samenvatting
List of publications
Author affilications
About the author
PhD Portfolio
Dankwoord

SUMMARY

Historically, the cornerstone of treatment of patients with metastatic urothelial cancer (mUC) consisted of different chemotherapeutic regimens. In 2014, efficacy of immune checkpoint inhibitors (ICIs) was shown for the first time in mUC, resulting in the registration of ICIs as second-line treatment for patients with mUC. Nowadays, multiple studies have shown efficacy of ICIs in earlier stages of UC. ICIs target co-inhibitory receptors on T cells, or their ligands on tumor or antigen presenting cells, and can thereby initiate or reactivate a T cell response against tumors. This can result in durable tumor responses, and possibly even cure a small proportion of patients with mUC.

A general introduction to this thesis and an overview of clinical trials on ICIs in different stages of UC is provided in **Chapter 1**. Thereby this chapter extends on the trials that were systematically reviewed in **Chapter 2**, including randomized controlled trials on ICIs in patients with mUC, as well as metastatic renal cell cancer, and prostate cancer. Collectively, these studies showed that ICIs can be (very) effective in a small proportion of patients with mUC, yet do not provide benefit to the majority of patients. In this thesis, we therefore aimed to identify novel biomarkers that can discriminate patients who respond to therapy with ICIs from those who do not. Potentially these biomarkers can be used for future up-front selection of patients. In addition, we aimed to improve our understanding of putative mechanisms underlying resistance to ICIs, which can give direction to future combination treatments to sensitize tumors to ICIs. For this, the prospective biomarker discovery trial RESPONDER was initiated in the Netherlands. In this study, patients with mUC were treated with pembrolizumab (anti-PD1), and fresh tumor biopsies and blood samples were collected from these patients at multiple timepoints before and during treatment. The samples were used for whole genome DNA and RNA sequencing analysis, and multiple advanced immune profiling methods.

A biomarker that is currently in use in clinical practice to select patients with mUC for treatment with ICIs is PD-L1 expression in tumor tissue. The predictive value of PD-L1 expression however differs per ICI and per treatment setting in which it is used. Possibly, this is a result of the differences per companion diagnostic assays with respect to antibody clone, required staining platform, and scoring algorithm. Therefore, we performed a comparison of PD-L1 expression by four companion diagnostic assays and one research antibody in **Chapter 3**. We found substantial concordance between companion diagnostic antibodies for PD-L1 expression on tumor and immune cells. The PD-L1 status according to each scoring algorithm was identical for all four companion diagnostic antibodies in 78% of patients. These results may warrant the interchangeable use of the companion diagnostic antibodies in the future, although additional studies are needed to assess their predictive value in patients treated with different types of ICIs.

In **Chapter 4**, we performed an extensive characterization of the genomic and transcriptomic landscape of mUC using metastatic tumor biopsies. We identified two major genomic subtypes based on mutational signatures, of which the most abundant subtype was related to APOBEC mutagenesis. At transcriptomic level, hierarchical clustering analysis revealed five subtypes of mUC that were related to the clusters of the consensus classifier for primary non-metastatic muscle invasive bladder cancer. Per transcriptomic subtype potential effective treatment strategies were proposed. Furthermore, at patient level, potential targetable genomic alterations were identified in almost all patients. Together, these data increased our understanding of the genomic biology of mUC and aid future development of more individualized treatment planning. Results on multiparameter flowcytometry analysis of blood samples, and multiplex immunofluorescence stainings of tumor biopsies collected in the RESPONDER trial are reported in **Chapter 5**. In blood, we observed that the fractions of CD4+ T cell subsets were different in responders compared to non-responders. At baseline, responders harbored a higher fraction of CD4+ T cells with an antigen-experienced phenotype, and upon treatment the fraction of CD4+ T cells that express co-stimulatory receptors increased. Furthermore, plasma levels of chemo-attractants where higher in responders at baseline. In tumor tissues, responders had a higher baseline density of CD4+ T helper-type 1 (Th1) cells than non-responders. These Th1 cells formed immune cell clusters with CD8+ T cells and CD11b+ myeloid cells upon treatment, which was not observed in non-responders. Collectively, these results showed that response to pembrolizumab in patients with mUC is associated with peripheral CD4+ T cell activation and local clustering of these cells into immune cell niches upon treatment.

In **Chapter 6,** an in-depth analysis of whole genome DNA and RNA sequencing data from metastatic tumor biopsies was performed. We correlated genomic tumor characteristics, such as genomic subtypes, tumor mutational burden (TMB), APOBEC mutagenesis, and specific alterations to response to treatment with pembrolizumab. We observed that high TMB and high APOBEC mutagenesis were associated with therapy response. Hierarchical clustering analysis using previously reported gene expression signatures related to T cells, non-T cell immune cells, and stromal resident cells and their products revealed three clusters of patients with a positive, neutral, or negative T cell-to-stroma enrichment (TSE) score. This score reflects the relative difference between expression scores of T cell versus stroma-related gene expression signatures. The majority of patients with a positive TSE score had a response to pembrolizumab. In contrast, none of the patients with a negative TSE score had an ongoing response after six months of treatment with pembrolizumab, and overall and progression-free survival were poor for these patients. The predictive value of the TSE score was confirmed in two independent cohorts of patients with UC treated with ICIs (IMvigor210 and ABACUS trial). Together, these results point towards the TSE score as a potential novel marker for

baseline stratification of patients with both primary and metastatic UC for treatment with pembrolizumab.

In **Chapter 7** we enumerated 18 immune cell populations in blood samples that were collected before and during treatment with pembrolizumab from patients with mUC. Similar numbers of all immune cell populations were observed in responders and non-responders prior to treatment. Assessing ratios of immune cell populations revealed that the ratio of mature neutrophils to T cells (MNTR) had the strongest association with overall and progression-free survival, outperforming the classical neutrophil-to-lymphocyte ratio and the PD-L1 combined positivity score. As none of the patients with a high MNTR obtained a response to pembrolizumab, this ratio can potentially be used for up-front patient selection.

Our main findings from whole genome DNA and RNA sequencing analyses and multiple immune profiling methods, including their strengths and weaknesses, are summarized and placed into perspective of the current literature in **Chapter 8**. Particularly, the potential value of the TSE score and MNTR for stratification of patients with mUC for treatment with ICIs is discussed in light of future translational and clinical studies. Furthermore, potential mechanisms underlying resistance to pembrolizumab are described, with emphasis on the lack of T cell numbers and cluster formation in tumors of non-responders, and potential strategies to overcome therapy resistance are suggested and discussed.

SAMENVATTING

Historisch gezien bestond de behandeling van patiënten met gemetastaseerd urotheelcarcinoom (mUC) uit chemotherapie. In 2014 werd effectiviteit van immuun checkpoint remmers (ICRs) voor het eerst aangetoond in mUC wat leidde tot registratie voor tweedelijns behandeling. Hedendaags hebben verschillende studies effectiviteit van ICRs in eerdere stadia van UC aangetoond. ICRs grijpen aan op remmende receptoren op T cellen, of hun liganden op tumor- of antigeen presenterende cellen, en initiëren of reactiveren daarmee een immuunrespons tegen tumorcellen. Dit kan resulteren in een langdurige anti-tumor respons en sommige patiënten met mUC mogelijk zelfs genezen. Een algemene inleiding op dit proefschrift en een overzicht van klinische studies naar ICRs in verschillende stadia van UC wordt gegeven in **Hoofdstuk 1**. Daarmee bouwt dit hoofdstuk voort op de studies die systematisch werden beoordeeld in **Hoofdstuk 2**, waaronder gerandomiseerde studies naar ICRs bij patiënten met gemetastaseerd UC, niercel- en prostaatcarcinoom. Deze studies toonden aan dat ICRs (zeer) effectief kunnen zijn voor een klein deel van patiënten met mUC, maar geen effect hebben bij de meerderheid van patiënten. Daarom was het doel van dit proefschrift om nieuwe biomarkers te identificeren die onderscheid kunnen maken tussen patiënten waarbij ICRs wel en niet effectief zijn. Mogelijk kunnen deze biomarkers in de toekomst gebruikt worden voor selectie van patiënten voor behandeling. Daarnaast was het doel om meer kennis te verkrijgen over mechanismen die ten grondslag liggen aan resistentie tegen ICRs, wat richting kan geven aan toekomstige gerichte combinatietherapieën om tumoren gevoelig te maken voor ICRs. Hiervoor werd in Nederland de prospectieve biomarker studie RESPONDER geïnitieerd. Binnen deze studie werden patiënten met mUC behandeld met pembrolizumab (anti-PD1), en werden op verschillende momenten voor en tijdens de behandeling tumor biopten en bloedmonsters afgenomen. In deze monsters werd het tumor genoom en transcriptoom in kaart gebracht door middel van geavanceerde *sequencing* technieken, en werden verschillende multiparameter kleuringstechnieken gebruikt voor immuun profilering.

Een bestaande biomarker voor selectie van patiënten met mUC voor behandeling met ICRs is de expressie van PD-L1 in tumorweefsel. De voorspellende waarde van PD-L1 expressie wisselt echter per type ICR en per behandellijn. Mogelijk liggen de verschillen met betrekking tot antilichaam kloon, het vereiste kleuringsplatform en de scoringsmethode per ICR-specifieke PD-L1 test hieraan ten grondslag. Daarom hebben we de PD-L1 expressie op basis van vier ICR-specifieke testen, en een test voor onderzoeksdoeleinden met elkaar vergeleken in **Hoofdstuk 3**. We vonden goede overeenstemming in PD-L1 expressie op tumor en immuun cellen tussen de verschillende ICR-specifieke testen. De PD-L1 status volgens de specifieke scoringsmethoden was hetzelfde voor alle vier ICR-specifieke testen in 78% van de patiënten. Deze resultaten

rechtvaardigen mogelijk het uitwisselbare gebruik van de ICR-specifieke PD-L1 testen in de toekomst, hoewel er aanvullende studies nodig zijn om hun voorspellende waarde te beoordelen bij patiënten die worden behandeld met verschillende soorten ICRs.

In **Hoofdstuk 4** hebben we het moleculaire landschap van mUC op DNA en RNA niveau gedetailleerd in kaart gebracht door biopten uit metastasen te onderzoeken. Gebaseerd op verschillende *mutational signatures* werden twee grote genomische subtypes van mUC geïdentificeerd, waarvan het meest voorkomende subtype gerelateerd was aan APOBEC mutagenese. Clustering analyse van het transcriptoom onthulde vijf subtypes van mUC die gedeeltelijk overeenkwamen met de consensus classificatie voor primair niet-gemetastaseerd UC. Per RNA subtype werden potentieel effectieve behandelstrategieën voorgesteld. Bovendien werd voor bijna alle patiënten een aanknopingspunt voor gerichte therapie geïdentificeerd aan de hand van DNA veranderingen. Samen verrijken deze resultaten onze kennis over de moleculaire achtergrond van mUC, en kunnen de resultaten als leidraad dienen voor de toekomstige ontwikkeling van meer geïndividualiseerde behandelstrategieën.

De resultaten van multiparameter flow cytometrie analyse van bloedmonsters, en van multiplex immuunfluorescentie kleuringen op weefsel biopten verzameld binnen de RESPONDER studie worden beschreven in **Hoofdstuk 5**. In bloed zagen we dat de frequenties van CD4+ T cel subsets verschillend was tussen responders en non-responders. Voor start van therapie hadden responders een hogere frequentie van CD4+ T cellen met fenotypische kenmerken passend bij eerdere blootstelling aan antigeen, gedurende de behandeling nam de frequentie van cellen die stimulerende receptoren tot expressie brengen toe. Daarnaast was de concentratie chemokines in plasma voor start van behandeling hoger in responders. In tumorweefsel van responders vonden we dat de dichtheid van CD4+ T helper 1 (Th1) cellen voor start van therapie hoger was dan in non-responders. Gedurende de behandeling vormden deze Th1 cellen clusters met CD8+ T cellen en CD11b+ myeloïde cellen, wat niet werd gezien in non-responders. Samen laten deze resultaten zien dat respons op pembrolizumab in patiënten met mUC geassocieerd is met CD4+ T cel activatie in bloed, en lokale clustering van immuun cellen in de tumor gedurende de behandeling.

In **Hoofdstuk 6** werd een diepgaande analyse verricht van DNA en RNA data verkregen uit biopten van metastasen. Hier relateerden we genomische tumor karakteristieken, zoals genomische subtypes, aantal mutaties (*tumor mutational burden*), APOBEC mutagenese, en specifieke mutaties aan respons op behandeling met pembrolizumab. We vonden dat een hoog aantal mutaties en veel APOBEC mutagenese waren geassocieerd met respons op behandeling. Hiërarchische clusteranalyse op basis van genexpressie *signatures* gerelateerd aan T cellen, non-T cel immuun cellen, en stromale cellen, toonde drie clusters

van patiënten met een positieve, neutrale of negatieve T cel-tot-stroma verrijkingsscore (in het Engels: TSE score). Deze nieuwe score vergelijkt de relatieve expressie van T cell versus stroma gerelateerde genexpressie *signatures*. De meerderheid van patiënten met een positieve TSE score had baat bij behandeling met pembrolizumab. Daarentegen zagen we dat géén van de patiënten met een negatieve TSE score na zes maanden nog een aanhoudende respons had op behandeling met pembrolizumab, en deze patiënten hadden een slechte algemene en progressievrije overleving. De voorspellende waarde van de TSE score werd bevestigd in twee onafhankelijke cohorten van patiënten met UC die werden behandeld met ICRs (IMvigor 210 en ABACUS studie). Samen wijzen deze resultaten erop dat de TSE score potentieel gebruikt kan worden voor de a priori stratificatie van patiënten met zowel primair als gemetastaseerd UC voor behandeling met pembrolizumab.

In **Hoofdstuk 7** hebben we 18 verschillende immuun cel populaties gekwantificeerd in bloed dat voorafgaand aan en gedurende behandeling met pembrolizumab werd verzameld van patiënten met mUC. Voor start van therapie waren de aantallen van alle immuun cel populaties vergelijkbaar tussen responders en non-responders. Analyse naar ratio's van verschillende immuun cel populaties liet zien dat de ratio van uitgerijpte neutrofielen tot T cellen (in het Engels: MNTR) de sterkste associatie had met algemene en progressievrije overleving, en dat deze associatie sterker was dan voor de klassieke ratio van neutrofielen tot lymfocyten en voor PD-L1 expressie in tumor weefsel. Aangezien géén van de patiënten met een hoge MNTR baat had bij behandeling met pembrolizumab kan deze ratio mogelijk gebruikt worden voor selectie van patiënten voorafgaand aan start van therapie.

Onze belangrijkste bevindingen uit tumor DNA en RNA analyses en verschillende methodes van immuun profilering, inclusief hun sterke en zwakke punten, worden samengevat en in perspectief van de huidige literatuur geplaatst in **Hoofdstuk 8**. Met name de potentiële waarde van de TSE score en MNTR voor stratificatie van patiënten met mUC voor behandeling met ICRs wordt besproken in het licht van toekomstige translationele en klinische studies. Daarnaast worden mechanismen beschreven die potentieel ten grondslag liggen aan resistentie tegen pembrolizumab, waarbij de nadruk wordt gelegd op het gebrek aan T cellen en de afwezigheid van clustering van immuun cellen in de tumor, en worden mogelijke strategieën om therapieresistentie te overwinnen gesuggereerd en besproken.

A

LIST OF PUBLICATIONS

Systematic review of immune checkpoint inhibition in urological cancers.
Maud Rijnders, Ronald de Wit, Joost L. Boormans, Martijn P.J. Lolkema, Astrid A.M. van der Veldt.
European Urology, 2017 Sep;72(3):411-423

Reply to Nelson Martinez Merizalde Balarezo, Mark Monroe Rivera, and Romina A. Tejada's Letter to the Editor re: Maud Rijnders, Ronald de Wit, Joost L. Boormans, Martijn P.J. Lolkema, Astrid A.M. van der Veldt. Systematic review of immune checkpoint Inhibition in urological cancers.
Maud Rijnders, Ronald de Wit, Joost L. Boormans, Martijn P.J. Lolkema, Astrid A.M. van der Veldt.
European Urology, 2018 Mar;73(3):e67-e68

PD-L1 antibody comparison in urothelial carcinoma
Maud Rijnders, Astrid A.M. van der Veldt, Tahlita C.M. Zuiverloon, Katrien Grünberg, Erik Thunnissen, Ronald de Wit, Geert J.L.H. van Leenders.
European Urology, 2019 Mar;75(3):538-540. Full text version in this thesis.

Reply to Thomas Gevaert, Markus Eckstein, Rodolfo Montironi, and Antonio Lopez-Beltran's Letter to the Editor re: Maud Rijnders, Astrid A.M. van der Veldt, Tahlita C.M. Zuiverloon, et al. PD-L1 antibody comparison in urothelial carcinoma.
Maud Rijnders, Astrid A.M. van der Veldt, Tahlita C.M. Zuiverloon, Katrien Grünberg, Erik Thunnissen, Ronald de Wit, Geert J.L.H. van Leenders.
European Urology, 2019 Jun;75(6):e160-e161

Anti-PD-1 efficacy in patients with metastatic urothelial cancer associates with intratumoral juxtaposition of T helper-type 1 and CD8+ T cells.
Maud Rijnders, Hayri E. Balcioglu, Debbie G.J. Robbrecht, Astrid A.M. Oostvogels, Rebecca Wijers, Maureen J.B. Aarts, Paul Hamberg, Geert J.L.H. van Leenders, J. Alberto Nakauma-González, Jens Voortman, Hans M. Westgeest, Joost L. Boormans, Ronald de Wit, Martijn P. Lolkema, Astrid A.M. van der Veldt, Reno Debets.
Clinical Cancer Research, 2022 Jan 1;28(1):215-226

Comprehensive Molecular Characterization Reveals Genomic and Transcriptomic Subtypes of Metastatic Urothelial Carcinoma
J. Alberto Nakauma-González‡, Maud Rijnders‡, Job van Riet, Michiel S. van der Heijden, Jens Voortman, Edwin Cuppen, Niven Mehra, Sandra van Wilpe, Sjoukje F. Oosting, L. Lucia Rijstenberg, Hans M. Westgeest, Ellen C. Zwarthoff, Ronald de Wit, Astrid A.M. van der Veldt, Harmen J. G. van de Werken‡, Martijn P. J. Lolkema‡, Joost L. Boormans‡.
European Urology, 2022 Apr;81(4):331-336

Reply to Yuxuan Song, Caipeng Qin, and Tao Xu's Letter to the Editor re: J. Alberto Nakauma-González, Maud Rijnders, Job van Riet, et al. Comprehensive molecular characterization reveals genomic and transcriptomic subtypes of metastatic urothelial carcinoma.
J. Alberto Nakauma-González, Maud Rijnders, Harmen J.G. van de Werken, Martijn P.J. Lolkema, Joost L. Boormans
European Urology, 2022 Jun 15:S0302-2838(22)02403-4

A blood-based immune marker for resistance to pembrolizumab in patients with metastatic urothelial cancer
Maud Rijnders, Debbie G.J. Robbrecht, Astrid A.M. Oostvogels, Mandy van Brakel, Joost L. Boormans, Maureen J.B. Aarts, Hayri E. Balcioglu, Paul Hamberg, Jens Voortman, Hans M. Westgeest, Martijn P. Lolkema, Ronald de Wit, Astrid A.M. van der Veldt, Reno Debets
Cancer Immunol Immunotherapy, 2022 Aug 17

Submitted manuscripts

T cell-to-stroma enrichment (TSE) score: a gene expression metric that predicts response to immune checkpoint inhibitors in patients with urothelial cancer
Maud Rijnders‡, J. Alberto Nakauma-González‡, Debbie G.J. Robbrecht, Alberto Gil-Jimenez, Maureen J.B. Aarts, Joost L. Boormans, Paul Hamberg, Michiel S. van der Heijden, Bernadett E. Szabados, Geert J.L.H. van Leenders, Niven Mehra, Jens Voortman, Hans M. Westgeest, Ronald de Wit, Astrid A.M. van der Veldt, Reno Debets‡, Martijn P. Lolkema‡
Under review at Nature Communications

Publications not belonging to this thesis

Differential quantities of immune checkpoint-expressing CD8 T cells in soft tissue sarcoma subtypes
Yarne Klaver, Maud Rijnders, Astrid Oostvogels, Rebecca Wijers, Marcel Smid, Dirk Grünhagen, Cornelis Verhoef, Stefan Sleijfer, Cor Lamers, Reno Debets.
Journal for Immunotherapy of Cancer, 2020 Aug;8(2):e000271

Genome wide aneuploidy detected in circulating DNA predicts for poor response to pembrolizumab in advanced urothelial cancer patients.
Pauline A.J. Mendelaar‡, Debbie G.J. Robbrecht‡, Maud Rijnders, Ronald de Wit, V. de Weerd, Teoman Deger, John W.M. Martens, Astrid A.M. van der Veldt, J. Alberto Nakauma-González, Saskia M. Wilting, Martijn P.J. Lolkema.
Molecular Oncology, 2022 May;16(10):2086-2097
‡These authors contributed equally.

AUTHOR AFFILIATIONS

Aarts, Maureen J.B.	Department of Medical Oncology, Maastricht University Medical Center+, The Netherlands
Balcioglu, Hayri E.	Department of Medical Oncology, Erasmus MC Cancer Institute, Rotterdam, The Netherlands
Boormans, Joost L.	Department of Urology, Erasmus MC Cancer Institute, Rotterdam, The Netherlands
Brakel van, Mandy	Department of Medical Oncology, Erasmus MC Cancer Institute, Rotterdam, The Netherlands
Cuppen, Edwin	Center for Molecular Medicine and Oncode Institute, University Medical Center Utrecht, Utrecht, the Netherlands Hartwig Medical Foundation, Amsterdam, the Netherlands
Debets, Reno	Department of Medical Oncology, Erasmus MC Cancer Institute, Rotterdam, The Netherlands
Gil-Jimenez, Alberto	Department of Molecular Carcinogenesis, the Netherlands Cancer Institute, Amsterdam, the Netherlands. Oncode Institute, Utrecht, the Netherlands
Grünberg, Katrien	Department of Pathology, Radboud University Medical Center, Nijmegen, The Netherlands
Hamberg, Paul	Department of Medical Oncology, Franciscus Gasthuis & Vlietland Hospital Rotterdam, The Netherlands
Heijden van der, Michiel S.	Departments of Medical Oncology and Molecular Carcinogenesis, the Netherlands Cancer Institute, Amsterdam, the Netherlands
Leenders van, Geert J.L.H	Department of Pathology, Erasmus MC Cancer Institute, University Medical Center, Rotterdam, The Netherlands
Lolkema, Martijn P.J.	Department of Medical Oncology, Erasmus MC Cancer Institute, Rotterdam, The Netherlands
Mehra, Niven	Department of Medical Oncology, Radboud University Medical Center, Nijmegen, the Netherlands
Nakauma-González, J. Alberto	Departments of Medical Oncology, Urology, and Cancer Computational Biology Center, Erasmus MC Cancer Institute, Rotterdam, The Netherlands
Oosting, Sjoukje F.	Department of Medical Oncology, University Medical Center Groningen, University of Groningen, Groningen, the Netherlands
Oostvogels, Astrid A.M.	Department of Medical Oncology, Erasmus MC Cancer Institute, Rotterdam, The Netherlands
Riet van, Job	Department of Medical Oncology, Urology, and Cancer Computational Biology Center, Erasmus MC Cancer Institute, Rotterdam, The Netherlands
Rijstenberg, L. Lucia	Department of Pathology, Erasmus MC Cancer Institute, University Medical Center, Rotterdam, The Netherlands
Robbrecht, Debbie G.J.	Department of Medical Oncology, Erasmus MC Cancer Institute, Rotterdam, The Netherlands
Szabados, Bernadett E.	Barts Cancer Institute, Queen Mary University of London, London, United Kingdom
Thunnissen, Erik	Department of Pathology, Free University Medical Center, Amsterdam, The Netherlands
Veldt van der, Astrid A.M.	Departments of Medical Oncology and Radiology & Nuclear Medicine, Erasmus MC Cancer Institute, Rotterdam, The Netherlands
Voortman, Jens	Department of Medical Oncology, Amsterdam UMC, Vrije Universiteit Amsterdam, Cancer Center Amsterdam, The Netherlands
Werken van de, Harmen J.G.	Department of Urology, and Cancer Computational Biology Center, Erasmus MC Cancer Institute, Rotterdam, The Netherlands
Westgeest, Hans M.	Department of Medical Oncology, Amphia Hospital Breda, The Netherlands
Wijers, Rebecca	Department of Medical Oncology, Erasmus MC Cancer Institute, Rotterdam, The Netherlands
Wilpe van, Sandra	Department of Medical Oncology, Radboud University Medical Center, Nijmegen, the Netherlands
Wit de, Ronald	Department of Medical Oncology, Erasmus MC Cancer Institute, Rotterdam, The Netherlands
Zuiverloon, Tahlita C.M.	Department of Urology, Erasmus MC Cancer Institute, Rotterdam, The Netherlands
Zwarthoff, Ellen C.	Department of Pathology, Erasmus MC Cancer Institute, University Medical Center, Rotterdam, The Netherlands

ABOUT THE AUTHOR

Maud Rijnders was born on the 25th of June 1991, in 's-Hertogenbosch, the Netherlands. She completed her secondary school education at the Jeroen Bosch College in 's-Hertogenbosch in 2009. After graduation, she moved to Rotterdam and started her medical training at the Erasmus University Rotterdam. In 2012 she obtained her Bachelor of Science degree. During Medical School, she was selected to participate in a program to obtain her Master of Science degree in Molecular Medicine at the Erasmus University Rotterdam. Within this program, she worked on a research project regarding chemotherapy resistance in breast cancer at the department of Molecular Genetics of the Erasmus Medical Center Rotterdam under supervision of Dr. P.L.J. de Keizer. Subsequently she went through her clinical rotations and conducted her senior medical internship at the department of Internal Medicine at the IJsseland hospital in Capelle aan den IJssel. In January 2016 she obtained her Medical degree. She then continued the Master of Science program with an internship at the Laboratory of Tumor Immunology at the Erasmus Medical Center Rotterdam, studying immunophenotypes in patients with soft tissue sarcomas under super vision of Dr. Y. Klaver and Prof. dr. R. Debets. She graduated and obtained her Master of Science degree in January 2017. After this she got appointed as a PhD candidate at the department of Medical Oncology, at the Erasmus MC Cancer Institute in Rotterdam. Here she was supervised by Prof. dr. R. de Wit, Prof. dr. R. Debets, Dr. A.A.M. van der Veldt, and Dr. J.L. Boormans. Her research projects on immunotherapy in patients with metastatic urothelial cancer are described in this thesis and were presented at various (inter)national conferences. From October 2021 onwards, she started working as a medical resident. In here future career, she hopes to combine her work as a medical doctor with scientific research to contribute to improving patient care.

PHD PORTFOLIO

Name PhD student:	Maud Rijnders
Erasmus MC Department:	Medical Oncology
Research School:	Molecular Medicine
PhD period:	March 2017 – Sept 2021
Promotors:	Prof. dr. R. de Wit, Prof. dr. R. Debets
Co-promotors:	Dr. A.A.M. van der Veldt, Dr. J.L. Boormans

	Year	Workload (ECTS)
1. PhD training		
1.1 General academic and research skills		
Research Integrity	2017	0,3
'Basiscursus Regelgeving Klinisch Onderzoek' (BROK)	2017	1,5
Basic human genetics course	2017	0,6
Basic Introduction Course on SPSS	2017	1,0
Advanced course on Applications in flow cytometry	2017	0,5
Survival analysis course	2018	0,6
Advanced immunology course	2018	4,5
Basic course on R	2018	1,1
R course of RNAseq analyses	2019	2,0
		12,1
1.2 Poster presentations		
Dutch Tumor Immunology Meeting, Breukelen	2018, 2019	0,5
Dutch Society for Immunology, European Congress Immunology	2018	0,5
Dutch Society for Immunology, annual meeting	2019	0,5
American Society of Clinical Oncology, annual meeting	2020	0,5
American Association for Cancer Research, annual meeting	2021	0,5
		2,5
1.3 Oral presentations		
Josephine Nefkens Institute scientific research meeting	2018, 2021	2,0
Tumor Immunology Platform meeting, Erasmus MC	2017-2021	4,0
Integraal Kankercentrum Nederland minisymposium urologic tumors	2017	1,0
Dutch Uro-Oncology Studygroup, annual meeting	2017-2019	3,0
Medical Oncology Research Meeting, Erasmus MC	2018	1,0
Dutch Society for Urology, bi-annual meeting	2018-2020	3,0
Jonge oncologen avond, Rotterdam	2018	1,0
Cancer Institute Research Day, Erasmus MC	2018, 2019	2,0
International Bladder Cancer Network, annual meeting	2018	1,0
Tour d'Europe, Rotterdam	2019	1,0
Academic Center of Excelence Tumor Immunology and Immune Therapy, Erasmus MC, annual symposium	2019, 2021	2,0
Scientific meeting Erasmus MC Cancer Institute	2019	1,0
Dutch Society for Immunology, annual meeting	2020	1,0
Dutch Tumor Immunology Meeting, Breukelen	2021	1,0
		24

	Year	Workload (ECTS)
1.4 (Inter)national conferences		
Molecular Medicine Day	2017	0,3
Dutch Uro-Oncology Studygroup, annual meeting	2017-2020	1,2
Dutch Tumor Immunology Meeting, Breukelen	2018, 2019	1,2
Dutch Society for Immunology, European Congress Immunology	2018	1,2
International bladder cancer network, annual meeting	2018-2020	1,5
Dutch Society for Immunology, annual meeting	2019, 2020	1,2
American Society of Clinical Oncology, annual meeting	2020	1,5
American Association for Cancer Research, annual meeting	2021	1,5
		11,1
1.5 Research meetings and other seminars		
Josephine Nefkens Institute scientific research meetings (~36x /year)	2017-2021	6,0
Josephine Nefkens Institute oncology lectures (~6x /year)	2017-2020	0,6
Tumor Immunology Platform meetings (~36x /year)	2017-2021	6,0
T cell consortium (TCC) meetings (~6x /year)	2017-2020	0,6
Immunology Seminars (~6x /year)	2017-2020	0,6
Medical Oncology Research Meeting (~10x/year)	2017-2021	1,0
Scientific meeting Erasmus MC Cancer Institute, annual symposium	2017-2020	0,5
Erasmus MC Cancer Institute annual research day	2017-2020	1,0
Vectra users day The Netherlands	2019	0,3
		16.6
Other		
Investigator meeting KEYNOTE-672	2018	0,6
RESPONDER trial, site initiation visits	2018, 2019	1,0
Scientific meeting Erasmus MC Cancer Institute – organisation and chair	2019	0,5
		2,1
2. Teaching		
2.1 Lecturing		
Master Nanobiology	2018	0,5
Minor Oncology	2019	0,5
Master Infection & Immunity	2021	0,5
		1,5
2.2 Supervising, Tutoring		
Thesis BSc student	2018, 2019	0,5
Thesis and practical supervision BSc student, 9 months	2019	3
		3,5
Total (28h workload = 1 ECTS)		73,4